University of Warsaw
Faculty of Physics
Institute of Theoretical Physics

Doctoral Thesis

Recursive Structures for Nahm Sums

Dmitry Noshchenko

Supervisor: Prof. Dr Hab. Piotr Sułkowski

October, 2021

Contents

Introduction

In the past half-century there has been a tendency towards unification in theoretical physics. Among the existing approaches, string theory provides a hypothetical framework for quantum gravity, filling the gap between Einstein's general relativity and the Standard Model of particle physics. Mathematically, better understood are the two-dimensional models of quantum gravity, given by ensembles of random matrices [1, 2, 3, 4, 5]. Another important player is the conformal field theory (CFT): on the one hand, it describes the embedding of a string in spacetime (string worldsheet, which is a surface with the conformal invariance), on the other hand – it governs the symmetries in 2d quantum gravity [6, 7, 8].

Nahm sums are central in this thesis. They were introduced by Werner Nahm [9, 10] as a generalization of character functions for rational conformal field theories in two dimensions [11, 12, 13, 14]. Correlations in such theories are described by a finite sum of holomorphic times anti-holomorphic functions of the moduli of surfaces with marked points. Character functions are the q-hypergeometric series which count states of a given conformal weight. Remarkably, they often have modularity properties, which allows to efficiently compute the fusion rules for observables. Nahm found the universal formula for such characters for $(2, k+2)$ minimal CFTs and conjectured the general form for all rational CFTs. The essential ingredient in Nahm's formula is a symmetric matrix C over rational numbers, which is unique for a given theory. He soon realized that the object might get more attention from both mathematical and physical communities.

Indeed, Nahm sums appeared many times outside the original context of CFTs. At first, as the generating series of Betti numbers of the moduli spaces of quiver representations [15, 16, 17], where C plays role of the adjacency matrix of a symmetric quiver. Later it was discovered that generating series of colored HOMFLY-PT polynomials for a knot [18, 19, 20] take form of a quiver series for some quivers [21, 22, 23, 24, 25, 26, 27]. This was rather exciting, since HOMFLY-PT polynomials, as shown by Edward Witten [28], are expectation values of Wilson loops in the Chern-Simons gauge theory on a 3-manifold. On the other hand, quivers are known to characterize a rather different kind of supersymmetric gauge theories: super-Yang-Mills theories, Argyres-Douglas models, etc. [29, 30, 31, 32, 33], and the knots-quivers correspondence connects topology of a knot to a three dimensional gauge theory represented by a quiver. This phenomenon captures a class of theories involved in the 3d-3d correspondence, which was conjectured even before the knots-quivers correspondence [34, 35, 36, 37]. Besides, Chern-Simons theory on a 3-sphere is known to be dual to open topological string theory on the resolved conifold [38, 39]. It turns out that from the M-theory point of view [40], the Nahm sums from quivers are partition functions which describe dynamics of M5 branes wrapping the knot conor-

mal inside the resolved conifold [24]. The duality between a knot and a gauge theory can be viewed as a choice of compactification for the corresponding M5 brane. In this picture quiver nodes correspond to basic Bogomol'nyi–Prasad–Sommerfield (BPS) states and the linking numbers correspond to their interactions, creating the infinite spectrum of bound states which are equal to motivic DT invariants of the corresponding quiver and are captured by the Nahm sum. Another interesting scenario concerns the asymptotic expansion of Jones polynomials for a hyperbolic knot [41, 42]. The Nahm data is given in terms of gluing matrices for ideal tetrahedra forming the complement of a hyperbolic knot. This approach is, however, different from the previous one. In this case the partition function for the Chern-Simons theory defined on a knot complement itself can be expressed as a Nahm sum.

Now we explain what are the "recursive structures", which are of main interest in this thesis. The early developments in 2d quantum gravity clarified the significance of matrix models. For them, there was a long-standing problem of finding the exact formula to compute correlation functions up to an arbitrary order. The ultimate answer was given by the topological recursion [3, 43, 44, 45]. Discovered within hermitian one-matrix model and soon taken into a much broader setting, topological recursion is the universal formula to compute correlation functions, given a spectral curve of a model. A determinant correlation function can be though of as a wave function, annihilated by the quantized spectral curve analogous to Schrödinger operator. For example, in the Chern-Simons theory such curves are knot A-polynomials [46], which are properly quantizable as Lagrangian submanifolds [47, 48]. It is conjectured that topological recursion applied to a deformed knot A-polynomial, computes colored HOMFLY-PT polynomials for this knot [49]. The associated quantum A-polynomials for knots were systematically studied in [50, 51]. From our perspective a particularly interesting class of spectral curves (a.k.a. quiver A-polynomials) comes from the Nahm sums for quivers, for which we explore both quantization properties and topological recursion. Besides, quantum A-polynomials themselves produce another type of recurrence relations [48], to which the Nahm sum is a distinguished solution. In order to match this recurrence with the topological recursion, we verify the consistency of the two partition functions obtained from the same quiver by using the Wentzel–Kramers–Brillouin (WKB) approximation.

A few years ago topological recursion was generalized to quantum Airy structures [52, 53, 54], i.e. a collection of differential operators which form Virasoro or $\mathcal{W}$-algebra. The main property of every quantum Airy structure is the existence of a unique partition function which is annihilated by the corresponding operators, and is tightly related to the topological recursion. This setup is closer to orbifold CFTs, because spectral curves are ramified, and it gives an automorphism of the corresponding $\mathcal{W}$-algebra. In this thesis we study the simplest case of r-Airy curve, related to the generalized Witten-Kontsevich matrix model [55, 56].

Summing up, the purpose of this thesis is to study the recursive structures (topological recursion, WKB analysis for quantum curve equations) for Nahm sums as well as local equivalences arising in the knots-quivers correspondence. Quantum Airy structures are the only exception, for which the relation to Nahm sums is not known to date. The results of this work are presented in the following papers[1]

[1]During my master studies I was working also on topics beyond the scope of this thesis. Results are summarised

- [57] Borot, G., Bouchard, V., Chidambaram, N. K., Creutzig, T., & Noshchenko, D. (2019). Higher Airy structures, W algebras and topological recursion (accepted in Memoirs of the AMS). arXiv: 1812.08738 [math-ph]

- [58] Larraguivel, H., Noshchenko, D., Panfil, M., & Sulkowski, P. (2020). Nahm sums, quiver A-polynomials and topological recursion. JHEP, 07, 151. arXiv: 2005.01776 [hep-th]

- [59] Noshchenko, D. (2021). Combinatorics of Nahm sums, quiver resultants and the K-theoretic condition. JHEP, 03, 236. arXiv: 2007.15398 [hep-th]

- [60] Jankowski, J., Kucharski, P., Larraguivel, H.,Noshchenko, D., & Sulkowski, P. (2021). Permutohedra for knots and quivers (accepted in Physical Review D) arXiv: 2105.11806 [hep-th]

The thesis consists of the following chapters:

- **Chapter 1.** We begin by defining Nahm sums for 2d rational CFTs and then proceed to quiver representations. After that we explain in brief the Chern-Simons theory, quantum knot invariants and the knots-quivers correspondence, which relates the generaing series of colored HOMFLY-PT polynomials of a knot to Nahm sums for some types of quivers. We give the M-theory setup in which the knots-quivers correspondence can be naturally considered. Finally we compute the semi-classical limit of the Nahm sums and define Nahm equations and quiver A-polynomial, both classical and quantum.

- **Chapter 2.** We study whether quiver A-polynomials are tempered. This property holds for all knot A-polynomials [46] and is closely related to quantization [48]. We focus on combinatorial structures of Newton polytopes for the Nahm sums, and give the positive answer for certain type of quivers. This is a preliminary step before the topological recursion, since if quiver A-polynomials are quantizable, it is expected that topological recursion gives a meaningful result. This chapter is based on [59].

- **Chapter 3.** We explain how the topological recursion arises from the matrix model formalism and provide its axiomatic definition in terms of an arbitrary spectral curve. We also relate the WKB expansion for a Schrödinger-like operator (quantum curve) to correlation functions computed by the topological recursion for the semi-classical limit of this operator. We apply the topological recursion to quiver A-polynomials and verify its consistency with the WKB method for a selection of quivers. This part is based on [58]. Next, we define quantum Airy structure as a collection of differential operators in relation to topological recursion. We focus on spectral curve $x = \frac{1}{r}\, y^r$ and especially on the case $r = 3$, whose symmetry algebra coincides with $\mathcal{W}(\mathfrak{sl}_3)$ algebra arising in conformal field theory. This part is based on [57].

in:

- Il'in, I., Noshchenko, D., & Perezhogin, A. (2015a). On classification of high-order integrable nonlinear partial differential equations. Chaos, Solitons & Fractals, 76 (100), 278–281. arXiv: 1611.09292.
- Noshchenko, D., & Perezhogin, A. (2016). On the Painleve property of a hydrodynamic system. In E. W. of Conferences (Ed.), (Vol. 11). doi:10.1051/e3sconf/20161100017

- **Chapter 4.** We switch our attention to the knots-quivers correspondence and study the local equivalence relation for Nahm sums connected to multi-cover skeins on quivers [25]. It helps to understand how quivers corresponding to the same knot are organized, moreover, it translates to identities between the corresponding Nahm sums. This chapter is based on [60].

Acknowledgements

I would like to thank, first of all, my supervisor Piotr Sułkowski for several years of fruitful collaboration, his hospitality and helpfulness during my PhD studies and thesis preparation. Besides I am grateful to all my friends and colleagues I met at University of Warsaw: Paweł Bączyk, Aditiya Bawane, Paweł Ciosmak, Shi Cheng, Jakub Jankowski, Maciej Konieczka, Aleksei Koshevarnikov, Piotr Kucharski, Hélder Larraguível, Miłosz Panfil, Carlos Perez, Tomasz Tarkowski and others, as well as collaborators abroad: Gaëtan Borot, Vincent Bouchard, Nitin Chidambaram and Thomas Creutzig. Special thanks go to Andrey Perezhogin, my first scientific mentor and a good friend from whom I got addicted to research, and Igor Il'in, who drove my scientific interests into the quantum realm.

The research conducted during my PhD studies and presented in this thesis was supported by the TEAM programme of the Foundation for Polish Science co-financed by the European Union under the European Regional Development Fund (POIR.04.04.00-00-5C55/17-00).

Chapter 1

Nahm sums, knots and quivers

Nahm sum is the main player in this thesis; remarkably, it appears in many contexts such as quiver representations, conformal field theories, knots and topological strings. We begin with the main definition and then proceed to various incarnations of Nahm sums, essential for our study. Recall that the q-Pochhammer symbol $(x,q)_n$ for integer n is defined as

$$(x,q)_n := \prod_{k=0}^{n-1}(1-xq^k). \tag{1.1}$$

Definition 1.0.1. *Nahm sum is the following q-hypergeometric series:*

$$\boxed{f_{A,B,C}(q) = \sum_{d_1,\ldots,d_m\geq 0} \frac{q^{Q(d)}}{(q;q)_{d_1}\ldots(q;q)_{d_m}}} \tag{1.2}$$

where $d=(d_1,\ldots,d_m)$ *and*

$$Q(d) = \frac{1}{2}d^TCd + Bd + A,$$

is a quadratic function determined by a symmetric $m\times m$ *matrix* C *with rational entries, a column vector* B *of length* m *and a scalar* A*.*

Example 1.0.1. The simplest example is the Nahm sum which counts partitions of natural numbers into d distinct summands:

$$\sum_{d\geq 0}\frac{q^{(d^2+d)/2}}{(q)_d} = \prod_{n=1}^{\infty}(1+q)^n \tag{1.3}$$

with $C_{11}=1, B=2, A=0$.

The original consideration of Werner Nahm comes from rational conformal field theories, which is our starting point here.

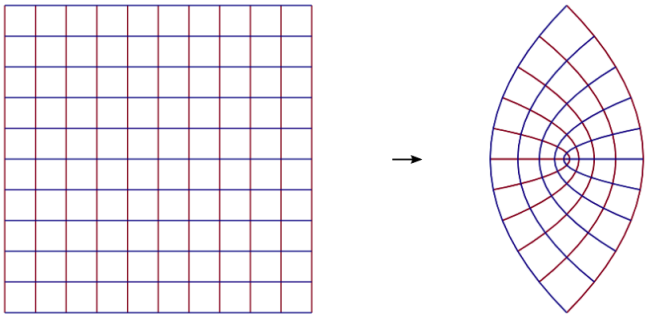

Figure 1.1: Conformal transformation in the plane.

1.1 Nahm sums from 2d rational CFTs

A two-dimensional conformal field theory (2d CFT) is a quantum field theory on a two-dimensional manifold, invariant under conformal transformations, figure 1.1. Historically important application of CFTs concerns various statistical systems at a critical point, where conformal invariance arises when the correlation distance tends to infinity [61, 62, 63]. Later it was realized that 2d CFT is a necessary framework for understanding string theory and quantum gravity [64, 14, 65, 66, 67]. Several notable examples of conformally invariant theories include minimal models, Liouville theory, massless free bosonic theories, Wess–Zumino–Witten models [4].

1.1.1 Conformal field theories in two dimensions

Consider the manifold $M = \mathbb{R}^d$ with flat metric $g_{\mu\nu}$. Let $\xi = (\xi^1, \dots, \xi^d), \xi' = (\xi'^1, \dots, \xi'^d)$ be the two coordinate charts on M. The elements of the conformal group can be presented as the functions

$$f: \ \xi \mapsto \xi'(\xi), \tag{1.4}$$

which change the metric in such way that

$$g_{\mu\nu}(\xi) \mapsto g'_{\mu\nu}(\xi') = \frac{\partial \xi^\alpha}{\partial \xi'^\mu} \frac{\partial \xi^\beta}{\partial \xi'^\nu} g_{\alpha\beta}(\xi), \tag{1.5}$$

where $g'_{\mu\nu}(\xi') = \Omega(\xi)\, g_{\mu\nu}(\xi)$ for some $\Omega > 0$. Therefore, they may distort the distance, but always preserve the angles between any two tangent vectors μ, ν.

We focus on the two dimensional theories, i.e. $d = 2$ and $g_{\mu\nu} = \delta_{\mu\nu}$. It is helpful to introduce complex coordinates $z = \xi^1 + i\xi^2$, $\overline{z} = \xi^1 - i\xi^2$. In this case conformal transformations $f(z), f(\overline{z})$ are analytic reparametrizations and their local algebra is infinite-dimensional. To define a quantum field theory, we need to introduce the fields $\Phi(z, \overline{z})$ which are called primary, as they transform nicely under conformal transformations:

$$\Phi(z, \overline{z}) = \left(\frac{\partial f}{\partial z}\right)^h \left(\frac{\partial \overline{f}}{\partial \overline{z}}\right)^{\overline{h}} \Phi(f(z), f(\overline{z})) \tag{1.6}$$

(here both h and $\overline{h}$ are real numbers, called the weights of $\Phi(z, \overline{z})$). The stress-energy tensor T_{ab}

can be diagonalized to have the non-vanishing holomorphic and anti-holomorphic components

$$T(z) = T_{11} + iT_{12}, \quad \overline{T}(z) = T_{11} - iT_{12}. \tag{1.7}$$

We can expand any of them as a series in z:

$$T(z) = \sum_{n=-\infty}^{\infty} L_n z^{-n-2} \tag{1.8}$$

In this expression the operators L_n are the generators of the analytic part of the conformal group. They form Virasoro algebra, which is a complex Lie algebra with the bracket

$$[L_i, L_j] = (i-j)L_{i+j} + \frac{c}{12}(i^3 - i)\delta_{i+j,0} \tag{1.9}$$

The constant c is one of the key characteristics of a CFT and is called the central charge. On another hand, $\overline{T}(z)$ gives rise to a similar set of operators, denoted by $\overline{L}_i$. Notice that the operators L_{-1}, L_0 and L_1 generate the $SL(2,\mathbb{R})$-subgroup of the conformal group consisting of translation, dilatation and special conformal transformation. The Hilbert space $\mathcal{H}$ for a CFT consists of the states, and each state is in bijection with some local operator (including Virasoro operators). Among all operators, primary fields play special role and correspond to the highest weight states of the Virasoro representations. They are usually denoted by $h_i, \overline{h}_i$.

A rational CFT can be described by a pair of vertex operator algebras: one is holomorphic and another one is anti-holomorphic. A vertex operator algebra (VOA) consists of states, fields and the state-field correspondence which satisfies certain set of axioms [68]. The space of states $V = \oplus_i V_i$ is a $\mathbb{Z}$-graded vector space. We may represent the space of states by the Fock space which is the polynomial ring of infinitely many variables: $\mathcal{F} = \mathbb{C}[b_{-1}, b_{-2}, \dots]$. It is also a graded vector space, i.e. each variable b_{-i} has degree i, which gives $\mathcal{F} = \oplus_i \mathcal{F}_i$, where $\mathcal{F}_i$ is the span of all homogeneous polynomials in $b_{-1}, b_{-2}, \dots$ of degree i. Then L_i as differential operators acting on the Fock space involve differentiation: $b_i = \frac{\partial}{\partial b_{-i}}$ for $i > 0$, and multiplication by b_{-i}:

$$L_k = \frac{1}{2} \sum_{m \in \mathbb{Z}} : b_m b_{k-m} : \quad \forall k \in \mathbb{Z} \tag{1.10}$$

where ": :" denotes the normal ordering:

$$: b_k b_l : = \begin{cases} b_l b_k & \text{if } k = -l, l \leq 0 \\ b_k b_l & \text{otherwise} \end{cases} \tag{1.11}$$

Remarkably, L_k defined above, satisfy the same algebra relation as in (1.9), and form the free-field representation of the Virasoro algebra.

Recall that the trace of exponential operator A is the summation over its spectrum $\Lambda(A)$ with multiplicities m_λ:

$$\mathrm{Tr}(e^A) = \sum_{\lambda \in \Lambda(A)} m_\lambda e^\lambda \tag{1.12}$$

Define the character function at the level i as

$$\chi_i(q) = \mathrm{Tr}_{\mathcal{F}_i}\left(q^{L_0-\frac{c}{24}}\right) = q^{h_i-\frac{c}{24}}\sum_{n=0}^{\infty} a_{in}q^n, \quad a_{in} \in \mathbb{Z}_{\geq 0}, \tag{1.13}$$

where the trace is taken over the i-th component of the Fock space. Analogously, $\overline{\chi}_i$ is defined by the spectrum of $\overline{L}_0$. In general, character functions are formal q-series. However, any rational CFT has the finite sets of characters $\chi_i, \overline{\chi}_i$, which are holomorphic (resp. anti-holomorphic) functions (not just formal series) which sometimes have nice modular properties. The partition function for such a theory is defined as

$$Z_{\mathrm{CFT}} = \sum_{i,j} n_{ij}\chi_i\overline{\chi_j} \tag{1.14}$$

where $n_{00} = 1$ and all n_{ij} are positive integers (can be equal to zero).

1.1.2 Nahm's definition

Our main references are [9, 10]. Among other things, it was shown that the character functions $\chi_i(q)$ for two-dimensional rational conformal field theories with an integrable perturbation [69, 70], for example all minimal models, have a canonical sum presentation. The (r, s) minimal model (or Virasoro minimal model) is a two-dimensional rational CFT whose space of states is built from finitely many irreducible representations of the Virasoro algebra, and whose central charge is determined by a pair of integers (r, s)

$$c(r, s) = 1 - 6\frac{(r-s)^2}{rs}. \tag{1.15}$$

For example:

- $(r, s) = (2, 3)$: Trivial CFT
- $(r, s) = (2, 5)$: Yang-Lee edge singularity [71, 72, 73, 74]
- $(r, s) = (3, 4)$: Critial Ising model [75, 74]

Consider the non-unitary $(2, k + 2)$ minimal model with central charge

$$c(2, k + 2) = 1 - 3\frac{k^2}{k+2} \tag{1.16}$$

and primary fields of conformal dimension

$$h_j = -\frac{j(k-j)}{2(k+2)}, \; j \in \{0, \ldots, \lfloor\frac{k}{2}\rfloor\} \tag{1.17}$$

As mentioned above, these CFTs are notable for having integrable deformations. Most importantly, their character functions are completely determined by a unique symmetric $m \times m$ matrix C, a column vector B of size m and a scalar A, all taking values in $\mathbb{Q}$. This formula reads

$$\chi_i(q) = \sum_{d_1,\dots,d_{\lfloor k/2\rfloor}\geq 0} \frac{q^{Q_i(d)}}{(q;q)_{d_1}\cdots(q;q)_{d_{\lfloor k/2\rfloor}}}, \tag{1.18}$$

where

$$Q_i(d) = \frac{1}{2}d^T C d + B_i d + h_i - \frac{c}{24}. \tag{1.19}$$

Note that the matrix C is the same for all characters χ_i of a given CFT This was the original motivation of Nahm, and later he generalized (1.18) to generic data A, B, C and m and studied its modular properties.

Example 1.1.1. A class of examples is related to Cartan matrices, or equivalently to Dynkin diagrams with the ADE classification [10]. The $(2, r+2)$ minimal model corresponds to the tadpole graph T_r. Recall that Cartan matrices for type A are $\mathcal{C}(A_r)_{ij} = -1$ for $|i-j| = 1$ and $\mathcal{C}(A_r)_{ij} = 0$ for $|i-j| > 1$. The tadpole diagram T_r (figure 1.2) is obtained by folding A_{2r} diagrams, so that $\mathcal{C}(T_r)_{rr} = 1$ and for all other entries $\mathcal{C}(T_r)_{ij} = \mathcal{C}(A_r)_{ij}$. In this case the corresponding Nahm sum is characterized by $C^{(2,k+2)} = \mathcal{C}^{-1}(T_k)$, so that $C_{ij}^{(2,k+2)} = \min(i,j)$. For example,

$$C^{(2,3)} = [\,1\,], \quad C^{(2,4)} = \begin{bmatrix} 1 & 1 \\ 1 & 2 \end{bmatrix}, \quad C^{(2,5)} = \begin{bmatrix} 1 & 1 & 1 \\ 1 & 2 & 2 \\ 1 & 2 & 3 \end{bmatrix}, \quad \dots \tag{1.20}$$

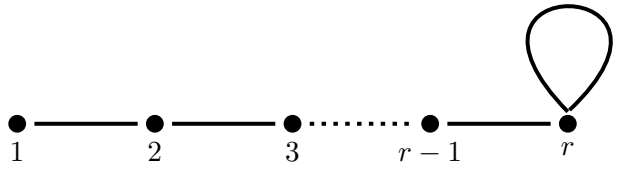

Figure 1.2: The tadpole Dynkin diagram T_r consists of r connected vertices and a loop.

Example 1.1.2. Quite recently [76] it was shown that the $(3,4)$ minimal model (critical Ising model) also has the character function taking form of the Nahm sum for the matrix

$$C^{(3,4)} = \begin{bmatrix} 8 & 3 \\ 3 & 2 \end{bmatrix}. \tag{1.21}$$

The character function takes form:

$$\chi_{(3,4)}(q) = \sum_{d_1,d_2\geq 0} \frac{q^{4d_1^2+3d_1d_2+d_2^2}}{(q;q)_{d_1}(q;q)_{d_2}}(1 - q^{d_1} + q^{d_1+d_2}) \tag{1.22}$$

1.2 Nahm sums for symmetric quivers

Although Nahm sums originated from 2d rational CFTs, we are primarily interested in a different appearance of this object. Namely, as a generating series of motivic Donaldson-Thomas

invariants for a symmetric quiver, or simply quiver series. They are known to encode some properties of the moduli space of quiver representations. We therefore review the basic quiver representation theory and explain the appearance of Nahm sums in this context [16, 77, 78, 79].

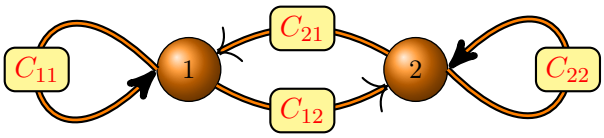

Figure 1.3: Symmetric quiver with $C_{ij} = 1,\ i,j = 1,2$ (the "uniform" quiver).

A quiver Q is a directed graph

$$Q = (Q_0, Q_1, h, t),$$

where Q_0, Q_1 are the sets of vertices and arrows, and h, t are the functions from Q_1 to Q_0, which for a given arrow give a "head" and a "tail" vertex. For example, if there are two vertices $1, 2$ connected by an arrow a from 1 to 2, then $ta = 1,\ ha = 2$ (figure 1.2). The arrow from a vertex to itself is called a loop; the number of loops for the i-th vertex is equal to C_{ii}.

A quiver representation of dimension vector $d = (d_1, \ldots, d_m) \in \mathbb{Z}^m$ is the following data associated to Q:

- To every vertex $i \in Q_0$ one associates a finite-dimensional vector space $V(i)$ over a field F, such that $d_i = \dim V(i)$
- to every arrow $a \in Q_1$, a linear map $V(a) : V(ta) \to V(ha)$.

Without loss of generality assume that $V(i) = F^{d_i},\ \forall i \in Q_0$ and denote $\mathrm{Mat}_{m,n}$ the set of all m by n matrices over F. We are not interested in particular representations, but rather in the representation space with a fixed dimension vector d:

$$\mathrm{Rep}_Q^d := \prod_{a \in Q_1} \mathrm{Mat}_{\dim(V(ha)),\dim(V(ta))} \tag{1.23}$$

Since any such matrix corresponds to $V(a)$ for some V, each point of (1.23) defines a representation. The group of automorphisms $\mathrm{Aut}(V)$ is defined as the orbit of

$$G := \prod_{i=1}^{m} \mathrm{GL}_{d_i}(F)$$

The latter acts on Rep_Q^d via conjugation:

$$(g)(V(a)) := (g_j V(a) g_i^{-1})_{(a:i\to j)}, \quad \forall\ a \in Q_1,\ g \in G \tag{1.24}$$

By definition, the orbits of G in Rep_Q^d are precisely the isomorphism classes of quiver represen-

tations of Q of dimension vector d (two representations are isomorphic if they are related by a change of bases of $F^{d_i},\ i=1,\dots,m$).

Take $F=\mathbb{F}_q$ (representations over a finite field), where $q=p^r$ and p is prime:

$$V(i)=\mathbb{F}_q^{d_i},\ \forall i\in Q_0$$

These are non-negative integers modulo q, i.e. $\mathbb{F}_q=\{0,1,2,\dots,q-1\}$ with modular multiplication. For a fixed d, denote

$$s_d:=\sum_{[V],\ \dim V=d}\frac{1}{|\mathrm{Aut}(V)|}, \tag{1.25}$$

where the summation is over all isomorphism classes $[V]$ of representations with dimension vector d, and $|\mathrm{Aut}(V)|$ is the size of the corresponding automorphism group (it is also finite). Because of this, the total number of representations of dimension vector d is

$$q^{\sum_{a\in Q_1}d_id_j}=q^{\sum_{i,j=1}^m C_{ij}d_id_j}$$

On another hand, the number of points in the orbit of V is $\frac{|G|}{|\mathrm{Aut}(V)|}$. Therefore,

$$q^{\sum_{i,j=1}^m C_{ij}d_id_j}=\sum_{[V],\ \dim V=d}\frac{|G|}{|\mathrm{Aut}(V)|}, \tag{1.26}$$

which gives

$$s_d=\frac{q^{\sum_{i,j=1}^m C_{ij}d_id_j}}{\prod_{i=1}^m|\mathrm{GL}_{d_i}(\mathbb{F}_q)|}, \tag{1.27}$$

where C is the adjacency matrix of Q, and

$$|\mathrm{GL}_n(\mathbb{F}_q)|=(q^n-1)(q^n-q)\dots(q^n-q^{n-1})=(-q)^{\frac{n(n-1)}{2}}(q;q)_n$$

The latter equality comes from counting of all admissible columns of a matrix in $\mathrm{GL}_n(\mathbb{F}_q)$. The first row can be anything but zero vector, hence the factor (q^n-1), the second row can be anything but the multiple of the first one, hence (q^n-q), and so on. The last step is assembling the generating series:

$$\sum_{d_1,\dots,d_m\geq 0}s_d\ x_1^{d_1}\dots x_m^{d_m} \tag{1.28}$$

where x_i are the formal generating parameters. In order to match (1.28) with (1.29), we apply rescaling

$$x_i^{d_i}\mapsto(-q)^{\frac{d_i(d_i-1)}{2}}x_i^{d_i}$$

In what follows, we allow q to be an arbitrary complex number.

Definition 1.2.1. *Nahm sums for a quiver Q are the infinite q-series*

$$P_C(x_1,\dots,x_m)=\sum_{d_1,\dots,d_m\geq 0}\frac{(-q^{1/2})^{\sum_{i,j=1}^m C_{ij}d_id_j}}{(q;q)_{d_1}\cdots(q;q)_{d_m}}x_1^{d_1}\cdots x_m^{d_m}, \tag{1.29}$$

where C_{ij} is the number of arrows from i to j in Q.

We also denote $P_{d_1,\ldots,d_m}$ q-coefficients of these series, so that

$$P_C(x_1,\ldots,x_m) = \sum_{d_1,\ldots,d_m\geq 0} P_{d_1,\ldots,d_m} x_1^{d_1}\cdots x_m^{d_m}. \tag{1.30}$$

In order to make a connection to (1.2), we can set $A = 0$ and define $x_i := q^{B_i}$. We therefore refer to (1.29) as the Nahm sum for a quiver, or simply quiver series. Remarkably, it can be written as an infinite product:

$$P_C(x_1,\ldots,x_m) = \prod_{d_1,\ldots,d_m\neq 0} \prod_{j\in\mathbb{Z}} \prod_{k\geq 0} (1-q^{k+(j-1)/2} x_1^{d_1}\ldots x_m^{d_m})^{\Omega_{d_1,\ldots,d_m;j}} \tag{1.31}$$

The exponents $\Omega_{d_1,\ldots,d_m;j}$ are called the motivic Donaldson-Thomas (DT) invariants [15, 16, 17], which were shown to be integer when C is symmetric [80]. From the physical perspective they correspond to BPS states of a supersymmetric gauge theory depending on a quiver and are related to the wall-crossing phenomenon [16, 81, 82, 83]. So far it is not clear what is the underlying theory, but the next section will shed some light on it.

1.3 Knots-quivers correspondence

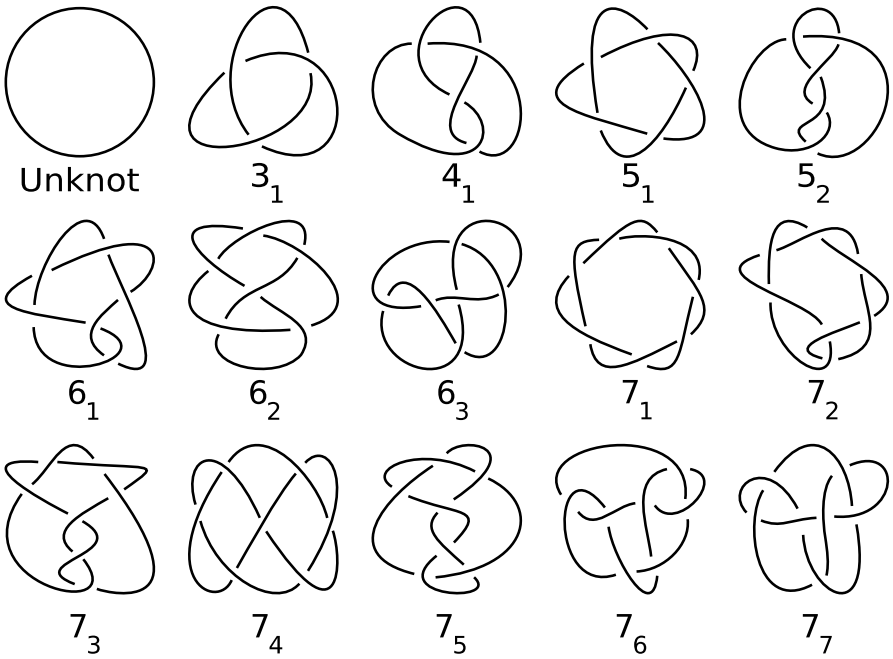

Figure 1.4: Planar diagrams of prime knots up to 7 crossings. Source: Wikipedia

A knot is a smooth embedding of a circle into a three-dimensional space; if several knots are tied together they form a link. Knots and links play an important role in theoretical high energy physics; this direction started from the groundbreaking paper by Edward Witten [28] who showed that quantum knot invariants arise from the Chern-Simons theory on a three-sphere S^3. We are interested in the knots-quivers correspondence, which relates the gauge theoretic invariants of

a knot to the representation theory of a quiver $Q[K]$ depending on a knot. Therefore, Nahm sums, quivers and knots share a common physical background which we discuss in this section.

Figure 1.4 shows planar diagrams of prime knots up to 7 crossings, labeled with Alexander–Briggs notation. The notation organizes knots by their crossing number: one writes the crossing number in a subscript to denote its order amongst all knots with that crossing number. The simplest ones are torus knots, which can be drawn on a surface of a two-dimensional torus (figure 1.5). They are characterized by a pair of integers (p, q), counting how many times the knot winds around a meridian and longitude cycles, respectively. Torus knots are special from several reasons: for example, they are related to matrix models [4]. Another two kinds are hyperbolic and satellite knots. In order to study knots, it is useful to introduce their invariants, i.e.

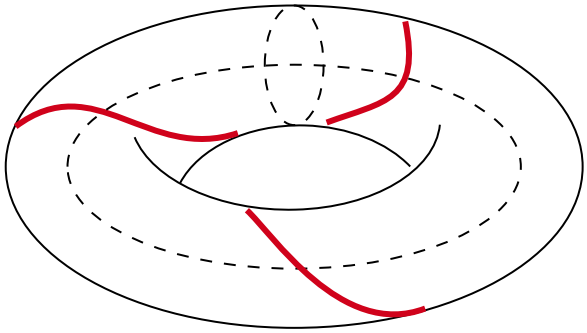

Figure 1.5: Trefoil knot is the $(2, 3)$ torus knot, also denoted as $T_{2,3}$.

quantities which are unchanged under smooth deformations of a knot. In practice polynomial invariants, although not being able to distinguish all possible knots, turn out to be efficient tools to work with, and, most importantly, connect knots to high energy physics.

1.3.1 Quantum knot polynomials via Chern-Simons theory

A gauge theory in 3 dimensions depends on a compact Lie group G. The fields are connections of the form

$$A = A_1(\xi)\, d\xi^1 + A_2(\xi)\, d\xi^2 + A_3(\xi)\, d\xi^3, \tag{1.32}$$

where $A_i(\xi)$ denote the elements of the Lie algebra of G.

Chern-Simons theory is the topological quantum field theory, meaning that its observables are invariant under continuous deformations of the underlying three-dimensional manifold. The theory is fixed by a choice of a 3-manifold M, a compact gauge group G, a gauge field A and a constant $k \in \mathbb{Z}$ (the "level"), which plays the role of a coupling constant. Its action is defined as

$$S_{\text{CS}} = \frac{k}{4\pi} \int_M \text{Tr}\left(A \wedge dA + \frac{2}{3} A \wedge A \wedge A\right) \tag{1.33}$$

The partition function is a Feynman path integral over the space of connections on M:

$$Z_{\text{CS}} = \int e^{iS_{\text{CS}}}\, \mathcal{D}A \tag{1.34}$$

Following Witten [28], let K be a knot or a link in M. For a given gauge field A, consider the

parallel transport (holonomy) around K which defines an element of the Lie group G. To define observables, imagine that we have a charged particle moving in a loop in M. Fix a representation R of G and define the *Wilson loop*:

$$W_R(K) = \mathrm{Tr}_R(P \exp \oint_K A) \tag{1.35}$$

Remarkably, its expectation value turns out to be a topological invariant of K in M, called a *quantum knot invariant*:

$$\langle W_R(K) \rangle = \int e^{iS_{\mathrm{CS}}} W_K(A)\, \mathcal{D}A \tag{1.36}$$

Choosing $G = U(N)$ and expressing the above formula in terms of

$$q = \exp\left(\frac{i\pi}{k+N}\right), \quad a = \exp\left(\frac{i\pi N}{k+N}\right), \tag{1.37}$$

we obtain the (unreduced) HOMFLY-PT polynomial $\overline{\mathcal{P}}_R^K(a,q)$ colored by R. Note that the expectation value (1.36) also depends on a framing, which is characterized by an integer f [19]. The framing affects the tangent "ribbon" to a knot by twisting it f times, so that $f = 0$ is the canonical choice which corresponds to the absence of such twists. The polynomials $\overline{\mathcal{P}}_R^K(a,q)$ are computed in the canonical framing, but could be easily framed by the formula

$$\overline{\mathcal{P}}_R^K(a,q) \quad \mapsto \quad a^{l(R)f} q^{\kappa(R)f}\, \overline{\mathcal{P}}_R^K(a,q), \tag{1.38}$$

where $l(R)$ is the total number of boxes in a Young diagram corresponding to R, and $\kappa(R) = l(R) + \sum_{j \in \mathrm{rows}(R)} (|j|^2 - 2j|j|)$.

We are interested in symmetric $(r+1)$-dimensional representations, labelled by a ribbon-like Young diagram $\lambda = S^r$:

$$S^r \quad = \quad \underbrace{\square\square\square\square\square}_{r \text{ boxes}} \tag{1.39}$$

and we simply use the label r instead of S^r. E.g. $r = 1$ corresponds to the fundamental representation.

Note that uncolored ($r = 1$) HOMFLY-PT polynomials were first defined via skein relations for the planar diagram of a knot. They also allow to compute them by hand for a few simple knots. For example, $\overline{\mathcal{P}}_1(a,q)$ can be defined by the initial condition for the unknot:

$$\overline{\mathcal{P}}_1^{0_1}(a,q) = \frac{a - a^{-1}}{q - q^{-1}}, \tag{1.40}$$

and for more complicated knots

$$a\overline{\mathcal{P}}_1^{L_+}(a,q) - a^{-1}\overline{\mathcal{P}}_1^{L_-}(a,q) = (q - q^{-1})\overline{\mathcal{P}}_1^{L_{0_1}}(a,q), \tag{1.41}$$

where $L_+, L_-, L_\circ$ correspond to the three types of crossings in figure 1.6. For the trefoil knot 3_1 we get

$$\overline{\mathcal{P}}_1^{3_1}(a,q) = \left(\frac{a^2}{q^2} + a^2q^2 - a^4\right) \overline{\mathcal{P}}_1^{0_1}(a,q). \tag{1.42}$$

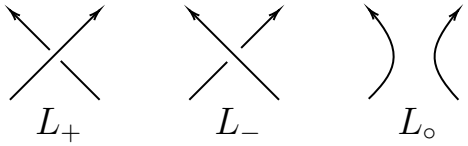

Figure 1.6: The three types of crossings on the plane

For us it is convenient to consider the reduced normalization for HOMFLY-PT polynomials which we denote as $\mathcal{P}_r(a,q)$, obtained after dividing by the unknot value, for example

$$\begin{aligned} \mathcal{P}_1^{0_1}(a,q) &= 1, \\ \mathcal{P}_1^{3_1}(a,q) &= \frac{a^2}{q^2} + a^2q^2 - a^4, \end{aligned} \tag{1.43}$$

and similarly for other knots. Therefore, for a given knot K one can associate the sequence of the reduced S^r-colored HOMFLY-PT polynomials:

$$\mathcal{P}_1^K(a,q),\ \mathcal{P}_2^K(a,q),\ \mathcal{P}_3^K(a,q),\ \ldots \tag{1.44}$$

(the index K will be often dropped, when fixed by the context). To finish this exposition, let us say that $a = q^r$ specialization for HOMFLY-PT polynomials gives quantum $\mathfrak{sl}_r$ invariants, in particular $r = 2$ corresponds to the Jones polynomial $J(q)$ [84].

1.3.2 HOMFLY-PT homologies

It has been conjectured and verified in numerous examples that quantum polynomials for a knot can be lifted to more powerful invariants called knot homologies. The procedure is called *categorification*. The inverse identification is based on the fact that such polynomials are Poincaré polynomials for the corresponding homology theory. Moreover, such homology theories conjecturally correspond to the algebras of BPS states for some gauge theories arising in 3d-3d correspondence. The pioneering paper on knot homologies by M. Khovanov [85] categorifies the Jones polynomial of a knot. Khovanov's construction is purely combinatorial, but the advantages are its well-definiteness and computability (e.g., the corresponding module is implemented in Mathematica package `Knot theory`). It opened many doors to physicists, and a new type of homology theory was soon conjectured for the uncolored HOMFLY-PT polynomial of a knot [86]. The next step was the precise construction of Khovanov-Rozansky homology [87, 88], which corresponds to $SL(N)$ invariants at arbitrary N. Lastly, but most importantly for us, entered the colored HOMFLY-PT homology [89] and its quadruply-graded version [90].

HOMFLY-PT homologies are generated by abelian groups $\mathcal{H}^R_{ijk}(K)$. We will deal with the reduced homology, corresponding to the reduced HOMFLY-PT polynomials. Denote the set of generators of the S^r-colored homology as

$$\mathscr{G}_r(K) = \{\mathcal{H}^{S^r}_{ijk}(K)\}. \tag{1.45}$$

Categorification then replaces the sequence (1.44) by its homological version:

$$\mathscr{G}_1(K),\ \mathscr{G}_2(K),\ \mathscr{G}_3(K),\ \ldots \tag{1.46}$$

Going from top to bottom, we can define colored superpolynomials, which generalize the colored HOMFLY-PT polynomials:

$$\mathcal{P}_r(a,q,t) = \sum_{i,j,k} a^i q^j t^k \dim \mathcal{H}^{S^r}_{ijk}(K) \equiv \sum_{i \in \mathscr{G}_r(K)} a^{a_i^{(r)}} q^{q_i^{(r)}} t^{t_i^{(r)}}. \tag{1.47}$$

Here the variables a and q are the same as in the HOMFLY-PT case (1.37), t is the Poincaré parameter, and we denote homological degrees of the generator $i \in \mathscr{G}_r(K)$ as triples $(a_i^{(r)}, q_i^{(r)}, t_i^{(r)})$. For $r = 1$ we will omit the upper indices and write $(a_i, q_i, t_i) \equiv (a_i^{(1)}, q_i^{(1)}, t_i^{(1)})$. If $t_i - a_i - q_i/2$ is constant for each $i \in \mathscr{G}_1(K)$ for some knot, such knot is called homologically thin [86] (all knots we consider in this thesis are homologically thin).

We can present the S^r-colored HOMFLY-PT homology as a diagram, so that every generator $i \in \mathscr{G}_r(K)$ is drawn as a dot with coordinates $(q_i^{(r)}, a_i^{(r)})$, sometimes decorated by $t_i^{(r)}$. Moreover, there are differentials (represented by arrows) acting on the homology. Their structure implies that all generators are aligned into two types of patterns – a zig-zag (consistsing of an odd number of generators) and a diamond (consisting of four generators). For example, homological diagrams for $(2, 2p+1)$ torus knots consist of only one zig-zag made of $2p+1$ generators.

Example 1.3.1. Consider the trefoil knot $T_{2,3}$. Its reduced, uncolored HOMFLY-PT homology

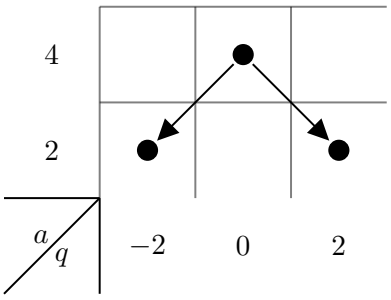

Figure 1.7: Reduced HOMFLY-PT homology of the trefoil knot consists of three generators and a pair of differentials.

can be read-off from the (uncolored) superpolynomial:

$$\mathcal{P}_1^{3_1}(a,q,t) = \frac{a^2}{q^2} t^0 + a^2 q^2 t^2 - a^4 q^0 t^3, \tag{1.48}$$

There are three monomials, each corresponding to a black dot in figure 1.3.1. The dots are drawn in the (a,q) plane encoding the degrees of the corresponding generators. Additionally, there is the t-grading (homological grading) which assigns an integer to each dot. The arrows are homology differentials, which can be guessed from some properties such as reflection symmetry $q \leftrightarrow \frac{1}{q}$ [91].

For $t = -1$ colored superpolynomials reduce to colored HOMFLY-PT polynomials that take

form of the Euler characteristic

$$\mathcal{P}_r(a,q) = \mathcal{P}_r(a,q,-1) = \sum_{i,j,k} a^i q^j (-1)^k \dim \mathcal{H}^{S^r}_{ijk}(K). \tag{1.49}$$

We stress that by $P_r(a,q,t)$ and $P_r(a,q)$ we denote reduced polynomials (equal to 1 for the unknot). We also consider generating functions of colored superpolynomials and colored HOMFLY-PT polynomials defined by

$$\mathcal{P}_K(x,a,q,t) = \sum_{r=0}^{\infty} \frac{x^r}{(q^2;q^2)_r} \mathcal{P}_r(a,q,t), \qquad \mathcal{P}_K(x,a,q) = \sum_{r=0}^{\infty} \frac{x^r}{(q^2;q^2)_r} \mathcal{P}_r(a,q). \tag{1.50}$$

Including q-Pochhammer symbols $(q^2;q^2)_r = \prod_{i=1}^{r}(1-q^{2i})$ in denominators provides a proper normalization as defined in [21, 22].

1.3.3 The statement of the knots-quivers correspondence

The knots-quivers correspondence begins from the observation that generating series of colored HOMFLY-PT polynomials (1.50) can be written in the form of a Nahm sum (1.29) for appropriate specialization of generating parameters x_i and a choice of the matrix C depending on a knot. Shown in various examples in [21], for two-bridge knots in [23], and for arborescent knots in [26], the knots-quivers correspondence has several important consequences. One such consequence is that Ooguri-Vafa invariants of a knot [40] obtain an interpretation in terms of motivic Donaldson-Thomas invariants for a symmetric quiver and are therefore integer numbers (recall the formula (1.31)), as has been conjectured before. On the other hand, the form (1.29) for colored superpolynomials for a knot implies that all of them are encoded in a finite data: the matrix C and additional parameters in the specialization of x_i. We are now ready to formulate the knots-quivers correspondence.

Definition 1.3.1. *We say that the symmetric quiver Q corresponds to the knot K if the generating function for superpolynomials (in reduced or unreduced normalization) takes form of the Nahm sum for Q:*

$$P_Q(\boldsymbol{x},q)|_{(-q)^{C_{ii}} x_i = x a^{a_i} q^{q_i} t^{t_i}} = \mathcal{P}_K(x,a,q,t). \tag{1.51}$$

The substitution $(-q)^{C_{ii}} x_i = x a^{a_i} q^{q_i} t^{t_i}$ is called the knots-quivers change of variables. Note that the quiver matrix for the unreduced case can be obtained by doubling the reduced quiver matrix and adding some additional arrows [21], which follows from

$$\overline{\mathcal{P}}_r(a,q) = a^{-r} q^r \frac{(a^2;q^2)_r}{(q^2;q^2)_r} \mathcal{P}_r(a,q) \tag{1.52}$$

where the factor in front of $\mathcal{P}_r(a,q)$ is the full r-colored HOMFLY-PT polynomial for an unknot. In this thesis, however, we will mostly focus on the reduced case. Denoting $a^{a_i} q^{q_i - C_{ii}} (-t)^{C_{ii}}$ as λ_i, we can write it shortly as

$$x_i = x\lambda_i \qquad \text{or} \qquad \boldsymbol{x} = x\boldsymbol{\lambda}. \tag{1.53}$$

The above correspondence can be also translated to the level of HOMFLY-PT polynomials,

simply by putting $t = -1$ in the knots-quivers change of variables.

Example 1.3.2. The generating series of the colored HOMFLY-PT polynomials for the f-framed unknot in the reduced normalization is

$$\sum_{r=0}^{\infty} x^r \frac{q^{f(r^2-r)}}{(q^2;q^2)_r}, \tag{1.54}$$

which means that the corresponding quiver is just one vertex with f loops, i.e. $C^{0_1} = [\, f \,]$.

Example 1.3.3. For the trefoil knot in framing $f = 0$, the generating function in the reduced normalization takes form

$$\sum_{r=0}^{\infty} \frac{\mathcal{P}_r(a,q)}{(q^2;q^2)_r} x^r = \sum_{d_1,d_2,d_3 \geq 0} \frac{q^{\sum_{i,j} C^{T_{2,3}}_{i,j} d_i d_j - 2d_1 - 3d_3} (-1)^{d_3} a^{2d_1+2d_2+4d_3}}{(q^2;q^2)_{d_1} (q^2;q^2)_{d_2} (q^2;q^2)_{d_3}} x^{d_1+d_2+d_3}, \tag{1.55}$$

where

$$C^{T_{2,3}} = \begin{bmatrix} 0 & 1 & 1 \\ 1 & 2 & 2 \\ 1 & 2 & 3 \end{bmatrix}. \tag{1.56}$$

The knots-quivers specialization in this case reads

$$\lambda = (a^2 q^{-2}, a^2, a^4 q^{-3} t). \tag{1.57}$$

Notice that $t = -1$ in the formula (1.55), which is the proper specialization to the HOMFLY-PT polynomials. In principle, one can keep t to obtain the generating series for colored superpolynomials.

1.3.4 String theory interpretation

It is known that Chern-Simons theory admits a string theory interpretation via a chain of dualities (a nice exposition is presented in [4]). As a consequence, invariants of knots and links from expectation values of Wilson loops obtain a "stringy" description. We need a particular kind of strings, namely topological strings (both open and closed), whose topological invariance comes from the so-called topological twist. The strings are compactified inside a Calabi-Yau threefold X (six real dimensions). There are two kinds of topological string theories considered in this thesis, which give rise to mirror symmetry between Calabi-Yau's X and $\tilde{X}$ [92, 93, 94], meaning that their correlation functions coincide:

1. **The A-model** defined on $X = T^*M$ for some three (real) dimensional manifold M. Additionally, there are N topological D-branes wrapping M. In the case of open topological strings it is dual to the Chern-Simons theory on M, where N is the size of the gauge group [95].

2. **The B-model** on a mirror Calabi-Yau threefold $\tilde{X}$ (relative to X) is defined by a spectral curve with a singularity, such that its resolution gives the defining equation for $\tilde{X}$. Such a curve does often correspond to an explicit matrix model [96].

Here we are focusing on the A-model (the B-model will appear next in relation to the topological recursion) and take $M = S^3$. As already noted, the Chern-Simons theory on S^3 is a topological open string theory on T^*S^3. Remarkably, T^*S^3 can be viewed as one of the two resolutions for the singular conifold (figure 1.8). In the neighbourhood of its singular point, the singular conifold looks like a cone with the base $S^3 \times S^2$. We can stretch the singularity in either S^2 or S^3 direction, to obtain the two different Calabi-Yau three-folds. The one in the bottom-right of figure 1.8 is called the resolved conifold, and the transition between the two resolutions is called the geometric transition. This corresponds to the *large N duality*, which is also the open/closed string duality [38].

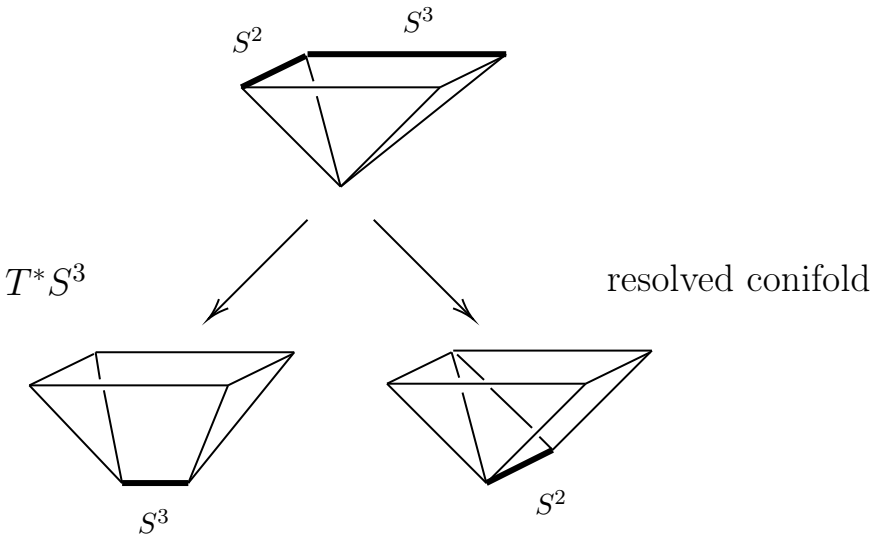

Figure 1.8: The two resolutions of the conifold singularity.

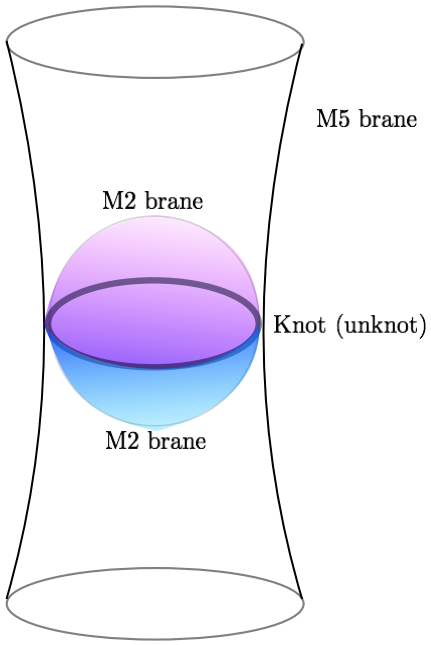

Figure 1.9: A knot (unknot) inside the resolved conifold.

One may ask the question: is it possible to provide an M-theory interpretation for the knots-

quivers correspondence? The answer hides in the Ooguri-Vafa setup, where there is an ambient manifold (spacetime) and certain types of branes arising as a solution to the equations of motion of 10-dimensional supergravity [40]:

Spacetime	Resolved conifold	$\times$	$\mathbb{R}^{1,4}$
M5 brane	Lagrangian submanifold L_K	$\times$	$\mathbb{R}^{1,2}$

(1.58)

A knot K (the unknot in figure 1.9) sits inside the resolved conifold. The knot conormal consists of planes orthogonal to tangent planes of the knot tubular neighbourhood. We can define the Lagrangian submanifold L_K as the M5 brane wrapping around the conormal of K. Additionally, there is an M2 brane which wraps holomorphic disks with the boundary on L_K; see, for example, [97] for the explicit description of these kinds of branes. For the unknot there are two basic holomorphic curves (basic disks, since they do not have handles, i.e. are homeomorphic to a hemisphere). The generating series of unreduced HOMFLY-PT polynomials has the following interpretation: *it counts M2-branes wrapping holomorphic curves with boundary on an M5-brane wrapping the knot conormal* [24]. Therefore, there should be a two-vertex quiver such that its Nahm sum coincides with the generating series for the unreduced colored HOMFLY-PT polynomials for the unknot. Such quiver is shown in figure 1.10. (the self-linking nubmer C_{22}

Figure 1.10: The two-vertex quiver for the unknot in the resolved conifold.

turns out to be non-zero, as shown in [24]). A similar picture is conjectured for any knot, given the following identifications:

- quiver nodes $\sim$ basic disks
- $C_{ij} \sim$ the linking number between the two basic disks

Moreover, in [24] the existence of low energy theory $T[L_K] \equiv T[Q]$ was proposed, which is a 3d $\mathcal{N} = 2$ theory of Chern-Simons type, such that its partition function coincides with the Nahm sum for the quiver $Q = Q[K]$, as predicted by the 3d-3d correspondence [34]. The BPS spectrum for such theory agrees with the motivic Donaldson-Thomas invariants for a symmetric quiver. The quiver nodes correspond to "basic" BPS states, while arrows encode their interactions and create the bound states, encoded in the infinite product form (1.31). To summarize, we have the following diagram which relates knots, topological strings, quivers and gauge theories:

$$\begin{array}{ccc} \text{knot } K & \longleftrightarrow & \text{quiver } Q \\ \updownarrow & & \updownarrow \\ \text{M5 brane wrapping } L_K \text{ inside } X & \longleftrightarrow & \text{3d } \mathcal{N}=2 \text{ theory } T[Q] \equiv T[L_K] \end{array} \tag{1.59}$$

1.4 Nahm equations and quiver A-polynomials

Another interesting invariant for a knot is the A-polynomial, arising as the eigenvalue locus for a representation $\pi_1(S^3 \setminus K) \mapsto SL(2,\mathbb{C})$, where $\pi_1(S^3 \setminus K)$ is the fundamental group of the knot complement [46]. Denoted as $A_K(l,m)$, this polynomial is parametrized by a pair of coordinates (l,m) – the longitude and meridian along the torus boundary of a knot complement. The A-polynomial is interesting for many reasons, particularly because it defines a Lagrangian submanifold in the Chern-Simons theory and therefore can be meaningfully quantized [47, 48]. Besides, quantum A-polynomial annihilates colored HOMFLY-PT polynomials, therefore can be considered within the dualities (1.59). Our goal is to define a similar object, but for an arbitrary symmetric quiver, not necessarily related to a knot, which we would call quiver A-polynomial $A_Q(x_1,\ldots,x_m)$, where m is the quiver size [24, 58]. It turns out that it is quantizable as well, but the explicit form of quantum A-polynomial is usually hard to find.

We proceed to the semi-classical approximation of the series (1.29):

$$P_C(x_1,\ldots,x_n) \simeq \int \frac{dz_1\cdots dz_m}{\bar{z}_1\cdots\bar{z}_m} \exp\Big(\frac{1}{\hbar}S_0 + S_1 + \hbar S_2 + \ldots\Big), \tag{1.60}$$

where $\hbar = \log q$, $S_k = S_k(x_1,\ldots,x_m,\bar{z}_1,\ldots,\bar{z}_m)$ and $\bar{z}_i = e^{\hbar d_i}$. The leading term is

$$S_0(x,\overline{z}) = \frac{1}{2}\sum_{i,j=1}^{m} C_{i,j}\log\overline{z}_i\log\overline{z}_j + \sum_{i=1}^{m}\left(\log\overline{z}_i\log(-1)^{c_{ii}}x_i + \mathrm{Li}_2(\overline{z}_i) - \frac{\pi^2}{6}\right). \tag{1.61}$$

In $\hbar \to 0$ limit we can evaluate integrals in (1.60) using the saddle point method, by finding stationary point of the leading term $\partial_{z_i} S_0(x,z)|_{z=\bar{z}} = 0$

$$\frac{1}{\bar{z}_i}\left(-\log(1-\bar{z}_i) + \log((-1)^{C_{ii}}x_i) + \sum_{j=1}^{m} C_{i,j}\log(\bar{z}_j)\right) = 0.$$

Taking the exponent of the right and left hand sides and multiplying by $1-\bar{z}_i$ we obtain the algebraic Nahm equations, which are somewhat similar to gluing equations of m simplices for a 3-dimensional manifold [42]:

$$\boxed{1 - z_i = (-1)^{C_{ii}}x_i\prod_{j=1}^{m} z_j^{C_{ij}}, \quad i = 1\ldots m} \tag{1.62}$$

where $(z_1,\ldots,z_m)$ is a solution to the saddle point equations

$$\frac{\partial}{\partial z_i} S_0(x_1,\ldots,x_m,\bar{z}_1,\ldots,\bar{z}_m) = 0. \tag{1.63}$$

We also introduce

$$y(x_1,\ldots,x_m) = e^{\sum_{i=1}^{m}\partial_{x_i}S_0(x,z)} = \prod_{i=1}^{m} y_i(x_1,\ldots,x_m) = \prod_{i=1}^{m} z_i. \tag{1.64}$$

1.4.1 Classical quiver A-polynomial

We can eliminate the variables z_i from the Nahm equations (1.62) to obtain a single polynomial, which we call *quiver A-polynomial* and denote as $A_C(x_1, \dots, x_m, y)$. Note that it defines a Lagrangian submanifold in the symplectic space with coordinates

$$(x_1, \dots, x_m, z_1, \dots, z_m) \in (\mathbb{C}^*)^m \times (\mathbb{C}^*)^m \tag{1.65}$$

and the symplectic form $\omega = \sum \frac{dx_i}{x_i} \wedge \frac{dy_i}{y_i}$. We can also take its principal specialization, which is a two-variable polynomial $A(a_1 x, \dots, a_m x, y)$ where a_i are complex numbers.

Example 1.4.1. Recall the polylogarithm function

$$\mathrm{Li}_m(z) := \sum_{n=1}^{\infty} \frac{z^n}{n^m}, \quad |z| < 1, \quad m = 1, 2, \dots, \tag{1.66}$$

which satisfy

$$\frac{d}{dz} \mathrm{Li}_m(z) = \frac{1}{z} \mathrm{Li}_{m-1}(z), \quad \mathrm{Li}_1(z) = -\log(1-z). \tag{1.67}$$

In the case of a quiver with one vertex and no loops we have

$$P_{[1]}(x) = \sum_{d \geq 0} \frac{x^d}{(q;q)_d} \tag{1.68}$$

Using $x^d = \exp\left(d \log(x)\right) = \exp\left(\frac{1}{\hbar} \log(z) \log(x)\right)$ and rewriting the leading term in the expansion

$$(q;q)_d \simeq \gamma \exp\left(\frac{1}{\hbar}\left(-\mathrm{Li}_2(z) + \frac{\pi^2}{6}\right) + \dots\right), \tag{1.69}$$

we get

$$S_0(x,z) = \mathrm{Li}_2(z) - \frac{\pi^2}{6} + \log(z)\log(x). \tag{1.70}$$

The saddle-point equation (1.63) takes form

$$z\frac{\partial}{\partial z} S_0(x,z) = -\log(1-z) + \log(x) = 0, \tag{1.71}$$

and after exponentiation it gives the Nahm equation for 1-vertex quiver without loops:

$$1 - z = x \tag{1.72}$$

If we set the number of loops to f, the Nahm sum takes form

$$P_{[f]}(x) = \sum_{d \geq 0} \frac{(-q^{1/2})^{fd^2} x^d}{(q;q)_d}, \tag{1.73}$$

resulting in two extra summands from $(-q^{1/2})^{fd^2}$ in $S_0(x,z)$: $\frac{f}{2}(\log(z))^2 + i\pi f \log(z)$. We

therefore obtain classical quiver A-polynomial for a one vertex quiver with f loops

$$A_{[f]}(x,y) = 1 - y - (-1)^f xy^f. \tag{1.74}$$

1.4.2 Quantum quiver A-polynomial

Since classical quiver A-polynomial for an m-vertiex quiver can be thought of as a Lagrangian in the symplectic space of dimension $2m$, it is natural to ask whether it is quantizable. The existence of quantum quiver A-polynomials is also predicted by the knots-quivers correspondence: it is known that quantum knot A-polynomials are quantizable [47] and can be also lifted to their t-deformed (homological) versions [48, 50, 51]. After a suitable change of variables, they annihilate the generating series for colored superpolynomials [98]. This, in principle, should extend to an arbitrary symmetric quiver, not necessarily related to a knot. Besides, the product form (1.31) encodes the motivic Donaldson-Thomas invaraints of a quiver and conjecturally corresponds to BPS invariants in the Ooguri-Vafa brane system considered in section 1.3.4. For example, such brane systems and their quiver descriptions include knots [21, 22, 23, 26, 24, 25] and strip geometries for topological strings [99]. It is natural to expect that for any symmetric quiver there is a brane system, which also implies that Nahm sums encode all information about such system. Therefore these invariants should be also recovered from a quantum quiver A-polynomial, and it must be well-defined, meaning that classical quiver A-polynomials must be quantizable. We discuss it more formally in the next chapter; here we show how the classical Nahm equations can be quantized, which leads to one definition of quantum quiver A-polynomial.

One can show [25, 58] that the promotion of z_i to operators $\hat{z}_i$ acting on x_j as $\hat{z}_i x_j = q^{\delta_{i,j}} x_j$ leads to the quantized version of the Nahm equations (1.62):

$$(1 - \hat{z}_i)\, P_C = \left((-1)^{C_{i,i}} x_i \prod_{j=1}^{m} \hat{z}_j^{C_{i,j}} \right) P_C\,. \tag{1.75}$$

To see this explicitly, we shift one index $d_k \mapsto d_k + 1$ in $P_{d_1,\ldots,d_m}$ (1.30), so that

$$P_{d_1,\ldots,d_k+1,\ldots,d_m} = \frac{(-q^{1/2})^{\sum_{i,j=1}^m C_{ij}(d_i+\delta_{ik})(d_j+\delta_{jk})}}{(q;q)_{d_1}\cdots(q;q)_{d_k+1}\cdots(q;q)_{d_m}} = \frac{(-q^{1/2})^{C_{kk}+2\sum_i^m C_{ki}d_i}}{1-q^{d_k+1}} P_{d_1,\ldots,d_m}\,, \tag{1.76}$$

which implies

$$\sum_{d_1,\ldots,d_m\geq 0} P_{d_1,\ldots,d_k+1,\ldots,d_m} \prod_{i=1}^{m} x_i^{d_i+\delta_{ki}} = \left[(1-\hat{z}_k)^{-1} (-q^{1/2})^{C_{kk}} \hat{x}_k \prod_{j=1}^{m} \hat{z}_j^{C_{kj}} \right] \cdot P_C(x_1,\ldots,x_m)\,, \tag{1.77}$$

and multiplying both sides by $(1-\hat{z}_k)$ leads to the equations (1.75). Much like in the classical case, we can reduce the quantum Nahm equations (1.75) to a single non-commutative polynomial, to which we refer as a *quantum quiver A-polynomial*. It is done by the non-commutative elimination from (1.75) with respect to $\hat{z}_1,\ldots,\hat{z}_m$:

$$\hat{A}_C(x_1,\ldots,x_m,\hat{y})P_C = 0, \qquad \hat{y} := \hat{z}_1\ldots\hat{z}_m. \tag{1.78}$$

Example 1.4.2. As an example consider the "uniform" quiver which is parametrized by a constant $f \geq 0$,

$$C = \begin{pmatrix} f & f & \dots & f \\ f & f & \dots & f \\ \vdots & \vdots & \ddots & \vdots \\ f & f & \dots & f \end{pmatrix}_{m\times m} \tag{1.79}$$

and whose quantum Nahm equations take form

$$\hat{z}_k P_C(x_1,\dots,x_m) = \left(1 - x_k(-q^{1/2}\hat{y})^f\right) P_C(x_1,\dots,x_m), \quad k = 1,\dots,m. \tag{1.80}$$

By eliminating $\hat{z}_k$ from the above equations, we obtain quantum quiver A-polynomial

$$\hat{A}_C(x_1,\dots,x_m,\hat{y}) = \prod_{k=1}^{m} \left(1 - x_k(-q^{1/2}\hat{y})^f\right) - \hat{y} \tag{1.81}$$

$$= \sum_{k=0}^{m} (-1)^{k(f+1)} q^{k^2 f/2} E_k(x_1,\dots,x_m)\hat{y}^{kf} - \hat{y} \tag{1.82}$$

where $E_k(x_1,\dots,x_m)$ are the elementary symmetric polynomials. Taking the semi-classical limit, we obtain

$$A_C(x_1,\dots,x_m,y) = \prod_{k=1}^{m} \left(1 - x_k(-y)^f\right) - y \tag{1.83}$$

By setting $x_i = x$, we obtain a two-variable polynomial whose locus of zeroes defines a genus zero curve

$$(1-(-1)^f x y^f)^m - y = 0, \qquad x(t) = \frac{1-t}{(-t^m)^f},\ y(t) = t^m. \tag{1.84}$$

1.4.3 Quiver A-polynomial and topological string B-model

In section 1.3.4 we have mentioned a duality between topological gauge theory and (open) topological strings, which involves Nahm sums for symmetric quivers.

- Topological gauge theory (Chern-Simons theory on a real 3-manifold M): computes quantum (gauge theoretic) invariants of M, in particular knot invariants when $M = S^3 \setminus K$.
- Topological string theory: counts various kinds of branes wrapping around objects in complex Calabi-Yau threefolds, such as the resolved conifold.

The Nahm sum for a quiver corresponding to a knot, generates colored HOMFLY-PT polynomials and at the same time can be interpreted as the A-model. Since the brane configuration is quite complicated (and involves the geometry of the knot conormal), we expect that the B-model is non-trivial and should capture a very interesting information. Moreover, we conjecture that it exists for every symmetric quiver, not necessarily related to a knot. The main ingredient for a B-model is the spectral curve, whose resolution gives an equation for the mirror Calabi-Yau (possibly with some brane configuration). In various theories there are different kinds of spectral curves:

- In $\mathcal{N} = 2$ supersymmetric gauge theory the complex curve is the Seiberg-Witten curve, and is related to the Ω-deformation [100, 101].
- In $SL(2, \mathbb{C})$ Chern-Simons theory with a Wilson loop, $A(x, y)$ is the knot A-polynomial. The parameter $\hbar$ is the coupling constant of Chern-Simons theory [46, 47].
- In matrix models, the B-model curve is the matrix model spectral curve, and $\hbar = 1/N$ controls the expansion in the inverse of matrix size [102].
- In topological string theory every curve $H(e^u, e^v)$ defines a (non-compact) Calabi-Yau threefold geometry [103, 4, 104], namely a hypersurface in $(\mathbb{C}^*)^2 \times \mathbb{C}$.

Topological recursion associates certain invariants to a spectral curve [3, 5, 105, 106]. These invariants can be then reinterpreted as open topological string invariants in the A-model, as stated in the remodelling conjecture [107], proved for smooth toric Calabi-Yau threefolds [108] and for orbifolds [109]. Therefore, the topological recursion builds the bridge between the two models. This motivates us to make the following consideration for an arbitrary symmetric quiver:

quiver A-polynomial $\equiv$ B-model spectral curve

Example 1.4.3. The simplest non-compact Calabi-Yau threefold is $\mathbb{C}^3$, also called the topological vertex [48] and is our A-model in this example. The related B-model spectral curve is given by

$$H(x, y) = 1 + y + xy^f. \tag{1.85}$$

It coincides with the quiver A-polynomial (1.74) after a change of sign of y. It also encodes the HOMFLY-PT polynomials for the framed unknot in the unreduced normalization [21].

Example 1.4.4. The second example is the ordinary conifold in framing $f = 2$ [48, 99]. Its B-model curve is

$$H(x, y) = 1 + y + xy^2 + Qxy \tag{1.86}$$

where $Q \in \mathbb{C}$ is the complex moduli called the Kahler parameter (the limit $Q \to 0$ shrinks the geometry to a single topological vertex in the same framing). The corresponding quiver encodes the HOMFLY-PT polynomials for the unknot in framing $f = 2$ and the unreduced normalization (see also section 1.3.4):

$$C = \begin{bmatrix} 2 & 1 \\ 1 & 1 \end{bmatrix}. \tag{1.87}$$

Chapter 2

Quantization of quiver A-polynomials

The aim of this chapter is to investigate whether quiver A-polynomials are quantizable by means of the K-theoretic condition stated in [48]. This check is independent from the existence of quantum Nahm equations from section 1.4.2, and serves as a preliminary step before the topological recursion calculation done in the next chapter. If this step fails, it is unlikely that topological recursion would give a meaningful answer, since the quantum theory will be ill-defined and there would be no proper physical description of quantum quiver A-polynomial. The quantization condition requires the only knowledge of a classical A-polynomial, and the condition states that it is quantizable if and only if its face polynomials (obtained from the faces of the Newton polytope) are all cyclotomic. If the answer is positive, it would be possible that quantum quiver A-polynomial can be recovered (independently from the quantization steps in section 1.4.2) from the classical quiver A-polynomial by means of topological recursion. We use the machinery of initial forms and mixed polyhedral decompositions to investigate the edges of the Newton polytope, and find that the face polynomials obey a remarkable combinatorial pattern. The result of this chapter are presented in [59].

2.1 Quantization problem in general

In classical mechanics the phase space of a physical system is a symplectic manifold (M, σ) of dimension $2m$, equipped with a closed non-degenerate 2-form ω, called symplectic. For example, in Newtonian mechanics $M = T^*\mathbb{R}^3$, where $\mathbb{R}^3$ is a configuration space. For our purpose we take M to be an open manifold with a complex structure. Using the local coordinates (the generalized positions and momenta), one can write

$$\omega = \sum_{i=1}^{m} dp_i \wedge dq_i \tag{2.1}$$

Another important object is the Liouville form θ, which exterior derivative gives the symplectic form:

$$d\theta = \omega \tag{2.2}$$

In local coordinates

$$\theta = \sum_{i=1}^{m} p_i dq_i \tag{2.3}$$

Recall that a submanifold L of (M, σ) is called Lagrangian if the two conditions are satisfied: $\dim L = m$, and $\omega|_L = 0$. The cohomology class in the first homology group $H^1(L, \mathbb{R})$ induced by the 1-form θ is called the Liouville class of L. It is trivial if all periods of $\theta|_L$ vanish.

We want to quantize our physical system, i.e. to replace the classical phase space by a Hilbert space $\mathcal{H}$ of non-commutative operators $\hat{p}_i, \hat{q}_i$. Moreover, we require a consistent quantization of (M, ω) with a selected L, which give rise to the wave-function Z supported on L. This requires L to satisfy some conditions [47, 48], which we are going to reveal. Define a phase function (action integral) S, such that $dS = \theta|_L$. The wave-function then takes form

$$Z \simeq e^{iS/\hbar} + O(\hbar^0) \tag{2.4}$$

(for simplicity we have assumed that L has a single component, otherwise one has to sum over all such components). Therefore,

- if $\theta|_L$ is exact, S is well-defined
- if the Liouville class of L is non-trivial, S depends on the choice of integration path in L, and a difference between two such choices S, S' is measured by a period of θ: $S - S' = \oint \theta$

In order for the leading term in (2.4) to be well-defined, all periods of θ must be integer multiples of $2\pi\hbar$. Taking into account the complex structure of M, we split

$$\theta = \alpha\theta_\alpha + i\beta\theta_\beta \tag{2.5}$$

for some real constants α, β, where $\theta_\alpha, \theta_\beta$ are real 1-forms. Since θ is complex-valued, the necessary conditions for L to be quantizable implies two independent sets of constraints:

$$\oint_\gamma \theta_\beta = 0 \quad \text{and} \quad \frac{1}{\pi}\oint_\gamma \theta_\alpha \in \mathbb{Q}\ , \quad \text{for any closed path } \gamma \text{ in } M \tag{2.6}$$

Example 2.1.1. (See [47] for the details.) Recall knot A-polynomial, whose zero locus parameterizes the space of all representations of the fundamental group for a knot [46]. It is parametrized by two complex non-zero numbers l, m, corresponding to the longitude and meridian along the torus boundary of the knot complement. We introduce the phase space $M = \mathbb{C}^* \times \mathbb{C}^*$ with coordinates $x = e^u, y = e^v,\ u, v \in \mathbb{C} \times \mathbb{C}$, and the symplectic form

$$\omega = \frac{dx}{x} \wedge \frac{dy}{y} \tag{2.7}$$

The role of Lagrangian submanifold is played by zero locus of an A-polynomial. The necessary

conditions for quantizability (2.6) are expressed in terms of x, y as follows:

$$\begin{aligned} \oint_\gamma \Big(\log|x| d(\arg y) - \log|y| d(\arg x) \Big) &= 0\,, \\ \frac{1}{\pi^2} \oint_\gamma \Big(\log|x| d\log|y| + (\arg y) d(\arg x) \Big) &\in \mathbb{Q} \end{aligned} \tag{2.8}$$

They are satisfied for all knots [46], giving a well-defined quantum operator (aka quantum curve, or non-commutative A-polynomial)

$$A(x,y) \;\rightsquigarrow\; \hat{A}(\hat{x},\hat{y}), \tag{2.9}$$

where $\hat{x}, \hat{y}$ obey the non-commutativity relation

$$\hat{y}\hat{x} = q\hat{x}\hat{y} \tag{2.10}$$

and such that

$$\lim_{q\to 1} A(\hat{x},\hat{y}) = A(x,y). \tag{2.11}$$

2.2 The K-theory criterion for quantization

2.2.1 Formulation

Suppose we have a polynomial $P(x,y)$ in two commutative variables. Its face polynomial in a single variable τ is obtained from monomials corresponding to a face (edge) of its Newton polygon. Starting from any endpoint of a face (decorating it by τ^0) and going consequently the opposite endpoint, we label each monomial by a power of τ. This gives a function $\gamma : (i,j) \mapsto k \mid x^i y^j \mapsto \tau^k$. A face polynomial is defined for every face of the Newton polygon of $P(x,y)$:

$$P|_{\text{face}}(\tau) = \sum_{(i,j)\in \text{face}} \text{coeff}_{x^i y^j} P(x,y) \cdot \tau^{\gamma(i,j)}. \tag{2.12}$$

Polynomial is called tempered if all its face polynomials are products of cyclotomic polynomials (in other words, all their roots are roots of unity). For example, $P(x,y) = x^2 - 2xy + y^2 - 2x - y + 1$ has 3 face polynomials (figure 2.1):

$$x^2 - 2x + 1 \mapsto (\tau-1)^2, \quad y^2 - y + 1 \mapsto \tau^2 - \tau + 1, \quad x^2 - 2xy + y^2 \mapsto (\tau-1)^2. \tag{2.13}$$

They are obviously cyclotomic, which means that $P(x,y)$ is tempered.

The following conjecture was stated in [48]:

Conjecture 2.2.1 (Quantization criterion)**.** *The curve in $\mathbb{C}^* \times \mathbb{C}^*$ is quantizable $\iff$ its defining polynomial is tempered.*

In [46] it was proven that A-polynomial is tempered for any knot K. Quiver A-polynomials are by far more general, and it is of our interest to investigate whether they are tempered or not which might yield interesting properties. However, we still have to fill the gap between conjecture 2.2.1 and the set of conditions (2.8).

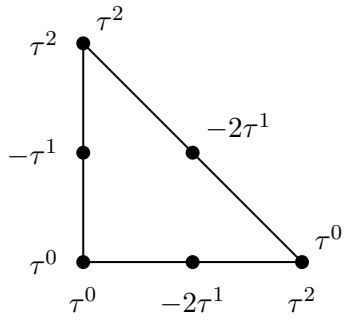

Figure 2.1: Newton polygon and face polynomials for $P(x, y)$.

2.2.2 Relation to algebraic K-theory

The exposition here is borrowed mostly from Milnor's classical book [110]. Informally speaking, the K-theory was invented to produce nice invariants of topological spaces – the so-called K-groups $\ldots, K_{-1}, K_0, K_1, K_2, \ldots$ (they are generally considered to be more powerful than (co)homology groups but harder to compute); in case of algebraic K-theory topological space is replaced by a field or a ring. Our main player is the group $K_2(F)$ of a field, which is a group of non-trivial relations satisfied by elementary matrices of any size with entries in F. Recall that elementary matrix $e_{ij}^{\lambda} \in \mathrm{GL}_n(F),\ i, j = 1 \ldots n$, differs from the identity matrix of size n by a single element λ in the (i, j)-th position, or a matrix obtained from such by elementary row/column operations. In other words, e_{ij}^{λ} generate the subgroup of elementary matrices in $\mathrm{GL}_n(F)$. They obey the commutation relations:

$$[e_{ij}^{\lambda}, e_{kl}^{\mu}] = \begin{cases} 1;\ j \neq k,\ i \neq l \\ e_{il}^{\lambda\mu};\ j = k,\ i \neq l \\ e_{kj}^{-\mu\lambda};\ j \neq k,\ i = l \end{cases} \tag{2.14}$$

One can consider an abstract group generated by the same relations, called Steinberg group $\mathrm{St}(n, F),\ n \geq 3$ (for $n < 3$ the relations degenerate):

$$\begin{aligned} x_{ij}^{\lambda} x_{ij}^{\mu} &= x_{ij}^{\lambda+\mu} \\ [x_{ij}^{\lambda}, x_{jl}^{\mu}] &= x_{il}^{\lambda\mu};\ i \neq l \\ [x_{ij}^{\lambda}, x_{kl}^{\mu}] &= 1;\ j \neq k,\ i \neq l \end{aligned} \tag{2.15}$$

There exists a homomorphism of groups:

$$\psi :\ \mathrm{St}(n, F) \to \mathrm{GL}_n(F), \quad \psi(x_{ij}^{\lambda}) = e_{ij}^{\lambda} \tag{2.16}$$

which associates an elementary matrix of size n to each element of $\mathrm{St}(n, F)$. Consider the $n \to \infty$ limit of the sequence

$$\mathrm{GL}_1(F) \subset \mathrm{GL}_2(F) \subset \mathrm{GL}_3(F) \subset \ldots, \tag{2.17}$$

where $\mathrm{GL}_i(F)$ is injected into $\mathrm{GL}_{i+1}(F)$ by the map

$$* \mapsto \begin{pmatrix} * & 0 \\ 0 & 1 \end{pmatrix}, \quad \forall * \in \mathrm{GL}_i(F) \tag{2.18}$$

This defines the group $\mathrm{GL}(F)$ as the union of all groups in the infinite sequence (2.17). Analogously, one can define $\mathrm{St}(F)$. Now we can define

$$K_2(F) := \ker \psi : \mathrm{St}(F) \to \mathrm{Id}(F), \tag{2.19}$$

where the kernel consists of those elements, which are mapped by ψ to an identity matrix in $\mathrm{GL}(F)$. For example, a 90° rotation matrix is elementary and can be written as a monomial in e_{ij}^{λ}:

$$e_{12}^1 e_{21}^{-1} e_{12}^1 = \begin{pmatrix} 0 & 1 \\ -1 & 0 \end{pmatrix} \tag{2.20}$$

Its period is equal to 4, i.e.

$$(e_{12}^1 e_{21}^{-1} e_{12}^1)^4 = \begin{pmatrix} 1 & 0 \\ 0 & 1 \end{pmatrix} \tag{2.21}$$

The relation (2.21) is non-trivial among the elementary matrices, thus producing an element in $K_2(\mathbb{R})$:

$$(x_{12}^1 x_{21}^{-1} x_{12}^1)^4 \in \ker \psi, \quad \psi\left((x_{12}^1 x_{21}^{-1} x_{12}^1)^4\right) = (e_{12}^1 e_{21}^{-1} e_{12}^1)^4 = \mathrm{Id}\,, \tag{2.22}$$

manifesting that "the relation holds". In general, such identities are of the form:

$$e_{i_1 j_1}^{\lambda_1} e_{i_2 j_2}^{\lambda_2} \dots e_{i_r j_r}^{\lambda_r} = \mathrm{Id} \quad \longleftrightarrow \quad x_{i_1 j_1}^{\lambda_1} x_{i_2 j_2}^{\lambda_2} \dots x_{i_r j_r}^{\lambda_r} \tag{2.23}$$

Following [111], we focus on the field $\mathbb{Q}(C)$ of rational functions x, y on a compact Riemann surface C. Since C is compact, there exists a minimal irreducible polynomial $P(x, y)$ which vanishes on C. E.g. if its genus is equal to 0, $x(t)$ and $y(t)$ provide a rational parametrization.

For any two elements x, y and a pair of elementary matrices

$$D_x = \begin{pmatrix} x & 0 & 0 \\ 0 & x^{-1} & 0 \\ 0 & 0 & 1 \end{pmatrix}, \quad D'_y = \begin{pmatrix} y & 0 & 0 \\ 0 & 1 & 0 \\ 0 & 0 & y^{-1} \end{pmatrix}, \tag{2.24}$$

define

$$\{x, y\} := uvu^{-1}v^{-1} \tag{2.25}$$

with $u = \psi^{-1}(D_x), v = \psi^{-1}(D'_y)$. This bracket is called the universal symbol of (x, y). The commutator evaluates to an identity matrix, therefore $\{x, y\} \in K_2(\mathbb{Q}(C))$. It turns out that for any field F, $K_2(F)$ is generated by the symbols $\{x, y\}$ [110]. The following theorem [111, 112, 48] is important for us:

Theorem 2.2.1.

$$\{x, y\}^N \in K_{2,\emptyset} \textit{ for some } N \in \mathbb{N} \Longleftrightarrow P(x, y) \textit{ is tempered} \tag{2.26}$$

where $K_{2,\emptyset}$ is the set of trivial elements in $K_2(\mathbb{Q}(C))$:

$$K_{2,\emptyset} := \bigcap_w \ker\lambda_w \quad \subset K_2(\mathbb{Q}(C)), \tag{2.27}$$

$w \in C$, and $\lambda_w : K_2 \to \mathbb{C}^*$ corresponds to the tame symbol:

$$(x,y)_w := (-1)^{w(x)w(y)} \frac{x^{w(y)}}{y^{w(x)}}\bigg|_w \tag{2.28}$$

Here $w(x)$ (or $w(y)$) equals to the degree of the leading term in $x(t)$ (or $y(t)$) around $t = w$. The tame symbol is a map $F^* \times F^* \to \mathbb{C}^*$, where $F^* := F \setminus \{0,1\}$. In fact every symbol on F, i.e. a map

$$F^* \times F^* \to A, \tag{2.29}$$

where A is any abelian group, gives rise to a unique homomorphism $K_2(F) \to A$ (proven by Matsumoto [111]). In the case of the tame symbol we simply denote this homomorphism by λ_w. Its kernel consists of all elements in $K_2(F)$, which are mapped to identity. Rephrasing, we can say that all tame symbols for any $w \in C$ are roots of unity. Comparing to the quantization conditions (2.8), we see that

$$\frac{1}{2\pi}\oint \log|x| d(\arg y) - \log|y| d(\arg x) \;=\; \log|(x,y)_p| \tag{2.30}$$

where the integral is over a small circle centered at p. This means that the quantization condition is closely related to algebraic K-theory. It turns out that the quantization criterion has many exciting implications: relation to modular forms and special values of Zeta function [111], Chern-Simons theory [48], knot theory [46], modularity properties of the Mahler measure and quantum dilogarithm [111, 112]. The proof of (2.26) is due to the fact that for each slope $\frac{p}{q}$ of $N(P)$, there is a valuation v such that $\frac{p}{q} = -\frac{v(x)}{v(y)}$. Moreover, the value of the tame symbol $(x,y)_v$ equals to the root of the corresponding face polynomial with this slope (details in [46]). In other words, by choosing (x,y), we have to evaluate tame symbols $(x,y)_w$ for each $w \in S$, where S is the set of zeroes and poles of x and y on C, and thus must be sure to get the roots of unity. It holds if and only if the polynomial $P(x,y)$ is tempered, i.e. quantizable.

Returning to the example in figure 2.1

$$P(x,y) = x^2 - 2xy + y^2 - 2x - y + 1, \tag{2.31}$$

Notice that $P(x,y)$ is not self-reciprocal, since

$$P(x^{-1},y^{-1}) \neq \pm x^p y^q P(x,y), \quad \text{for some integers } p,q \tag{2.32}$$

which means it cannot be realized as an A-polynomial for some knot [46]. The slopes are $0, \infty, -1$. The face polynomials are $(\tau-1)^2, (\tau-1)^2, \tau^2 - \tau + 1$. All of them are obviously

cyclotomic. Choose the rational parametrization, e.g.:

$$x(t) = \frac{t^2+t+1}{(t-1)^2},\ y(t) = \frac{3t^2}{(t-1)^2} \tag{2.33}$$

Now compute the tame symbols at $w \in S$ for this parametrization. In our case the set of zeroes and poles S of $x(t)$ and $y(t)$ is

$$S = \{0, 1, \zeta_3^{(1)}, \zeta_3^{(2)}\}, \tag{2.34}$$

where $\zeta_3^{(1)}, \zeta_3^{(2)}$ are two complex-conjugated cubic roots of unity. We get:

$$\text{horizontal}: (x,y)_0 = 1, \quad \text{slope "}-1\text{"}: (x,y)_1 = 1, \quad \text{vertical}: (x,y)_{\zeta_3^{(i)}} = \zeta_3^{(i)}. \tag{2.35}$$

For instance,

$$(x,y)_0 = (-1)^{0\cdot 2}\frac{x(t)^2}{y(t)^0}\Big|_{t=0} = 1, \tag{2.36}$$

since $x(t) = 1 + 3t + 6t^2 + O(t^3)$, and $y(t) = 3t^2 + O(t^3)$ around $w = 0$, this gives $w(x) = 0$ and $w(y) = 2$. As we see, each of the values $(x,y)_0, (x,y)_1, (x,y)_{\zeta_3^*}$ corresponds to a root of some face polynomial. All of them are roots of unity, which shows that $P(x,y)$ (2.31) is tempered, i.e. the K-theoretic property holds for the underlying curve. Also, by computing the tame symbols we indeed see the surjection, but not the bijection between valuations and slopes (of course in this example one of the face polynomials has degree two and is irreducible, thus giving the two distinct roots with the same slope).

2.3 Are quiver A-polynomials tempered?

It is known from the preceding work on the knots-quivers correspondence [24, 25] that a symmetric quiver Q defines a 3d $\mathcal{N} = 2$ gauge theory $T[Q]$, see section 1.3.4. By analogy with the Chern-Simons case (2.7), the role of Lagrangian submanifold is played by multi-variable quiver A-polynomial $A(x_1, \ldots, x_m, y)$ with respect to symplectic form

$$\omega = \sum_{i=1}^{m} \frac{dx_i}{x_i} \wedge \frac{dy_i}{y_i} \tag{2.37}$$

where m is the number of nodes, x_i are summation variables in the quiver series and y_i are associated to the Nahm equations. Furthermore, the quiver series count holomorphic curves inside Calabi-Yau manifold (resolved conifold) with boundary on a Lagrangian, and is a subject of 3d-3d correspondence. This setup predicts the existence of quantum quiver A-polynomial, which has been studied in [58]. Therefore it is natural to ask whether quiver A-polynomials are tempered. Luckily, in many examples we can compute the face polynomials and confirm that they are cyclotomic. Our main conjecture is

Conjecture 2.3.1. *Quiver A-polynomials are tempered, for any symmetric quiver.*

In the remaining part of this chapter we confirm the conjecture for quivers consisting of m disjoint vertices with $\alpha_1, \ldots, \alpha_m$ self-loops. Since the adjacency matrix takes the diagonal form,

we refer to such quivers as *diagonal*. The choice is dictated by the combinatorial properties of the resultant polytope, which in this case has the structure of a zonotope (projection of a hypercube onto a space of lower dimension). It greatly simplifies calculation of the face polynomials, expressing them recursively in terms of mixed decompositions of the corresponding Minkowski sums.

2.4 Combinatorics of quiver resultants

We therefore start from explaining the combinatorial machinery of mixed resultants and initial forms. The exposition is based on [113] and [114]. Fix a non-negative integer m and a collection $\mathbf{A} = \{A_0, \dots, A_m\}$ of finite subsets $A_i \subset \mathbb{Z}^m,\ n_i = |A_i|$. Their convex hulls $Q_i = \mathrm{conv}(A_i) \subset \mathbb{R}^m$ are integral polytopes of dimension at most m. Take a generic $(m+1)$-tuple $(f_0, \dots, f_m)$ of Laurent polynomials supported on $\mathbf{A}$:

$$f_i(z_1, \dots, z_m) = \sum_{\mathbf{a} \in A_i} c_{i,\mathbf{a}} \mathbf{z}^{\mathbf{a}},\ i = 0, \dots, m. \tag{2.38}$$

Since f_i are generic, $c_{i,\mathbf{a}} \neq 0$ simultaneously for all $\mathbf{a} \in A_i,\ i = 0, \dots, m$. Therefore we may present the system $\{f_i = 0\}_{i=0}^m$ geometrically as a point

$$(c_{0,A_0}, \dots, c_{m,A_m}) \in \mathbb{P}^{n_0-1} \times \cdots \times \mathbb{P}^{n_m-1}, \tag{2.39}$$

where c_{i,A_i} is the n_i-tuple of coefficients of f_i. Consider now all tuples (2.38) having a common root $\mathbf{z}' \in (\mathbb{C} \setminus \{0\})^m : \{f_i(\mathbf{z}') = 0\}_{i=0}^m$. Taken simultaneously, they define a set of projective points, which closure we denote by $\overline{Z}$. In general $\overline{Z}$ is an irreducible hypersurface in $\mathbb{P}^{n_0-1} \times \cdots \times \mathbb{P}^{n_m-1}$. However, for some bad choices of $\mathbf{A}$, $\overline{Z}$ may have codimension bigger than one.

Definition 2.4.1. *Given a set* $\mathbf{A}$*, the sparse mixed resultant* $\mathcal{R}_{\mathbf{A}}$ *is the unique irreducible polynomial with integral coefficients* $c_{i,\mathbf{a}}$*, which vanishes on* $\overline{Z}$ *if* $\mathrm{codim}(\overline{Z}) = 1$*, and* $\mathcal{R}_{\mathbf{A}} := 1$ *if* $\mathrm{codim}(\overline{Z}) \geq 2$*. Additionally, the sub-resultant* $\mathcal{R}_{\mathbf{A}'}$ *is defined as the sparse mixed resultant for a proper subset* $\mathbf{A}' \subset \mathbf{A}$*.*

Example 2.4.1. Since $m = 0$ implies $\mathrm{conv}(\mathbf{A}) = \mathbf{A}$, the fist non-trivial case is $m = 1$. The choice $A_0 = \{0, 1\},\ A_1 = \{0, 1, 2\}$ gives

$$\begin{aligned} f_0 &= c_{0,0} + c_{0,1} z \\ f_1 &= c_{1,0} + c_{1,1} z + c_{1,2} z^2 \end{aligned} \tag{2.40}$$

with the two intervals $Q_0 = [0:1]$ and $Q_1 = [0:2]$. The system $\{f_1 = 0, f_2 = 0\}$ corresponds to a point $((c_{0,0} : c_{0,1}), (c_{1,0} : c_{1,1} : c_{1,2}))$. We get by eliminating the variable z:

$$\mathcal{R}_{\{0,1\},\{0,1,2\}} = c_{1,0} c_{0,1}^2 - c_{1,1} c_{0,0} c_{0,1} + c_{1,2} c_{0,0}^2 \tag{2.41}$$

which agrees with the classical resultant. The polytope $N(\mathcal{R}_{\{0,1\},\{0,1,2\}})$ is a triangle in $\mathbb{R}^5$, and $\mathcal{R}_{\{0,1\},\{0,1,2\}} = 0$ is the defining equation for the hypersurface $\overline{Z}$ in $\mathbb{P}^1 \times \mathbb{P}^2$. Indeed, in (2.41) there are 5 parameters (only 3 of them are independent), but equating it to zero drops the

dimension by 1, so $\dim \overline{Z} = 2$. E.g., if we remove a monomial from f_0

$$\begin{aligned} \tilde{f}_0 &= \cancel{c_{0,0}} + c_{0,1}z \\ f_1 &= c_{1,0} + c_{1,1}z + c_{1,2}z^2 \end{aligned} \tag{2.42}$$

this gives $\mathcal{R}_{\{1\},\{0,1,2\}} = c_{0,1}$.

The next ingredient, necessary for our study, is defined below.

Definition 2.4.2. *Given a polynomial $P(x_1, \dots, x_m)$ and an integer vector $\omega = (\omega_1, \dots, \omega_m)$, the initial form $init_\omega$ of P with respect to ω is a sum of all monomials in P which weight is maximal with respect to ω:*

$$init_\omega(P) := v^k P(v^{-\omega_1}x_1, \dots, v^{-\omega_m}x_m)|_{v=0} \tag{2.43}$$

(the exponent k is chosen such that $v = 0$ gives no infinities).

E.g. in example 2.4.1 the choice $\omega = (0, 1, 1, 0, 2)$ gives the initial form

$$init_\omega = v^3\, \mathcal{R}_{\{0,1\},\{0,1,2\}}(c_{0,0}, v^{-1}c_{0,1}, v^{-1}c_{1,0}, c_{1,1}, v^{-2}c_{1,2})\big|_{v=0} = c_{1,0}c_{0,1}^2. \tag{2.44}$$

It is important to mention that for any face of the Newton polytope $N(P)$ one can associate an initial form. Namely, if ω is the normal vector to some face, then $init_\omega$ is the restriction of P to this face, meaning that we are left only with monomials belonging to the face. We will use this fact when dealing with the resultant polytope $N(\mathcal{R}_{\mathbf{A}})$.

It's time to get back to Nahm equations (1.62). We would like to treat them from the perspective of (2.38) by writing

$$\begin{cases} 0 = F_0 = a_0 + a_1 z_1 \dots z_m \\ \hline 0 = F_1 = b_{1,0} + b_{1,1}z_1 + b_{1,2}\prod_{j=1}^m z_j^{C_{1,j}} \\ \vdots \\ 0 = F_m = b_{m,0} + b_{m,1}z_m + b_{m,2}\prod_{j=1}^m z_j^{C_{m,j}} \end{cases} \tag{2.45}$$

We also define the Nahm supports $\mathbf{A}_C = \{\mathrm{supp}(F_i)\}_{i=0\dots m}$, $\mathbf{b} = \{b_{i,j}\},\ i = 0 \dots m,\ j = 1, 2$.

Definition 2.4.3. *Quiver resultant is the sparse mixed resultant for the Nahm supports:*

$$\mathcal{R}_C := \mathcal{R}_{\mathbf{A}_C}(a_0, a_1, \mathbf{b}). \tag{2.46}$$

Therefore, we have the chain of specializations – quiver resultant produces quiver A-polynomial, which gives the two-variable polynomial after the principal specialization:

$$\begin{aligned} A_C(x_1, \dots, x_m, y) &= \mathcal{R}_C\left(y, -1 \mid 1, -1, (-1)^{C_{1,1}}x_1 \mid \dots \mid 1, -1, (-1)^{C_{m,m}}x_m\right), \\ A_C(x, y) &= A_C(a_1 x, \dots, a_m x, y). \end{aligned} \tag{2.47}$$

Next, recall that the Minkowski sum $Q = \sum_{i=0}^m Q_i$ of subsets $Q_0, \dots, Q_m \subset \mathbb{R}^n$ is simply the vector sum of all their elements. For example, the system (2.45) with $m = 2$ and $C = \mathrm{diag}(\alpha, \beta)$

gives three segments $Q_i = \mathrm{conv}(F_i),\ i = 0 \dots 2$. Their Minkowski sum is a hexagon, shown in figure 2.2. This is also an example of a zonotope (a projection of a hypercube onto a lower

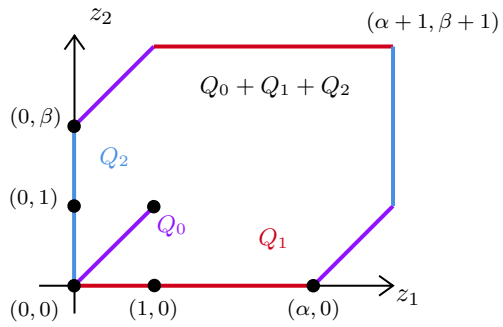

Figure 2.2: The Minkowski sum $Q = Q_0 + Q_1 + Q_2$ for the system (2.45) with $m = 2$ and $C = \mathrm{diag}(\alpha, \beta)$.

dimensional space: in this case 3-cube onto the plane). Its boundary zones are purple, red and blue edges, corresponding respectively to Q_0, Q_1 and Q_2. For an arbitrary diagonal quiver, its Minkowski sum inherits a similar structure (such quivers with larger number of vertices correspond to higher dimensional zonotopes).

Note that for any quiver with m vertices $\dim N(\mathcal{R}_C) = m$. In order to unify calculations for higher dimensional polytopes, we use the diagrammatic convention. Each diagram consists of several rows corresponding to an equation and dots representing the non-zero monomials, for example we can remove some monomials from the system (2.45) by crossing them out, and get

$$\begin{array}{l} a_0 + a_1 z_1 \dots z_m \\ \hline b_0 + b_1 z_1 + b_2 z_1^{C_{1,1}} \dots z_m^{C_{1,m}} \\ c_0 + \cancel{c_1 z_2} + c_2 z_1^{C_{2,1}} \dots z_m^{C_{2,m}} \\ d_0 + \cancel{d_1 z_3} + d_2 z_1^{C_{3,1}} \dots z_m^{C_{3,m}} \end{array} \quad \simeq \quad \begin{array}{|c|} \hline \bullet\ \bullet \\ \bullet\ \bullet \\ \bullet\ \quad \bullet \\ \bullet\ \quad \bullet \\ \hline \end{array} \tag{2.48}$$

Recall that mixed decomposition of Q coming from a polynomial system, is a partition by cells, each of them being a Minkwoski sum corresponding to a sub-resultant for some proper subsets $A'_0 \subset A_0, \dots, A'_m \subset A_m$.

Example 2.4.2. Figure 2.3 shows a mixed decomposition for the configuration in figure 2.2. Let us determine the corresponding cells:

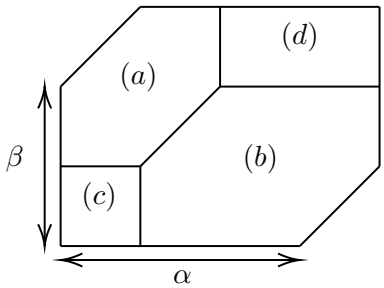

Figure 2.3: An example of mixed decomposition for the system (2.45) with $m = 2$ and $C = \mathrm{diag}(\alpha, \beta)$.

$$(a)\quad \begin{matrix} a_0 + a_1 z_1 z_2 \\ b_{1,0} + b_{1,1} z_1 + \cancel{b_{1,2} z_1^2} \\ \cancel{b_{2,0}} + b_{2,1} z_2 + b_{2,2} z_2^2 \end{matrix} \quad \simeq \quad \begin{vmatrix} \bullet & \bullet \\ \bullet & \bullet \\ & \bullet \end{vmatrix} \qquad (b)\quad \begin{matrix} a_0 + a_1 z_1 z_2 \\ \cancel{b_{1,0}} + b_{1,1} z_1 + b_{1,2} z_1^2 \\ b_{2,0} + b_{2,1} z_2 + \cancel{b_{2,2} z_2^2} \end{matrix} \quad \simeq \quad \begin{vmatrix} \bullet & \bullet \\ & \bullet \\ \bullet & \end{vmatrix}$$

$$(c)\quad \begin{matrix} a_0 + \cancel{a_1 z_1 z_2} \\ b_{1,0} + b_{1,1} z_1 + \cancel{b_{1,2} z_1^2} \\ b_{2,0} + b_{2,1} z_2 + \cancel{b_{2,2} z_2^2} \end{matrix} \quad \simeq \quad \begin{vmatrix} \bullet & \\ \bullet & \bullet \\ \bullet & \bullet \end{vmatrix} \qquad (d)\quad \begin{matrix} \cancel{a_0} + a_1 z_1 z_2 \\ \cancel{b_{1,0}} + b_{1,1} z_1 + b_{1,2} z_1^2 \\ \cancel{b_{2,0}} + b_{2,1} z_2 + b_{2,2} z_2^2 \end{matrix} \quad \simeq \quad \begin{vmatrix} \bullet & \\ \bullet & \bullet \\ \bullet & \bullet \end{vmatrix} \tag{2.49}$$

Now we see that the Minkowski sums of these two collections of sub-supports indeed produce the two hexagons (a) and (b). E.g., (a) gives $\tilde{Q}_0 = [(0,0) : (1,1)]$, $\tilde{Q}_1 = [(0,0) : (1,0)]$, $\tilde{Q}_2 = [(0,1) : (0,2)]$. Analogously, the two rectangular cells correspond to the sub-resultants (c) and (d).

In what follows, we associate an initial form to a mixed decomposition, so that each hexagonal cell contributes as a binomial, while each rectangular cell gives a monomial factor. Namely, given the data

- a collection $\mathbf{A} = \{A_0, \dots, A_m\}$ of subsets in $\mathbb{Z}^m$
- a mixed decomposition $\mathcal{MD}(Q)$, where $Q = \sum_{i=1}^m \mathrm{conv}(A_i)$

we define

$$init_{\mathcal{MD}(Q)}(c_{0,0}, c_{0,1}, \dots) := \prod_{\text{“rectangles”}} \times \prod_{\text{“hexagons”}} = \mu \prod_{\iota \in \mathcal{MD}(Q)} \tilde{\mathcal{R}}_\iota^{k_\iota}, \tag{2.50}$$

where $\mu = \prod_{\iota'} \mu_{\iota'}^{(k_{\iota'})}$ is a monomial in variables $\mu_{\iota'}$ for a rectangle ι' in $\mathcal{MD}(Q)$. On another hand, each $\tilde{\mathcal{R}}_\iota$ is a sub-resultant, which diagram gives a hexagonal cell ι. The latter product is taken over all hexagonal cells in $\mathcal{MD}(Q)$, and the exponents k_ι and $k_{\iota'}$ are chosen uniquely such that the volume of ι equals to the total degree of $\tilde{\mathcal{R}}_\iota^{k_\iota}$, for every cell ι, and for ι' the volume of a rectangular cell ι' simply equals to $k_{\iota'}$.

The correspondence between mixed decompositions and initial forms of the sparse mixed resultant is due to the fact that $init_{\mathcal{MD}(Q)}$ is in fact the initial form for $\mathcal{R}_{\mathbf{A}}$ [114, 115]. This allows to associate a mixed decomposition to each face of the resultant polytope, and then study their initial forms. Let us illustrate how it works using the example in figure 2.3. We claim that it gives the initial form:

$$a_0 a_1^{(\alpha-1)(\beta-1)} (a_0^{\alpha-1} b_2 c_1^{\alpha-1} + a_1^{\alpha-1} b_1 c_0^{\alpha-1})(a_0^{\beta-1} c_2 b_1^{\beta-1} + a_1^{\beta-1} c_1 b_0^{\beta-1}) \tag{2.51}$$

We can take $\omega = [\,(0,0),\,(0,1,1),\,(1,1,1)\,] + const$, where $const$ is an arbitrary constant vector. Here, hexagons are the two distinct binomial factors, while rectangles contribute to the monomial in (2.51). This gives the following picture (Figure 2.4). Indeed, the sparse mixed resultants from (a) and (b) are $\tilde{\mathcal{R}}_{(a)} = a_0^{\beta-1} c_2 b_1^{\beta-1} + a_1^{\beta-1} c_1 b_0^{\beta-1}$, $\tilde{\mathcal{R}}_{(b)} = a_0^{\alpha-1} b_2 c_1^{\alpha-1} + a_1^{\alpha-1} b_1 c_0^{\alpha-1}$. The exponents $k_{(a)}$ and $k_{(b)}$ are equal to 1, since the total degrees of $\tilde{\mathcal{R}}_{(b)}$ and $\tilde{\mathcal{R}}_{(a)}$ are equal to $2(\alpha-1)+1$ and $2(\beta-1)+1$, correspondingly, which agrees with the areas of the two hexagons (a) and (b). On the monomial side, we have the two degeneracies: in the first one, a_0 survives,

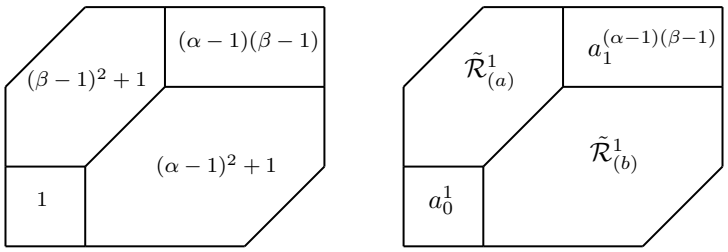

Figure 2.4: This mixed decomposition gives rise to the initial form (2.51), computed as the product over all its cells

and the area of (c) is equal to $k_{(c)} = 1$, so a_0^1. In the second one, a_1 survives and the area is $k_{(d)} = (\alpha-1)(\beta-1)$. Making a product of them gives the expression (2.51).

Additionally, we will call a diagram (respectively, its initial form) simple, if it does not have the middle monomials in $F_1, \ldots, F_m$, e.g. $\left|\begin{smallmatrix}\bullet & \bullet \\ \bullet & \bullet \\ \bullet & \bullet\end{smallmatrix}\right|$ is simple, whereas $\left|\begin{smallmatrix}\bullet & \bullet \\ \bullet & \bullet & \bullet \\ \bullet & \bullet\end{smallmatrix}\right|$ is not.

2.5 Case studies: quivers with $C = C^{\mathrm{diag}(\alpha_1,\ldots,\alpha_m)}$

2.5.1 Two-vertex quivers

In the case of quivers with two vertices, without loss of generality we consider

$$C^{\mathrm{diag}(\alpha,\beta)} = \begin{bmatrix}\alpha & 0 \\ 0 & \beta\end{bmatrix}, \qquad \alpha, \beta \geq 2. \tag{2.52}$$

Note that the non-diagonal case can be obtained by transformation

$$A(x_1, \ldots, x_m, y) \mapsto A(x_1 y^f, \ldots, x_m y^f, y), \tag{2.53}$$

which only dilates the polytopes but does not alter their face polynomials (except for the two degenerate cases $f = 0$ and $f = 1$, which we exclude). It affect the quiver matrix in a simple way:

$$\begin{bmatrix}\alpha & 0 \\ 0 & \beta\end{bmatrix} \mapsto \begin{bmatrix}\alpha+f & f \\ f & \beta+f\end{bmatrix}. \tag{2.54}$$

Therefore, we consider the polynomial system (2.45) which in this case takes form

$$\begin{cases} 0 = F_0 = a_0 + a_1 z_1 z_2 \\ 0 = F_1 = b_0 + b_1 z_1 + b_2 z_1^\alpha \\ 0 = F_2 = c_0 + c_1 z_2 + c_2 z_2^\beta \end{cases} \tag{2.55}$$

For generic α, β the resultant polytope $N(\mathcal{R}_{\mathbf{A}})$ coincides with the Gelfand-Kapranov-Zelevinsky (GKZ) polytope $N_{2,2}$, depicted in figure 2.5 [113, 116]. By definition, GKZ polytope is the Newton polytope of a classical resultant of two polynomials:

$$\begin{cases} f_0 = \tilde{a}_0 + \tilde{a}_1 z + \ldots \tilde{a}_{m'} z^{m'} \\ f_1 = \tilde{b}_0 + \tilde{b}_1 z + \ldots \tilde{b}_{n'} z^{n'} \end{cases} \quad \longrightarrow \quad N_{m',n'} := N\left(\mathrm{res}_z(f_0, f_1)\right). \tag{2.56}$$

When $(m', n') = (2, 2)$, this system is equivalent to (2.55) with $(\alpha, \beta) = (2, 2)$. It implies that $N(\mathcal{R}_{\mathbf{A}}) = N_{2,2}$ for $(\alpha, \beta) = (2, 2)$. However, varying $\alpha, \beta \geq 2$ in (2.55) does not change the polytope, since it corresponds to dilation of the lattice of $\mathbf{A}$, which is an affine transformation. Therefore, $N(\mathcal{R}_{\mathbf{A}}) = N_{2,2}$ for any $\alpha, \beta \geq 2$.

Example 2.5.1. Take $C = \mathrm{diag}(2, 2)$. Eliminating z_1, z_2 from (2.55), we obtain quiver resultant and quiver A-polynomial:

$$\begin{aligned} \mathcal{R}_{\mathrm{diag}(2,2)}(a_0, a_1, \mathbf{b}) &= (a_0^2 b_2 c_2 - a_1^2 b_0 c_0)^2 + a_0 a_1 \, (a_0 b_2 c_1 + a_1 b_1 c_0)(a_0 b_1 c_2 + a_1 b_0 c_1), \\ A_{\mathrm{diag}(2,2)}(x_1, x_2, y) &= \mathcal{R}(y, -1, -1, 1, x_1, -1, 1, x_2) \\ &= (x_1 x_2 y^2 - 1)^2 - y \, (x_1 y + 1)(x_2 y + 1) \\ &= x_1^2 x_2^2 y^4 + x_1 x_2 y^3 - 2 x_1 x_2 y^2 + x_1 y^2 + x_2 y^2 + y + 1. \end{aligned} \tag{2.57}$$

The resultant polytope encodes the powers of monomials shown as blue nodes in figure 2.5. For

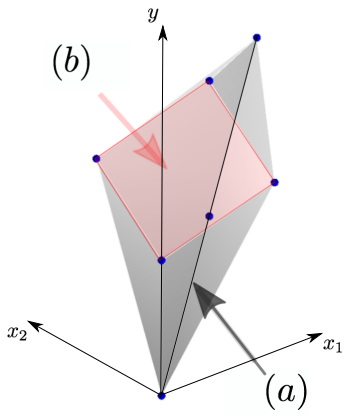

Figure 2.5: The resultant polytope $N_{2,2}$ for a two-vertex quiver.

example, the convex hull of $(x_1 x_2 y^2 - 1)^2$ gives the edge (a), while $-y \, (x_1 y + 1)(x_2 y + 1)$ gives the 2-dimensional face (b). The latter belongs to the plane

$$1 + x_1 + x_2 - y = 0 \tag{2.58}$$

with normal vector $\omega = (1, 1, -1)$. We can rescale the variables x_1, x_2, y with respect to ω:

$$A_{\mathrm{diag}(2,2)}(c^1 x_1, c^1 x_2, c^{-1} y) = (x_1 x_2 y^2 - 1)^2 - c^{-1} y \, (x_1 y + 1)(x_2 y + 1) \tag{2.59}$$

for some $c \neq 0$, separating the faces of the polytope. As the result, we get the two distinguished initial forms:

$$init_a = (x_1 x_2 y^2 - 1)^2, \qquad init_b = y \, (x_1 y + 1)(x_2 y + 1). \tag{2.60}$$

Let us move to the unspecialized case (2.57). The first initial form corresponds to binomial $(a_0^2 b_2 c_2 - a_1^2 b_0 c_0)^2$. The overall square comes from the areal factor of the largest hexagon in figure 2.6, left. The total degree is equal to the volume of the corresponding cell. The binomial $a_0^2 b_2 c_2 - a_1^2 b_0 c_0$ is also the sub-resultant for $b_1 = c_1 = 0$.

The second initial form corresponds to $a_0 a_1 \, (a_0 b_2 c_1 + a_1 b_1 c_0)(a_0 b_1 c_2 + a_1 b_0 c_1)$. It splits

into the product of four distinct sub-resultants, representing the four distinct cells of the mixed decomposition in figure 2.6, right:

$$\begin{aligned} b_0 = c_2 = 0, \qquad & a_0b_2c_1 + a_1b_1c_0 \\ b_2 = c_0 = 0, \qquad & a_0b_1c_2 + a_1b_0c_1 \\ a_1 = b_2 = c_2 = 0, \qquad & a_0 \\ a_0 = b_0 = c_0 = 0, \qquad & a_1 \end{aligned} \tag{2.61}$$

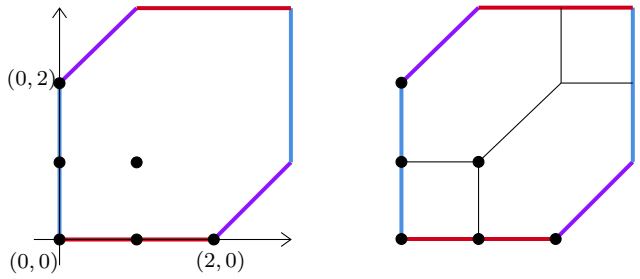

Figure 2.6: Mixed decompositions in (z_1, z_2)-plane: for $init_a$ (left) and $init_b$ (right).

Moving to the general case $\alpha, \beta \geq 2$, we have to introduce an operator which implements the rule for computing the exponents k_ι in (2.50).

Definition 2.5.1. *Given a binomial* $\eta^{\mathbf{p}} + \theta^{\mathbf{q}}, \mathbf{p} = (p_1, \ldots, p_k), \mathbf{q} = (q_1, \ldots, q_k)$, *define*

$$\mathrm{GCD}\left(\eta^{\mathbf{p}} + \theta^{\mathbf{q}}\right) := \left(\eta^{\frac{\mathbf{p}}{\mathrm{GCD}(\mathbf{p},\mathbf{q})}} + \theta^{\frac{\mathbf{q}}{\mathrm{GCD}(\mathbf{p},\mathbf{q})}}\right)^{\mathrm{GCD}(\mathbf{p},\mathbf{q})}, \tag{2.62}$$

where $\mathrm{GCD}(\mathbf{p}, \mathbf{q})$ *acts on the two vectors component-wise. Also, for any integer* $s \geq 1$

$$\mathrm{GCD}\left(\prod_{i=1\ldots s} (\eta^{\mathbf{p}_i} + \theta^{\mathbf{q}_i})\right) = \prod_{i=1\ldots s} \mathrm{GCD}(\eta^{\mathbf{p}_i} + \theta^{\mathbf{q}_i}) \tag{2.63}$$

For example:

$$\begin{aligned} \mathrm{GCD}\left(a_0^2b_2^2c_2 + a_1^2b_0^2c_0\right) &= a_0^2b_2^2c_2 + a_1^2b_0^2c_0, \\ \mathrm{GCD}\left(a_0^4b_2^2c_2^2 + a_1^4b_0^2c_0^2\right) &= (a_0^2b_2c_2 + a_1^2b_0c_0)^2. \end{aligned} \tag{2.64}$$

Proposition 2.5.1. *The Newton polytope* $N(\mathcal{R})$ *for the system (2.55) supports the following simple initial forms:*

$$init_a = \left|\begin{smallmatrix}\bullet & \bullet \\ \bullet & \\ \bullet & \bullet\end{smallmatrix}\right| = \mathrm{GCD}\left(a_0^{\alpha\beta}b_2^{\beta}c_2^{\alpha} + (-1)^{\alpha\beta+\alpha+\beta}a_1^{\alpha\beta}b_0^{\beta}c_0^{\alpha}\right),$$

$$init_b = \left|\begin{smallmatrix}\bullet & \bullet \\ \bullet & \bullet \\ & \bullet\end{smallmatrix}\right| \times \left|\begin{smallmatrix}\bullet & \bullet \\ & \bullet \\ \bullet & \end{smallmatrix}\right| = a_0 a_1^{(\alpha-1)(\beta-1)}(a_0^{\alpha-1}b_2c_1^{\alpha-1} + a_1^{\alpha-1}b_1c_0^{\alpha-1})(a_0^{\beta-1}c_2b_1^{\beta-1} + a_1^{\beta-1}c_1b_0^{\beta-1}),$$

$$init_c = \left|\begin{smallmatrix}\bullet & \bullet \\ \bullet & \\ \bullet & \end{smallmatrix}\right| = a_1^{\alpha(\beta-1)}b_0^{\beta-1}(a_0^{\alpha}b_2c_1^{\alpha} + a_1^{\alpha}b_0c_2^{\alpha}),$$

$$init_d = \left|\begin{smallmatrix}\bullet & \bullet \\ \bullet & \bullet \\ \bullet & \end{smallmatrix}\right| = a_1^{(\alpha-1)\beta}c_0^{\alpha-1}(a_0^{\beta}b_1^{\beta}c_2 + a_1^{\beta}b_2^{\beta}c_0),$$

$$init_e = \left|\begin{smallmatrix}\bullet & \bullet \\ & \bullet \\ \bullet & \end{smallmatrix}\right| = a_0^{\beta}c_2 \cdot \mathrm{GCD}\left(a_0^{(\alpha-1)\beta}b_2^{\beta}c_2^{\alpha-1} + (-1)^{(\alpha-1)\beta+(\alpha-1)+\beta}a_1^{(\alpha-1)\beta}b_1^{\beta}c_0^{\alpha-1}\right),$$

$$init_f = \left|\begin{smallmatrix}\bullet & \bullet \\ \bullet & \\ & \bullet\end{smallmatrix}\right| = a_0^{\alpha}b_2 \cdot \mathrm{GCD}\left(a_0^{\alpha(\beta-1)}b_2^{\beta-1}c_2^{\alpha} + (-1)^{(\alpha-1)\beta+(\alpha-1)+\beta}a_1^{\alpha(\beta-1)}b_0^{\beta-1}c_1^{\alpha}\right),$$

$$init_g = \left|\begin{smallmatrix}\bullet & \bullet \\ & \bullet \\ & \bullet\end{smallmatrix}\right| = a_0^{\alpha+\beta-1}b_2c_2 \cdot \mathrm{GCD}\left(a_0^{(\alpha-1)(\beta-1)}b_2^{\beta-1}c_2^{\alpha-1} + \right.$$
$$\left.(-1)^{(\alpha-1)(\beta-1)+(\alpha-1)+(\beta-1))}a_1^{(\alpha-1)(\beta-1)}b_1^{\beta-1}c_1^{\alpha-1}\right),$$

$$init_h = \left|\begin{smallmatrix}\bullet & \bullet \\ \bullet & \bullet \\ \bullet & \bullet\end{smallmatrix}\right| = a_1^{\alpha\beta-1}b_0^{\beta-1}c_0^{\alpha-1}(a_0b_1c_1 + a_1b_0c_0),$$

where a, b, c, d, e, f, g, h are the faces of $N(\mathcal{R})$ (Figure 2.7), and diagrams on the right correspond to distinct binomial factors.

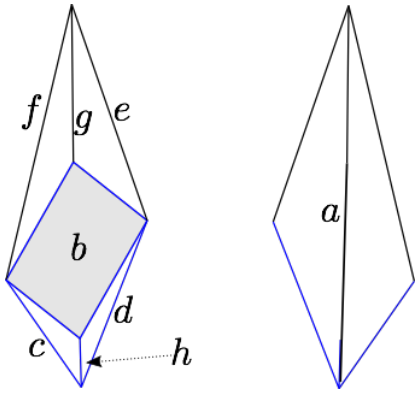

Figure 2.7: The Newton polytope $N_{2,2}$ with the initial forms (2.55), as viewed from the top (left) and bottom (right). Blue faces do not have other points rather than the vertices

Proof. Every binomial factor in $init_a, init_b, \ldots$ correspond to a sub-resultant, whose diagram is given on the right side of each expression in Proposition 2.5.1. Let's associate mixed decompositions to these initial forms, as shown in figure 2.8. This provides a desired combinatorial interpretation of the faces. Each hexagon in a mixed decomposition gives the distinct binomial factor in the corresponding initial form, and all rectangles together determine the monomial prefactor. The GCD operator has the following interpretation: each $k_\iota \geq 1$ in (2.50) is uniquely fixed when (α, β) are fixed, so that the total degree of $\tilde{\mathcal{R}}_\iota^{k_i}$ equals to the area of the ι-th cell of a mixed decomposition.

E.g., for $init_a$ there is only a single hexagon (the top-left in Figure 2.8), which is Q itself – so there is no monomial prefactor. This hexagon gives the sub-resultant $\tilde{\mathcal{R}} = a_0^{\alpha\beta}b_2^{\beta}c_2^{\alpha} +$

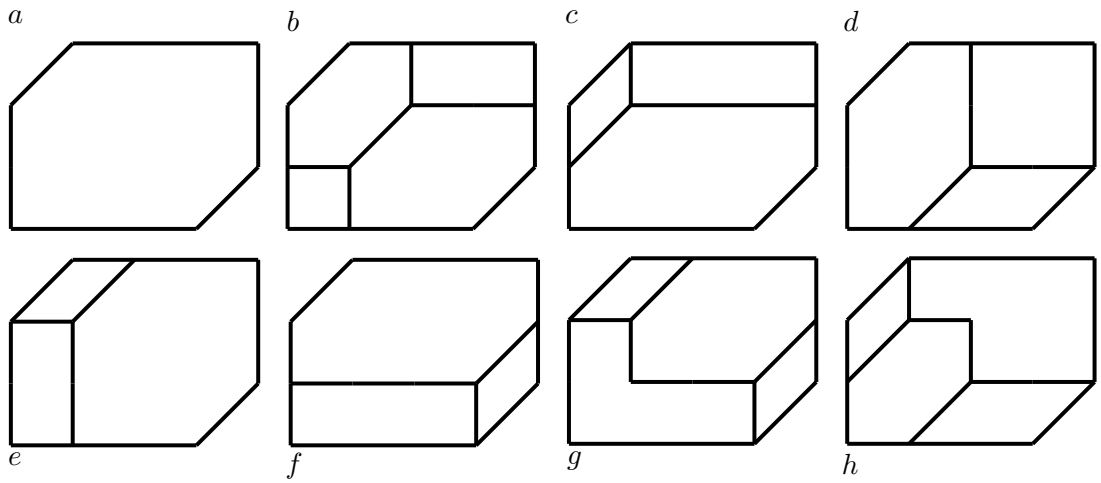

Figure 2.8: mixed decompositions of Q, associated to the faces of $N_{2,2}$

$(-1)^{\alpha\beta+\alpha+\beta}a_1^{\alpha\beta}b_0^{\beta}c_0^{\alpha}$. We see that the area of Q is $\alpha\beta+\alpha+\beta$, so if α and β are not co-prime, it would give $k>1$, hence

$$init_a = \mathrm{GCD}\left(a_0^{\alpha\beta}b_2^{\beta}c_2^{\alpha} + (-1)^{\alpha\beta+\alpha+\beta}a_1^{\alpha\beta}b_0^{\beta}c_0^{\alpha}\right).$$

In the case of $init_b$ we have two hexagons (giving the two distinct binomial factors) and two quadrangles for the monomial: the bottom square is a_0, and the top quadrangle is $a_1^{(\alpha-1)(\beta-1)}$ (compare with Figure 2.3). To sum up, by using the mixed decompositions a, b, c, d, e, f, g, h we completely described the bijection between the faces and simple initial forms, which completes the proof.

□

Having the above said, we conclude that quiver A-polynomial for any two-vertex quiver is tempered, with its face polynomials all being binomials. It follows directly from factorization formulas for the initial forms a, b, c, d, e, f, g, h. The polytope $N(\mathcal{R})$ projects onto $N(A)$ in such a way that the faces of $N(\mathcal{R})$ do not overlap each other (colliding the axes x_1 and x_2 in figure 2.5). Binomiality of the initial forms of Proposition 2.5.1 translates to the corresponding face polynomials, which shows that $A(x,y)$ is tempered for every quiver of the form (2.52).

2.5.2 Three-vertex quivers

In the case of quivers with three vertices it is not sufficient to consider only diagonal quivers to cover all possible cases. However, for us this scenario is important because it is still tractable from the same perspective as the two-vertex case. We therefore consider for $\alpha, \beta, \gamma \geq$

$$C^{\mathrm{diag}(\alpha,\beta,\gamma)} = \begin{bmatrix} \alpha & 0 & 0 \\ 0 & \beta & 0 \\ 0 & 0 & \gamma \end{bmatrix}, \qquad \begin{cases} F_0 = a_0 + a_1 z_1 z_2 z_3 \\ F_1 = b_0 + b_1 z_1 + b_2 z_1^{\alpha} \\ F_2 = c_0 + c_1 z_2 + c_2 z_2^{\beta} \\ F_3 = d_0 + d_1 z_3 + d_2 z_3^{\gamma} \end{cases} \tag{2.65}$$

and introduce the initial forms $init_{\phi_{p,q}}$ (which we will shortly write as $\phi_{p,q}$, at the same time referring to the corresponding face of $N(\mathcal{R})$), labelled by $p, q \geq 0$. They are given by products over all permutations of diagrams with p rows of the form [••] and q rows of the form [••], such that $p+q=m$ (the red color is just for a better visual distinction between the two cases). The only exception is $\phi_{0,0}$, which rows are of the form [• •]. For $m=3$, there are five such forms:

$\phi_{0,0} =$  $\phi_{3,0} =$  $\phi_{0,3} =$ 

$\phi_{2,1} =$  $\times$  $\times$  (2.66)

$\phi_{1,2} =$  $\times$  $\times$ 

For example, let us illustrate how $\phi_{0,3}$ is calculated. From the corresponding diagram in (2.66) we get

$$a_0 = -a_1 z_1 z_2 z_3,\ z_1^{\alpha-1} = -\frac{b_1}{b_2},\ z_2^{\beta-1} = -\frac{c_1}{c_2},\ z_3^{\gamma-1} = -\frac{d_1}{d_2} \tag{2.67}$$

To find the binomial factor, we compute the mixed resultant for this system. Raising the first equation to the power $(\alpha-1)$ immediately eliminates z_1:

$$a_0^{(\alpha-1)} = (-a_1 z_2 z_3)^{(\alpha-1)} \left(-\frac{b_1}{b_2}\right) \tag{2.68}$$

Consequently, we raise it to $(\beta-1)$ and $(\gamma-1)$ and getting rid of numerators, to obtain

$$\begin{aligned} &\Big(a_0^{(\alpha-1)(\beta-1)(\gamma-1)} b_2^{(\beta-1)(\gamma-1)} c_2^{(\alpha-1)(\gamma-1)} d_2^{(\alpha-1)(\beta-1)} + \\ &(-1)^{(\alpha-1)+(\beta-1)+(\gamma-1)+1} a_1^{(\alpha-1)(\beta-1)(\gamma-1)} b_1^{(\beta-1)(\gamma-1)} c_1^{(\alpha-1)(\gamma-1)} d_1^{(\alpha-1)(\beta-1)}\Big) \end{aligned} \tag{2.69}$$

The binomial part of $\phi_{0,3}$ is equal to the GCD applied to (2.69). A genuine guess of the arrangement of three-dimensional blocks (figure 2.9) gives the monomial expression. We therefore obtain (analogously for other diagrams):

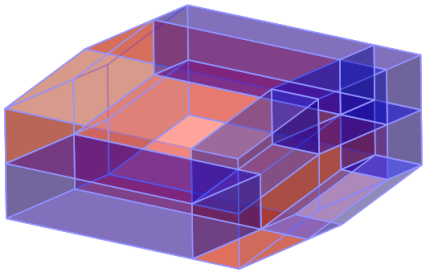

Figure 2.9: The mixed decomposition induced by $\phi_{0,3}$: the red cells correspond to three binomials in (2.70), while the union of blue cells uniquely determines the monomial $\mu_{0,3}$.

$$
\begin{aligned}
\phi_{0,0} &= \mathrm{GCD}\left(a_0{}^{\alpha\,\beta\,\gamma} b_2{}^{\beta\,\gamma} c_2{}^{\alpha\,\gamma} d_2{}^{\alpha\,\beta} + (-1)^{\sigma+1}\, a_1{}^{\alpha\,\beta\,\gamma} b_0{}^{\beta\,\gamma} c_0{}^{\alpha\,\gamma} d_0{}^{\alpha\,\beta}\right),\\
\phi_{3,0} &= \mu_{3,0}\cdot(a_0 b_1 c_1 d_1 - a_1 b_0 c_0 d_0),\\
\phi_{2,1} &= \mu_{2,1}\cdot \mathrm{GCD}\left(\left(a_0{}^{\alpha-1} b_2 c_1{}^{\alpha-1} d_1{}^{\alpha-1} + (-1)^{\alpha+1}\, a_1{}^{\alpha-1} b_1 c_0{}^{\alpha-1} d_0{}^{\alpha-1}\right)\times\right.\\
&\quad \left(a_0{}^{\beta-1} c_2 b_1{}^{\beta-1} d_1{}^{\beta-1} + (-1)^{\beta+1}\, a_1{}^{\beta-1} c_1 b_0{}^{\beta-1} d_0{}^{\beta-1}\right)\times\\
&\quad \left.\left(a_0{}^{\gamma-1} d_2 b_1{}^{\gamma-1} c_1{}^{\gamma-1} + (-1)^{\gamma+1}\, a_1{}^{\gamma-1} d_1 b_0{}^{\gamma-1} c_0{}^{\gamma-1}\right)\right),\\
\phi_{1,2} &= \mu_{1,2}\cdot \mathrm{GCD}\left(\left(a_0{}^{(\beta-1)(\gamma-1)} b_1{}^{(\beta-1)(\gamma-1)} c_2{}^{\gamma-1} d_2{}^{\beta-1} + \right.\right.\\
&\quad \left.(-1)^{\beta+\gamma+1}\, a_1{}^{(\beta-1)(\gamma-1)} b_0{}^{(\beta-1)(\gamma-1)} c_1{}^{\gamma-1} d_1{}^{\beta-1}\right)\times\\
&\quad \left(a_0{}^{(\alpha-1)(\gamma-1)} c_1{}^{(\alpha-1)(\gamma-1)} b_2{}^{\gamma-1} d_2{}^{\alpha-1} + \right.\\
&\quad \left.(-1)^{\alpha+\gamma+1}\, a_1{}^{(\alpha-1)(\gamma-1)} c_0{}^{(\alpha-1)(\gamma-1)} b_1{}^{\gamma-1} d_1{}^{\alpha-1}\right)\times\\
&\quad \left(a_0{}^{(\alpha-1)(\beta-1)} d_1{}^{(\alpha-1)(\beta-1)} b_2{}^{\beta-1} c_2{}^{\alpha-1} + \right.\\
&\quad \left.\left.(-1)^{\alpha+\beta+1}\, a_1{}^{(\alpha-1)(\beta-1)} d_0{}^{(\alpha-1)(\beta-1)} b_1{}^{\beta-1} c_1{}^{\alpha-1}\right)\right),\\
\phi_{0,3} &= \mu_{0,3}\cdot \mathrm{GCD}\left(a_0^{(\alpha-1)(\beta-1)(\gamma-1)} b_2^{(\beta-1)(\gamma-1)} c_2^{(\alpha-1)(\gamma-1)} d_2^{(\alpha-1)(\beta-1)} + \right.\\
&\quad \left.(-1)^{(\alpha-1)+(\beta-1)+(\gamma-1)+1} a_1^{(\alpha-1)(\beta-1)(\gamma-1)} b_1^{(\beta-1)(\gamma-1)} c_1^{(\alpha-1)(\gamma-1)} d_1^{(\alpha-1)(\beta-1)}\right),
\end{aligned}
\tag{2.70}
$$

where $\sigma = \alpha\,\beta\,\gamma + \alpha\,\beta + \alpha\,\gamma + \beta\,\gamma$, and the monomials are:

$$
\begin{aligned}
\mu_{3,0} &= a_1^{\alpha\beta\gamma-1} b_0^{\beta\gamma-1} c_0^{\alpha\gamma-1} d_0^{\alpha\beta-1},\\
\mu_{2,1} &= a_0 a_1{}^{\alpha\,\beta\,\gamma-\alpha-\beta-\gamma+2} b_0{}^{(\beta-1)(\gamma-1)} c_0{}^{(\alpha-1)(\gamma-1)} d_0{}^{(\alpha-1)(\beta-1)},\\
\mu_{1,2} &= a_0{}^{\alpha+\beta+\gamma-2} a_1{}^{(\alpha-1)(\beta-1)(\gamma-1)} b_2 c_2 d_2,\\
\mu_{0,3} &= a_0^{\alpha\beta+\alpha\gamma+\beta\gamma-\alpha-\beta-\gamma+1} b_2^{\beta+\gamma-1} c_2^{\alpha+\gamma-1} d_2^{\alpha+\beta-1}.
\end{aligned}
\tag{2.71}
$$

Our next step is to show that the initial forms $\{\phi_{p,q}\}_{p+q=m}$ completely determine the resultant polytope and compute the corresponding face polynomials for a diagonal quiver of an arbitrary size.

2.5.3 Arbitrary number of vertices

Consider the quiver $C = \mathrm{diag}(\alpha_1, \ldots, \alpha_m)$, $\alpha_i \geq 2$, $m \geq 2$ and initial forms $\{\phi_{p,q}\}$, where we indicate the [••]-type rows by $I = \{i_1, \ldots, i_p\}$, and [••]-type rows by $K = \{k_1, \ldots, k_q\}$.

Proposition 2.5.2. *Let $I = \{i_1, \ldots, i_p\}$, $K = \{k_1, \ldots, k_q\}$, $p + q = m$. Define*

$$
\begin{aligned}
\varphi_{I,K} := &\left(a_0 \prod_{i\in I} b_{i,1}\right)^{\prod_{k\in K}(\alpha_k-1)} \prod_{k\in K} b_{k,2}^{\prod'_{k'\in K}{}^{k'\neq k}(\alpha_{k'}-1)} + \\
&(-1)^{1+\sum_{k\in K}\prod'_{k'\in K}{}^{k'\neq k}(\alpha_{k'}-1)} \left(a_1 \prod_{i\in I} b_{i,0}\right)^{\prod_{k\in K}(\alpha_k-1)} \prod_{k\in K} b_{k,1}^{\prod'_{k'\in K}{}^{k'\neq k}(\alpha_{k'}-1)}
\end{aligned}
\tag{2.72}
$$

where the product $\prod'$ *equals to* 1 *if* $q = 1$. *Then*

$$\phi_{p,q} := \mu_{p,q} \cdot \prod_{\substack{I,K\subset\{1,\dots,m\}\\ |I|=p,|K|=q}} \mathrm{GCD}(\varphi_{I,K}) \tag{2.73}$$

are well-defined initial forms, where the product is taken over all $\frac{m!}{p!q!}$ *choices of the subsets* I, K, *and the monomial* $\mu_{p,q}$ *is given by*

$$\begin{aligned}\mu_{p,q} =& a_0^{1+\sum_{|K'|=1\dots q-1}\prod_{k'\in K'}(\alpha_{k'}-1)} a_1^{\sum_{|K'|=q+1\dots m}\prod_{k'\in K'}(\alpha_{k'}-1)} \times \\ & \prod_{i=1\dots m} b_{i,0}^{\sum_{|K'|=q-2\dots m-1}\prod_{k'\in K'}(\alpha_{k'}-1)} \; b_{i,2}^{\delta(q)+\sum_{|K'|=1\dots q-2}\prod_{k'\in K'}(\alpha_{k'}-1)} \end{aligned} \tag{2.74}$$

where $\delta(q) = 0$ *if* $q \le m-1$, *and* $\delta(q) = 1$ *otherwise.*

Proof. To get the expression for $\varphi_{I,K}$, we write the first equation in (2.45)

$$a_0 = -a_1 z_1 \dots z_m, \tag{2.75}$$

and then raise the right and left hand sides consequently to powers $(\alpha_k - 1)$, where $k \in K$ corresponds to [••]-type rows, and plug $z_k^{\alpha_k - 1} = -\frac{b_{k,1}}{b_{k,2}}$ in order to eliminate the variables $z_1, \dots, z_m$. To compute the monomials, we denote by (π) the set of all permutations of rows in a diagram which are not marked as blue, e.g.

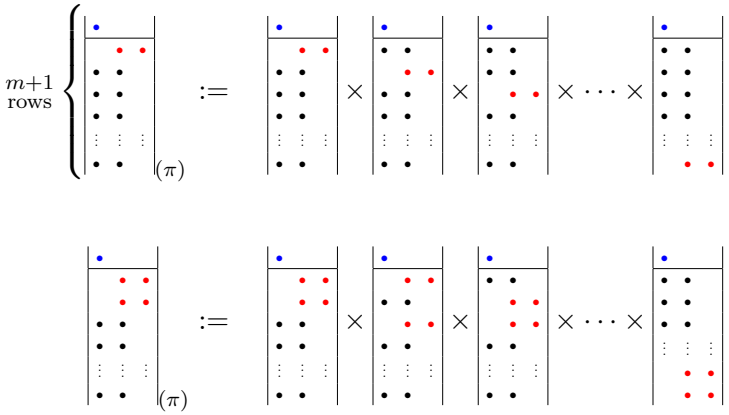

(2.76)

The number of such permutations is equal to

$$\frac{m!}{(\#\text{black rows})! \cdot (\#\text{red rows})!} \tag{2.77}$$

Note that the operation "×" is commutative, since it corresponds to a union of the corresponding cells in the mixed decomposition. The blue dot indicate the equation fixed under permutation. For example, in (2.76) it corresponds to $\tilde{F}_0 = a_0 + \cancel{a_1 z_1 \dots z_m}$. Therefore, this diagram contributes to a_0 in the expression (2.74). On another hand, all diagrams contributing to a_1 correspond to $\tilde{F}_0 = \cancel{g_0} + a_1 z_1 \dots z_m$, and so on. Our claim is that the following diagrams

completely determine (2.74)

a_0 : 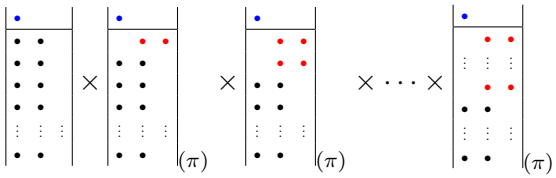 , unless #red rows $\leq q-1$ (2.78)

a_1 : 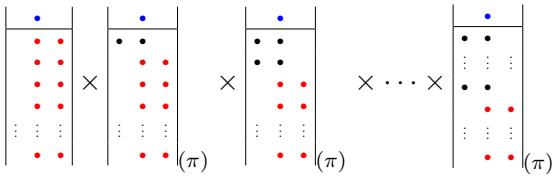 , unless #red rows $\geq q+1$ (2.79)

$b_{i,0}$: 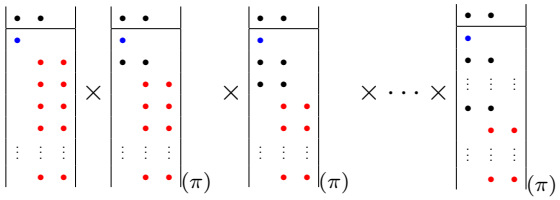 , unless #red rows $\geq q+1$ (2.80)

$b_{i,2}$: 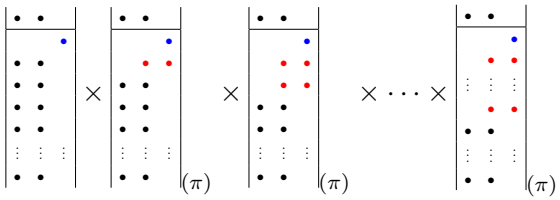 , unless #red rows $\leq q-1$ (2.81)

where the number of red rows is equal to $|K'|$ in (2.74). For example, the exponent of a_0 in (2.74) is equal to $1+\sum_{|K'|=1\ldots q-1}\prod_{k'\in K'}(\alpha_{k'}-1)$, which is obtained by summing the volumes of cells (2.78)

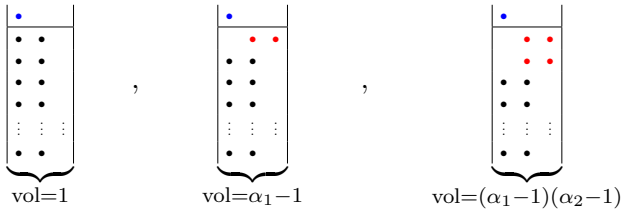

(2.82)

In the first case we are left with $\tilde{F}_0=a_0$ and $\tilde{F}_i=b_{i,0}+b_{i,2}z,\ i=1\ldots m$, which corresponds to $\tilde{Q}$ being a m-cube with $\mathrm{Vol}(\tilde{Q})=1$. Similarly, each j-th row highlighted by red, gives the factor (α_j-1) to the volume of $\tilde{Q}$. Calculating the volumes for each diagram for $a_0, a_1, b_{*,0}, b_{*,2}$ and summing them up in each case, we obtain the exponents (2.74). Besides, one can verify that the total degree of $\phi_{p,q}$ is equal to the total volume $\mathrm{Vol}(Q)$. We have

$$\mathrm{Vol}(Q)=\alpha_1\ldots\alpha_m+\sum_{j=1}^{m}\alpha_1\ldots\cancel{\alpha_j}\ldots\alpha_m. \tag{2.83}$$

Take $\mathcal{MD}(Q)=Q$, which corresponds to the bottom edge of $N(\mathcal{R}_C)$ and gives

$$\phi_{0,0}:=\mathrm{GCD}\left(a_0^{\prod\alpha_j}\prod b_{j,2}^{\prod_{j'\neq j}\alpha_{j'}}+(-1)^{\prod\alpha_j+\sum\prod\alpha_{j'}}a_1^{\prod\alpha_j}\prod b_{j,0}^{\prod_{j'\neq j}\alpha_{j'}}\right)\simeq \tag{2.84}$$
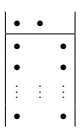

The GCD operator does not change the total degree of a polynomial, therefore the degree of $\phi_{0,0}$ is equal to the right hand side of (2.83). On another hand, since the cell is unique and equals to Q itself, its total degree is equal to the volume of Q. For $m = 2$ we have the complete set

$$\{\phi_{p,q}\} = \{\phi_{0,0}\} \cup \{\phi_{2,0},\ \phi_{0,2},\ \phi_{1,1}\}. \tag{2.85}$$

E.g.,

$$\phi_{1,1} = a_0 a_1^{(\alpha_1-1)(\alpha_2-1)}(a_0^{\alpha_1-1}b_2c_1^{\alpha_1-1} + a_1^{\alpha_1-1}b_1c_0^{\alpha_1-1})(a_0^{\alpha_2-1}c_2b_1^{\alpha_2-1} + a_1^{\alpha_2-1}c_1b_0^{\alpha_2-1}) \tag{2.86}$$

(recall (2.51)). The volume $\mathrm{Vol}(Q) = \alpha_1\alpha_2 + \alpha_1 + \alpha_2$. We see that the condition $\deg(\phi_{1,1}) = \mathrm{Vol}(Q)$ is satisfied. Analogously, for $m = 3$ it can be checked from the formulas (2.70). For arbitrary m it then follows by induction. Indeed, increasing m by one amounts to adding one extra row to all diagrams we have, and also introducing some new diagrams. Since the volume of a cell given by a diagram is the product over all its rows, the individual volumes are modified as

$$\begin{aligned}
\tilde{\alpha}_1 \dots \tilde{\alpha}_m &\mapsto \tilde{\alpha}_1 \dots \tilde{\alpha}_m\tilde{\alpha}_{m+1} \\
\tilde{\alpha}_1 \dots \cancel{\tilde{\alpha}_j} \dots \tilde{\alpha}_m &\mapsto \tilde{\alpha}_1 \dots \cancel{\tilde{\alpha}_j} \dots \tilde{\alpha}_m\tilde{\alpha}_{m+1},\ j \neq m+1 \\
\tilde{\alpha}_1 \dots \cancel{\tilde{\alpha}_j}, \cancel{\tilde{\alpha}_{j'}} \dots \tilde{\alpha}_m &\mapsto \tilde{\alpha}_1 \dots \cancel{\tilde{\alpha}_j}, \cancel{\tilde{\alpha}_{j'}} \dots \tilde{\alpha}_m\tilde{\alpha}_{m+1},\ j, j' \neq m+1 \\
&\vdots
\end{aligned} \tag{2.87}$$

where $\tilde{\alpha}_i := \alpha_i - 1$. But this picture is not yet symmetric, since $\tilde{\alpha}_{m+1}$ is never crossed out. To make it fully symmetric, we have to take the permutation classes (π) in both binomial (2.72) and monomial (2.74) parts. When we sum up the volumes of all cells in $\phi_{p,q}$ with $p + q = m$, some cancellations occur (i.e. in the total volume all monomials $\alpha_{i_1} \dots \alpha_{i_k}$ with $k < m - 1$ are cancelled), which results in (2.83). The same type of cancellation happens if we add one extra dimension, since the formula is symmetrized (thanks to the permutations involved), and only the number of factors is increased by one. Therefore, $\{\phi_{p,q}\}$ are well-defined initial forms for any $m \geq 2$. □

The following result implies that for any m-vertex quiver with $C = \mathrm{diag}(\alpha, \dots, \alpha)$ its quiver A-polynomial is tempered, and therefore quantizable.

Theorem 2.5.1. *The initial forms $\{\phi_{p,q}\}_{p+q=m}$ are in bijection with face polynomials for a diagonal quiver if and only if $(\alpha_1, \dots, \alpha_m) = (\alpha, \dots, \alpha)$, as shown in figure 2.10.*

Proof. We have

$$\phi_{0,0}^{\min} = (-1)^{\prod \alpha_j + \sum \prod \alpha_{j'}} a_1^{\prod \alpha_j} \prod b_{j,0}^{\prod_{j' \neq j} \alpha_{j'}}, \qquad \phi_{0,0}^{\max} = a_0^{\prod \alpha_j} \prod b_{j,2}^{\prod_{j' \neq j} \alpha_{j'}}. \tag{2.88}$$

These monomials produce the highest powers of y in the quiver A-polynomial and correspond to the marked vertices of $N(A)$ in figure 2.10, where we denote $\phi_0 := \phi_{0,0}$. Let us write explicitly

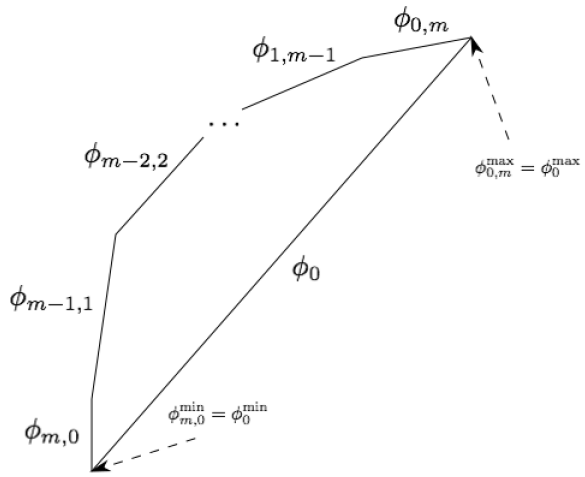

Figure 2.10: The Newton polygon for quiver A-polynomial with $C = \mathrm{diag}(\alpha, \dots, \alpha)$.

the extremal monomials for $\phi_{p,q}$:

$$\begin{aligned}
\phi_{p,q}^{\min} &= \mu_{p,q} \cdot \prod_{\pi(I,K)} (-1)^{1+\sum_{k\in K}\prod_{\substack{k'\in K\\ k'\neq k}}(\alpha_{k'}-1)} \left(a_1 \prod_{i\in I} b_{i,0}\right)^{\prod_{k\in K}(\alpha_k-1)} \prod_{k\in K} b_{k,1}^{\prod_{\substack{k'\in K\\ k'\neq k}}(\alpha_{k'}-1)} \\
\phi_{p,q}^{\max} &= \mu_{p,q} \cdot \prod_{\pi(I,K)} \left(a_0 \prod_{i\in I} b_{i,1}\right)^{\prod_{k\in K}(\alpha_k-1)} \prod_{k\in K} b_{k,2}^{\prod_{\substack{k'\in K\\ k'\neq k}}(\alpha_{k'}-1)}
\end{aligned} \tag{2.89}$$

For example, the first few monomials project onto (x, y) plane as

$$\begin{aligned}
\phi_{m,0}^{\min}: \ (0,0), \quad \phi_{m,0}^{\max}: \ (0,1), \\
\phi_{m-1,1}^{\min}: \ (0,1), \quad \phi_{m-1,1}^{\max}: \ \left(m, 1+\sum_{i=1\dots m}(\alpha_i - 1)\right)
\end{aligned} \tag{2.90}$$

where $(x_i, y_i) = (\deg(\phi_*^{\min/\max}, x), \deg(\phi_*^{\min/\max}, y))$. The vertical edge given by $\phi_{m,0}$ is always presented in $A(x, y)$, since it encodes the analytic branch of $y(x)$.

Now we discuss how a mixed decomposition can be further partitioned by dividing each cell into even smaller cells. This implements a map sending a face to its sub-face. We can think of it acting on the two mutually dual levels: 1) the level of mixed decompositions, and 2) the level of diagrams. If we have a simple initial form supported on a face, we can apply this map to each of its diagrams as follows. Take a diagram which corresponds to some $\varphi_{I,K}$ in (2.72):

$$\varphi_{I,K} \ = \tag{2.91}$$

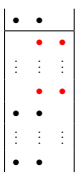

and perform the following steps:

1. in the first equation F_0, highlight the leftmost (rightmost) dot, by putting it into the "box"

2. in the rest of equations $F_1, \dots, F_m$, do the same for the rightmost (leftmost) dots: either

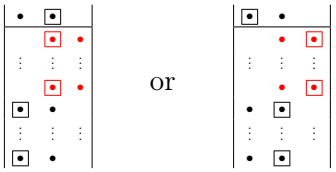

(2.92)

3. copy this diagram as many times as the number of its rows, every time removing one of the dots which are not in the box:

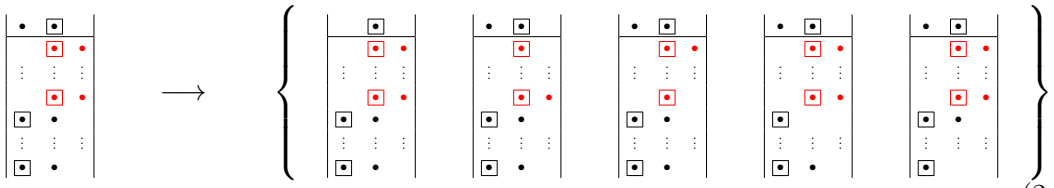

(2.93)

which corresponds to the map

$$\text{edge} \qquad \longrightarrow \qquad \text{vertex}$$

4. the resulting diagrams correspond to a vertex of $N(\mathcal{R})$: a tail or a head of an edge given by $\varphi_{I,K}$ (if the leftmost or rightmost configuration is chosen, respectively)

Therefore, if we have just a single diagram (remember that it always corresponds to an edge), there are only two options: detalization gives either its head or tail vertex, since we assume that the head is always above the tail). On another hand, if the face has a bigger dimension, we can apply detalization to each of its diagrams independently, each time choosing either a head or a tail. In this way, all possible choices generate the complete set of sub-faces (figure 2.11 shows an example of such partition).

This shows how the aforementioned steps apply. For example, the underlined diagrams in figure 2.11 form the pattern (2.93). The choice of either rightmost or leftmost boxes implements the cubical flip inside each hexagon. In figure 2.7 the middle mixed decomposition corresponds to the 2-dimensional face b, whereas each of the four subdivisions give one of its edges.

Let's prove an important intermediate statement, which clarifies the incidence relations for $\{\phi_{p,q}\}$.

Proposition 2.5.3. $\phi^{\max}_{m-i,i} = \phi^{\min}_{m-i-1,i+1}, \ \forall i = 0 \dots m; \ m \geq 2.$

Proof. We check whether $\phi^{\max}_{2,1} = \phi^{\min}_{1,2}$ for $C = \operatorname{diag}(\alpha_1, \alpha_2, \alpha_3)$. Firstly, we subdivide $\phi_{2,1} \ =$

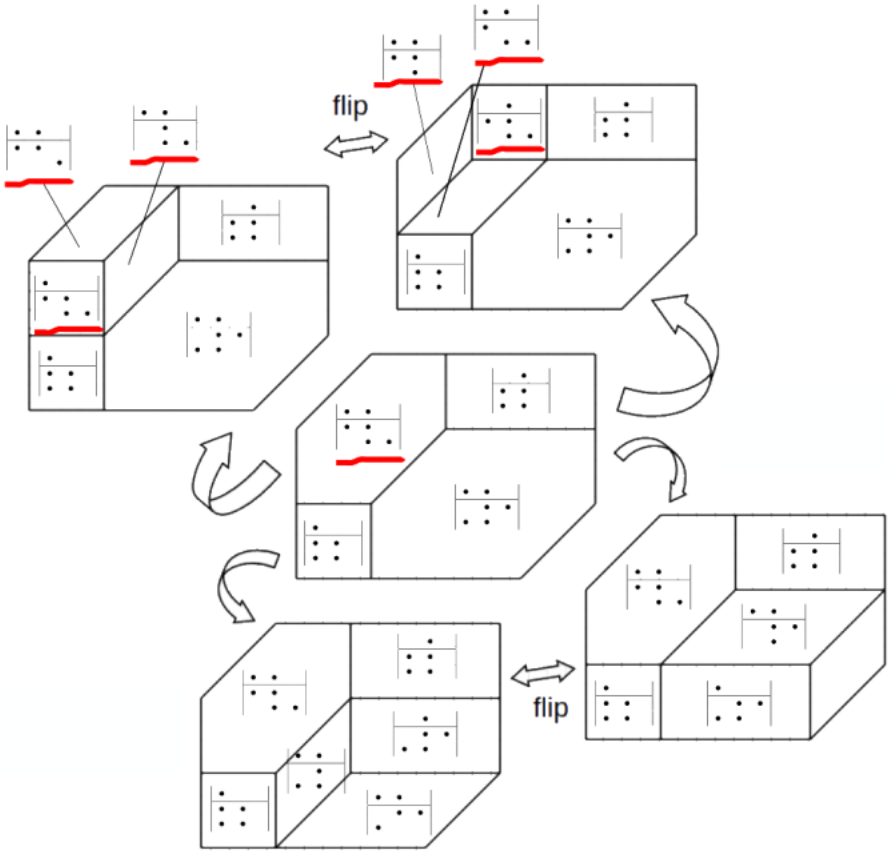

Figure 2.11: Four distinct subdivisions of $\phi_{1,1}$, which are related by cubical flips.

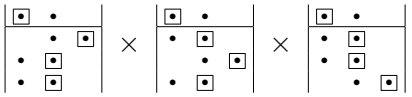 as follows

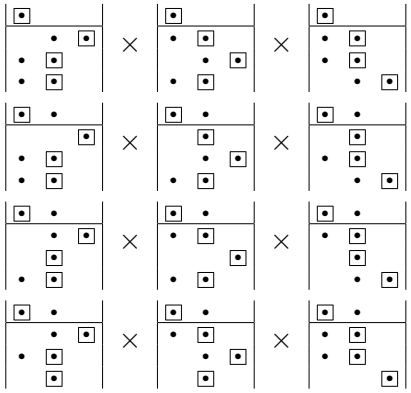

(2.94)

The boxed monomials remain non-zero and we do not cross them out. This results in the decomposition of each diagram in $\phi_{2,1}$ into four copies forming a column in (2.94), all of which define $\phi_{2,1}^{\max}$. The monomial $\mu_{2,1}$:

(a_0) :  (a_1) : 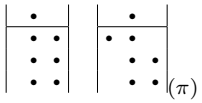 $(b_{*,0})$: 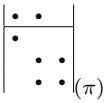

(2.95)

Now we do the same thing for $\phi_{1,2}$ $=$ 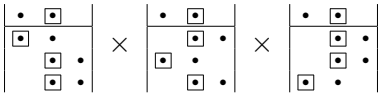 .

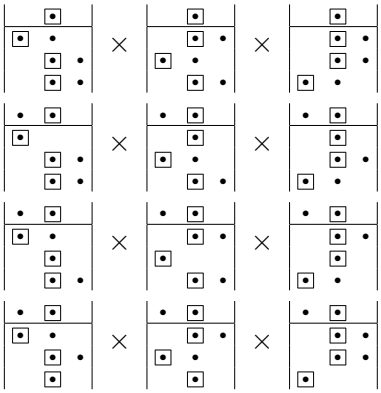

(2.96)

The monomial $\mu_{1,2}$:

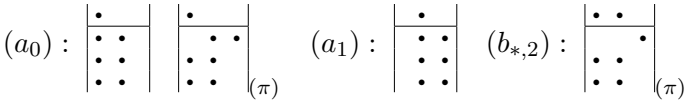

(2.97)

We see that the binomial counterparts of both $\phi^{\max}_{1,2}$ and $\phi^{\min}_{2,1}$ have the identical collections of $b_{*,1}$-diagrams. Moreover, it immediately extends to any $\phi_{p,q}$, since detalizing any of $b_{*,1}$ corresponds to taking a row of the form [••] or [••]. So, in order to get the maximum (minimum), we remove the left (right) neighbouring "•", which results in the same diagram. Next, comparing the a_0- and a_1-diagrams, we see that those ones, which are in the binomial part of $\phi^{\min}_{2,1}$, coincide with the μ-part in $\phi^{\max}_{2,1}$, and vice versa. This is also true for $b_{*,2}$ counterpart (follows from Proposition 2.5.2). Therefore, the two extremal monomials are equal. This rule extends to any p, q (the only difference is that we have to consider larger permutations), hence the claim. □

Returning to theorem 2.5.1, it is left to show that after the principal specialization (2.47) the x- and y-degrees of each monomial in $\phi_{p,q}$ grow linearly. In other words they project onto the same segment and $\phi_{p,q}$ gives a face polynomial of $A_C(x, y)$.

$\mathcal{H}^{(1)}_{p,q}$	$\mathcal{H}^{(2)}_{p,q}$	$\mathcal{H}^{(3)}_{p,q}$
min	min	min
min	min	max
min	max	min
min	max	max
max	min	min
max	min	max
max	max	min
max	max	max

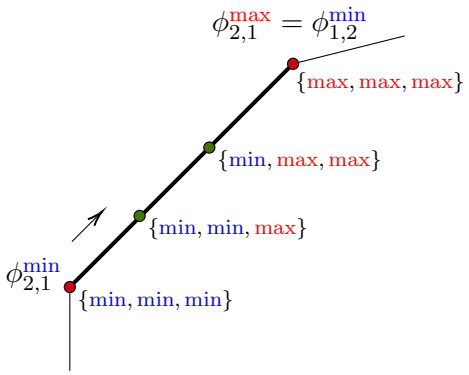

Figure 2.12: The principal specialization of $\phi_{2,1}$ (analogously for $\phi_{1,2}$).

Compare $\phi_{2,1}$ and $\phi_{1,2}$. Each of them contains three distinct binomial factors $\mathcal{H}^{(i)}_{p,q}$ and monomials given by the triples min/max, figure 2.5.3. We perform the following steps: make

the a_1 (a_0) dot frozen: $\boxed{\bullet}$, along with all the leftmost (rightmost) b-type dots, as in (2.94). Then duplicate the diagram by removing each non-frozen dot, to obtain a collection of diagrams corresponding to a single coefficient in a non-negative power (to define extremal monomial).

Recall that the binomial counterpart of $\phi_{2,1}^{\min}$ does not depend on neither a_0 nor $b_{i,2}$, which means that the (x,y)-coordinates of the minimal monomial are completely fixed by $\mu_{2,1}$. Moving to the next order gives an increment to both x- and y- degrees of $\mu_{2,1}$ (which we denote as $\tilde{\mu}_x$ and $\tilde{\mu}_y$). For the fist increment, we replace a single "min" by "max", say, in $\mathcal{H}_s := \mathcal{H}_{p,q}^{(s)}$ for $s \in \{1,2,3\}$. This amounts to changing the frozen configuration, so that the a_0-degree gets the increment $+\prod_{j\in K'_s}(\alpha_j - 1)$, where K'_s is attached to $\mathcal{H}_s$. If we do that again, we modify yet another factor $\mathcal{H}_{s'}$, getting the increment: $a_0 \mapsto a_0 + \prod_{j\in K'_{s'}}(\alpha_j - 1)$, and so on, until we reach $\phi_{2,1}^{\max} \simeq (\max, \max, \max)$.

Therefore, each time by switching min to max, we get the increments for the (x,y)-coordinates of a monomial on the edge of $N(A)$:

$$x \mapsto x + \sum_{r=1\ldots m} \prod_{j\in K'_s\setminus\{r\}} (\alpha_j - 1), \quad y \mapsto y + \prod_{j\in K'_s} (\alpha_j - 1), \tag{2.98}$$

We see that the increment, being a function of $(\alpha_1, \ldots, \alpha_m)$, is non-linear. Now it becomes clear by looking at (2.98) that it is linear only when α_i are all equal. Of course the (x,y)-degree of the monomial does not depend on permutation (i.e. $(\min, \min, \max)$ and $(\max, \min, \min)$ are indistinguishable after the (x,y)-projection). Therefore, eight monomials of $\phi_{2,1}$ (or $\phi_{1,2}$) are mapped onto four points on the edge of $N(A)$. The endpoints of an edge in figure 2.5.3 correspond to minimal and maximal powers of a_0 and the corresponding diagram has an identity permutation only, which shows that such extremal monomial is unique. On another hand, intermediate points on a face always correspond to several permutations and therefore produce several monomials. If $\alpha_i = \alpha$ for $i = 1, \ldots, m$, then all monomials of $\phi_{p,q}$ lie on the same edge of the Newton polygon and therefore completely describe the face polynomial, which completes the proof of theorem 2.5.1. □

Summing up, we have confirmed that quiver A-polynomial for $C = \mathrm{diag}(\alpha, \ldots, \alpha)$ is tempered. Although we were not able to prove it for an arbitrary quiver, there is a lot of evidence for the statement to be true. In the next chapter we proceed to topological recursion for the Nahm sums and use the advantage that quiver A-polynomial is quantizable in a class of examples.

Chapter 3

Topological recursion for Nahm sums and quantum Airy structures

In this chapter we verify whether Nahm sums can be reconstructed by means of the topological recursion. We select several two-vertex quivers with genus zero quiver A-polynomials (in the principal specialization) and apply to them the topological recursion. If the results are positive, then topological recursion can in principle compute all invariants encoded in a quiver, such as quantum knot polynomials, counts of topological strings, lattice paths, and other related objects. In general the A-model for a quiver is not known, but we know that its partition function takes form of the Nahm sum. Besides, there is a good amount of evidence that such A-model exists [24] (as in the case of the knots-quivers correspondence), and one way to confirm the existence of the A-model, is to postulate the B-model and apply the topological recursion. If the latter is functorial, the A-model should be well-defined. Therefore our main focus is on the topological recursion wave functions constructed from classical quiver A-polynomials and verification whether the $\hbar$-expansions of Nahm sums agree with the perturbative result given by the topological recursion, order by order in $\hbar$. The results of section 3.5 are presented in [58].

Another interesting class of examples comes from quantum Airy structures, which generalize the topological recursion and take form of an algebra of differential operators. They are closely related to vertex operator algebras and orbifold CFTs. To a date, such structures are not known for Nahm sums. However, there is an evidence suggesting such a relation, for example in the context of the refined volume conjecture [117]. We investigate one version of such structure, related to a spectral curve with non-simple ramification point. The results of section 3.6.2 are presented in [57].

3.1 A bird's-eye view on topological recursion

Topological recursion originated from Hermitian one-matrix model [3]. Shortly after it was found that this recursion admits a diagrammatic description in terms of punctured surfaces [118, 119]. The next step was its generalization to the case of an arbitrary spectral curve [120]. Subsequently it was realized that the recursion has numerous applications, which go beyond the matrix models formalism (see, for example, [121] for a brief survey).

An essential ingredient for the topological recursion (at least in its original formulation) is a spectral curve. In the next section we will derive spectral curves for matrix models and then proceed to the general definition. In short, topological recursion spectral curve is a pair of complex-valued meromorphic functions (one of them has to be a ramified cover) on a Riemann surface which obey some polynomial equation. In practice we start from a defining polynomial and find its parametrization to obtain the initial data for the recursion (different choice of parametrization leads to different result of the recursion computation). There are two kinds of curves that we consider:

$$\begin{aligned} P(x,y) = 0,\ (x,y) \in \mathbb{C}\times\mathbb{C} \qquad & \text{usual variables} \\ A(e^u, e^v) = 0,\ (u,v) \in \mathbb{C}\times\mathbb{C} \qquad & \text{exponential variables} \end{aligned} \tag{3.1}$$

For example, all hermitian matrix models with polynomial potential lead to spectral curves in usual variables (where the the topological recursion was first detected). On another hand, knot A-polynomials, topological strings and quivers correspond to exponential variables.

So what kind of invariants does the topological recursion compute? By definition, it assigns an infinite tower of correlation differentials to a given spectral curve. Such differentials are denoted as $\omega_{g,n}$ and represented as punctured surfaces (figure 3.1) of genus g and n marked points (boundaries). The condition $2g-2+n>0$ manifests that $\omega_{0,1}$ and $\omega_{0,2}$ are the initial

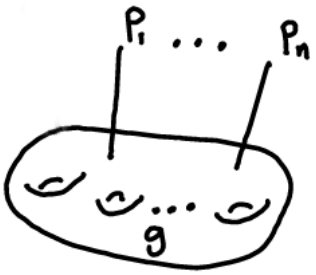

Figure 3.1: Pictorial presentation of $\omega_{g,n}$.

data for the recursion, which then runs over the Euler characteristic of such differentials. From the bird's-eye view, the topological recursion consists of the two main steps:

1. solving the problem for the simplest topologies: $\omega_{0,1}$ (a disk), $\omega_{0,2}$ (a cylinder), $\omega_{0,3}$ (a pair of pants)

2. understanding the behaviour when the topologies are glued (like a pair of pants), or, in another direction, degenerated (one removes a pair of pants or degenerates the surface)

3.2 Topological recursion from matrix models

We start by reviewing matrix models, spectral curves, loop equations, and from these derive the topological recursion. Most of the material is nicely exposed in the lectures [122]. We are focusing on the one-matrix integral, which is an instance of closed partition function (3.56):

$$Z = \langle 1 \rangle := \int dM \exp\left\{-N \operatorname{Tr} V(M)\right\} \tag{3.2}$$

where M is a $N \times N$ complex matrix, and $V(M)$ is the potential, which we assume to be polynomial in M. Additionally, we take M to be hermitian. In this case the integral (3.2) is also called hermitian. Integration measure is

$$dM = \prod_{i<j}^{N} d\,(\mathrm{Re}\ M_{ij})\, d\,(\mathrm{Im}\ M_{ij}) \prod_{i=1}^{N} dM_{ii} \tag{3.3}$$

The matrix integral (3.2) admits $\frac{1}{N}$-expansion in only even powers of $\frac{1}{N}$ (with $\hbar = \frac{1}{N^2}$):

$$Z = e^{\tilde{F}}, \quad \tilde{F} = N^2 \tilde{F}_0 + \tilde{F}_1 + \frac{1}{N^2}\tilde{F}_2 + O(\frac{1}{N^3}). \tag{3.4}$$

The simplest non-trivial case of cubic potential would be:

$$Z = \int dM \exp\left\{-N\,\mathrm{Tr}\left(t_2\frac{M^2}{2} + t_3\frac{M^3}{3}\right)\right\}, \tag{3.5}$$

where t_2 and t_3 are continuous parameters ("times"). To warm up, let us show that such integral already knows something about the topology of Riemann surfaces. Denote the Gaussian counterpart

$$Z_0 := \int dM \exp\left\{-N\,\mathrm{Tr}\left(t_2\frac{M^2}{2}\right)\right\} \tag{3.6}$$

and expand $\frac{Z}{Z_0}$ in powers of N:

$$\frac{1}{Z_0}\int dM e^{-N\,\mathrm{Tr}(M^2)}\left(1 - N\frac{t^3}{3}\,\mathrm{Tr}(M^3) + \frac{N^2}{2!}\left(\frac{t^3}{3}(\mathrm{Tr}(M^3))^2\right) - \frac{N^3}{3!}\left(\frac{t^3}{3}(\mathrm{Tr}(M^3))^3\right) + \dots\right) \tag{3.7}$$

The powers of traces can be written as

$$\begin{aligned}
\mathrm{Tr}(M^3) &= \sum_{i,j,k} M_{ij}M_{jk}M_{ki}, \\
\mathrm{Tr}(M^4) &= \sum_{i,j,k,l} M_{ij}M_{jk}M_{kl}M_{li}, \\
\left(\mathrm{Tr}(M^3)\right)^2 &= \sum_{\substack{i_1,j_1,k_1 \\ i_2,j_2,k_2}} M_{i_1j_1}M_{j_1k_1}M_{k_1i_1}M_{i_2j_2}M_{j_2k_2}M_{k_2i_2},
\end{aligned} \tag{3.8}$$

and so on. Using Wick's theorem which states that

$$\frac{1}{Z_0}\int DM e^{-N\,\mathrm{Tr}(M^2)} M_{i_1,j_1}M_{i_2,j_2}\dots M_{i_{2n},j_{2n}} = \sum_{\text{complete pairings}} \overbrace{M^{(1)}M^{(2)}}\overbrace{M^{(3)}M^{(4)}}\dots \tag{3.9}$$

(for odd number of M's it is always zero), where each pairing is given by a simple formula:

$$\overbrace{M\ M} = \frac{1}{Nt_2}\delta_{i_1j_2}\delta_{j_2i_1}, \tag{3.10}$$

we can rewrite the expansion (3.7) as a sum over graphs (Feynman diagrams). Figure 3.2 shows how it works for $\mathrm{Tr}(M^4) = \sum_{i,j,k,l} M_{ij}M_{jk}M_{kl}M_{li}$: we connect pairs of indices to make

a directed graph, and then perform all possible identifications according to (3.9), which results into "fattened" graphs, also called *ribbon graphs*. They can be drawn on Riemann surfaces of various genera. Therefore, $\frac{1}{N}$-expansion of matrix integral can be re-written as an infinite sum over such graphs. It appears that the graphs can be re-collected according to the genus of the corresponding surfaces, and we obtain the genus expansion of our closed partition function Z. The closed free energy would then have an expansion:

$$\tilde{F} = \sum_{g=0}^{\infty} N^{2g-2} \tilde{F}_g \tag{3.11}$$

which terms are represented by graphs.

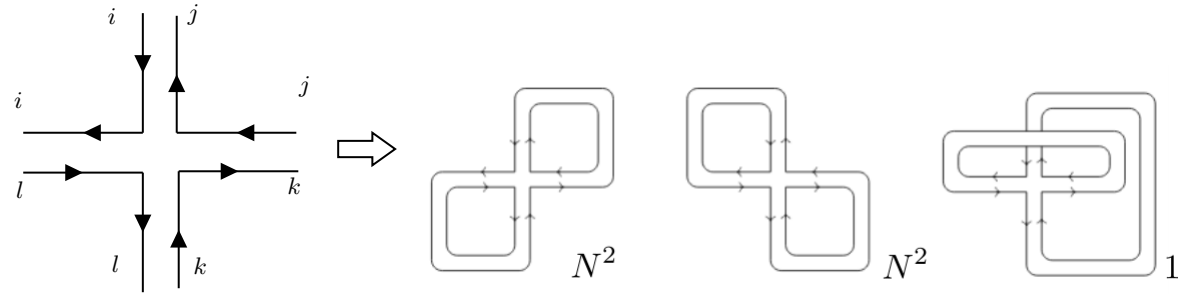

Figure 3.2: Applying Wick's theorem to $\mathrm{Tr}(M^4)$ leads to the following three ribbon graphs, two of them being planar; corresponding powers of $\frac{1}{N}$ are Euler characteristics $\chi(G) = \#\text{vertices} - \#\text{edges} + \#\text{faces}$

Using the fact that M is hermitian, and the measure (3.3) is invariant upon conjugation $M \mapsto UMU^\dagger$, where U is a unitary matrix, we can diagonalize $M = U\Lambda U^\dagger$ with $\Lambda = \mathrm{diag}(\lambda_1, \ldots, \lambda_N)$, and re-write (3.2) as an integral over eigenvalues:

$$Z = \int \prod_{i=1}^{N} d\lambda_i \Delta^2(\lambda) \exp\left\{ -N \sum_{i=1}^{N} V(\lambda_i) \right\} \tag{3.12}$$

where $\Delta = \prod_{1 \le i < j \le N} (\lambda_j - \lambda_i)$ is Vandermonde determinant. We can put the Vandermonde further into the exponential:

$$Z = \int \prod_{i=1}^{N} d\lambda_i \exp\left\{ -N \sum_{i=1}^{N} V(\lambda_i) + \sum_{i \neq j} \log|\lambda_i - \lambda_j| \right\} \tag{3.13}$$

This integral encodes distribution of eigenvalues. It resembles the Coulomb gas of particles. Therefore, for large N we can apply saddle-point approximation to the integral to obtain spectral curve, which determines universal properties of our matrix integral. Denote

$$S(\lambda_1, \ldots, \lambda_N) = -N \sum_{i=1}^{N} V(\lambda_i) + \sum_{i \neq j} \log|\lambda_i - \lambda_j| \tag{3.14}$$

the action; and assume polynomiality of V. The saddle points are given by the critical points

of the action: $\frac{\partial S}{\partial \lambda_i} = 0$, which gives

$$V'(\lambda_i) = \frac{2}{N} \sum_{æ \neq i} \frac{1}{\lambda_i - \lambda_j},\ i = 1 \dots N \tag{3.15}$$

where $V'(x) := \frac{dV}{dx}$. Since V is polynomial, we are guaranteed to have finitely many solutions to (3.15). Let's pick any such solution $(\overline{\lambda}_1, \dots, \overline{\lambda}_N)$ and define the resolvent:

$$W(x) := \frac{1}{N} \sum_{i=1}^{N} \frac{1}{x - \overline{\lambda}_i} \tag{3.16}$$

where x is a continuous parameter. It can be shown to satisfy Riccati equation:

$$W(x)^2 + \frac{1}{N} W'(x) = V'(x) W(x) - P(x)\ . \tag{3.17}$$

Define $\overline{W} := \lim_{N \to \infty} W$. The equation (3.17) in the large N limit transforms into the algebraic equation for $\overline{W}$:

$$\overline{W}^2 - V \overline{W} + \overline{P} = 0 \tag{3.18}$$

This shows that $\overline{W}$ is a multi-valued function on the complex plane. Alternatively, we can think of it as a single valued function, but living on a two-sheet covering of the complex plane (the two sheets correspond to branches of 3.18). This picture gives geometry of a Riemann surface, which we denote by Σ. We get:

$$\overline{W}(x(t)) = y(t), \tag{3.19}$$

where $y : \Sigma \to \mathbb{C}$ is single-valued and meromorphic fucntion on Σ. Therefore, from the matrix model we naturally obtain a triple

$$(\Sigma, x(t), y(t)) \tag{3.20}$$

where $x(t)$ and $y(t)$ are two meromorphic functions on Σ. These two functions satisfy the equation:

$$y^2 - V'(x) y + \overline{P}(x) = 0 \tag{3.21}$$

which defines the *spectral curve* for our matrix model, where $\overline{P}(x) := V'(x)\overline{W}(x) - \overline{W}(x)^2$. For example, gaussian integral Z_0 (3.6) gives:

$$\overline{W} = \frac{1}{2}(x - \sqrt{x^2 - 4}) \tag{3.22}$$

We are interested in correlation functions for our model, e.g., the moments:

$$\left\langle \operatorname{Tr} M^k \right\rangle = \frac{1}{Z_0} \int dM (\operatorname{Tr} M^k) \exp\{-N\ \operatorname{Tr} V(M)\} \tag{3.23}$$

And we also define matrix model wave function as the following integral:

$$\psi(x) := \left\langle \operatorname{Tr} \frac{1}{x - M} \right\rangle \tag{3.24}$$

Its expansion has form:

$$\psi(x) \simeq \exp\left(\frac{1}{\hbar}S_0(x) + S_1(x) + \hbar S_2(x) + O(\hbar^2)\right), \tag{3.25}$$

i.e. all powers of $\hbar$ are involved, starting from $\frac{1}{\hbar}$ (compare with the closed partition function (3.2), where we had only even powers of $\hbar$). One can use the following identity

$$\sum_{i,j}\int_\Gamma dM\,\frac{\partial}{\partial M_{ij}}\left(\left(M^k\right)_{ij}\,e^{-N\,\mathrm{Tr}\,V(M)}\right) = 0\ . \tag{3.26}$$

to compute the first *loop equation*:

$$\sum_{l=0}^{k-1}\Big\langle\,\mathrm{Tr}\,M^l\,\mathrm{Tr}\,M^{k-l-1}\Big\rangle - N\Big\langle\,\mathrm{Tr}\,M^kV'(M)\Big\rangle = 0\ . \tag{3.27}$$

More generally, we may use

$$\sum_{i,j}\int_\Gamma dM\,\frac{\partial}{\partial M_{ij}}\left((M^{\mu_1})_{ij}\,\mathrm{Tr}\,M^{\mu_2}\cdots\mathrm{Tr}\,M^{\mu_n}\,e^{-N\,\mathrm{Tr}\,V(M)}\right) = 0\ . \tag{3.28}$$

Which then results into more general loop equation for moments:

$$\begin{aligned}\sum_{l=0}^{\mu_1-1}\Big\langle\,\mathrm{Tr}\,M^l\,\mathrm{Tr}\,M^{\mu_1-l-1}\prod_{i=2}^{n}\mathrm{Tr}\,M^{\mu_i}\Big\rangle + \sum_{j=2}^{n}\mu_j\Big\langle\,\mathrm{Tr}\,M^{\mu_1+\mu_j-1}\prod_{\substack{i=2\\ i\neq j}}^{n}\mathrm{Tr}\,M^{\mu_i}\Big\rangle = \\ N\Big\langle\,\mathrm{Tr}\,V'(M)M^{\mu_1}\prod_{i=2}^{n}\mathrm{Tr}\,M^{\mu_i}\Big\rangle\,.\end{aligned} \tag{3.29}$$

Now our aim is to re-write the loop equation for general correlation functions, not only moments. Recall that we had the resolvent (3.16), for which we now put the index "one":

$$W_1(x) = \left\langle\sum_{i=1}^{N}\frac{1}{x-\lambda_i}\right\rangle = \left\langle\,\mathrm{Tr}\,\frac{1}{x-M}\right\rangle = \sum_{\mu=0}^{\infty}x^{-\mu-1}\left\langle\,\mathrm{Tr}\,M^\mu\right\rangle\ . \tag{3.30}$$

We define higher (connected) correlation functions as follows:

$$W_n(x_1,\cdots x_n) = \left(\frac{\beta}{2}\right)^{\frac{n}{2}}\left\langle\,\mathrm{Tr}\,\frac{1}{x_1-M}\cdots\mathrm{Tr}\,\frac{1}{x_n-M}\right\rangle_{\mathrm{c}}, \tag{3.31}$$

where the cumulant $\langle\ \rangle_{\mathrm{c}}$ is defined from the summation formula:

$$\langle p_{\mu_1,\ldots,\mu_l}\rangle = \sum_{k=1}^{l}\sum_{\sqcup I_j=\{\mu_1,\ldots,\mu_l\}}\prod_{j=1}^{k}\langle p_{I_j}\rangle_{\mathrm{c}}\,, \tag{3.32}$$

meaning that the expectation values of $p_\mu = \prod_{j=1}^{\ell} \operatorname{Tr} M^{\mu_j}$, are the sums over partitions:

$$\langle p_{(\mu_1)} \rangle = \langle p_{(\mu_1)} \rangle_{\mathrm{c}} \ , \tag{3.33}$$

$$\langle p_{(\mu_1,\mu_2)} \rangle = \langle p_{(\mu_1,\mu_2)} \rangle_{\mathrm{c}} + \langle p_{(\mu_1)} \rangle \langle p_{(\mu_2)} \rangle \ , \tag{3.34}$$

$$\langle p_{(\mu_1,\mu_2,\mu_3)} \rangle = \langle p_{(\mu_1,\mu_2,\mu_3)} \rangle_{\mathrm{c}} + \langle p_{(\mu_1)} \rangle \langle p_{(\mu_2,\mu_3)} \rangle_{\mathrm{c}} + \langle p_{(\mu_2)} \rangle \langle p_{(\mu_1,\mu_3)} \rangle_{\mathrm{c}} + \langle p_{(\mu_3)} \rangle \langle p_{(\mu_1,\mu_2)} \rangle_{\mathrm{c}} + \langle p_{(\mu_1)} \rangle \langle p_{(\mu_2)} \rangle \langle p_{(\mu_3)} \rangle \ . \tag{3.35}$$

For instance,

$$\langle p_{(\mu_1,\mu_2,\mu_3)} \rangle_{\mathrm{c}} = \langle p_{(\mu_1,\mu_2,\mu_3)} \rangle - \langle p_{(\mu_1)} \rangle \langle p_{(\mu_2,\mu_3)} \rangle - \langle p_{(\mu_2)} \rangle \langle p_{(\mu_1,\mu_3)} \rangle - \langle p_{(\mu_3)} \rangle \langle p_{(\mu_1,\mu_2)} \rangle + 2 \langle p_{(\mu_1)} \rangle \langle p_{(\mu_2)} \rangle \langle p_{(\mu_3)} \rangle \ . \tag{3.36}$$

One can show (as a consequence of (3.29)) that the following recursion holds for W_n:

$$W_{n+2}(x,x,I) + \sum_{J \subset I} W_{1+|J|}(x,J)\, W_{1+n-|J|}(x, I \backslash J) + \sum_{i=1}^{n} \frac{\partial}{\partial x_i} \frac{W_n(x, I \backslash \{x_i\}) - W_n(I)}{x - x_i} = N \Big(V'(x) W_{n+1}(x,I) - P_n(x;I) \Big) \ , \tag{3.37}$$

where $I = \{x_1, \dots, x_n\}$, and

$$P_n(x; x_1, \dots, x_n) := \left(\frac{\beta}{2} \right)^{\frac{n+1}{2}} \left\langle \operatorname{Tr} \frac{V'(x) - V'(M)}{x - M} \prod_{i=1}^{n} \operatorname{Tr} \frac{1}{x_i - M} \right\rangle_{\mathrm{c}} \tag{3.38}$$

We are already very close to topological recursion. In fact, it would be a re-formulation of the equation (3.37).

We need to define recursion on two parameters: g (genus) and n (the number of marked points). For this purpose, we use the topological expansion of a (connected) correlation function as the formal asymptotic expansion:

$$W_n = \sum_{g=0}^{\infty} N^{2-2g-n} W_{g,n} \ . \tag{3.39}$$

Now plugging this into (3.37) and determining the first few orders, we get:

$$W_{0,1} = \frac{1}{2} \left(V' - M\sqrt{\sigma} \right) \qquad \text{where} \qquad (V')^2 - 4P_{0,0} = M^2 \sigma \ , \tag{3.40}$$

Next, for $W_{0,2}$:

$$W_{0,2}(x,x') = \frac{\frac{\partial}{\partial x'}\frac{W_{0,1}(x)-W_{0,1}(x')}{x-x'} + P_{0,1}(x;x')}{V'(x)-2W_{0,1}(x)} , \tag{3.41}$$

$$= -\frac{1}{2(x-x')^2} + \frac{\frac{\partial}{\partial x'}\frac{M(x')\sqrt{\sigma(x')}}{2(x-x')} + \frac{\partial}{\partial x'}\frac{V'(x)-V'(x')}{2(x-x')} + P_{0,1}(x;x')}{M(x)\sqrt{\sigma(x)}} . \tag{3.42}$$

It is useful to rewrite correlation functions as differential forms on the Riemann sphere:

$$\omega_{g,n}(z_1,\dots,z_n) = W_{g,n}(x_1,\dots,x_n)dx_1\dots dx_n + \delta_{g,0}\delta_{n,2}\frac{dx_1 dx_2}{(x_1-x_2)^2} , \tag{3.43}$$

where $x_i = x(z_i)$. For example,

$$\omega_{0,2} = B\left(z,z'\right) = \frac{dz\ dz'}{(z-z')^2} . \tag{3.44}$$

which is the fundamental 2nd kind differential on the Riemann sphere. Introducing the *recursion kernel*

$$K(z,z') = \frac{1}{2w(z')dx(z')}\int_{\frac{1}{z'}}^{z'} B(z,\cdot) = \frac{1}{2w(z')dx(z')}\left(\frac{1}{z-z'} - \frac{1}{z-\frac{1}{z'}}\right)dz , \tag{3.45}$$

we finally obtain for $2g-2+n>0$:

$$\begin{aligned}\omega_{g,n}(z_1,\cdots z_n) = \sum_{\eta=\pm1}\operatorname*{Res}_{z=\eta} K(z_1,z)\Bigg[&\omega_{g-1,n+1}(z,\tfrac{1}{z},z_2,\cdots z_n) \\ &+ {\sum_{\substack{h+h'=g\\ I\sqcup I'=\{z_2,\cdots z_n\}}}}' \omega_{h,1+|I|}(z,I)\omega_{h',1+|I'|}(\tfrac{1}{z},I')\Bigg] ,\end{aligned} \tag{3.46}$$

where the modified summation $\sum'$ excludes the terms $(h,I)=(0,\emptyset)$ and $(h,I)=(g,\{z_2,\cdots z_n\})$. The formula (3.46) is the topological recursion for matrix model of the type (3.2). $\omega_{g,n}$ possess the following properties:

- $\omega_{g,n}(z_1,\dots,z_n)$ is a rational, symmetric function of $z_1,\dots,z_n$,
- they have poles at $z_i=\pm1$ only,
- the antisymmetry property

$$2g-2+n>0 \quad\Longrightarrow\quad \omega_{g,n}(\tfrac{1}{z_1},\dots,z_n) = -\omega_{g,n}(z_1,\dots,z_n) . \tag{3.47}$$

The punchline is that the correlation functions are completely determined by the loop equations (here considered for the one-cut case, but it also holds in a much greater generality). Also,

$\omega_{g,0}$ need to be defined separately from (3.46):

$$g \geq 2: \quad \omega_{g,0} := \frac{1}{2-2g} \sum_a \mathrm{Res}_{q \to a} \ \omega_{g,1}(q)\, \Phi(q) \tag{3.48}$$

where $d\Phi = \omega_{0,1}$. Notice that if the potential V does not depend on "times", $\omega_{g,0}$ are simply scalars. If the times are switched on, they become rational functions of times.

3.3 Topological recursion: axiomatic definition

In the previous section we have showed how the topological recursion follows from the matrix model loop equations. On another hand, instead of proving it as a theorem, we may take it as a definition. This would open new perspectives for an enormous number of problems, for which the matrix model is not known, but there is a suitable spectral curve.

Definition 3.3.1. *Topological recursion spectral curve is the data*

$$\{\Sigma_0,\ x(t),\ y(t),\ \omega_{0,2}(t_1,t_2)\} \tag{3.49}$$

where Σ_0 is a Riemann surface of a non-negative genus, $x(t)$ and $y(t)$ are meromorphic functions on Σ_0, and $\omega_{0,2}(t_1,t_2)$ is a fundamental bi-differential (Bergman kernel), which is symmetric and has a double pole on diagonal. Moreover, there are values of t such that $dx(t) = 0$.

We also define meromorphic differential $\omega_{0,1} = ydx$. Note that if Σ_0 is of genus zero, then $\omega_{0,2}$ has a canonical form

$$\omega_{0,2}(t_1,t_2) = \frac{dt_1 dt_2}{(t_1-t_2)^2} + \text{holomorphic terms.} \tag{3.50}$$

Denote *Ram* the set of ramification points of $x(t)$, that is, the set of zeroes of dx together with

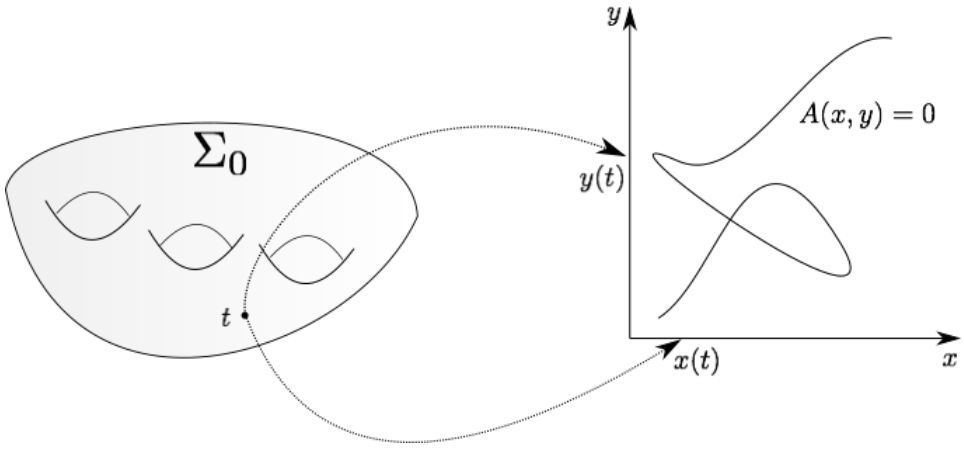

Figure 3.3: Topological recursion spectral curve.

the set of poles of x of order ≥ 2. For each $a \in Ram$, denote σ_a a local Galois involution, s.t.

$u(\sigma_a(t)) = u(t)$, and $\sigma_a(a) = a$. Also, introduce the recursion kernel:

$$K(t_1, t_2, t_3) = \frac{\frac{1}{2}\int_{\xi=t_3}^{t_2} \omega_{0,2}(t_1, \xi)}{\omega_{0,1}(t_2) - \omega_{0,1}(t_3)} \tag{3.51}$$

Definition 3.3.2. *Topological recursion is the assignment of an infinite tower of correlation differentials $\omega_{g,n}(t_1, \ldots, t_n)$ to a spectral curve, such that for for $2g - 2 + n \geq 0$*

$$\begin{aligned}\omega_{g,n}(t_1, \ldots, t_n) = \sum_{a \in Ram} \mathrm{Res}_{t \to a} K(t_1, t, \sigma_a(t))[\omega_{g-1,n+1}(t, \sigma_a(t), t_2, \ldots, t_n) + \\ \sum_{\substack{g_1+g_2=g \\ I_1 \cup I_2 = \{t_2, \ldots, t_n\}}}{}' \omega_{g_1,1+|I_1|}(t, I_1)\omega_{g_2,1+|I_2|}(\sigma_a(t), I_2)],\end{aligned} \tag{3.52}$$

where $\sum'$ excludes $\omega_{0,1}$ and $\omega_{0,2}$ from the summation.

Note that in this definition all ramification point are assumed to be simple, i.e. all zeroes of dx are of degree one. For higher order ramification points, there is a straightforward generalization [123]. Correlation differentials $\omega_{g,n}$ enjoy many nice properties, in particular, they are meromorphic and fully symmetric under permutation of its variables. The only poles of $\omega_{g,n}$ are at ramification points of S.

Example 3.3.1. According to the remodelling theorem [107, 124, 108, 109], topological recursion computes open and closed topological string invariants from a spectral curve as the B-model curve. Consider an open topological string partition function [4], such that its logarithm has a perturbative expansion:

$$Z_{\text{open}} = \exp F, \;\; F = \sum_{g=0}^{\infty} \hbar^{g-1} F_g, \tag{3.53}$$

where F is called the (open) free energy. The perturbation coefficients F_i encode enumerative invariants of moduli spaces for topological strings (Gromov-Witten invariants). The free energy can be written as:

$$F_g = \sum_{n \geq 1} \frac{1}{n!} \sum_{i_1, \ldots, i_n \in I} F_{g,n}(i_1, \ldots, i_n) x_{i_1} \cdot \cdots \cdot x_{i_n} \tag{3.54}$$

By means of the topological recursion, the coefficients $F_{g,n}(i_1, \ldots, i_n)$ are defined from $\omega_{g,n}$:

$$\sum_{i_1, \ldots, i_n} F_{g,n}(i_1, \ldots, i_n) \equiv \omega_{g,n} \quad (2g - 2 + n > 0) \tag{3.55}$$

On another hand, closed partition function Z_{closed} would have an expansion only in even powers of $\hbar$:

$$Z_{\text{closed}} = \exp \tilde{F}, \;\; \tilde{F} = \sum_{g=0}^{\infty} \hbar^{2g-2} \tilde{F}_g, \tag{3.56}$$

where $\tilde{F}$ is the (closed) free energy. It is related to the topological recursion in a different way:

$$\tilde{F}_g \equiv \omega_{g,0} \tag{3.57}$$

3.4 Reconstructing WKB from the topological recursion

Having defined the topological recursion, we proceed to the next step. Our goal is to analyse quiver A-polynomials, and we need quantum curves which annihilate the Nahm sums and the semi-classical limit of whose gives classical quiver A-polynomials, suitable for the topological recursion. On the other hand, quantum quiver A-polynomials produce their own recursions which allow to compute the corresponding Nahm sum. Therefore we return to the quantization problem, considered earlier in the second chapter, in order to define these recursions, and then make a connection to the topological recursion. If the quiver correspons to a knot, then the recursion also encodes HOMFLY-PT polynomials for this knot; however, in the next section we will consider general quivers and their quantum A-polynomials in relation to topological recursion.

3.4.1 Quantum curves as the recursion relations

We focus on the case of exponential variables necessary for the case of knots, quivers and topological strings [47, 4, 48][1]

$$x = e^u, \qquad y = e^v, \tag{3.58}$$

where $(u, v) \in (\mathbb{C}^*)^2$ describe the classical phase space. To quantize it, one has to promote the variables x, y to their non-commutative versions $\hat{x}, \hat{y}$ subject to relation

$$\hat{y}\hat{x} = q\hat{x}\hat{y}. \tag{3.59}$$

If a classical curve (Lagrangian in $(\mathbb{C}^*)^2$) given by equation $P(x, y) = 0$ is quantizable, it means that there exists a well-defined Schrödinger-like operator ("quantum curve"), given by the non-commutative (or quantum) polynomial

$$\hat{P}(\hat{x}, \hat{y}) = \sum_{i,j} c_{i,j}(q)\hat{x}^i\hat{y}^j, \tag{3.60}$$

which enjoys the following properties:

- $c_{i,j}(q)$ are rational in q,
- $\lim_{q\to 1} \hat{P}(\hat{x}, \hat{y}) = P(x, y)$,
- there exist a unique solution $\psi(x)$ to the quantum curve equation

$$\hat{P}(\hat{x}, \hat{y})\psi(x) = 0. \tag{3.61}$$

Quantum A-polynomials for quivers produce their own type of recursion. Since $\hat{A}_C$ annihilates the Nahm sum, it can be translated to a linear q-difference equation dual to $\hat{A}_C$, encoding the recursion for the q-coefficients of P_C [127, 128] (this applies to any q-holonomic sequence). For example, if some generating function $G(x, q) = \sum_{k=0}^{\infty} G_k(q)x^k$ is annihilated by $\hat{A}(\hat{x}, \hat{y})$, then

[1] The case of usual variables is worked out in [125], see also [126] for an overview.

$G_k(q)$ for every k satisfies the n-term linear recursion

$$\hat{A}^*(\hat{l},\hat{m})G_k(q)=0 \tag{3.62}$$

such that

$$\begin{aligned}\hat{l}G(x,q)&=\sum_{k=0}^{\infty}G_{k+1}(q)x^k=\frac{1}{x}\left(G(q,x)-G_0(q)\right),\\ \hat{m}G(x,q)&=\sum_{k=0}^{\infty}G_k(q)(qx)^k=G(qx,q).\end{aligned} \tag{3.63}$$

The two quantum polynomials (after a suitable choice of the initial condition) are related by

$$\hat{A}^*(\hat{x},\hat{y})\equiv\hat{A}(\hat{x}^{-1},\hat{y}). \tag{3.64}$$

Let us note that in the case of quivers corresponding to a knot we have the normalized generating series of HOMFLY-PT polynomials

$$\mathcal{P}_K(x,a,q)=\sum_{r=0}^{\infty}\frac{x^r}{(q^2;q^2)_r}\mathcal{P}_r(a,q). \tag{3.65}$$

The presence of the q-Pochhammer in the denominator modifies the formula (3.64) as follows:

$$\hat{A}^*(\hat{x},\hat{y})\equiv\hat{A}(\hat{x}^{-1}(1-\hat{y}^2),\hat{y}), \tag{3.66}$$

from which we obtain the relation between knot and quiver A-polynomials when C corresponds to a knot:

$$\hat{A}_K(\hat{x},\hat{y})\equiv\ \hat{A}_{C[K]}\ (\hat{x}_1,\ldots,\hat{x}_m,\hat{y})\Big|_{\substack{x_i=\hat{x}^{-1}(1-\hat{y}^2)\\ i=1\ldots m}} \tag{3.67}$$

Example 3.4.1. Consider the sequence of r-coloured Jones polynomials for a knot K:

$$J_1^K(q),\ J_2^K(q),\ J_3^K(q),\ \ldots \tag{3.68}$$

They satisfy a linear q-difference equation [129]

$$\hat{A}_K\ (\hat{l},\hat{m})J_r^K(q)=0, \tag{3.69}$$

where $\hat{A}_K$ is a polynomial in $\hat{l},\hat{m}$ such that

$$\hat{l}J_r^K(q)=J_{r+1}^K(q),\quad \hat{m}J_r^K(q)=q^rJ_r^K(q) \tag{3.70}$$

E.g., for the trefoil knot the polynomial $\hat{A}_K$ can be written as the three-term recursion

$$J_r^{3_1}(q)=\frac{q^{-1}\hat{m}+q^4\hat{m}^{-4}-\hat{m}^{-1}-q^1\hat{m}^{-2}}{q^{1/2}(q^{-1}\hat{m}-q^2\hat{m}^{-1})}\hat{l}^{-1}J_r^{3_1}(q)+\frac{q^4\hat{m}^{-4}-q^3\hat{m}^{-2}}{q^2\hat{m}^{-1}-q^{-1}\hat{m}}\hat{l}^{-2}J_r^{3_1}(q) \tag{3.71}$$

with the initial condition $J_0^{3_1}(q)=0$, $J_1^{3_1}(q)=1$. The AJ conjecture [47] relates it to the knot

A-polynomial by evaluating $q = 1$ in (3.71), which gives (up to a normalizing monomial)

$$A_{T_{2,3}}(l, m) = (l - 1)(lm^3 + 1) \tag{3.72}$$

To adopt it for our notation, we change the variables $l \mapsto y, m \mapsto \frac{1}{x}$ and write

$$A_{T_{2,3}}(x, y) = (y - 1)(x^3 + y) \tag{3.73}$$

(this can be matched with the database [130]). We can also reconstruct the generating series for Jones polynomials by converting $\hat{A}^*$ to $\hat{A}$. The latter can be lifted to the quantum (super) A-polynomial for r-coloured HOMFLY-PT superpolynomials and takes form [50, 51]

$$\hat{A}(\hat{x}, \hat{y}) = a_0 + a_1\hat{y} + a_2\hat{y}^2\,, \tag{3.74}$$

where

$$\begin{aligned} a_0 &= \frac{a^2t^4(\hat{x} - 1)\hat{x}^3(1 + aqt^3\hat{x}^2)}{q(1 + at^3\hat{x})(1 + at^3q^{-1}\hat{x}^2)} \\ a_1 &= -\frac{a(1 + at^3\hat{x}^2)\big(q - q^2t^2\hat{x} + t^2(q^2 + q^3 + at + aq^2t)\hat{x}^2 + aq^2t^5\hat{x}^3 + a^2qt^6\hat{x}^4\big)}{q^2(1 + at^3\hat{x})(1 + at^3q^{-1}\hat{x}^2)} \\ a_2 &= 1 \end{aligned}$$

and, to relate it to (3.71), one has to take $a = q^r, t = -1$ and apply the transformation (3.64). Finally, it can be related to a quiver A-polynomial for the corresponding quiver (1.56) via a chain of knots-quiver specializations [21]. The quiver A-polynomial can be computed as the resultant from the Nahm equations (1.62):

$$\begin{aligned} A_{C[T_{2,3}]}(x_1, x_2, \sqrt{y}) = y^4{x_1}^2 + y^3x_3{x_2}^2 - y^3x_1x_2 - 2\,y^2x_1x_3 + 2\,y^2x_2x_3 - y^2x_1 - \\ yx_2x_3 + yx_1 + yx_3 + {x_3}^2 - x_3. \end{aligned} \tag{3.75}$$

Taking specialization $x_i = x^{-1}(1 - y^2)$ we obtain:

$$\frac{\left(y^2 - 1\right)^3 (x - 1)\left(y^6 + x\right)}{x^3} \tag{3.76}$$

which agrees up to a factor with the knot A-polynomial after exchanging x and y. To this end, we can also include a and t dependence to obtain (3.74) from (3.75).

Analogous recursion relations can be obtained for an arbitrary quiver, given its quantum quiver A-polynomial (1.78). However, we are not guaranteed that such quantum polynomial is unique. In fact we want to check whether the topological recursion reconstructs the same quantum polynomial, annihilating the corresponding Nahm sum. The relation between topological recursion and quantum polynomials is established from the form of topological recursion wave function, which we consider in the next section.

3.4.2 WKB method and topological recursion wave function

The quantum curve equation (3.61) can be solved recursively by the ansatz

$$\psi(x) = \exp\left(\frac{1}{\hbar}S_0(x) + S_1(x) + \hbar S_2(x) + \dots\right), \tag{3.77}$$

where the leading term is determined from the classical curve (solving $y = y(x)$ from $P(x, y) = 0$):

$$S_0(x) = \int \log y(x)\frac{dx}{x} \tag{3.78}$$

Such procedure is known as the WKB method, and $\psi(x)$ is called the WKB solution, which we denote as ψ_{WKB}.

On another hand, we can apply the topological recursion to $P(x, y)$ to find $\omega_{g,n}$'s which can be integrated and re-assembled into the topological recursion wave function, much like in the matrix model case:

$$\psi_{TR}(t) = \exp\left(\frac{1}{\hbar}S_0^{TR}(t) + S_1^{TR}(t) + \hbar S_2^{TR}(t) + \dots\right) \tag{3.79}$$

where

$$S_0^{TR} := \int \omega_{0,1}, \quad S_1^{TR} := -\frac{1}{2}\log(\frac{du}{dt}), \tag{3.80}$$

and for $k > 1$:

$$S_k^{TR} := \sum_{2g-2+n=k-1} \frac{1}{n!}\int_{t_0}^{t}\cdots\int_{t_0}^{t}\omega_{g,n}(t_1, \dots, t_n), \tag{3.81}$$

where all integration is (typically) from $t_0 \in \mathbb{R}$ to t, and t_0 shall coincide with one of the zeroes of $x(t)$. For example,

$$\begin{aligned} S_2^{TR} =& \frac{1}{3!}\iiint \omega_{0,3} + \int \omega_{1,1} \\ S_3^{TR} =& \frac{1}{4!}\iiiint \omega_{0,4} + \frac{1}{2!}\iint \omega_{1,2} \\ S_4^{TR} =& \frac{1}{5!}\underbrace{\int\cdots\int}_{5 \text{ times}}\omega_{0,5} + \frac{1}{3!}\iiint \omega_{1,3} + \frac{1}{5!}\int \omega_{2,1} \end{aligned} \tag{3.82}$$

Note that this wave function is annihilated by the topological recursion quantum curve, which we denote as $\hat{A}_{TR}$ (we will conduct the explicit calculations in the case of quivers). In many cases (e.g. Hermitean one-matrix model) the topological recursion wave function (3.79) defined purely from spectral curve data agrees with the matrix model wave function (3.24). In particular, we will test this conjecture for quiver partition functions in the next chapter. By rewriting it as a function of x and using the "hierarchy of equations" technique we can recover the candidate quantum curve order by order of $\hbar$, starting only from the classical data:

$$\hat{P}(\hat{x}, \hat{y}) = \hat{P}_0(\hat{x}, \hat{y}) + \hbar\hat{P}_1(\hat{x}, \hat{y}) + \dots \tag{3.83}$$

with $\hat{P}_0(\hat{x}, \hat{y}) = P(x, y)$. The natural problem is to match the two approaches to quantization,

i.e. to establish the relation between (3.60) and (3.83). It is a highly non-trivial check, because the quantum curves are usually constructed independently from TR (e.g. knots or topological strings). In case when $\psi_{TR} \equiv \psi_{WKB}$, one says that WKB is reconstructed from the topological recursion. It is conjectured that this holds for a large class of spectral curves. The conjecture has been proven for a class of genus 0 curves in the usual variables [125], but remains open in general. In the next section we will study the consistency problem for a class of two-vertex quivers and their A-polynomials.

3.5 Nahm sums and quiver A-polynomials from topological recursion

In this section we present the original results [58] and investigate whether the Nahm sums (1.29) can be realized as the wave-functions (3.79) associated to the underlying classical quiver A-polynomial. If true, then the $\hbar \to 0$ expansion of the Nahm sum and the quantum quiver A-polynomial (1.78) can be determined, order by order in $\hbar$, by the topological recursion. More precisely, we make the following

Conjecture 3.5.1. *The Nahm sums from quivers are reconstructed by the topological recursion, so that*

$$\psi_{TR}(x) \equiv x^{\alpha_0} P_C(q^{\alpha_1} x, \ldots, q^{\alpha_m} x). \tag{3.84}$$

where $\alpha_0, \ldots, \alpha_m$ are rational numbers, which depend on the choice of the quiver.

The monomial x^{α_0} appears as the normalization prefactor (on the level of quantum quiver A-polynomial it corresponds to rescaling of $\hat{y}$ by some power of q) – the topological recursion wave function does not incorporate this feature, and we have to take into account and also find the proper exponents $\alpha_1, \ldots, \alpha_m$. Therefore, we have to compare the two expansions in $\hbar$:

- ψ_{TR} given by (3.79) on the topological recursion side,
- the WKB expansion ψ_{WKB} (3.77) of the quiver generating series, where $\hat{P}(\hat{x}, \hat{y}) = \hat{A}(\hat{x}, \hat{y})$.

We verify whether the conjecture 3.5.1 holds in various simple examples. Our choice of quivers relies on the following criterion: the corresponding A-polynomials have genus 0 and are admissible (i.e. they are irreducible and have maximal number of ramification points); to this end we appropriately identify generating parameters $x_1 = \pm x_2 = x$ (so that the A-polynomial is irreducible), and introduce framing if necessary (so that the number of ramification points is maximal). In what follows, we analyze our statement and provide topological recursion calculations for the following quivers:

- 1-vertex quiver in arbitrary framing f, encoded in the matrix $C = [f]$; this quiver captures topological string amplitudes for $\mathbb{C}^3$ geometry, as well as extremal colored HOMFLY-PT polynomials of the framed unknot,
- uniform quivers $C_{ij} = const$, of size 2 and independently of arbitrary size, with identification $x_i = x$,

- a quiver $C = \begin{bmatrix} 2 & 1 \\ 1 & 1 \end{bmatrix}$ with identification $x_1 = -x_2 = x$; this quiver captures full colored HOMFLY-PT polynomials for the unknot,
- a quiver $C = \begin{bmatrix} 3 & 1 \\ 1 & 1 \end{bmatrix}$ with identification $x_1 = x_2 = x$; this quiver encodes extremal colored invariants of the left-handed trefoil knot,
- a quiver $C = \begin{bmatrix} 2 & 0 \\ 0 & -1 \end{bmatrix}$ with identification $x_1 = -x_2 = x$,
- a quiver $C = \begin{bmatrix} 2 & 2 \\ 2 & 1 \end{bmatrix}$ with identification $x_1 = x_2 = x$,
- a quiver $C = \begin{bmatrix} 3 & 2 \\ 2 & 1 \end{bmatrix}$ with identification $x_1 = x_2 = x$; this quiver encodes extremal colored invariants of the right-handed trefoil knot,
- a quiver $C = \begin{bmatrix} 2 & 0 \\ 0 & 2 \end{bmatrix}$ with identification $-x_1 = x_2 = x$,

We find agreement between Nahm sums and topological recursion calculations in all cases, apart from one subtlety for diagonal quivers (the last example). Namely, in this case one term in the quantum A-polynomial determined from the topological recursion appears to have a different ordering than the operator that annihilates the Nahm sum. It would be important to explain this discrepancy.

3.5.1 One-vertex quiver, $m = 1$

We start from the case $m = 1$, associated to a single vertex quiver with f loops. Note that it was also analyzed in [131, 48] from the viewpoint of topological strings. Besides it encodes the reduced HOMFLY-PT polynomials of the unknot [21]. At first we analyze $f = 2$ case, and then arbitrary framing f.

Framing $f = 2$

We begin with the smallest framing value $f = 2$ for which the quiver A-polynomial has maximal number of ramification points and therefore is admissible for the topological recursion. The quantum and classical quiver A-polynomials are

$$\hat{A}(\hat{x}, \hat{y}) = q\hat{x}\hat{y}^2 + \hat{y} - 1, \qquad A(x, y) = xy^2 + y - 1. \tag{3.85}$$

The Newton polygon $N(A)$ is shown in figure 3.4. It has no interior points which implies that the curve has genus zero, besides all face polynomials are simply binomials, which are cyclotomic and therefore this A-polynomial is quantizable (this also holds for an arbitrary framing which we will consider next). Note that the Nahm sum is recovered as the solution to this quantum

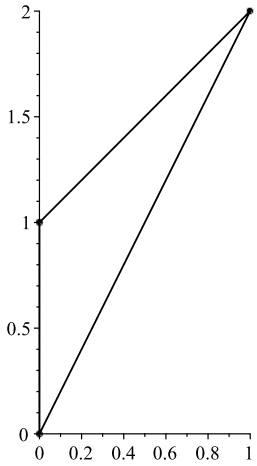

Figure 3.4: The Newton polygon $N(A)$ for the quiver A-polynomial (3.85).

A-polynomial. The leading terms in the WKB solution for the Nahm sum take form:

$$\begin{aligned} S_0 &= -\mathrm{Li}_2(1-y) - (\log y)^2, \\ S_1 &= -\frac{1}{2}\log\frac{(1-y)y}{x} - \frac{1}{2}\log\left(-\frac{dx}{dy}\right) = -\frac{3}{2}\log y - \frac{1}{2}\log\left(-\frac{dx}{dy}\right). \end{aligned} \tag{3.86}$$

We consider the following rational parametrization

$$x(t) = \frac{1-t}{t^2}, \qquad y(t) = t, \tag{3.87}$$

with $t \in [0, 2]$. This corresponds to the choice of branch of $y(x)$:

$$y(x) = \frac{-1+\sqrt{1+4x}}{2x}. \tag{3.88}$$

Next, we conduct the topological recursion calculations (3.80) in the parametrization (3.87) and find

$$\begin{aligned} S_0^{TR} &= \int \log y \frac{dx}{x} = -\mathrm{Li}_2(1-y) - (\log y)^2 = S_0, \\ S_1^{TR} &= -\frac{1}{2}\log\frac{1}{x}\frac{dx}{dt} = -\frac{1}{2}\log\frac{-2+y}{xy^3}. \end{aligned} \tag{3.89}$$

As a result, the leading term exactly gives S_0 in (3.86), however for the second one with S_1 in (3.86) we get

$$S_1^{TR} = S_1 + \frac{1}{2}\log(-x) + \frac{3}{2}\log y. \tag{3.90}$$

Therefore we propose the following relation between $P_C(x)$ and $\psi_{TR}(x)$

$$P_C(q^{3/2}x) = ix^{-1/2}\psi_{TR}(x). \tag{3.91}$$

Furthermore, from the quantum Nahm equations (1.75) we obtain the following quantum quiver A-polynomial annihilating $\psi(x)_{TR}$ (which agrees with the result in [48])

$$\hat{A}_{TR}(\hat{x},\hat{y}) = \hat{A}(q^{3/2}\hat{x}, q^{-1/2}\hat{y}) = q^{3/2}\hat{x}\hat{y}^2 + q^{-1/2}y - 1. \tag{3.92}$$

The next step is to confirm that S_k^{TR} with $k > 1$ can be consistently computed from the above relations and the result matches with the corresponding coefficient in the Nahm sum expansion. Analysing the ramification points, we obtain the first point $\frac{d\log x(t)}{dt}|_{t=t^*} = 0$ arising for $t^* = 2$. Another (conjugate) point, defined from $x(t) = x(\bar{t})$ for $\bar{t}$ in the neighbourhood of t^*, takes form $\bar{t} = \frac{t}{t-1}$. This allows to write the differential 1-form

$$\omega(t,\bar{t}) = (\log y(t) - \log y(\bar{t}))\,\frac{dx(t)}{x(t)} = \log(t-1)\frac{-2+t}{t(1-t)}dt. \tag{3.93}$$

The Bergman kernel for genus 0 curves and the associated recursion kernel read

$$\begin{aligned} dE_{t,\bar{t}}(t') &= \frac{1}{2}\int_{\xi=\bar{t}}^{t} B(\xi,t') = -\frac{t}{2}\frac{2-t}{(t'(t-1)-t)(t'-t)}dt', \\ K(t',t,\bar{t}) &= \frac{dE_{t,\bar{t}}(t')}{\omega(t,\bar{t})} = \frac{t^2}{2}\frac{1-t}{(t'(t-1)-t)(t'-t)}\frac{1}{\log(t-1)}\frac{dt'}{dt}. \end{aligned} \tag{3.94}$$

Knowing them, we can compute

$$\omega_{0,2}(\bar{q},t_1) = \frac{d\bar{q}dt}{(\bar{q}-t)^2} = -\frac{1}{1-q^2}\frac{dqdt}{(\bar{q}-t)^2}, \tag{3.95}$$

to get from (3.52)

$$\begin{aligned} \omega_{1,1}(t) &= -\frac{16-16t+t^2}{24(2-t)^4}dt, \\ \omega_{0,3}(t_1,t_2,t_3) &= \frac{4dt_1dt_2dt_3}{(t_1-2)^2(t_2-2)^2(t_3-2)^2}. \end{aligned} \tag{3.96}$$

Finally we can compute S_2^{TR} as in (3.82), and for $t = -\infty$ we find

$$S_2^{TR}(t) = \frac{-4-10t+t^2}{24(t-2)^3}. \tag{3.97}$$

In order to compare this expression with the corresponding coefficient $S_2(x)$ from the Nahm sum, we need to express S_2^{TR} as a function of x. However, we find that there are two branches:

$$t_\pm(x) = \frac{-1 \pm \sqrt{1+4x}}{2x}, \tag{3.98}$$

and we choose the one with $y(x=0) = 1$, since this corresponds to $t_+(x)$ and reflects the property of the Nahm sum which is equal to one when $x = 0$. Therefore we obtain

$$S_2^{TR}(x) = \frac{-4-10y(x)+y(x)^2}{24(y(x)-2)^3}, \tag{3.99}$$

which confirms the consistency with the WKB expansion of the corresponding Nahm sum.

As a double-check, we can compute S_2^{TR} with another base point $t_0 = 1$:

$$S_2^{TR}(t) = -\frac{-4 + 22t - 31t^2 + 13t^3}{24(t-2)^3}, \tag{3.100}$$

and this time to plug the different branch $t_-(x)$ (the two are related by the Galois involution $t_-(x) = t_+(x)/(1 - t_+(x))$) and we end up with the exact same answer:

$$S_2^{TR}(x) = -\frac{-4 + 22t_-(x) - 31t_-^2(x) + 13t_-^3(x)}{24(t_-(x)-2)^3} = -\frac{-4 - 10y(x) + y(x)^2}{24(y(x)-2)^3}. \tag{3.101}$$

Arbitrary framing f

Our next case is one-vertex quiver in arbitrary framing f. The quiver A-polynomials are

$$\hat{A}(\hat{x}, \hat{y}) = q\hat{x}\hat{y}^f + \hat{y} - 1, \qquad A(x, y) = xy^f + y - 1. \tag{3.102}$$

We choose the rational parametrization

$$x(t) = \frac{1-t}{t^f}, \qquad y(t) = t. \tag{3.103}$$

Since we know that $S_0^{TR}(x)$ reproduces the leading term automatically, we continue to S_1^{TR} from (3.80) and we match the two expressions: $S_1(x)$ in WKB expansion and the result by topological recursion

$$S_1^{TR}(x) = S_1(x) + \frac{1}{2}\log x + \frac{f+1}{2}\log y + \frac{1}{2}\log(-1)^{f+1}. \tag{3.104}$$

The presence of extra terms in the right hand side of the above formula can be compensated by rescaling the variables and multiplying the wave function by the overall factor $x^{1/2}$, and we conjecture that in this case

$$\psi_{TR}(x) = (-1)^{(f+1)/2} x^{1/2} P_C(q^{(f+1)/2} x), \tag{3.105}$$

which gives the full agreement of the leading terms $S_1(x)$ and $S_2(x)$ with the topological recursion. Next, the quantum A-polynomial annihilating $\psi_{TR}(x)$ can be determined from the leading terms and is given by

$$\hat{A}_{TR}(\hat{x}, \hat{y}) = \hat{A}(q^{(f+1)/2}\hat{x}, q^{-1/2}\hat{y}) = (-1)^f q^{(f+1)/2}\hat{x}\hat{y}^f + q^{-1/2}\hat{y} - 1. \tag{3.106}$$

What is left is to compute S_k^{TR} for several $k > 1$ and verify the formula (3.105). The ramification point for (3.103) is $t^* = f/(f-1)$. The conjugate point, however, does not admit a closed form expression, but for our calculations it is sufficient to write

$$\begin{aligned} \bar{t} = & t^* - (t - t^*) + \frac{2(f^2-1)}{3f}(t-t^*)^2 - \frac{4(f^2-1)^2}{9f^2}(t-t^*)^3 + \\ & + \frac{2(f-1)^3(22f^3 + 57f^2 + 57f + 22)}{135f^3}(t-t^*)^4 + \mathcal{O}((t-t^*)^5). \end{aligned} \tag{3.107}$$

We further find $\omega(t_1, t_2)$, one-form dE and the recursion kernel

$$\begin{aligned}
\omega(t,\bar{t}) &= (\log t - \log \bar{t})\frac{f(t-1)-t}{t(1-t)}dt,\\
dE_{t,\bar{t}}(t') &= \frac{1}{2}\frac{t-\bar{t}}{(t'-t)(t'-\bar{t})}dt',\\
K(t',t,\bar{t}) &= \frac{dE_{t,\bar{t}}(t')}{\omega(t,\bar{t})} = \frac{1}{2}\frac{\bar{t}-t}{(t'-t)(t'-\bar{t})}\frac{t(1-t)}{f(t-1)-t}\frac{1}{\log \bar{t}/t}\frac{dt'}{dt}.
\end{aligned} \tag{3.108}$$

which gives

$$\begin{aligned}
\omega_{1,1}(t) &= \frac{1}{24(f-1)^4}\frac{-t^2(f-1)^4 + 2tf(f^3-2f^2+3f-2) - f^4}{(t-t^*)^4},\\
\omega_{0,3}(t_1,t_2,t_3) &= \frac{f^2}{(f-1)^4}\frac{1}{(t_1-t^*)^2(t_2-t^*)^2(t_3-t^*)^2},
\end{aligned} \tag{3.109}$$

and also some higher differentials (we will omit their full expression but rather present the final result). Given that, we can compute $S_2^{TR}(t)$ and $S_3^{TR}(t)$ from (3.82). Fixing the base point $t_0 = -\infty$, we get

$$\begin{aligned}
S_2^{TR}(t) &= -\frac{1}{(f-1)^4}\frac{-(f-1)^4t^2 + f(f-1)(3-3f+2f^2)t + f^2(-f^2+f+3)}{24(t-t^*)^3},\\
S_3^{TR}(t) &= -\frac{ft(t-1)\left[2f^4(t-1)^2 - 8f^2 - (9f^2-14f+9)ft(t-1) + 2t^2\right]}{48(f(1-t)+t)^6}.
\end{aligned} \tag{3.110}$$

In order to express everything in terms of x, we use the regular branch and find

$$t(x) = 1 + (-1)^{f+1}x + fx^2 + \frac{1}{2}(-1)^f(f-3f^2)x^3 + \frac{1}{3}f(1-6f+8f^2)x^4 + \dots \tag{3.111}$$

Finally, from the computer program we find that $S_2^{TR}(x)$ and $S_3^{TR}(x)$ re-expressed in terms x fully agree with those from the Nahm sum, therefore reproducing the WKB expansion as proposed in the conjecture (3.105).

3.5.2 Uniform two-vertex quivers, $m = 2$

The next example is the uniform quiver with $m = 2$ and $f = 1$, which adjacency matrix is

$$C = \begin{bmatrix} 1 & 1 \\ 1 & 1 \end{bmatrix} \tag{3.112}$$

The quantum and classical quiver A-polynomials read

$$\hat{A}(\hat{x},\hat{x},\hat{y}) = \quad q^2\hat{x}^2\hat{y}^2 + 2\sqrt{q}\hat{x}\hat{y} - \hat{y} + 1, \tag{3.113}$$

$$A(x_1,x_2;y) = \quad y^2x_1x_2 + (x_1+x_2-1)\,y + 1, \tag{3.114}$$

$$A(x,x,y) = \quad (xy+1)^2 - y = 0. \tag{3.115}$$

The Newton polygon $N(A)$ is shown in figure 3.5. It has no interior points which implies that the curve has genus zero, besides the only face polynomial which contains three monomials is

factorized into binomial, which means that the quantization condition holds in this case. Notice

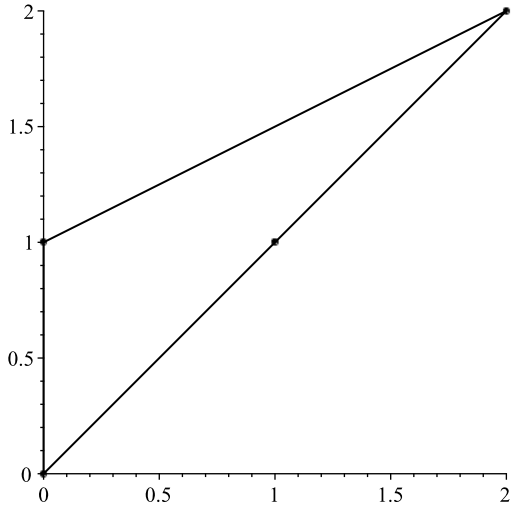

Figure 3.5: The Newton polygon $N(A)$ for the quiver A-polynomial (3.115).

that we use specialization $x_1 = x, x_2 = x$, and the following rational parametrization

$$x(t) = \frac{t-1}{t^2}, \qquad y(t) = t^2. \tag{3.116}$$

Note that $t(x) = \frac{1-\sqrt{1-4x}}{2x}$ is regular at $x = 0$. Our aim is to check whether the related Nahm sum with the above specialization of x_i can be reconstructed by means of the topological recursion. In other words, we need to match the two quantum polynomials (one is the quantum quiver A-polynomial, another one annihilates the topological recursion wave function) by finding the exponents $\alpha_1, \alpha_2, \beta$ such that

$$\hat{A}(q^{\alpha_1}x, q^{\alpha_2}x; q^{\beta}\hat{y})\psi_{TR}(x) = 0. \tag{3.117}$$

In order to find these exponents we solve this equation perturbatively using the ansatz (3.79). From the parametrization (3.116) we find

$$\begin{aligned} S_0^{TR} &= \int \frac{1}{x} \ln \frac{(X-1)^2}{4x^2} dx, \\ S_1^{TR} &= -\frac{1}{2}\Big(\ln(2) + \ln\Big(\frac{(X+4x-1)x}{(X+2x-1)(X-1)} \Big) \Big), \end{aligned} \tag{3.118}$$

where we denote $X := \sqrt{1-4x}$. The $\hbar^0$ term in (3.117) vanishes automatically, however vanishing of the $\hbar$ term imposes the constants for α_1, α_2 and we get

$$\alpha_1 = \alpha_2 = 1, \qquad \beta = -\frac{1}{2}. \tag{3.119}$$

Remarkably, it fixes the topological recursion quantum curve

$$\hat{A}_{TR}(\hat{x}, \hat{y}) = \hat{A}(q^{\alpha_1}x, q^{\alpha_2}x; q^{\beta}\hat{y}) = q^3\hat{x}^2\hat{y}^2 + 2\,q\hat{x}\hat{y} - \frac{\hat{y}}{\sqrt{q}} + 1. \tag{3.120}$$

The last check is that higher coefficients S_K^{TR} of the topological recursion wave function also reproduce the solution to this quantum curve equation. We consider

$$\hat{A}_{TR}(\hat{x},\hat{y})\exp\Big(\frac{1}{\hbar}S_0^{TR}+S_1^{TR}+\sum_{k=1}^{\infty}\hbar^k S_k\Big)=0, \tag{3.121}$$

keeping in mind (3.118) and (3.120), and compute

$$\begin{aligned} S_2 =&\frac{12\,x^2+3\,X-14\,x+4}{24X^3},\\ S_3 =&\frac{\left(4\,x^2-2\,x-1\right)x\,(2\,Xx-X+4\,x-1)}{8X^7}. \end{aligned} \tag{3.122}$$

In order to verify that these terms can be obtained as well from the topological recursion, we return again to the classical curve (3.115) and its rational parametrization (3.116). The two ramification point are $t^*=2$ and $t^*=0$. The second point corresponds to $x=\infty$, which also must be taken into account when computing the topological recursion correlation functions.

Having said the above, we compute

$$\begin{aligned} \omega_{1,1} =&\frac{t_1}{4\,(t_1-2)^4}-\frac{1}{4}\,(t_1-2)^{-4}-\frac{1}{48}\,(t_1-2)^{-2}-\frac{1}{16}\,{t_1}^{-2},\\ \omega_{0,3} =&\frac{2}{(t_1-2)^2\,(-2+t_2)^2\,(t_3-2)^2}, \end{aligned} \tag{3.123}$$

Now we can compute S_2^{TR} by the formula (3.81)

$$\begin{aligned} S_2^{TR} =&-\frac{t^3-7\,t^2+12\,t-6}{12t\,(t-2)^3}+\frac{{t_0}^3-7\,{t_0}^2+12\,t_0-6}{12t_0\,(t_0-2)^3}+\\ &+\frac{(t-t_0)^2}{3\,(t-2)^3\,(t_0-2)^2}-\frac{(t-t_0)^2}{3\,(t-2)^2\,(t_0-2)^3}. \end{aligned} \tag{3.124}$$

By setting the integration limit $t_0=1$ ($x(t_0)=0, y(t_0)=1$), we obtain the same result as in (3.122) up to a constant (which is always irrelevant in our considerations, as it can be absorbed into a normalization prefactor of the wave function)

$$S_2^{TR}=\frac{4\,t^4-13\,t^3+19\,t^2-16\,t+6}{12t\,(t-2)^3}=S_2+\frac{1}{24}. \tag{3.125}$$

Analogously, using the integration limit $t_0=1$, we get

$$S_3^{TR}=\frac{(t-1)^3\left(t^4+2\,t^3-6\,t^2+8\,t-4\right)}{4t^2\,(t-2)^6}, \tag{3.126}$$

which also agrees with (3.122).

Let us also consider the second choice of the integration limit, which is $t_0=-\infty$. In this

case we find

$$S_2^{TR} = -\frac{-6+8t-7t^2+t^3}{12t(t-2)^3} = S_2 + \frac{1}{24}, \qquad S_3^{TR} = \frac{4-12t+14t^2-8t^3+t^4+t^5}{4t^2(t-2)^6} = S_3, \tag{3.127}$$

which again can be successfully matched with (3.122).

Summing up, the topological recursion indeed reconstructs the Nahm sum for the quiver (3.112), up to the shifts (3.119) in (3.117), and with carefully chosen integration limit either $t_0 = 1$ or $t_0 = -\infty$.

3.5.3 Uniform quivers of arbitrary size m

The next class of examples are now quivers of size $m \times m$ with all entries equal to f. The explicit form of classical quiver A-polynomial for generic m is not known, but we know that it can be parametized by

$$x(t) = \frac{1-t}{(-t^m)^f}, \qquad y(t) = t^m, \tag{3.128}$$

which implies

$$S_0^{TR} = -m\mathrm{Li}_2(1-t) - \frac{m}{2} fm(\log t)^2, \qquad S_1^{TR} = -\frac{1}{2}\log\frac{t-fm(t-1)}{t(t-1)}. \tag{3.129}$$

From the form of S_1^{TR} we conjecture

$$\psi_{TR}(x) = x^{1/2} P_C(q^{(f+1)/2}x). \tag{3.130}$$

In this case the associated Nahm sum is annihilated by the operator $\hat{A}(\hat{x},\hat{y})$ (1.81). If we consider the same rescalings as in (3.130), we can predict the form of the topological recursion quantum operator:

$$\hat{A}_{TR}(\hat{x},\hat{y}) = \hat{A}(q^{(f+1)/2}\hat{x}, q^{-1/2}\hat{y}) = \left(1-(-1)^f q^{(f+1)/2}\hat{x}\hat{y}^f\right)^m - q^{-1/2}\hat{y}. \tag{3.131}$$

To check the consistency, we may take $m = 2$ and $f = 1$ which gives (3.120).

Our aim is therefore to confirm the proposal (3.130) with the help of the topological recursion. The ramification points are $t_1^* = mf/(mf-1)$ and $t_2^* = 0$. We can decompose

$$S_k^{TR} = S_k^{TR,t_1^*} + S_k^{TR,t_2^*}, \tag{3.132}$$

where the first term on the right hand side encodes contribution from the first ramification point and is the same as for the one-vertex quiver (section 3.5.1):

$$S_k^{TR,t_1^*} \equiv S_k^{TR,(m,f)}(t) = m^{1-k} S_k^{TR,(1,mf)}, \tag{3.133}$$

where $S_k^{TR,(m,f)}$ denotes the term for a uniform quiver, coming from the topological recursion. In particular, $S_k^{TR,(1,n)}$ have been already computed in section 3.5.1. Introducing $n = mf$ and

$t^* = n/(n-1)$, we find

$$S_2^{TR,(m,f)} = -\frac{1}{m(n-1)^4}\frac{-(n-1)^4t^2 + n(n-1)(3-3n+2n^2)t + n^2(-n^2+n+3)}{24(t-t^*)^3}, \quad (3.134)$$

$$S_3^{TR,(m,f)} = -\frac{nt(t-1)}{m^2(n-1)^6}\frac{2n^4(t-1)^2 - 8n^2 - (9n^2-14n+9)nt(t-1) + 2t^2}{48m^2(n(1-t)+t)^6}. \quad (3.135)$$

The next step is to analyse contributions from the second ramification point $t_2^* = 0$. Its conjugate point is given by $\frac{1-t}{t^n} = \frac{1-\bar{t}(t)}{\bar{t}(t)^n}$ (for $n = mf$). We thus write $\bar{t}(t) = atp(t)$ where a is a constant and $p(t)$ is a polynomial in t such that $p(0) = 1$, satisfying the equation $(1-t)a^n p(t)^n = (1-ap(t))$. We denote solutions of this equation by $(a_k, p_k(t))$ for $k = 1, \dots, n$, with $a_k = \exp\left(\frac{2\pi i k}{n}\right)$, so that $(a_n = 1, p_n(t) = 1)$, and all other solutions implement Galois involutions $\bar{t}_k(t) = a_k t p_k(t)$. Furthermore,

$$\omega^{(k)}(t,\bar{t}) = (\log y(t) - \log y(\bar{t}_k))\frac{n(t-1)-t}{t(1-t)}dt = (\log a_k^m + m\log p_k(t))\frac{t-n(t-1)}{t(1-t)}dt, \quad (3.136)$$

leading to the recursion kernel

$$K^{(k)}(t',t,\bar{t}) = \frac{1}{2}\frac{\bar{t}_k - t}{(t'-t)(t'-\bar{t}_k)}\frac{t(1-t)}{mf(t-1)-t}\frac{1}{\log a_k^m + m\log p_k(t)}\frac{dt'}{dt}. \quad (3.137)$$

Having said the above, we compute the topological recursion differentials

$$\omega_{1,1}^{(k)}(t) = \begin{cases} \frac{1}{2m}\frac{a_k}{(1-a_k)^2 t^2}, & a_k^m = 1, \\ 0, & a_k^m \neq 1. \end{cases}, \qquad \omega_{0,3}^{(k)}(t_1,t_2,t_3) = 0, \quad (3.138)$$

This allows to express the contribution from t_2^* in (3.132) as the sum over integers k divisible by f

$$S_2^{TR,t_2^*} = -\frac{1}{2mt}\sum_{\substack{k=1 \\ k|f}}^{m-1}\frac{a_k}{(1-a_k)^2}, \quad (3.139)$$

For the one-vertex quiver there are no such contributions, since $n = f$. However, they are always present for uniform quivers of size $m \geq 2$. Denoting

$$A_m := \sum_{k=1}^{n-1}\frac{b^k}{(1-b^k)^2}, \qquad b := e^{2\pi i/m}, \quad (3.140)$$

we can write the complete expression

$$S_2^{TR}(t) = \frac{1}{m}S_2^{TR,(1,mf)}(t) - \frac{A_m}{2mt}, \quad (3.141)$$

which agrees with the S_2 term in the WKB expansion of the generating series for the uniform quiver, taken (3.130) into account.

To this end, let us also confirm the agreement for the term S_3. For the first ramification point the extra contributions appear only for $\omega_{1,1}$ and therefore $\omega_{0,4}$ is not changed comparing

with the one vertex quiver. But $\omega_{1,2}$ undergoes the change by adding the correction term

$$\frac{A_m}{m}\operatorname*{Res}_{q\to t^*} q^{-2}K^{(k)}(t_1,q,\bar{q})\omega_{0,2}(\bar{q},t_2). \tag{3.142}$$

We obtain the relation

$$-\frac{A_m}{m(t^*)^2(t_2-t^*)^2}\operatorname*{Res}_{q\to t^*}K^{(k)}(t_1,q,\bar{q}) = -\frac{t^*(1-t^*)}{2m^2n(t_1-t^*)^2(t_2-t^*)^2}\frac{a_k}{(1-a_k)^2}. \tag{3.143}$$

Consider now the second ramification point $t_2^* = 0$. We conclude that there are no extra contributions to $\omega_{0,4}$ and the potential contribution to $\omega_{1,2}$ comes only from the second term

$$2\operatorname*{Res}_{q\to 0}K^{(k)}(t_1,q,\bar{q})\,\omega_{1,1}(q)\omega_{0,2}(\bar{q},t_2) = \frac{A_m a_k}{2m^2t_1^2t_2^2}. \tag{3.144}$$

Taken together, (3.143) and (3.144) contribute to $\omega(t_1,t_2)$ as

$$\frac{A_m}{2m^2}\Big(-\frac{t^*(1-t^*)}{n(t_1-t^*)^2(t_2-t^*)^2}+\sum_{\substack{k=1\\k|f}}^{n-1}\frac{a_k}{t_1^2t_2^2}\Big) \tag{3.145}$$

which gives the correct form of S_3^{TR}. Summing over the roots of unity we obtain

$$S_3^{TR} = \frac{1}{m^2}S_3^{TR,(1,mf)} - \frac{A_m}{4m^2}\frac{t^*(1-t^*)}{n(t-t^*)^2}, \tag{3.146}$$

which is indeed consistent with (3.130).

3.5.4 Quiver $\left[\begin{smallmatrix}2&1\\1&1\end{smallmatrix}\right]$

Another interesting example is a quiver encoded in a matrix

$$C = \begin{bmatrix}2&1\\1&1\end{bmatrix} \tag{3.147}$$

In particular, we know that this quiver encodes colored HOMFLY-PT polynomials of the unknot in framing $f = 1$ and the unreduced normalization (section 1.3.4). This value of f is the minimal framing such that the quiver A-polynomial in its principal specialization has maximal number of ramification points. Quite importantly, it allows to check whether the topological recursion reconstructs colored HOMFLY-PT polynomials for a knot.

The quiver A-polynomial for (3.147) takes form

$$A(x_1,x_2;y) = x_1y^2 - x_2y + y - 1. \tag{3.148}$$

We consider specialization $x_1 = x, x_2 = -x$, which leads to an irreducible curve[2]

$$A(x,-x,y) = xy^2 + (x+1)\,y - 1 = 0 \tag{3.149}$$

[2]The choice $x_1 = x_2 = x$ leads to a reducible curve $A(x,x;y) = (y-1)(xy+1)$.

which Newton polygon $N(A)$ is shown in figure 3.6. It has no interior points which implies that the curve has genus zero, besides all face polynomials are simply binomials, which are cyclotomic and therefore this A-polynomial is quantizable. We choose the following rational

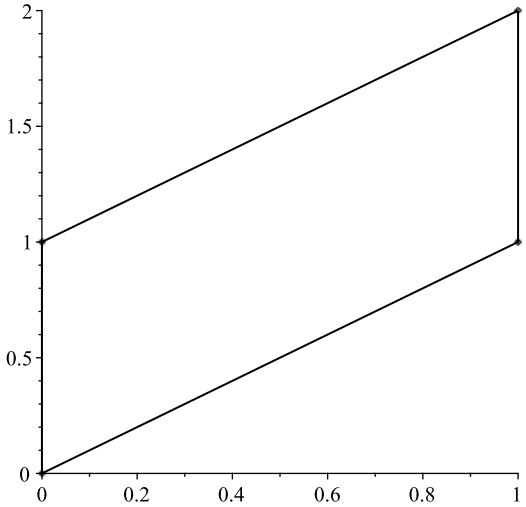

Figure 3.6: The Newton polygon $N(A)$ for the quiver A-polynomial (3.149).

parametrization

$$x(t) = -\frac{t-1}{t\,(t+1)}, \qquad y(t) = t, \tag{3.150}$$

and the inverse function, regular at $x = 0$

$$t(x) = \frac{-x - 1 + \sqrt{x^2 + 6\,x + 1}}{2x}. \tag{3.151}$$

The corresponding quantum quiver A-polynomial for $x_1 = -x_2 = x$ is of the form

$$\hat{A}(x, -x, \hat{y}) = qx\hat{y}^2 + \sqrt{q}x\hat{y} + \hat{y} - 1. \tag{3.152}$$

In order to verify that the Nahm sum and the quantum quiver A-polynomial with the above identification of variables can be reconstructed by the topological recursion, we employ the strategy used in the previous cases. We begin with the conjectural relation between the quantum quiver A-polynomial and the topological recursion wave function

$$\hat{A}(q^{\alpha_1}x, -q^{\alpha_2}x, q^{\beta}\hat{y})\psi_{TR}(x) = 0. \tag{3.153}$$

By analysing it order by order in $\hbar$ and matching S_1^{TR} with S_1, we find that

$$\alpha_1 = \frac{3}{2}, \quad \alpha_2 = 1, \quad \beta = -\frac{1}{2}. \tag{3.154}$$

This implies

$$\hat{A}_{TR}(\hat{x}, \hat{y}) = \hat{A}(q^{3/2}x, -qx, q^{-1/2}\hat{y}) = q^{3/2}x\hat{y}^2 + x\hat{y} + q^{-1/2}\hat{y} - 1. \tag{3.155}$$

Next we confirm that higher order terms also agree with the topological recursion. We can use

the same ansatz as before

$$\hat{A}_{TR}(\hat{x},\hat{y})\exp\Big(\frac{1}{\hbar}S_0^{TR}+S_1^{TR}+\sum_{k=1}^{\infty}S_k\Big)=0, \tag{3.156}$$

to find

$$\begin{aligned} S_2 =&\frac{(8\,x^2X+3\,x^3+13\,xX+21\,x^2+3\,X+21\,x+3)X^2}{12(x+3-2\,\sqrt{2})^3(x+3+2\,\sqrt{2})^3},\\ S_3 =&-\frac{(x^2-4\,x+11)(3\,x+X+1)x(x+1)X^2}{16(x+3-2\,\sqrt{2})^4(x+3+2\,\sqrt{2})^4}, \end{aligned} \tag{3.157}$$

where $X:=\sqrt{x^2+6x+1}$.

We now show that the topological recursion correctly reproduces the above terms S_k. In this case the ramification points for the parametrization (3.150) are just zeros of dx

$$1+\sqrt{2},1-\sqrt{2}. \tag{3.158}$$

The conjugate point is given by $\bar{t}=\frac{t+1}{t-1}$. In order to simplify calculations, we present the recursion kernel as a product of a rational function in t and t_1 and a logarithmic function

$$K(t,\bar{t},t_1)=\frac{t-t^3}{2\,((t_1-1)\,t-t_1-1)\,(t_1-t)}\times\frac{1}{\ln t-\ln\frac{t+1}{t-1}}, \tag{3.159}$$

Taking the product of their Laurent expansions, we obtain

$$\omega_{0,3}(t_1,t_2,t_3)=\frac{P_{0,3}}{Q_{0,3}},\qquad \omega_{1,1}(t_1)=\frac{P_{1,1}}{Q_{1,1}}, \tag{3.160}$$

where

$$\begin{aligned} P_{0,3} =&((10\,{t_3}^2+8\,t_3+2){t_2}^2+(8\,{t_3}^2+8\,t_3)t_2+2\,{t_3}^2+2){t_1}^2+\\ &+8\,(t_3t_2+1)((t_3+1)t_2+t_3-1)t_1+(2\,{t_3}^2+2){t_2}^2+\\ &+(8\,t_3-8)t_2+2\,{t_3}^2-8\,t_3+10,\\ Q_{0,3} =&(-2+(t_1-1)\sqrt{2})(t_1-1+\sqrt{2})(-1-\sqrt{2}+t_2)^2(2+(t_1-1)\sqrt{2})\times\\ &\times(-1-\sqrt{2}+t_3)^2(t_1-1-\sqrt{2})(-1+\sqrt{2}+t_2)^2(-1+\sqrt{2}+t_3)^2,\\ P_{1,1} =&\,2\,({t_1}^2+1)({t_1}^4-16\,{t_1}^3+2\,{t_1}^2+16\,t_1+1)({t_1}^2-2\,t_1-1)^2,\\ Q_{1,1} =&\,-3\,(-2+(t_1-1)\sqrt{2})^3(2+(t_1-1)\sqrt{2})^3(t_1-1+\sqrt{2})^3(t_1-1-\sqrt{2})^3. \end{aligned} \tag{3.161}$$

We continue with S_2^{TR} (3.81), keeping t_0 as a parameter, to get

$$S_2^{TR}=\frac{(t_0-t)(tt_0+1)}{12(t_0^2-2t_0-1)^3(t^2-2t-1)^3}P(t,t_0), \tag{3.162}$$

where

$$\begin{aligned} P(t,t_0) = {} & t^4{t_0}^4 - 10\,t^4{t_0}^3 - 10\,t^3{t_0}^4 - 14\,t^4{t_0}^2 + 96\,t^3{t_0}^3 - 14\,t^2{t_0}^4 - 14\,t^4t_0 + \\ & + 4\,t^3{t_0}^2 + 4\,t^2{t_0}^3 - 14\,t{t_0}^4 - 11\,t^4 - 48\,t^3t_0 - 4\,t^2{t_0}^2 - 48\,t{t_0}^3 - 11\,{t_0}^4 + \\ & + 14\,t^3 - 4\,t^2t_0 - 4\,t{t_0}^2 + 14\,{t_0}^3 - 14\,t^2 + 96\,tt_0 - 14\,{t_0}^2 + 10\,t + 10\,t_0 + 1. \end{aligned} \tag{3.163}$$

Finally, we confirm that that S_2 in (3.157) agrees with (3.162) if we take $t_0 = 1$ (note that the property $x(t_0) = 0, y(t_0) = 1$ holds for this value of t_0). Analogously, we find S_3^{TR}, and with the same value of $t_0 = 1$ it is given by

$$S_3^{TR} = \frac{(11\,t^4 + 26\,t^3 + 12\,t^2 - 6\,t + 1)(t^2 - 2\,t - 1)^6(t^2 + 1)(t - 1)^3(t + 1)t}{8(t - 1 - \sqrt{2})^{12}(t - 1 + \sqrt{2})^{12}}, \tag{3.164}$$

which agrees with S_3 in (3.157).

Summing up, we have confirmed that the topological recursion determines the Nahm sum for the quiver (3.147), as well as the corresponding quantum quiver A-polynomial (3.152), order by order in $\hbar$.

3.5.5 Quiver $\left[\begin{smallmatrix} 3 & 1 \\ 1 & 1 \end{smallmatrix}\right]$

The next representative quiver in our sequence is given by

$$C = \begin{bmatrix} 3 & 1 \\ 1 & 1 \end{bmatrix} \tag{3.165}$$

This case is also interesting because it relates to extremal colored HOMFLY-PT polynomials of the left-handed trefoil knot in framing $f = 1$, and also (in a different framing) counting of Duchon paths [132]. As a result, we would be able (at least in principle) to verify that the topological recursion reconstructs colored knot polynomials [133, 49, 48] and lattice path counts.

The quantum and classical quiver A-polynomials are of the form

$$\hat{A}(x_1, x_2, \hat{y}) = \quad q^{\frac{3}{2}}x_1\hat{y}^3 + (q^3x_2^2 - q^{\frac{3}{2}}x_2)\hat{y}^2 + ((q+1)\sqrt{q}x_2 - 1)\hat{y} + 1, \tag{3.166}$$

$$A(x, x, y) = \quad xy^3 + (x^2 - x)y^2 + (2x - 1)y + 1. \tag{3.167}$$

The Newton polygon $N(A)$ is shown in figure 3.7. Despite the fact that it has one interior point, we find the explicit rational parametrization which implies that the curve has genus zero, besides all face polynomials can be factorized to binomials, which are cyclotomic and therefore this A-polynomial is quantizable. We also use the following parametrization

$$x(t) = \frac{t+1}{t(t^2 - t - 1)}, \quad y(t) = \frac{t^2(t-1)}{t^2 - t - 1}. \tag{3.168}$$

Similarly as in earlier examples we compare the subleading term S_1 from the saddle point expansion of the corresponding Nahm sum with the topological recursion result, and find the

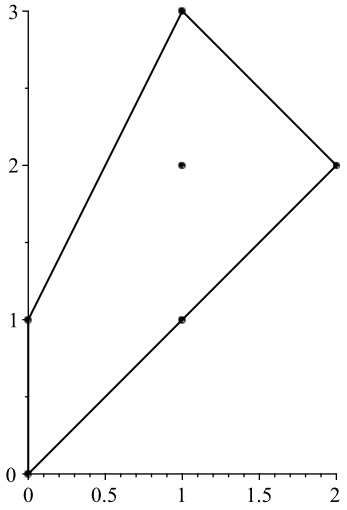

Figure 3.7: The Newton polygon $N(A)$ for the quiver A-polynomial (3.167).

quantum polynomial which annihilate the topological recursion wave function

$$\begin{aligned}\hat{A}_{TR}(\hat{x},\hat{y}) &= \hat{A}(q^2x, qx, q^{-\frac{1}{2}}\hat{y}) \\ &= q^2x_1\hat{y}^3 + (q^4x_2^2 - q^{\frac{3}{2}}x_2)\hat{y}^2 + ((q+1)qx_2 - q^{-\frac{1}{2}})\hat{y} + 1.\end{aligned} \tag{3.169}$$

Unfortunately, in this case we were not able to write analytically higher order terms. Still, the above result confirms that the topological recursion formalism reconstructs the Nahm sum at the subleading order (up to $\hbar^1$ term), and since the quantum operator (3.169) is defined uniquely from this subleading order, we conjecture that it consistently recovers all the coefficients of the Nahm sum to an arbitrary order.

3.5.6 Quiver $\left[\begin{smallmatrix}2 & 0\\ 0 & -1\end{smallmatrix}\right]$

Now we consider the quiver

$$C = \begin{bmatrix}2 & 0\\ 0 & -1\end{bmatrix} \tag{3.170}$$

The quantum and classical quiver A-polynomials are of the form

$$\hat{A}(x_1,x_2,\hat{y}) = \quad q^3x_1^2\hat{y}^4 + x_1\hat{y}^3 - \left(q^{3/2}(q+1)x_1x_2 + x_1 + \sqrt{q}x_2\right)\hat{y}^2 + \sqrt{q}x_2\hat{y} + qx_2^2, \tag{3.171}$$

$$A(x,-x,y) = \quad x(xy^4 + y^3 + 2\,xy^2 - y + x) = 0. \tag{3.172}$$

Notice that here we use the specialization $x_1 = x$ and $x_2 = -x$, which leads to the irreducible classical spectral curve given by $\frac{1}{x}A(x,-x,y)$ (we simply get rid of the x prefactor since it does not contribute to the topological recursion). The corresponding Newton polygon $N(A)$ is shown in figure 3.8. It has no interior points which implies that the curve has genus zero, besides all face polynomials can be factorized into binomials, which are cyclotomic and therefore this A-polynomial is quantizable. Our choice of parametrization for this curve is

$$x(t) = -\frac{(t-1)(t+1)t}{(t^2+1)^2}, \qquad y(t) = t. \tag{3.173}$$

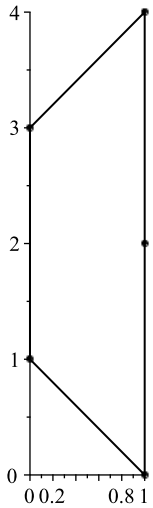

Figure 3.8: The Newton polygon $N(A)$ for the quiver A-polynomial (3.172).

Proceeding as in previous sections, we compute S_0^{TR} and S_1^{TR} by the formula (3.80) and find the quantum polynomial annihilating the topological recursion wave function up to a subleading order

$$\hat{A}_{TR} = q^3 x^2 \hat{y}^4 + q^{-1} x \hat{y}^3 + q^{3/2} (q+1) x^2 \hat{y}^2 - x\hat{y} + q x^2. \tag{3.174}$$

Next, we analyse the equation

$$\hat{A}_{TR}(\hat{x}, \hat{y}) \exp\Big(\frac{1}{\hbar} S_0^{TR} + S_1^{TR} + \sum_{k=1}^{\infty} S_k \Big) = 0, \tag{3.175}$$

order by order in $\hbar$, to find

$$\begin{aligned} S_2 = &- \frac{(x-1)(144x^3+144x^2+11x+11)}{60(16x^2-1)^2} - \frac{x(368x^2+77)X}{48(16\,x^2-1)^2} + \\ &+ \frac{(448x^4-540x^2+7)X^2}{48(16x^2-1)^2} - \frac{(432x^2-7)xX^3}{48(16x^2-1)^2}, \end{aligned} \tag{3.176}$$

where X denotes any solution of the equation $xX^4 + X^3 + 2\,xX^2 - X + x = 0$.

The next step is to confirm that the same form of S_2 is computed by the topological recursion. From the parametrization (3.173) we find the four ramification points

$$\sqrt{2}-1, -1-\sqrt{2}, 1-\sqrt{2}, 1+\sqrt{2}, \tag{3.177}$$

and the two recursion kernels which are associated to pairs of ramification points

$$\begin{aligned} K_{-1\pm\sqrt{2}} &= - \frac{t(t-1)(t+1)(t^2+1)}{2(t^2-2t-1)(t_1-t)(p_1 t+t_1+t-1)} \times \frac{1}{\ln t - \ln(-t+1) + \ln(t+1)}, \\ K_{1\pm\sqrt{2}} &= - \frac{t(t-1)(t+1)(t^2+1)}{2(t^2+2t-1)(t_1-t)(p_1 t-t_1-t-1)} \times \frac{1}{\ln t - \ln(t+1) + \ln(t-1)}. \end{aligned} \tag{3.178}$$

In the present case, poles of x (residues at infinity) do not contribute, since they cannot be canceled by zeros of y. We therefore find that the integration limit is $t_0 = 1$, so that $x(t_0) = 0$

and $y(t_0) = 1$, and we obtain

$$S_2^{TR} = \frac{(t-1)^2}{48(t-1+\sqrt{2})^3(-t+\sqrt{2}-1)^3(-t+1+\sqrt{2})^3(t+1+\sqrt{2})^3} \times \\ \times (17t^{10} + 132t^9 + 181t^8 + 144t^7 - 118t^6 - 232t^5 - 118t^4 + 144t^3 + 181t^2 + 132t + 17) \tag{3.179}$$

which agrees with (3.176). We conclude that the Nahm sum is reconstructed by the topological recursion in this case too.

3.5.7 Quiver $\begin{bmatrix} 2 & 2 \\ 2 & 1 \end{bmatrix}$

Another quiver that we consider is

$$C = \begin{bmatrix} 2 & 2 \\ 2 & 1 \end{bmatrix} \tag{3.180}$$

The quantum and classical quiver A-polynomials are of the form

$$\hat{A}(x_1, x_2, \hat{y}) = \quad q^{15/2}x_1^2x_2\hat{y}^5 - 2q^{5/2}x_1x_2\hat{y}^3 - qx_1\hat{y}^2 + (q^{1/2}x_2 - 1)\hat{y} + 1, \tag{3.181}$$

$$A(x_1, x_2, y) = \quad x_1^2x_2y^5 - 2x_1x_2y^3 - x_1y^2 + (x_2 - 1)y + 1. \tag{3.182}$$

We choose specialization $x_1 = x_2 = x$, for which we obtain[3]

$$\hat{A}(x, x, y) = \quad q^{15/2}x^3\hat{y}^5 - (q+1)q^{5/2}x^2\hat{y}^3 - qx\hat{y}^2 + \sqrt{q}x\hat{y} - \hat{y} + 1, \tag{3.183}$$

$$A(x, x, y) = \quad x^3y^5 - 2x^2y^3 - xy^2 + (x-1)y + 1 = 0. \tag{3.184}$$

for which the the Newton polygon $N(A)$ is shown in figure 3.9. Despite the fact that it has one interior point, we find the explicit rational parametrization which implies that the curve has genus zero, besides all face polynomials can be factorized to binomials, which are cyclotomic and therefore this A-polynomial is quantizable. The classical polynomial can be parametrized by

$$x(t) = \frac{t^4}{(t+1)(t^2-t-1)^2}, \qquad y(t) = \frac{(t+1)(t^2-t-1)}{t^3}. \tag{3.185}$$

Unfortunately, due to a high order of the A-polynomial we were not able to write down explicitly the exact expressions in topological recursion calculation. Nonetheless, we can still confirm the consistency up to the subleading order. Namely, computing S_1^{TR} as in (3.80), using the parametrization (3.185) and substituting the result to

$$\hat{A}(q^{\alpha_1}x, q^{\alpha_2}x, q^{\beta}\hat{y})\psi_{TR}(x) = 0, \tag{3.186}$$

we find that

$$\alpha_1 = -\frac{1}{2}, \qquad \alpha_2 = 0, \qquad \beta = \frac{1}{2}, \tag{3.187}$$

[3]Notice that specialization $x_1 = -x_2 = x$ gives a reducible curve

$$A(x, -x, y) = (xy^2 - 1)\big((xy(xy^2 - 1) + 1) + y\big).$$

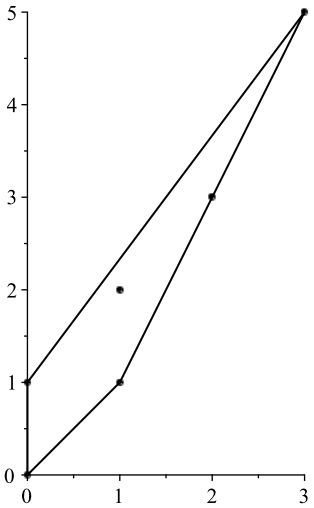

Figure 3.9: The Newton polygon $N(A)$ for the quiver A-polynomial (3.184).

confirms the agreement at the subleading order. This solution implies the form of the topological recursion quantum polynomial

$$\hat{A}_{TR} = q^9 x^3 \hat{y}^5 - (q+1)\, q^{7/2} x^2 \hat{y}^3 - q^{3/2} x \hat{y}^2 + q x \hat{y} - q^{1/2} \hat{y} + 1, \tag{3.188}$$

and we expect that the terms S_k^{TR} for higher k also agree with it.

3.5.8 Quiver $\left[\begin{smallmatrix} 3 & 2 \\ 2 & 1 \end{smallmatrix}\right]$

Our next example is

$$C = \begin{bmatrix} 3 & 2 \\ 2 & 1 \end{bmatrix} \tag{3.189}$$

The Nahm sum for this remarkable quiver encodes extremal colored HOMFLY-PT polynomials of the right-handed trefoil knot and also counts certain Duchon paths [132]. Again, we have a possibility to confirm that topological recursion computes quantum knot invariants [133, 49, 48], and to discover novel links between the recursion and path counting problems.

In this case the quantum and classical quiver A-polynomial take form

$$\hat{A}(x_1, x_2; \hat{y}) = \quad q^4 {x_1}^2 \hat{y}^5 - (q+1)\sqrt{q} x_1 \hat{y}^3 + \sqrt{q} x_1 \hat{y}^2 + \left(-\sqrt{q} x_2 + 1\right) \hat{y} - 1, \tag{3.190}$$

$$A(x, x; y) = \quad y(xy^2 - 1)^2 + xy(y-1) - 1, \tag{3.191}$$

with identification $x_1 = x_2 = x$ for the classical A-polynomial, for which the The Newton polygon $N(A)$ is shown in figure 3.10. Despite the fact that it has one interior point, we find the explicit rational parametrization which implies that the curve has genus zero, besides all face polynomials can be factorized to binomials, which are cyclotomic and therefore this A-polynomial is quantizable. We use the following parametrization

$$x(t) = -\frac{\left(t^2 + t - 1\right)^2}{t^4 \left(t - 1\right)}, \qquad y(t) = \frac{t\left(t-1\right)}{t^2 + t - 1}. \tag{3.192}$$

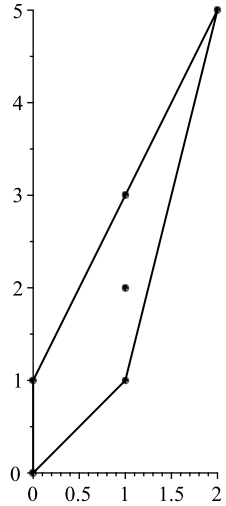

Figure 3.10: The Newton polygon $N(A)$ for the quiver A-polynomial (3.191).

Unfortunately, in this case we were not able to write down the exact results for higher order terms for the wave function (3.79). However the subleading term can still be matched with the topological recursion. This comparison gives

$$\hat{A}(q^{\alpha_1}x, q^{\alpha_2}x, q^{\beta}\hat{y})\,\psi_{TR}(x) = 0 \tag{3.193}$$

with

$$\alpha_1 = -1,\ \alpha_2 = 0,\ \beta = \frac{1}{2}, \tag{3.194}$$

and the topological recursion quantum curve takes form

$$\hat{A}_{TR} = q^{9/2}x^2\hat{y}^5 - (q+1)\,qx\hat{y}^3 + \sqrt{q}x\hat{y}^2 + (-qx + \sqrt{q})\,\hat{y} - 1 \tag{3.195}$$

which confirms our conjecture at the subleading order.

3.5.9 Quiver $\left[\begin{smallmatrix}2 & 0\\ 0 & 2\end{smallmatrix}\right]$

To finish the exposition we consider the diagonal quiver with

$$C = \begin{bmatrix}2 & 0\\ 0 & 2\end{bmatrix}, \tag{3.196}$$

examined earlier in relation to the quantization condition (section 2.5.1). To our amusement, we obtain an unexpected result – namely, the quantum curve determined by the topological recursion appears to be slightly different from the quantum quiver A-polynomial that annihilates the corresponding Nahm sum. But unlike in all previous examples, this difference cannot be absorbed by rescaling the variables of the quantum polynomial. Taking into account the fact that this quiver has passed the K-theoretic criterion for quantization, we believe that this phenomenon deserves further analysis. Here we are interested in the specialization $x_1 = -x, x_2 = x$ (although we have verified that the anomaly described above, also appears for different specializations)

which gives the specialized quantum and classical quiver A-polynomials[4]

$$\hat{A}(-x,x,\hat{y}) = \quad q^9x^4\hat{y}^4 + q^3x^2\hat{y}^3 + (q+1)\,q^2x^2\hat{y}^2 - \hat{y} + 1, \tag{3.197}$$

$$A(-x,x,y) = \quad x^4y^4 + x^2y^3 + 2\,x^2y^2 - y + 1 = 0. \tag{3.198}$$

The classical polynomial has the Newton polygon shown in figure 3.11, and is a two-dimensional projection of the polytope in figure 2.5. The quiver A-polynomial in this case has four branches

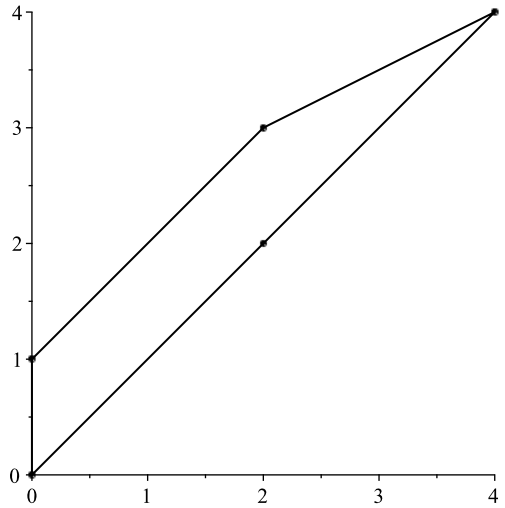

Figure 3.11: The Newton polygon $N(A)$ for the quiver A-polynomial (3.198).

and four parametrizations. For $x = \frac{(t-1)(t+1)t}{(t^2+1)^2}$, the y coordinate for those different branches is parametrized by

$$y_1 = \frac{\left(t^2+1\right)^2}{t^2\,(t-1)\,(t+1)}, \qquad y_2 = -\frac{\left(t^2+1\right)^2}{(t-1)\,(t+1)}, \qquad y_3 = \frac{\left(t^2+1\right)^2}{(t+1)^2\,t}, \qquad y_4 = -\frac{\left(t^2+1\right)^2}{(t-1)^2\,t}. \tag{3.199}$$

Computing now S_1^{TR} as in (3.80), and taking into account the structure of S_2^{TR} we find the four candidate quantum curves for the topological recursion wave function:

$$\begin{aligned}
\hat{A}^{(1)}_{TR}(\hat{x},\hat{y}) &= q^{10}x^4\hat{y}^4 + q^{7/2}x^2\hat{y}^3 + (q+1)\,q^{5/2}x^2\hat{y}^2 + 1 - \sqrt{q}\hat{y},\\
\hat{A}^{(2)}_{TR}(\hat{x},\hat{y}) &= q^{10}x^4\hat{y}^4 + q^{5/2}x^2\hat{y}^3 + (q+1)\,q^{5/2}x^2\hat{y}^2 + 1 - \frac{\hat{y}}{\sqrt{q}},\\
\hat{A}^{(3)}_{TR}(\hat{x},\hat{y}) &= q^{10}x^4\hat{y}^4 + q^{7/2}x^2\hat{y}^3 + (q+1)\,q^{5/2}x^2\hat{y}^2 - \frac{\hat{y}}{\sqrt{q}} + \underline{q^{1/2}}\,(q-1)\,x\hat{y}^2 + 1,\\
\hat{A}^{(4)}_{TR}(\hat{x},\hat{y}) &= q^{10}x^4\hat{y}^4 + q^{7/2}x^2\hat{y}^3 + (q+1)\,q^{5/2}x^2\hat{y}^2 - \frac{\hat{y}}{\sqrt{q}} + \underline{q^{3/2}}\left(q^{-1}-1\right)x\hat{y}^2 + 1.
\end{aligned} \tag{3.200}$$

The underlined monomial coefficients are defined uniquely by matching the S_2 term (if they are not included, then some unwanted logarithmic additional terms appear in higher S_k's). The two parametrizations (x,y_1) and (x,y_2) are related by $t \mapsto \frac{1}{t}$, while (x,y_3) and (x,y_4) are related by $t \mapsto -\frac{1}{t}$. Note that for (x,y_3) and (x,y_4), the underlined term $(q^{\pm 1}-1)xy^2$ vanishes when $q \to 1$, which means that it is non-trivially generated by quantum effects.

[4]The specialization $x_1 = x_2 = x$ leads to reducible polynomial $A(x,x,y) = \left(x^2y^2 - 2\,xy - y + 1\right)(xy+1)^2$.

To this end, we need to match either of the quantum polynomials in (3.200) with the operator (3.197). The closest solution we can get is

$$\hat{A}^{(1)}_{TR}(q^{1/4}x, q^{-1/2}\hat{y}) = \hat{A}^{(2)}_{TR}(q^{-3/4}x, q^{1/2}\hat{y}) = q^9x^4\hat{y}^4 + q^{5/2}x^2\hat{y}^3 + (q+1)\,q^2x^2\hat{y}^2 - \hat{y} + 1. \quad (3.201)$$

Comparing it with the quantum quiver A-polynomial (3.197), we see that the difference appears only in one monomial: instead its prefactor $q^{5/2}$ we would expect the prefactor q^3. Note that the missing $q^{1/2}$ can be taken care of by changing the ordering of operators, and writing this monomial as $q^{5/2}x^2\hat{y}^3 = q^3x(\hat{y}^{-1/2}x\hat{y}^{1/2})\hat{y}^3$.

Summing up, we have verified that topological recursion applied to classical quiver A-polynomials of genus zero indeed reproduces the corresponding Nahm sums and quantum quiver A-polynomials for a class of two-vertex quivers. However, one counter-example (the case $C = \left[\begin{smallmatrix} 2 & 0 \\ 0 & 2 \end{smallmatrix}\right]$) suggests that the relation between topological recursion wave function and quantum quiver A-polynomial must be more involved than (3.84) and deserves a further study.

3.6 Quantum Airy structures

In the remaining part of this chapter we take a turn from the previously chosen direction and consider quantum Airy structures [52, 53, 54, 134, 135, 136] which generalize the topological recursion and are possibly related to orbifold CFTs [137] and their character functions.

One of the notable properties of the topological recursion is the symmetry of $\omega_{g,n}(t_1, \ldots, t_n)$ under permutation of its arguments. This allows to reformulate the recursion as a system of differential operators, called quantum Airy structure. The name is after the Airy spectral curve [138] $x = y^2$, which is the simplest spectral curve with an infinite-dimensional algebra of symmetries – Virasoro algebra (1.9). On one hand, it can be shown that topological recursion formula (3.52) arises from a particular form of these differential operators. On the other hand, such operators provide a representation of Virasoro or $\mathcal{W}$-algebras [6, 139], so that many physical systems with the underlying symmetry algebra (but when the spectral curve is not known or even does not exist) can be still explored by means of the topological recursion.

3.6.1 Quadratic order

We start by reviewing the case of (infinite-dimensional) quadratic quantum Airy structures [52, 53] which can be associated to spectral curves with simple ramification.

Definition 3.6.1. *Quadratic quantum Airy structure is an infinite family $\{L_i\}_{i\geq 0}$ of differential operators with scalar coefficients $A^i_{a,b}, B^i_{a,b}, C^i_{a,b}, D^i$, of the form*

$$L_i = \hbar\partial_{x_i} - \sum_{a,b\in I} \left(\tfrac{1}{2}\, A^i_{a,b}x_ax_b + \hbar\, B^i_{a,b}x_a\partial_{x_b} + \tfrac{\hbar^2}{2}\, C^i_{a,b}\partial_{x_a}\partial_{x_b}\right) - \hbar D^i\,, \quad (3.202)$$

which span a Lie algebra with structure constants $f^a_{i,j}$

$$[L_i, L_j] = \sum_a \hbar\, f^a_{i,j}\, L_a\,, \quad (3.203)$$

Therefore, a quantum Airy structure (3.202) is completely determined by its numerical coefficients (note that they are not related to the Nahm data A, B, C, and C does not denote the symmetric matrix in this context). Essentially the two conditions (3.202) and (3.203) guarantee the existence and uniqueness of a partition function (which is sometimes referred as the topological recursion partition function) for every quantum Airy structure:

$$Z = \exp\left(\sum_{g\geq 0} \hbar^{g-1} F_g\right), \quad F_g = \sum_{n\geq 1} \frac{1}{n!} \sum_{i_1,\dots,i_n \in I} F_{g,n}(i_1,\dots,i_n) x_{i_1}\dots x_{i_n}, \tag{3.204}$$

which satisfies the constraints

$$L_i \cdot Z = 0, \quad \forall i \geq 0 \tag{3.205}$$

From the equation $L_i \cdot Z = 0$ we deduce that $F_{0,3}(i,j,k) = A^i_{j,k}$, $F_{1,1}(i) = D^i$, and for $2g-2+n \geq 2$ and $J = \{i_2,\dots,i_n\}$ we obtain the recursion for the free energy coefficients:

$$\begin{aligned} F_{g,n}(i_1, J) = &\sum_{m=2}^{n} B^{i_1}_{i_m,a} F_{g,n-1}(a, J\setminus\{i_m\}) \\ &+ \tfrac{1}{2} C^{i_1}_{a,b}\Big(F_{g-1,n+1}(a,b,J) + \sum_{\substack{J'\sqcup J''=I \\ h'+h''=g}} F_{h',1+|J'|}(a,J') F_{h'',1+|J''|}(b,J'')\Big). \end{aligned} \tag{3.206}$$

This is completely equivalent the topological recursion formula (3.52). The symmetry of $F_{g,n}(i_1,\dots,i_n)$ under permutations of the indices follows directly from the Lie algebra condition (3.203). Notice that we do not use a spectral curve in the definition of quantum Airy structure. On another hand, we have claimed that the latter is a reformulation of the topological recursion. In order to see this relation, write the local parametrization in the neighbourhood of the ramification point $t = a$

$$x(t) = \frac{z(t)^2}{2} + x(a), \tag{3.207}$$

and introduce

$$\xi_{a,k}(t) := \frac{(2k+1)dz(t)}{z(t)^{2k+2}}, \quad \xi^*_{a,k}(t) := \frac{z(t)^{2k+1}}{(2k+1)}, \quad \theta_a(t) := (y(t - y(\iota(t))dx(t))^{-1} dz(t)|_{t=a}. \tag{3.208}$$

(we can also write $\theta_a(t) = \sum_{m\geq -1} p_{m,r}\, z^{2m}(t)\,(dz(t))^{-1}$). The above definitions allow us to present the correlation functions in the following form:

$$\omega_{g,n}(t_1,\dots,t_n) = \sum_{\substack{i_1,\dots,i_n \\ j=1\dots m}} F_{g,n}(i_1,\dots,i_n)\, \xi_{a_j,i_1}(t_{i_1})\dots\xi_{a_j,i_n}(t_{i_n}) \tag{3.209}$$

Plugging this expansion into (3.52), we obtain the recursion (3.206), which shows that quantum Airy structures are equivalent to topological recursion in case when the coefficients A, B, C, D

arise from a spectral curve with simple ramification points, i.e. when

$$A^{(k_1,a)}_{(k_2,r_2),(k_3,r_3)} = \operatorname{Res}_{t\to a}\xi^*_{k_1,a}(t)\,d\xi^*_{k_2,r_2}(t)\,d\xi^*_{k_3,r_3}(t)\,\theta_a(t), \tag{3.210}$$

$$B^{(k_1,a)}_{(k_2,r_2),(k_3,r_3)} = \operatorname{Res}_{t\to a}\xi^*_{k_1,a}(t)\,d\xi^*_{k_2,r_2}(t)\,\xi_{k_3,r_3}(t)\,\theta_a(t), \tag{3.211}$$

$$C^{(k_1,a)}_{(k_2,r_2),(k_3,r_3)} = \operatorname{Res}_{t\to a}\xi^*_{k_1,a}(t)\,\xi_{k_2,r_2}(t)\,\xi_{k_3,r_3}(t)\,\theta_a(t), \tag{3.212}$$

$$D^{(k,r)} = \delta_{k,0}\big(\tfrac{p_{-1,r}}{2}\,\phi_{0,2} + \tfrac{p_{0,r}}{8}\big) + \delta_{k,1}\tfrac{p_{-1,r}}{24} \tag{3.213}$$

where $\phi_{0,2}$ is the constant term in the expansion of $\omega_{0,2}$ around $(t_1,t_2)=(a,a)$ in local coordinates. Since the index a corresponds to a ramification point, in general for a single spectral curve there are several copies of quantum Airy structure at each ramification point.

The most important example is the 2-Airy quantum Airy structure, which operators are usually denoted by $\mathcal{L}_i := L_{i+1}$, and the first three of them are:

$$\begin{aligned}
\mathcal{L}_{-1} &= \hbar\partial_{x_0} - \frac{1}{2}x_0^2 - \sum_{k\geq 0}\hbar x_k\partial_{x_{k+1}}\\
\mathcal{L}_0 &= \hbar\partial_{x_1} - \sum_{k\geq 0}\hbar\frac{2k+1}{3}\,x_k\partial_{x_k} - \frac{\hbar}{24}\\
\mathcal{L}_1 &= \hbar\partial_{x_2} - \sum_{k\geq 0}\hbar\frac{(2k+3)(2k+1)}{15}x_k\partial_{x_{k+1}} - \frac{\hbar^2}{30}\,\partial_{x_0}^2
\end{aligned} \tag{3.214}$$

The underlying spectral curve is the 2-Airy curve $x=\frac{y^2}{2}$, for which we have $z(t)=t$, $x(t)=t^2$, $y(t)=t$, $\theta(t)=(t^2dt)^{-1}$ and $a=0$. The operators $\mathcal{L}_i$ span the positive part of Witt algebra:

$$[\mathcal{L}_i,\mathcal{L}_j] = (j-i)\mathcal{L}_{i+j}, \quad \forall i,j\geq 0. \tag{3.215}$$

The partition function is the famous Witten-Kontsevich generating series [138]:

$$Z = \exp\left\{\sum_{g\geq 0}\sum_{n\geq 1}\sum_{k_1,\dots,k_n\geq 0}\frac{\hbar^{g-1}}{n!}\left(\int_{\overline{\mathcal{M}}_{g,n}}\psi_1^{k_1}\cup\cdots\cup\psi_n^{k_n}\right)x_{k_1}\cdots x_{k_n}\right\} \tag{3.216}$$

encoding the intersection classes ψ_i on the compactified moduli space $\overline{\mathcal{M}}_{g,n}$ of Riemann surfaces of genus g with n marked points. Note that we can obtain the completion to Virasoro algebra from the 2-Airy quantum Airy structure (3.214). Apply the transformation $x\mapsto x,\ y\mapsto x^k y$ for some fixed $k>1$. Computation of the coefficients (3.210) and the correction term gives:

$$\begin{aligned}
\mathcal{L}_{-2} &= x_0 - x_0x_1 - \hbar\sum_{k\geq 0}(2k+1)x_{k+2}\partial_k\\
\mathcal{L}_{-3} &= x_1 - x_0x_2 - \hbar\sum_{k\geq 0}(2k+1)x_{k+3}\partial_k - \frac{1}{2}\\
&\ \ \vdots\\
\mathcal{L}_{-n-1} &= x_{n-1} - \sum_{k+l=n}\frac{x_kx_l}{2} - \hbar\sum_{k\geq 0}(2k+1)x_{k+l+1}\partial_k, \quad n\geq 3
\end{aligned} \tag{3.217}$$

Then the union of positive and negative parts will give the full Virasoro algebra with $c = 2$. In order to match it with (3.215), we can set $L_{-i} := \mathcal{L}_{-i+1}$, $\forall i \geq 1$. Note that the correction term $-\frac{1}{2}\hbar^0$ in L_{-2} is fixed uniquely from the Lie bracket condition.

3.6.2 Higher order

We are ready to generalize quadratic quantum Airy structures from the previous section to an arbitrary order and describe the original result of [57] in its simplest incarnation. The main motivation comes from the fact that the topological recursion in the form (3.52) does not allow for spectral curves with non-simple ramification points. However, such curves quite often appear in physics. For example, the curve $x = y^r$, which we consider in this section, corresponds to the generalized Witten-Kontsevich matrix model [55, 56]. Some other curves with higher ramification may correspond to general B-model toric geometries [140]. In order to capture these types of models, the generalized topological recursion for higher ramification has been introduced [141, 123]. We will not discuss this formalism explicitly, but rather as a form of higher quantum Airy structure. This algebraic point of view has many advantages, in particular it can be approached in at least two ways: 1) either starting from a particular local data (local 1-forms) to compute the corresponding operators, or 2) from an ideal of differential operators, translate them into the form of recursion. The two ways turn out to be completely equivalent when the underlying symmetry algebra is an infinite dimensional conformal algebra of type A_r (recall the ADE classification for semi-simple Lie algebras). Let us also note that by the conformal algebra A_2 we mean Virasoro algebra which corresponds to $\mathfrak{sl}_2$, and more generally for A_r we mean $\mathcal{W}(\mathfrak{sl}_r)$ algebra [6]. In this thesis we focus on the first approach which is closer to the notion of spectral curve.

Let $t \in \mathbb{C}$ and $x(t)$ be a ramified function of t. We also denote R the set of ramification points (zeroes of dx), and

$$r \,:\, R \to \{1, 2, \ldots\}$$

the order of the ramification points of $x(t)$ (in the quadratic case we have $r = 1$ for all ramification points). If $a \in R$, we introduce a local coordinate $z_a(t)$ analogously to (3.207), such that

$$x(t) = \frac{z_a(t)^{r_a}}{r_a} + x(a),$$

which is well-defined up to the choice of a r_p-th root of unity.

We denote $\sigma_a(t)$ the conjugate point in the neighborhood U_a of a such that $z_a(\sigma_a(t)) = u_a z_a(t)$, i.e. there are several such points related by the Galois symmetry:

$$\left\{z, \sigma_a(t), \ldots, \sigma_a^{r_a-1}(t)\right\}$$

The most important ingredient is the linearly independent family of holomorphic (respectively meromorphic) 1-forms $\xi^*_{p,i}(z)$ (respectively $\xi_{p,i}(z)$), indexed by $p \in R$ and integers $i \geq 0$. They

generalize the 1-forms (3.208) for a simple ramification and are defined by

$$\xi^*_{p,i}(z) = \begin{cases} \frac{(z_a(z))^{i+1}}{i+1} & \text{if } z \in U_p \\ 0 & \text{otherwise} \end{cases}, \qquad \xi_{p,i}(z) = \operatorname*{Res}_{\tilde{z}\to p} \frac{(i+1)\mathrm{d}z_a(\tilde{z})}{(z_a(\tilde{z}))^{i+2}} \Big(\int_a^{\tilde{z}} \omega_{0,2}(\cdot, z) \Big)$$

In particular we can write the local expansion of $\omega_{0,2}$ in terms of these 1-forms as

$$\omega_{0,2}(z_1, z_2) \underset{\substack{z_1\to p_1 \\ z_2\to p_2}}{\approx} \sum_{i\geq 0} \mathrm{d}\xi^*_{p_1,i}(z_1)\xi_{p_2,i}(z_2)$$

Let $\theta(z) = \sum_{r\in\mathbb{Z}} t_r z^r (\mathrm{d}z)^{-1}$, where t_r are constants (they are fixed by a choice of spectral curve). We use the double square bracket notation for symmetrization with respect to a root of unity. For example,

$$[\![f(z)g(z)]\!]_r = \sum_{a\neq b} f(\vartheta_a^r z)g(\vartheta_b^r z), \quad \vartheta_k^r = e^{2i\pi\frac{k}{r}},$$

and we can continue by induction:

$$[\![f(z)g(z)h(z)]\!] = [\![f(z)[\![g(z)h(z)]\!]]\!], \qquad \dots$$

We also fix a ramification point a, omitting the corresponding index in the 1-forms, and define the scalars for $2 \leq r' \leq r$ which generalize the coefficients (3.210) as

$$\begin{aligned}
C^i[\ \,|\, k_1, k_2, \dots, k_{r'}] &= \operatorname*{Res}_{z\to p} \theta(z)\xi^*_i(z)[\![\xi_{k_1}(z)\xi_{k_2}(z)\dots\xi_{k_{r'}}(z)]\!]_l \\
C^i[k_1 \,|\, k_2, \dots, k_{r'}] &= \operatorname*{Res}_{z\to p} \theta(z)\xi^*_i(z)[\![d\xi^*_{k_1}(z)\xi_{k_2}(z)\dots\xi_{k_{r'}}(z)]\!]_{r'} \\
&\vdots \\
C^i[k_1, k_2, \dots, k_{r'-1} \,|\, k_{r'}] &= \operatorname*{Res}_{z\to p} \theta(z)\xi^*_i(z)[\![d\xi^*_{k_1}(z)\dots d\xi^*_{k_2}(z)\xi_{k_{r'}}(z)]\!]_{r'} \\
C^i[k_1, k_2, \dots, k_{r'} \,|\, \ ] &= \operatorname*{Res}_{z\to p} \theta(z)\xi^*_i(z)[\![d\xi^*_{k_1}(z)d\xi^*_{k_2}(z)\dots d\xi^*_{k_{r'}}(z)]\!]_{r'}
\end{aligned} \tag{3.218}$$

For any $g \geq 0$ and $n \geq 1$ such that $2g-2+n > 0$, there exists scalars $F_{g,n}[\boldsymbol{\nu}]$ indexed by $\boldsymbol{\nu} \in \overline{R}^n$ among which only finitely many are non-zero, and such that

$$\omega_{g,n}(z_1, \dots, z_n) = \sum_{\boldsymbol{\nu}\in\overline{R}} F_{g,n}[\boldsymbol{\nu}] \prod_{i=1}^n \xi_{\nu_i}(z_i) \tag{3.219}$$

Besides, these scalars satisfy a recursion on $2g-2+n > 0$, which generalize the topological recursion formula (3.52) to the case of arbitrary ramification [141, 123].

We now define our main object of interest.

Definition 3.6.2. *Quantum r-Airy structure is a collection of differential operators of degree at most r, defined by coefficients (3.218)*

$$H_{i\geq 0} = -\hbar(\partial_i - D^i) + \sum_{m+n=1}^{r} \frac{\hbar^n}{m!n!} \sum_{\substack{i_1,\dots,i_m \\ j_1,\dots,j_n}} C^i[i_1, \dots, i_m \,|\, j_1, \dots, j_n]\, x_{i_1}\dots x_{i_m}\partial_{j_1}\dots\partial_{j_n}, \tag{3.220}$$

where D^i are so-called quantum correction terms, fixed by the form of C.

According to [52], for every system of differential operators $\{H_i\}_{i\geq 0}$ of the form (3.220) with arbitrary C not necessarily equal to (3.218), which form a Lie ideal

$$[H_i, H_j] = \sum_{k=0}^{\infty} g_{i,j}^k H_k, \tag{3.221}$$

where $g_{i,j}^k$ could be differential operators as well, there is a unique partition function

$$Z = \exp\left(\sum_{2g-2+n>0} \frac{\hbar^{g-1}}{n!} \sum_{\nu_1,\ldots,\nu_n \in \overline{R}} F_{g,n}[\nu_1,\ldots,\nu_n] \prod_{i=1}^{n} x_{\nu_i} \right) \tag{3.222}$$

annihilated by these operators

$$H_i \cdot Z = 0, \quad \forall i \geq 0 \tag{3.223}$$

In particular, for the r-Airy structure (3.220) the corresponding partition function Z is related to generalized Witten-Kontsevich matrix integral [55, 56], and the spectral curve is $x = \frac{1}{r} y^r$. For a spectral curve with multiple ramification points, at each of them exists a copy of quantum r-Airy structure given by (3.218), so that the values of C differ for various ramification points because the local parametrization around these points is not universal. As an interesting consequence, for such curves there is not just one, but several partition functions of the form (3.222). In the remaining part we discuss the case of a spectral curve with double ramification point.

Example 3.6.1. Consider spectral curve $x = \frac{1}{3} y^3$ with double ramification point $a = 0$ and choose local coordinate $z_a(t) = t$, so that $y = t$ and $x(z(t)) = \frac{t^3}{3}$. Evaluating (3.218) and plugging them into (3.220), we find the operators $L_i := H_{2i},\ W_i := H_{2i+1},\ i \geq 0$,

$$\begin{aligned} [L_i, L_j] &= \sum_{a=0}^{\infty} \hbar f_{ij}^a L_a,\ i,j,a \in \iota_1 \\ [W_i, L_j] &= \sum_{a=0}^{\infty} \hbar g_{ij}^a W_a,\ i,a \in \iota_2,\ j \in \iota_1 \end{aligned} \tag{3.224}$$

such that $\deg(L_i) = 2,\ \deg(W_i) = 3$, $\iota_1 \cup \iota_2 = \mathbb{Z},\ \iota_1 \cap \iota_2 = \emptyset$, and

$$\begin{aligned} f_{ij}^a &= C^j[a \,|\, a] - C^i[j \,|\, a] \\ g_{ij}^a &= C^j[a \,|\, a] - C^i[j \,|\, a] + \frac{\hbar}{2} \sum_{k,l\geq 0} \left(C^i[\ \,|\, k,l] C^j[k \,|\, l,a] - C^j[\ \,|\, k,l] C^i[k \,|\, l,a] \right) \end{aligned} \tag{3.225}$$

In order to identify the algebra structure we examine the form of commutators (3.224) in Math-

ematica and confirm that they generate $\mathcal{W}(\mathfrak{sl}_3)$ algebra with central charge $c = 3$ [142]

$$\begin{aligned}
[L_i, L_j] &= (i-j)L_{i+j} + \frac{c}{12} i(i^2-1)\delta_{i+j,0} \\
[L_i, W_j] &= (2i-j)W_{i+j} \\
[W_i, W_j] &= (i-j)(\frac{1}{15}(i+j+3)(i+j+2) - \frac{1}{6}(i+2)(j+2))L_{i+j} + \\
&\qquad \beta(i-j)\Lambda_{i+j} + \frac{c}{360} i(i^2-1)(i^2-4)\delta_{i+j,0}
\end{aligned} \tag{3.226}$$

where $\Lambda_m = \sum\limits_{n\leq -2} L_n L_{n-m} + \sum\limits_{n>-2} L_{m-n} L_n - \frac{c}{10}(m+3)(m+2)L_m,\ i,j,m \in \mathbb{Z},\ c,\beta \in \mathbb{C}$.

The explicit form of the coefficients (3.218) is given below.

$$\begin{aligned}
C^i[j,k\,|\,] =& \frac{1}{3}\delta_{d_i+d_j+d_k,7} \frac{\sum\limits_{a,b\in\{d_j,d_k\}}{}' \zeta_{3,1}^{a-1}\zeta_{3,2}^{b-1} - \sum\limits_{\substack{a\in\{d_j,d_k\}\\ c=1..2}} \zeta_{3,c}^{a-1}}{(d_i-1)(\zeta_{3,1}-1)(\zeta_{3,2}-1)} \\
C^i[j\,|\,k] =& \frac{1}{3}\delta_{d_i+d_j-d_k,5} \frac{(d_k-1)\left(\sum\limits_{a,b\in\{0,2-d_j,d_k\}}{}' \zeta_{3,1}^{1-a}\zeta_{3,2}^{1-b} - \sum\limits_{\substack{a\in\{2-d_j,d_k\}\\ c=1..2}} \zeta_{3,c}^{1-a}\right)}{(d_i-1)(\zeta_{3,1}-1)(\zeta_{3,2}-1)} \\
C^i[\,|\,j,k] =& \frac{1}{3}\delta_{d_i-d_j-d_k,3} \frac{(d_k-1)(d_j-1)\left(\sum\limits_{a,b\in\{0,d_j,d_k\}}{}' \zeta_{3,1}^{1-a}\zeta_{3,2}^{1-b} - \sum\limits_{\substack{a\in\{d_j,d_k\}\\ c=1..2}} \zeta_{3,c}^{1-a}\right)}{(d_i-1)(\zeta_{3,1}-1)(\zeta_{3,2}-1)} \\
C^i[j,k,l\,|\,] =& -\frac{1}{9}\delta_{d_i+d_j+d_k+d_l,12} \frac{\sum\limits_{a,b\in\{d_j,d_k,d_l\}}{}' \zeta_{3,1}^{a-1}\zeta_{3,2}^{b-1}}{(d_i-1)(\zeta_{3,1}-1)(\zeta_{3,2}-1)} \\
C^i[j,k\,|\,l] =& -\frac{1}{9}\delta_{d_i+d_j+d_k-d_l,10} \frac{(d_l-1)\sum\limits_{a,b\in\{d_j,d_k,2-d_l\}}{}' \zeta_{3,1}^{a-1}\zeta_{3,2}^{b-1}}{(d_i-1)(\zeta_{3,1}-1)(\zeta_{3,2}-1)} \\
C^i[j\,|\,k,l] =& -\frac{1}{9}\delta_{d_i+d_j-d_k-d_l,8} \frac{(d_l-1)(d_k-1)\sum\limits_{a,b\in\{d_j,2-d_k,2-d_l\}}{}' \zeta_{3,1}^{a-1}\zeta_{3,2}^{b-1}}{(d_i-1)(\zeta_{3,1}-1)(\zeta_{3,2}-1)} \\
C^i[\,|\,j,k,l] =& -\frac{1}{9}\delta_{d_i-d_j-d_k-d_l,6} \frac{(d_j-1)(d_k-1)(d_l-1)\sum\limits_{a,b\in\{d_j,d_k,d_l\}}{}' \zeta_{3,1}^{1-a}\zeta_{3,2}^{1-b}}{(d_i-1)(\zeta_{3,1}-1)(\zeta_{3,2}-1)}
\end{aligned} \tag{3.227}$$

where $\sum'$ excludes $a = b$ from summation. Note that $C^i[j,k\,|\,]$ is non-zero only for $i \in \{0,1\}$ and $(j,k) = (0,1)$ and $(0,0)$, respectively. Also, $j - k = 2 - i$ for $C^i[j\,|\,k],\ , i \geq 0$ and $j + k = i - 3$ for $C^i[\,|\,j,k],\ i \geq 3$.

Summing up, we have defined a quantum r-Airy structure which generalizes quadratic Airy structure. This notion turns out to be equivalent to topological recursion applied to spectral curve $x = \frac{1}{r}\, y^r$, and in the case of higher ramification point ($r > 2$) such system of operators is consistent with the generalized topological recursion. Besides, we have confirmed that the

case of double ramification point ($r = 3$) corresponds to $\mathcal{W}(\mathfrak{sl}_3)$ algebra arising in conformal field theory. In fact, [57] studies much more general scenario with an arbitrary semi-simple Lie algebra, by using the formalism of vertex operator algebras. It allows to conjecture that higher Airy structures are related to orbifold CFTs, but this relation is still to be explored.

Chapter 4

Local equivalences of quivers

In this chapter we define and study the local equivalence relation for quivers, which can be applied recursively to a given quiver matrix in order to compute all equivalent matrices. The results of section 4.5 are presented in [60]. Our motivation comes from the uniqueness problem in the knots-quivers correspondence. Already in [21] it was noticed that there exist more than one quiver corresponding to the same knot (the phenomenon we call a quiver degeneracy). For example, in [25] the two quivers were identified for the figure eight knot:

$$C^{4_1} = \begin{bmatrix} 0 & 0 & -1 & 0 & -1 \\ 0 & 2 & 0 & 1 & -1 \\ -1 & 0 & -1 & 0 & -2 \\ 0 & 1 & 0 & 1 & -1 \\ -1 & -1 & -2 & -1 & -2 \end{bmatrix}, \qquad \tilde{C}^{4_1} = \begin{bmatrix} 0 & 0 & -1 & 0 & -1 \\ 0 & 2 & 0 & 1 & 0 \\ -1 & 0 & -1 & -1 & -2 \\ 0 & 1 & -1 & 1 & -1 \\ -1 & 0 & -2 & -1 & -2 \end{bmatrix}. \tag{4.1}$$

The first one is the same as in [21], but the second differs only by a permutation of some entries which cannot be obtained by a simple relabelling of the vertices. Both quivers, however, produce the same generating functions of colored HOMFLY-PT polynomials after the knots-quivers change of variables (1.53) for a suitable choice of a_i, q_i, l_i. Therefore in order to identify all possible degeneracies, the necessary step is to determine the local transformation of the quiver matrices which makes such identification. This is of course is justified by the identities between the corresponding Nahm sums (because the two partition functions must be equal after such specialization). Our plan is as follows:

- Firstly, we analyse directly what kind of constraints arise from a single degeneracy (when the two quivers correspond to the same knot).
- Secondly, we recall the *unlinking* operation on quivers defined in [25], which generates various identities between the Nahm sums.
- Thirdly, we formulate and prove the local equivalence theorem with the help of unlinking, establishing the sufficient condition for the local equivalence of quivers.
- Finally, we find all equivalent quivers for knots which differ by a single transposition of elements of their quiver matrices from the quivers in [21]. We cover the infinite families of torus and twist knots, as well as knots $6_2, 6_3, 7_3$.

4.1 Preliminary analysis of a quiver degeneracy

We begin with introducing an equivalence relation which captures quiver degeneracies:

Definition 4.1.1. *Assume that quiver Q corresponds to the knot K and quiver Q' corresponds to the knot K' in the sense of the definition 1.3.1. We define*

$$Q \sim Q' \quad \Longleftrightarrow \quad P_Q(\boldsymbol{x},q)\big|_{\boldsymbol{x}=x\boldsymbol{\lambda}} \equiv P_{Q'}(\boldsymbol{x},q)\big|_{\boldsymbol{x}=x\boldsymbol{\lambda}'}\,, \tag{4.2}$$

where

$$\lambda_i = \lambda_i' = a^{a_i} q^{q_i - C_{ii}} (-t)^{C_{ii}}, \quad C_{ii} = t_i \quad \forall i \in Q_0 = Q_0'. \tag{4.3}$$

This is clearly an identity between the two Nahm sums corresponding to each quiver. It also means that the two knots K, K' share the same HOMFLY-PT homology. In what follows, we take $K = K'$ which is sufficient for our case studies (we do not consider different knots which share the same HOMFLY-PT homology, such as mutant knots [143]). The main question is: what are the general conditions for two quivers to be equivalent? In order to answer this question we compare the two Nahm sums involved in (4.2) order by order in x. The linear terms cancel automatically, since $C_{ii} = t_i$ are completely fixed by the knots-quivers specialization (4.3), which is the same for both Q and Q'. Let us focus on terms proportional to x^2:

$$\begin{aligned} \frac{P_2(a,q,t)x^2}{(1-q^2)(1-q^4)} &= \sum_{i\in Q_0} \frac{(-q)^{4C_{ii}} x^2 \lambda_i^2}{(1-q^2)(1-q^4)} + \sum_{i,j\in Q_0, i\neq j} \frac{(-q)^{C_{ii}+2C_{ij}+C_{jj}} x^2 \lambda_i \lambda_j}{(1-q^2)(1-q^2)} \\ &= \sum_{i\in Q_0'} \frac{(-q)^{4C_{ii}} x^2 \lambda_i^2}{(1-q^2)(1-q^4)} + \sum_{i,j\in Q_0', i\neq j} \frac{(-q)^{C_{ii}+2C'_{ij}+C_{jj}} x^2 \lambda_i \lambda_j}{(1-q^2)(1-q^2)}, \end{aligned} \tag{4.4}$$

where we used (4.3) to write $\lambda_i = \lambda_i'$ and $C_{ii} = C'_{ii}$. From there we already see something interesting: the only difference between Q and Q' can appear in non-diagonal terms C_{ij} and C'_{ij}. Since equation (4.4) needs to hold for all a and t (which are independent from C_{ij} and C'_{ij}), we require the equality between coefficients of each monomial in these variables. The only possibility of having $Q \neq Q'$ satisfying (4.2) comes from $C_{ij} \neq C'_{ij}$. Let us focus on the requirement

$$\lambda_a \lambda_b = q^{2s} \lambda_c \lambda_d \tag{4.5}$$

for some $s \in \mathbb{Z}$ and λ_a, λ_b, λ_c, λ_d being pairwise different. It allows to re-write the quadratic term (4.4) as

$$\lambda_a \lambda_b (-q)^{C_{aa}+C_{bb}} \left(q^{2C_{ab}} + q^{-2s+2C_{cd}} \right) = \lambda_a \lambda_b (-q)^{C_{aa}+C_{bb}} \left(q^{2C'_{ab}} + q^{-2s+2C'_{cd}} \right), \tag{4.6}$$

where we used $C_{aa} + C_{bb} = C_{cc} + C_{dd}$ that comes from the comparison of t powers in $\lambda_a \lambda_b = q^{2s} \lambda_c \lambda_d$. There is only one non-trivial way to satisfy (4.4):

$$C'_{ab} = C_{cd} - s, \quad C'_{cd} = C_{ab} + s. \tag{4.7}$$

For $s = 0$ it translates to the transposition of matrix entries $C_{ab} \leftrightarrow C_{cd}$. Proceeding to the cubic

order, we get

$$\begin{aligned}\frac{P_3(a,q,t)x^3}{(1-q^2)(1-q^4)(1-q^6)} &= \sum_{i\in Q_0}\frac{(-q)^{9C_{ii}}x^3\lambda_i^3}{(1-q^2)(1-q^4)(1-q^6)}\\ &+\sum_{i,j\in Q_0,i\neq j}\frac{(-q)^{4C_{ii}+4C_{ij}+C_{jj}}x^3\lambda_i^2\lambda_j}{(1-q^2)(1-q^4)(1-q^2)}\\ &+\sum_{i,j,k\in Q_0,i\neq j\neq k}\frac{(-q)^{C_{ii}+2C_{ij}+C_{jj}+2C_{jk}+C_{kk}+2C_{ik}}x^3\lambda_i\lambda_j\lambda_k}{(1-q^2)(1-q^2)(1-q^2)},\end{aligned} \tag{4.8}$$

so we have to look for terms containing $\lambda_a\lambda_b$ or $\lambda_c\lambda_d$. They are given by

$$\begin{aligned}\frac{x^3\lambda_a\lambda_b}{(1-q^2)(1-q^4)(1-q^6)}\Big[&(-q)^{4C_{aa}+4C'_{ab}+C_{bb}}\lambda_a+(-q)^{4C_{bb}+4C'_{ab}+C_{aa}}\lambda_b\\ &+(1+q^2)(-q)^{C_{aa}+2C'_{ab}+C_{bb}+2C_{bc}+C_{cc}+2C_{ac}}\lambda_c\\ &+(1+q^2)(-q)^{C_{aa}+2C'_{ab}+C_{bb}+2C_{bd}+C_{dd}+2C_{ad}}\lambda_d\\ &+(1+q^2)\sum_{i\in Q_0\backslash\{a,b,c,d\}}(-q)^{C_{aa}+2C'_{ab}+C_{bb}+2C_{bi}+C_{ii}+2C_{ai}}\lambda_i\Big]\end{aligned} \tag{4.9}$$

and

$$\begin{aligned}\frac{x^3\lambda_c\lambda_d}{(1-q^2)(1-q^4)(1-q^6)}\Big[&(-q)^{4C_{cc}+4C'_{cd}+C_{dd}}\lambda_c+(-q)^{4C_{dd}+4C'_{cd}+C_{dd}}\lambda_d\\ &+(1+q^2)(-q)^{C_{cc}+2C'_{cd}+C_{dd}+2C_{ad}+C_{aa}+2C_{ac}}\lambda_a\\ &+(1+q^2)(-q)^{C_{cc}+2C'_{cd}+C_{dd}+2C_{bd}+C_{bb}+2C_{bc}}\lambda_b\\ &+(1+q^2)\sum_{i\in Q_0\backslash\{a,b,c,d\}}(-q)^{C_{cc}+2C'_{cd}+C_{dd}+2C_{di}+C_{ii}+2C_{ci}}\lambda_i\Big]\end{aligned} \tag{4.10}$$

for $P_{Q'}(\boldsymbol{x},q)\big|_{\boldsymbol{x}=x\boldsymbol{\lambda}}$ and analogous terms without prime symbols for $P_Q(\boldsymbol{x},q)\big|_{\boldsymbol{x}=x\boldsymbol{\lambda}}$. Since $\lambda_a\lambda_b = q^{2s}\lambda_c\lambda_d$, imposing the equality between $P_{Q'}(\boldsymbol{x},q)\big|_{\boldsymbol{x}=x\boldsymbol{\lambda}}$ and $P_Q(\boldsymbol{x},q)\big|_{\boldsymbol{x}=x\boldsymbol{\lambda}}$ implies conditions for sums of terms from both (4.9) and (4.10) for λ_a, λ_b, λ_c, λ_d and each λ_i, $i\in Q_0\backslash\{a,b,c,d\}$:

$$\begin{aligned}&\lambda_a\Big[(-q)^{4C_{aa}+4C'_{ab}+C_{bb}+2s}+(1+q^2)(-q)^{C_{cc}+2C'_{cd}+C_{dd}+2C_{ad}+C_{aa}+2C_{ac}}\Big]\\ &\quad=\lambda_a\Big[(-q)^{4C_{aa}+4C_{ab}+C_{bb}+2s}+(1+q^2)(-q)^{C_{cc}+2C_{cd}+C_{dd}+2C_{ad}+C_{aa}+2C_{ac}}\Big],\end{aligned} \tag{4.11}$$

$$\begin{aligned}&\lambda_b\Big[(-q)^{4C_{bb}+4C'_{ab}+C_{aa}+2s}+(1+q^2)(-q)^{C_{cc}+2C'_{cd}+C_{dd}+2C_{bd}+C_{bb}+2C_{bc}}\Big]\\ &\quad=\lambda_b\Big[(-q)^{4C_{bb}+4C_{ab}+C_{aa}+2s}+(1+q^2)(-q)^{C_{cc}+2C_{cd}+C_{dd}+2C_{bd}+C_{bb}+2C_{bc}}\Big],\end{aligned} \tag{4.12}$$

$$\begin{aligned}&\lambda_c\Big[(-q)^{4C_{cc}+4C'_{cd}+C_{dd}}+(1+q^2)(-q)^{C_{aa}+2C'_{ab}+C_{bb}+2C_{bc}+C_{cc}+2C_{ac}+2s}\Big]\\ &\quad=\lambda_c\Big[(-q)^{4C_{cc}+4C_{cd}+C_{dd}}+(1+q^2)(-q)^{C_{aa}+2C_{ab}+C_{bb}+2C_{bc}+C_{cc}+2C_{ac}+2s}\Big],\end{aligned} \tag{4.13}$$

$$\begin{aligned}&\lambda_d\Big[(-q)^{4C_{dd}+4C'_{cd}+C_{cc}}+(1+q^2)(-q)^{C_{aa}+2C'_{ab}+C_{bb}+2C_{bd}+C_{dd}+2C_{ad}+2s}\Big]\\ &\quad=\lambda_d\Big[(-q)^{4C_{dd}+4C_{cd}+C_{cc}}+(1+q^2)(-q)^{C_{aa}+2C_{ab}+C_{bb}+2C_{bd}+C_{dd}+2C_{ad}+2s}\Big],\end{aligned} \tag{4.14}$$

$$\begin{aligned}&\lambda_i\Big[(-q)^{C_{aa}+2C'_{ab}+C_{bb}+2C_{bi}+C_{ii}+2C_{ai}+2s}+(-q)^{C_{cc}+2C'_{cd}+C_{dd}+2C_{di}+C_{ii}+2C_{ci}}\Big]\\&\quad=\lambda_i\Big[(-q)^{C_{aa}+2C_{ab}+C_{bb}+2C_{bi}+C_{ii}+2C_{ai}+2s}+(-q)^{C_{cc}+2C_{cd}+C_{dd}+2C_{di}+C_{ii}+2C_{ci}}\Big].\end{aligned}\tag{4.15}$$

In each equation we have to match three q-monomials on both sides in a non-trivial way. For example, in (4.11) we must take

$$\begin{aligned}4C_{aa}+4C'_{ab}+C_{bb}+2s&=C_{cc}+2C_{cd}+C_{dd}+2C_{ad}+C_{aa}+2C_{ac}+2,\\C_{cc}+2C'_{cd}+C_{dd}+2C_{ad}+C_{aa}+2C_{ac}&=4C_{aa}+4C_{ab}+C_{bb}+2s,\\C_{cc}+2C'_{cd}+C_{dd}+2C_{ad}+C_{aa}+2C_{ac}+2&=C_{cc}+2C_{cd}+C_{dd}+2C_{ad}+C_{aa}+2C_{ac},\end{aligned}\tag{4.16}$$

or

$$\begin{aligned}4C_{aa}+4C'_{ab}+C_{bb}+2s&=C_{cc}+2C_{cd}+C_{dd}+2C_{ad}+C_{aa}+2C_{ac},\\C_{cc}+2C'_{cd}+C_{dd}+2C_{ad}+C_{aa}+2C_{ac}&=C_{cc}+2C_{cd}+C_{dd}+2C_{ad}+C_{aa}+2C_{ac}+2,\\C_{cc}+2C'_{cd}+C_{dd}+2C_{ad}+C_{aa}+2C_{ac}+2&=4C_{aa}+4C_{ab}+C_{bb}+2s.\end{aligned}\tag{4.17}$$

Analogous matching for equations for (4.12-4.14), combined with $C_{aa}+C_{bb}=C_{cc}+C_{dd}$ and (4.7), leads to two possible ways for non-trivial pairwise cancellation:

$$\begin{aligned}C_{ab}+s&=C_{cd}-1,\\C_{aa}+C_{cd}&=C_{ad}+C_{ac}+s+1,\\C_{bb}+C_{cd}&=C_{bd}+C_{bc}+s+1,\\C_{ab}+C_{cc}+s&=C_{bc}+C_{ac},\\C_{ab}+C_{dd}+s&=C_{bd}+C_{ad}\end{aligned}\quad\text{or}\quad\begin{aligned}C_{ab}+s&=C_{cd}+1,\\C_{aa}+C_{cd}&=C_{ad}+C_{ac}+s,\\C_{bb}+C_{cd}&=C_{bd}+C_{bc}+s,\\C_{ab}+C_{cc}+s&=C_{bc}+C_{ac}+1,\\C_{ab}+C_{dd}+s&=C_{bd}+C_{ad}+1.\end{aligned}\tag{4.18}$$

Combining (4.18) with $C_{aa}+C_{bb}=C_{cc}+C_{dd}$, we deduce that $s=0$. Putting it in equations (4.11)-(4.15) and performing the analogous matching of terms, we learn that:

$$C_{cd}=C_{ab}-1,\qquad C_{ci}+C_{di}=C_{ai}+C_{bi}-\delta_{ai}-\delta_{bi}\quad\forall i\in Q_0\tag{4.19}$$

$$\text{or}\qquad C_{ab}=C_{cd}-1,\qquad C_{ai}+C_{bi}=C_{ci}+C_{di}-\delta_{ci}-\delta_{di}\quad\forall i\in Q_0.\tag{4.20}$$

These conditions are required for the transposition $C_{ab}\leftrightarrow C_{cd}$ to lead to an equivalent quiver.

4.2 Unlinking operation

The main topic in [25] is the *multi-cover skein relation* for symmetric quivers. It was motivated by the invariance of the q-series counting generalized holomorphic curves under bifurcations of basic disks (recall section 1.3.4). One can express such bifurcations as the two elementary operations on quivers – linking and unlinking. As they reproduce the same kind of equality between the corresponding Nahm sums, without loss of a generality we focus on the case of unlinking (figure 4.1). Consider a symmetric quiver Q and fix $a,b\in Q_0$. The unlinking of nodes a,b is defined as a transformation of Q leading to a new quiver $\widetilde{Q}$ such that:

- There is a new node n: $\widetilde{Q}_0=Q_0\cup n$.

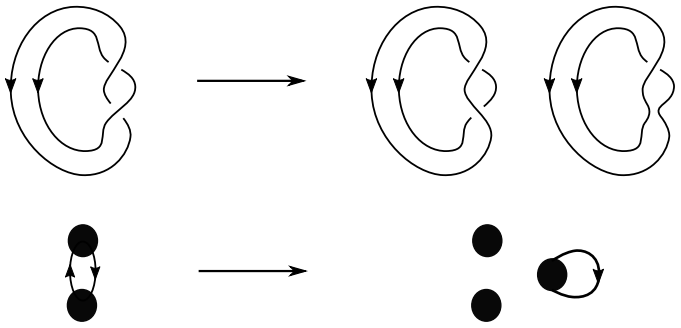

Figure 4.1: Unlinking of the two basic disks (top) and quiver description (bottom). Source: [25]

- The quiver matrix entries associated to this node are taken as follows

$$\begin{aligned} \widetilde{C}_{ab} &= C_{ab} - 1, & \widetilde{C}_{nn} &= C_{aa} + 2C_{ab} + C_{bb} - 1, \\ \widetilde{C}_{in} &= C_{ai} + C_{bi} - \delta_{ai} - \delta_{bi}, & \widetilde{C}_{ij} &= C_{ij} \quad \text{for all other cases,} \end{aligned} \tag{4.21}$$

  where δ_{ij} is a Kronecker delta.

To illustrate this principle, we relate the two quivers in the bottom of figure 4.1 by unlinking, corresponding respectively to

$$C = \begin{bmatrix} C_{aa} & C_{ab} \\ C_{ba} & C_{bb} \end{bmatrix} = \begin{bmatrix} 0 & 1 \\ 1 & 0 \end{bmatrix} \qquad \longrightarrow \qquad \widetilde{C} = \begin{bmatrix} \widetilde{C}_{aa} & \widetilde{C}_{ab} & \widetilde{C}_{an} \\ \widetilde{C}_{ba} & \widetilde{C}_{bb} & \widetilde{C}_{bn} \\ \widetilde{C}_{na} & \widetilde{C}_{nb} & \widetilde{C}_{nn} \end{bmatrix} = \begin{bmatrix} 0 & 0 & 0 \\ 0 & 0 & 0 \\ 0 & 0 & 1 \end{bmatrix}. \tag{4.22}$$

Most importantly, as proved in [25], the unlinking accompanied by the substitution $x_n = q^{-1}x_a x_b$ preserves the Nahm sum for the quiver:

$$P_Q(\boldsymbol{x}, q) = P_{\widetilde{Q}}(\boldsymbol{x}, q)\Big|_{x_n = q^{-1}x_a x_b}. \tag{4.23}$$

4.3 Local equivalence theorem

Having said the above, we formulate the following

Theorem 4.3.1. *Consider a quiver Q for the knot K with the adjacency matrix C and another quiver Q' with C' such that $Q'_0 = Q_0$ and $\lambda'_i = \lambda_i \ \forall i \in Q_0$ (λ_i comes from the knots-quivers change of variables 1.53). If Q and Q' are related by a sequence of disjoint transpositions*

$$C_{ab} \leftrightarrow C_{cd}, \qquad C_{ba} \leftrightarrow C_{dc} \tag{4.24}$$

for some pairwise different $a, b, c, d, \in Q_0$, such that

$$\lambda_a \lambda_b = \lambda_c \lambda_d, \tag{4.25}$$

and either

$$C_{ab} = C_{cd} - 1, \qquad C_{ai} + C_{bi} = C_{ci} + C_{di} - \delta_{ci} - \delta_{di}, \quad \forall i \in Q_0 \tag{4.26}$$

or

$$C_{cd} = C_{ab} - 1, \qquad C_{ci} + C_{di} = C_{ai} + C_{bi} - \delta_{ai} - \delta_{bi}, \quad \forall i \in Q_0, \tag{4.27}$$

then Q is equivalent to Q'.

Proof. Assume that Q corresponds to K, $Q'_0 = Q_0$, $\lambda'_i = \lambda_i$ $\forall i \in Q_0$, and $C'_{ij} = C_{ij}$ except one transposition $C_{ab} \leftrightarrow C_{cd}$ for some pairwise different $a, b, c, d \in Q_0$. We require

$$\lambda_a\lambda_b = \lambda_c\lambda_d, \quad C_{cd} = C_{ab} - 1, \quad C_{ci} + C_{di} = C_{ai} + C_{bi} - \delta_{ai} - \delta_{bi}, \quad i \in Q_0 \tag{4.28}$$

and analogously for C' (the case $C_{ab} = C_{cd} - 1$ correspond to changing labels $ab \leftrightarrow cd$). In order to show that Q' also corresponds to K, we connect Q' to Q by transformations preserving the Nahm sums, namely unlinking nodes a, b in Q and nodes c, d in Q':

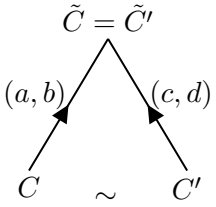

By definition, unlinking expresses $\tilde{C}$ and $\tilde{C}'$ in terms of C as follows

$$\begin{aligned}
&\widetilde{C}_{ij} = C_{ij} \quad \forall i,j \in Q_0\backslash\{a,b\} && \widetilde{C}'_{ij} = C'_{ij} \quad \forall i,j \in Q_0\backslash\{c,d\} \\
&\widetilde{C}_{ab} = C_{ab} - 1 && \widetilde{C}'_{cd} = C'_{cd} - 1 \\
&\widetilde{C}_{in} = C_{ai} + C_{bi} - \delta_{ai} - \delta_{bi}, && \widetilde{C}'_{in} = C'_{ci} + C'_{di} - \delta_{ci} - \delta_{di}, \\
&\widetilde{C}_{nn} = C_{aa} + 2C_{ab} + C_{bb} - 1, && \widetilde{C}'_{nn} = C'_{cc} + 2C'_{cd} + C'_{dd} - 1.
\end{aligned} \tag{4.29}$$

Therefore we can relate the entries of $\tilde{C}$ and $\tilde{C}'$:

$$\begin{aligned}
&\widetilde{C}'_{ab} = C'_{ab} = C_{cd} = C_{ab} - 1 = \widetilde{C}_{ab}, \\
&\widetilde{C}'_{cd} = C'_{cd} - 1 = C_{ab} - 1 = C_{cd} = \widetilde{C}_{cd}, \\
&\widetilde{C}'_{an} = C'_{ac} + C'_{ad} = C_{ac} + C_{ad} = C_{aa} + C_{ab} - 1 = \widetilde{C}_{an}, \\
&\widetilde{C}'_{bn} = C'_{bc} + C'_{bd} = C_{bc} + C_{bd} = C_{ab} + C_{bb} - 1 = \widetilde{C}_{bn}, \\
&\widetilde{C}'_{cn} = C'_{cc} + C'_{cd} - 1 = C'_{ac} + C'_{bc} = C_{ac} + C_{bc} = \widetilde{C}_{cn}, \\
&\widetilde{C}'_{dn} = C'_{cd} + C'_{dd} - 1 = C'_{ad} + C'_{bd} = C_{ad} + C_{bd} = \widetilde{C}_{dn}, \\
&\widetilde{C}'_{in} = C'_{ci} + C'_{di} = C_{ci} + C_{di} = C_{ai} + C_{bi} = \widetilde{C}_{in}, \quad \forall i \in Q_0\backslash\{a,b,c,d\}, \\
&\widetilde{C}'_{nn} = C'_{cc} + 2C'_{cd} + C'_{dd} - 1 = C_{cc} + 2C_{ab} + C_{dd} - 1 = C_{cc} + 2C_{ab} + C_{dd} - 1 = \widetilde{C}_{nn}, \\
&\widetilde{C}'_{ij} = C'_{ij} = C_{ij} = \widetilde{C}_{ij} \quad \text{for all other cases,}
\end{aligned} \tag{4.30}$$

which shows that the two quivers agree: $\widetilde{Q}' = \widetilde{Q}$. Since we have a freedom to choose the knots-quivers change of variables for the new nodes created when unlinking (for the old ones we have $\lambda'_i = \lambda_i$), we can take

$$\widetilde{\lambda}'_n = q^{-1}\lambda_c\lambda_d = q^{-1}\lambda_a\lambda_b = \widetilde{\lambda}_n, \tag{4.31}$$

and use the property that unlinking preserves the corresponding Nahm sum, to get

$$P_{Q'}(\boldsymbol{x},q)\big|_{x_i=x\lambda_i'} = P_{\widetilde{Q}'}(\boldsymbol{x},q)\Big|_{x_i=x\lambda_i',\, x_n=x\widetilde{\lambda}_n'} = P_{\widetilde{Q}}(\boldsymbol{x},q)\Big|_{x_i=x\lambda_i,\, x_n=x\widetilde{\lambda}_n} = P_Q(\boldsymbol{x},q)\big|_{x_i=x\lambda_i}\,.$$

Therefore we conclude

$$P_{Q'}(\boldsymbol{x},q)\big|_{\boldsymbol{x}=x\boldsymbol{\lambda}'} = P_Q(\boldsymbol{x},q)\big|_{\boldsymbol{x}=x\boldsymbol{\lambda}} = P_K(x,a,q,t), \tag{4.32}$$

which means that Q' also corresponds to K, as we wanted to show. □

Recall that the knots-quivers change of variables (1.53) for Nahm sum when C corresponds to a knot, introduces the parameters

$$\lambda_i = a^{a_i} q^{q_i - C_{ii}} (-t)^{C_{ii}},\ \ i = 1 \dots m, \tag{4.33}$$

where m is the size of quiver matrix and, in our case studies, also the number of generators of the uncolored HOMFLY-PT homology for a knot. In practice, for various quivers corresponding to knots we start from looking for quadruples $\lambda_a, \lambda_b, \lambda_c, \lambda_d$ that satisfy the condition $\lambda_a\lambda_b = \lambda_c\lambda_d$. We refer to such a quadruple $a, b, c, d \in Q_0$ as a *pairing*. If all the conditions in theorem 4.3.1 hold, we call such pairing a *symmetry*. For example, the two quivers for 4_1 knot are related by such transposition, therefore they are equivalent:

$$\begin{array}{c} \\ \lambda_1 \\ \lambda_2 \\ \lambda_3 \\ \lambda_4 \\ \lambda_5 \\ \\ \end{array}\!\!\begin{array}{c} \begin{array}{ccccc} \lambda_1 & \lambda_2 & \lambda_3 & \lambda_4 & \lambda_5 \end{array} \\ \left[\begin{array}{ccccc} 0 & 0 & -1 & 0 & -1 \\ 0 & 2 & 0 & 1 & -1 \\ -1 & 0 & -1 & 0 & -2 \\ 0 & 1 & 0 & 1 & -1 \\ -1 & -1 & -2 & -1 & -2 \end{array}\right] \end{array} \xleftrightarrow{\lambda_2\lambda_5=\lambda_3\lambda_4} \left[\begin{array}{ccccc} 0 & 0 & -1 & 0 & -1 \\ 0 & 2 & 0 & 1 & 0 \\ -1 & 0 & -1 & -1 & -2 \\ 0 & 1 & -1 & 1 & -1 \\ -1 & 0 & -2 & -1 & -2 \end{array}\right]. \tag{4.34}$$

Moreover, there are no other pairings which satisfy this conditions, and some extra analysis shows that this is the complete set of equivalent quivers for 4_1 knot. Besides, in the case of 3_1 knot and the reduced HOMFLY-PT homology the quiver (1.56) has only 3 nodes and does not support this type of transformation, therefore is unique. Importantly, symmetries of quivers are tightly related to homological diagrams for knots. After the change of variables (1.53), each pairing $\lambda_a\lambda_b = \lambda_c\lambda_d$ gives the vector identity $\vec{v}_a + \vec{v}_b = \vec{v}_c + \vec{v}_d$, where $\vec{v}_i = (q_i, a_i)$ encodes the position of the homology generator corresponding to λ_i. This identity can be interpreted as a requirement that the centers of mass for pairs of nodes $\{a, b\}$ and $\{c, d\}$ coincide (assuming that masses of all nodes are equal). We draw it as a parallelogram with the diagonals ab and cd, as shown in figure 4.2.

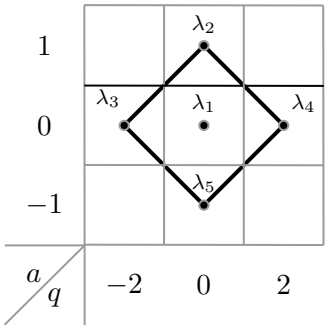

Figure 4.2: Generators of the uncolored, reduced HOMFLY-PT homology for 4_1 knot. The parallelogram corresponds to pairing $\lambda_2\lambda_5 = \lambda_3\lambda_4$.

4.4 Quiver matrices and HOMFLY-PT homologies for torus and twist knots

Here we describe quiver matrices for some torus and twist knots, found in [21]. This would be our input data in the next section.

The first family we consider are the $(2, 2p+1)$ (another notation is $T_{2,2p+1}$) torus knots, with the homology diagram consisting of one zig-zag made of $2p+1$ generators, figure 4.3. These knots are $3_1 = (2,3), 5_1 = (2,5), 7_1 = (2,7)$, and so on. It is convenient way to think of a zig-zag as a several wedges ($\wedge$) joined one by one, for example 3_1 knot corresponds to just a single wedge. Of course if there are two wedges connected at a node, this connecting node has the same label for both wedges. The quiver matrix for $T_{2,2p+1}$ knot is given by

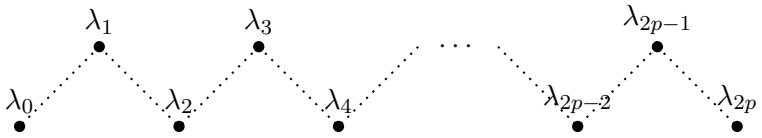

Figure 4.3: Generators of the uncolored, reduced HOMFLY-PT homology for $T_{2,2p+1}$ knot.

$$C^{T_{2,2p+1}} = \begin{bmatrix} 0 & 1 & 1 & 3 & 3 & \dots & 2p-1 & 2p-1 \\ 1 & 2 & 2 & 3 & 3 & \dots & 2p-1 & 2p-1 \\ 1 & 2 & 3 & 4 & 4 & \dots & 2p & 2p \\ 3 & 3 & 4 & 4 & 4 & \dots & 2p-1 & 2p-1 \\ 3 & 3 & 4 & 4 & 5 & \dots & 2p & 2p \\ \vdots & \vdots & \vdots & \vdots & \vdots & \ddots & \vdots & \vdots \\ 2p-1 & 2p-1 & 2p & 2p-1 & 2p & \dots & 2p & 2p \\ 2p-1 & 2p-1 & 2p & 2p-1 & 2p & \dots & 2p & 2p+1 \end{bmatrix}, \tag{4.35}$$

so that λ_i corresponds to $C_{ii} = i - \delta_{1,1}$. The homological degrees t_i are encoded in the diagonal of (4.35)

$$(t_i) = (0, 2, 3, 4, 5, \dots, 2p, 2p+1). \tag{4.36}$$

Moreover, the parameters a_i and l_i (and so q_i) in the knots-quivers change of variables (1.53)

are determined by

$$\sum_i a_i d_i = 2pr + 2\alpha_1 = 2p(d_1 + d_2 + d_4 + \ldots + d_{2p}) + 2(p+1)(d_3 + d_5 + \ldots + d_{2p+1}), \quad (4.37)$$

$$\begin{aligned}\sum_i l_i d_i = &-2pd_1 + 2(1-p)d_2 + \big(2(1-p)-3\big)d_3 + \\ &+ 2(2-p)d_4 + \big(2(2-p)-3\big)d_5 + \\ &\quad\vdots \\ &+ 2(p-1-p)d_{2(p-1)} + \big(2(p-1-p)-3\big)d_{2(p-1)+1} + \\ &+ 2(p-p)d_{2p} + \big(2(p-p)-3\big)d_{2p+1}.\end{aligned} \quad (4.38)$$

Example 4.4.1. In order to illustrate how the values of t_i, a_i, q_i determine the homology diagram in figure 4.3, take the $T_{2,5}$ knot ($p = 2$). The quiver matrix is given by

$$C^{T_{2,5}} = \begin{bmatrix} 0 & 1 & 1 & 3 & 3 \\ 1 & 2 & 2 & 3 & 3 \\ 1 & 2 & 3 & 4 & 4 \\ 3 & 3 & 4 & 4 & 4 \\ 3 & 3 & 4 & 4 & 5 \end{bmatrix} \quad (4.39)$$

We can see that there are 5 homology generators, and from the main diagonal we can read-off their homological degrees

$$(t_1, t_2, t_3, t_4, t_5) = (0, 2, 3, 4, 5). \quad (4.40)$$

To determine the positions of the generators, we use the formulas (4.37), (4.38) and $q_i = l_i + t_i$, to get

$$\begin{aligned}(a_1, a_2, a_3, a_4, a_5) &= (4, 4, 6, 4, 6), \\ (l_1, l_2, l_3, l_4, l_5) &= (-4, -2, -5, 0, -3), \\ (q_1, q_2, q_3, q_4, q_5) &= (-4, 0, -2, 4, 2).\end{aligned} \quad (4.41)$$

We can draw the corresponding points in the (a, q) plane (figure 4.4). A similar analysis shows

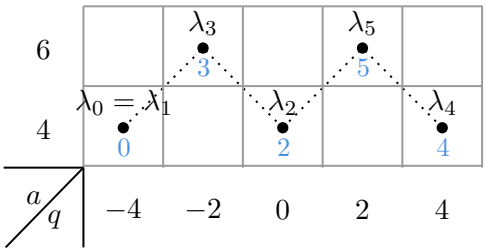

Figure 4.4: Generators of the uncolored, reduced HOMFLY-PT homology for $T_{2,5}$ knot.

the zig-zag shape (figure 4.3) for an arbitrary $T_{2,2p+1}$ knot.

The second family of our interest includes the $TK_{2|p|+2}$ twist knots, with the homology consisting of several diamonds (figure 4.5, left). They include knots $4_1, 6_1, 8_1$, and so on. For

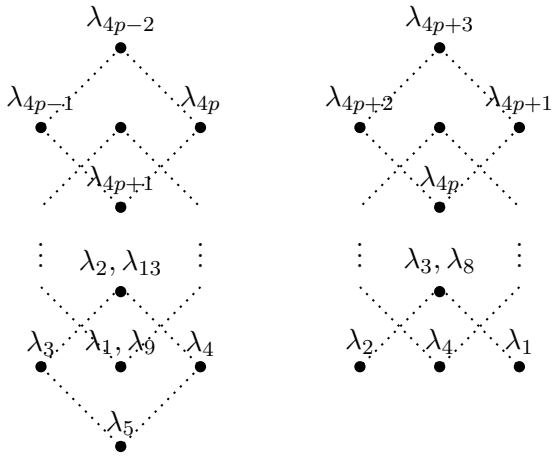

Figure 4.5: Generators of the uncolored, reduced HOMFLY-PT homologies for $TK_{2|p|+2}$ (on the left) and TK_{2p+1} (on the right) knots.

example, 4_1 knot corresponds just to a single diamond, shown in figure 4.2. The quiver matrix is given by

$$C^{TK_{2|p|+2}} = \begin{bmatrix} F_0 & F & F & F & \cdots & F & F \\ F^T & D_1 & R_1 & R_1 & \cdots & R_1 & R_1 \\ F^T & R_1^T & D_2 & R_2 & \cdots & R_2 & R_2 \\ F^T & R_1^T & R_2^T & D_3 & \cdots & R_3 & R_3 \\ \vdots & \vdots & \vdots & \vdots & \ddots & \vdots & \vdots \\ F^T & R_1^T & R_2^T & R_3^T & \cdots & D_{|p|-1} & R_{|p|-1} \\ F^T & R_1^T & R_2^T & R_3^T & \cdots & R_{|p|-1}^T & D_{|p|} \end{bmatrix}, \tag{4.42}$$

where

$$F_0 = [0]\,, \qquad F = \begin{bmatrix} 0 & -1 & 0 & -1 \end{bmatrix}, \tag{4.43}$$

$$D_k = \begin{bmatrix} 2k & 2k-2 & 2k-1 & 2k-3 \\ 2k-2 & 2k-3 & 2k-2 & 2k-4 \\ 2k-1 & 2k-2 & 2k-1 & 2k-3 \\ 2k-3 & 2k-4 & 2k-3 & 2k-4 \end{bmatrix}, \qquad R_k = \begin{bmatrix} 2k & 2k-2 & 2k-1 & 2k-3 \\ 2k-1 & 2k-3 & 2k-2 & 2k-4 \\ 2k & 2k-1 & 2k-1 & 2k-3 \\ 2k-2 & 2k-3 & 2k-2 & 2k-4 \end{bmatrix}. \tag{4.44}$$

The element F_0 represents a zig-zag of length 1, i.e. a single homology generator, while the diagonal blocks D_k represent diamonds (up to a permutation of homology generators and an overall shift). The identification with λ_i's in D_k and R_k goes as follows:

	λ_{4k-2}	λ_{4k-1}	λ_{4k}	λ_{4k+1}
λ_{4k-2}	$2k$	$2k-2$	$2k-1$	$2k-3$
λ_{4k-1}	$2k-2$	$2k-3$	$2k-2$	$2k-4$
λ_{4k}	$2k-1$	$2k-2$	$2k-1$	$2k-3$
λ_{4k+1}	$2k-3$	$2k-4$	$2k-3$	$2k-4$

	λ_{4k-2}	λ_{4k-1}	λ_{4k}	λ_{4k+1}
$\lambda_{4k'-2}$	$2k$	$2k-1$	$2k$	$2k-2$
$\lambda_{4k'-1}$	$2k-2$	$2k-3$	$2k-1$	$2k-3$
$\lambda_{4k'}$	$2k-1$	$2k-2$	$2k-1$	$2k-2$
$\lambda_{4k'+1}$	$2k-3$	$2k-4$	$2k-3$	$2k-4$

(4.45)

This means that D_k encodes interactions of nodes nodes within one diamond, while R_k encodes interactions of nodes from two diamonds labelled by r, r'.

The knots-quivers change of variables (1.53) for the $TK_{2|p|+2}$ knot can be read-off from

$$\begin{aligned}(-1)^{\sum_i p_i d_i} &= (-1)^{(d_3+d_4)+(d_7+d_8)+\ldots+(d_{4|p|-1}+d_{4|p|})+2(d_5+d_9+\ldots+d_{4|p|+1})},\\ \sum_i a_i d_i &= 2d_2+0d_3+0d_4-2d_5+\\ &\quad +4d_6+2d_7+2d_8+0d_9+\\ &\quad \vdots\\ &\quad +2|p|d_{4|p|-2}+(2|p|-2)\,d_{4|p|-1}+(2|p|-2)\,d_{4|p|}+(2|p|-4)\,d_{4|p|+1},\\ \sum_i l_i d_i &= -2d_2-d_3+d_4+2d_5+\\ &\quad -4d_6-3d_7-1d_8+0d_9+\\ &\quad \vdots\\ &\quad -2|p|d_{4|p|-2}+(1-2|p|)\,d_{4|p|-1}+(3-2|p|)\,d_{4|p|}+(4-2|p|)\,d_{4|p|+1}.\end{aligned} \tag{4.46}$$

$$\begin{aligned}(-1)^{\sum_i p_i d_i} &= (-1)^{(d_3+d_4)+(d_7+d_8)+\ldots+(d_{4|p|-1}+d_{4|p|})+2(d_5+d_9+\ldots+d_{4|p|+1})},\\ \sum_i a_i d_i &= 2d_2+0d_3+0d_4-2d_5+\\ &\quad +4d_6+2d_7+2d_8+0d_9+\\ &\quad \vdots\\ &\quad +2|p|d_{4|p|-2}+(2|p|-2)\,d_{4|p|-1}+(2|p|-2)\,d_{4|p|}+(2|p|-4)\,d_{4|p|+1},\\ \sum_i l_i d_i &= -2d_2-d_3+d_4+2d_5+\\ &\quad -4d_6-3d_7-1d_8+0d_9+\\ &\quad \vdots\\ &\quad -2|p|d_{4|p|-2}+(1-2|p|)\,d_{4|p|-1}+(3-2|p|)\,d_{4|p|}+(4-2|p|)\,d_{4|p|+1}.\end{aligned} \tag{4.47}$$

The third family we consider are the $TK_{2|p|+1}$ knots, with the homology consisting of p diamonds and a zig-zag made of one generator, so altogether it has $4p+1$ generators. They include $5_2, 7_2, 9_2$ and other knots. Quiver matrices for TK_{2p+1} twist knots are

$$C^{TK_{2p+1}} = \begin{bmatrix} D_1 & R_1 & R_1 & R_1 & \cdots & R_1 & R_1\\ R_1^T & D_2 & R_2 & R_2 & \cdots & R_2 & R_2\\ R_1^T & R_2^T & D_3 & R_3 & \cdots & R_3 & R_3\\ R_1^T & R_2^T & R_3^T & D_4 & \cdots & R_4 & R_4\\ \vdots & \vdots & \vdots & \vdots & \ddots & \vdots & \vdots\\ R_1^T & R_2^T & R_3^T & R_4^T & \cdots & D_{p-1} & R_{p-1}\\ R_1^T & R_2^T & R_3^T & R_4^T & \cdots & R_{p-1}^T & D_p \end{bmatrix}, \tag{4.48}$$

where the block elements in the first row and column are

$$D_1 = \begin{bmatrix} 2 & 1 & 2\\ 1 & 0 & 1\\ 2 & 1 & 3 \end{bmatrix}, \qquad R_1 = \begin{bmatrix} 1 & 2 & 1 & 2\\ 0 & 2 & 0 & 1\\ 1 & 3 & 2 & 3 \end{bmatrix}, \tag{4.49}$$

and all other elements, for $k>1$, take the form

$$D_k = \begin{bmatrix} 2k-3 & 2k-2 & 2k-3 & 2k-2\\ 2k-2 & 2k & 2k-1 & 2k\\ 2k-3 & 2k-1 & 2k-2 & 2k-1\\ 2k-2 & 2k & 2k-1 & 2k+1 \end{bmatrix}, \qquad R_k = \begin{bmatrix} 2k-3 & 2k-2 & 2k-3 & 2k-2\\ 2k-1 & 2k & 2k-1 & 2k\\ 2k-2 & 2k & 2k-2 & 2k-1\\ 2k-1 & 2k+1 & 2k & 2k+1 \end{bmatrix}. \tag{4.50}$$

In this case D_1 represents a zig-zag of the same form as for the trefoil knot, and D_k (for $k>1$) represent diamonds (up to a permutation of homology generators and an overall constant shift).

For this family of knots the change of variables (1.53) is given by

$$(-1)^{\sum_{i=3}^{4p+1} t_i d_i} = (-1)^{(d_3+d_4)+(d_7+d_8)+\ldots+(d_{4p-1}+d_{4p})+2(d_5+d_9+\ldots+d_{4p+1})}$$

$$\begin{aligned}
\sum_{i=3}^{4p+1} a_i d_i = {} & 2(d_3+d_4) + 4d_5 + \\
& + 2d_6 + 4d_7 + 4d_8 + 6d_9 + \\
& + 4d_{10} + 6d_{11} + 6d_{12} + 8d_{13} + \\
& \vdots \\
& + 2(p-1)d_{4p-2} + 2pd_{4p-1} + 2pd_{4p} + 2(p+1)d_{4p+1}
\end{aligned} \tag{4.51}$$

$$\begin{aligned}
\sum_{i=2}^{4p} l_i d_i = {} & -2d_4 - 3d_5 + \\
& - d_6 - 2d_7 - 4d_8 - 5d_9 + \\
& - 3d_{10} - 4d_{11} - 6d_{12} - 7d_{13} + \\
& \vdots \\
& + (1-2p)d_{4p-2} + (2-2p)d_{4p-1} + (-2p)d_{4p} + (-1-2p)d_{4p+1}.
\end{aligned} \tag{4.52}$$

4.5 Local equivalences for knots

Here we identify for quivers from section 4.4 all transpositions of arrows satisfying the conditions of theorem 4.3.1. We call them local symmetries, because they give rise to equivalent quivers. We study the three infinite families of knots mentioned before, and additionally $6_2, 6_3$ and 7_3 knots. The ordering of homological generators is fixed consistently with the ordering of quiver nodes in section 4.4 and allows to enumerate the wedges and diamonds in figures 4.3 and 4.5 by an index $r = 0, \ldots, p$. We also denote pairings by

$$\lambda_a \lambda_b = \lambda_c \lambda_d \quad \Longleftrightarrow \quad \begin{pmatrix} a & b \\ c & d \end{pmatrix} \tag{4.53}$$

Proposition 4.5.1. *Quiver matrices (4.35), (4.42) and (4.48) have the following local symmetries*

$$\begin{aligned}
T_{2,2p+1}: \quad & \begin{pmatrix} 2r & 2r'+3 \\ 2r+3 & 2r' \end{pmatrix}, \ \begin{pmatrix} 2r+3 & 2r'+2 \\ 2r+2 & 2r'+3 \end{pmatrix} \\
TK_{2|p|+2}: \quad & \begin{pmatrix} 4r-1 & 4r' \\ 4r & 4r'-1 \end{pmatrix}, \ \begin{pmatrix} 4r-1 & 4r'-2 \\ 4r-2 & 4r'-1 \end{pmatrix}, \ \begin{pmatrix} 4r+1 & 4r' \\ 4r & 4r'+1 \end{pmatrix}, \\
& \begin{pmatrix} 4r+1 & 4r''-2 \\ 4r'+1 & 4r'-2 \end{pmatrix}, \ \begin{pmatrix} 4 & 4p-1 \\ 5 & 4p-2 \end{pmatrix} \\
TK_{2p+1}: \quad & \begin{pmatrix} 2 & 4r'+3 \\ 3 & 4r'+2 \end{pmatrix}, \ \begin{pmatrix} 2 & 4r'+1 \\ 1 & 4r'+2 \end{pmatrix}, \ \begin{pmatrix} 2 & 4p+1 \\ 3 & 4p \end{pmatrix}, \ \mathcal{S}^T_{2|p|+2}
\end{aligned} \tag{4.54}$$

such that $r' = r+1$, $r'' = r+2$, *and*

$$\mathcal{S}^T_{2|p|+2} := \begin{pmatrix} 4r+2 & 4r'+1 \\ 4r+1 & 4r'+2 \end{pmatrix}, \begin{pmatrix} 4r & 4r'+1 \\ 4r+1 & 4r' \end{pmatrix}, \begin{pmatrix} 4r+2 & 4r'+3 \\ 4r+3 & 4r'+2 \end{pmatrix}, \begin{pmatrix} 4r & 4r''+3 \\ 4r' & 4r'+3 \end{pmatrix}. \tag{4.55}$$

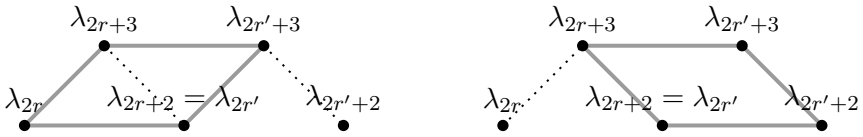

Figure 4.6: The two local symmetries for quiver matrix (4.35).

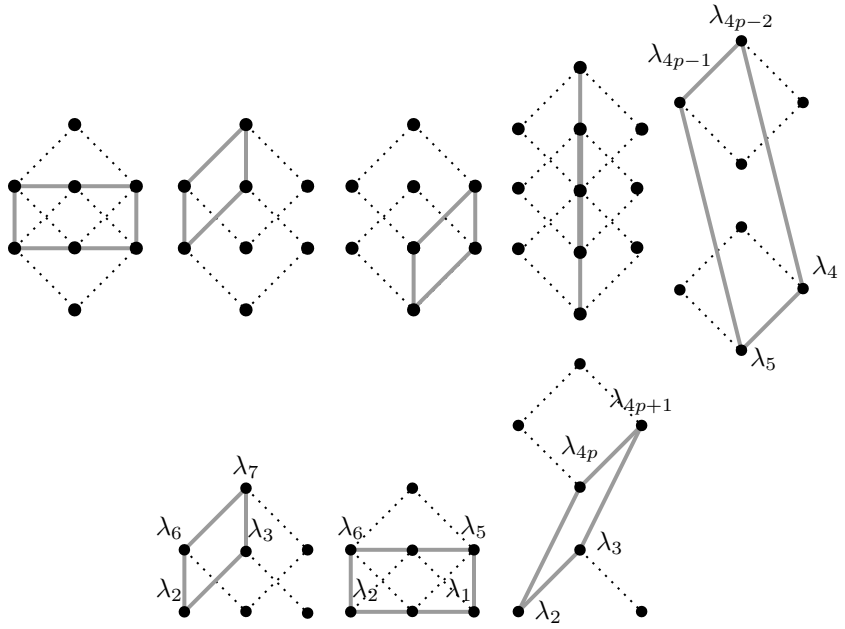

Figure 4.7: The five local symmetries for quiver matrices (4.42), top, and the three local symmetries for quiver matrices (4.48), bottom. The missing labels for the first four diagrams indicate that these symmetries are shared between (4.42) and (4.48).

These symmetries can be drawn as parallelograms on the corresponding homological diagrams (figures 4.6 and 4.7). Below we give a comprehensive analysis of each of the three infinite families of knots. It is followed by the analysis of $6_2, 6_3, 7_3$ knots.

4.5.1 Torus knots $T_{2,2p+1}$: $3_1, 5_1, 7_1, \ldots$

For this family of knots, the homology diagram is a chain of p consecutive wedges (figure 4.3), and we label them by $r = 0, \ldots, p-1$. Note that $\lambda_0 = \lambda_1$ corresponds to x_1, while λ_i corresponds to x_i. This notation is convenient, since elsewhere in the formulas we can simply assign $r = 0$ to the leftmost wedge. Note that the quiver matrix (4.35) can be presented as

$$\begin{array}{lllll} i,j \text{ both odd or even:} & C_{ij} = j-1, & i=j: & C_{jj} = j, & \\ i \text{ odd, } j \text{ even:} & C_{ij} = j, & j \text{ even:} & C_{1j} = j-1, & (4.56) \\ i \text{ even, } j \text{ odd:} & C_{ij} = j-2+\delta_{i+1,j}, & j \text{ odd:} & C_{1j} = j-2. & \end{array}$$

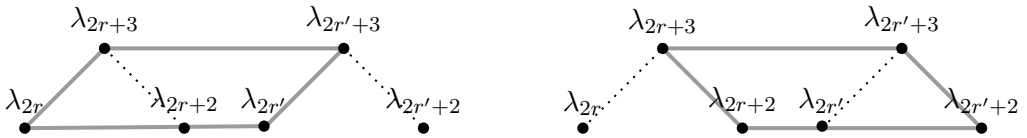

Figure 4.8: The two kinds of pairings between wedges.

Suppose that a pairing is made of generators from only two wedges, not necessarily joined together (figure 4.8). A direct check of conditions (table 4.1) shows that it is a local symmetry if and only if $r' = r + 1$, meaning that these wedges are actually connected. In order to confirm that there are no other symmetries, we consider the four consecutive wedges labelled by $r < r' < r'' < r'''$. In consequence equation (4.56) leads to the four cases

$$1)\quad C_{ab} = 2r'' + 1,\ C_{cd} = 2r' + 1 \qquad 2)\quad C_{ab} = 2r'' + 2,\ C_{cd} = 2r' + 1$$

$$3)\quad C_{ab} = 2r''' + 1,\ C_{cd} = \begin{cases} 2r' + 1,\ r'' = r' + 1 \\ 2r'',\ r'' > r' + 1 \end{cases} \qquad 4)\quad C_{ab} = 2r''' + 2,\ C_{cd} = 2r'' + 1$$

It follows that the condition $|C_{ab} - C_{cd}| = 1$ cannot be met, which shows that the only local symmetries are indeed those in figure 4.6.

Pairing $b = c + 3, d = a + 3$

$a = a$
$b = c + 3$
$c = c$
$d = a + 3$

$$\begin{pmatrix} a & \boxed{b-2} & c-1 & d-2 \\ \boxed{b-2} & b & b-2 & b-1 \\ c-1 & b-2 & c & c \\ d-2 & b-1 & c & d \end{pmatrix}$$

$s < a$, odd	$a + (b-1) = c + (d-1)$
$s < a$, even	$(a-1) + (b-2) =$
	$(c-1) + (d-2)$
$s > b$, odd	$(s-2) + (s-1) =$
	$(s-2) + (s-1)$
$s > b$, even	$(s-1) + s = (s-1) + s$
$d < s < c$, odd	$(s-2) + (b-1) \neq c + (s-1)$
$d < s < c$, even	$(s-1) + (b-2) \neq (c-1) + d$
$s = a + 2$	$(i+1) + (j-2) \neq$
	$(k-1) + (l-1)$
$s = c + 1$	$(s-2) + (j-1) \neq$
	$(s-1) + (s-1)$

Pairing $b = c + 1, d = a + 1$

$a = a$
$b = c + 1$
$c = c$
$d = a + 1$

$$\begin{pmatrix} a & b-2 & c-1 & d-1 \\ b-2 & b & b-1 & b-1 \\ c-1 & b-1 & c & \boxed{c} \\ d-1 & b-1 & \boxed{c} & d \end{pmatrix}$$

$s < d$, odd	$a + (b-1) = c + (d-1)$
$s < d$, even	$(a-1) + (b-2) =$
	$(c-1) + (d-2)$
$s > c$, odd	$(s-2) + (s-1) =$
	$(s-2) + (s-1)$
$s > c$, even	$(s-1) + s = (s-1) + s$
$a < s < b$, odd	$(s-2) + (b-1) \neq c + (s-1)$
$a < s < b$, even	$(s-1) + (b-2) \neq (c-1) + d$

Table 4.1: The local symmetries of quivers (4.35) for $T_{2,2p+1}$ torus knots.

4.5.2 Twist knots $TK_{2|p|+2}$: $4_1, 6_1, 8_1, \ldots$

For this family of knots, the homology diagram consists of p diamonds and an extra dot (figure 4.5). Table 4.2 shows all possible pairings which can occur between the homology diamonds for this family of knots.

2 diamonds

a	$\underline{4r-1}$	$\underline{4r-1}$	$\underline{4r+1}$	$4r+1$	$\underline{4r+1}$	$4r$	$4r+1$	$4r-1$	$4r$	$4r+1$
b	$\underline{4r'}$	$\underline{4r'-2}$	$\underline{4r'}$	$4r'-2$	$\underline{4r'-2}$	$4r'-2$	$4r'-1$	$4r'$	$4r'-1$	$4r'-2$
c	$\underline{4r}$	$\underline{4r-2}$	$\underline{4r}$	$4r-1$	$\underline{4r}$	$4r-2$	$4r-1$	$4r-2$	$4r-2$	$4r-2$
d	$\underline{4r'-1}$	$\underline{4r'-1}$	$\underline{4r'+1}$	$4r'$	$\underline{4r'-1}$	$4r'$	$4r'+1$	$4r'+1$	$4r'+1$	$4r'+1$

3 diamonds, equally distant

$4r-2$ $4r''$ $4r'-2$ $4r'$	$4r-2$ $4r''-1$ $4r'-2$ $4r'-1$	$4r-1$ $4r''+1$ $4r'-1$ $4r'+1$	$4r-1$ $4r''$ $4r'-1$ $4r'$	$4r$ $4r''+1$ $4r'$ $4r'+1$	$4r-2$ $4r''+1$ $4r'-1$ $4r'$	$4r+1$ $4r''-2$ $4r'-1$ $4r'$	$4r$ $4r''-1$ $4r'+1$ $4r'-2$	$4r-2$ $4r''+1$ $4r'+1$ $4r'-2$
$4r-1$ $4r''-2$ $4r'-1$ $4r'-2$	$4r$ $4r''-1$ $4r'$ $4r'-1$	$4r$ $4r''-2$ $4r'$ $4r'-2$	$4r-1$ $4r''$ $4r'+1$ $4r'-2$	$\underline{4r+1}$ $\underline{4r''-2}$ $\underline{4r'+1}$ $\underline{4r'-2}$				

3 diamonds, shifted up / down

$4r+1$ $4r''+1$ $4r'-1$ $4r'$	$4r+1$ $4r''$ $4r'$ $4r'-2$	$4r-1$ $4r''+1$ $4r'-1$ $4r'-2$	$4r$ $4r''+1$ $4r'$ $4r'-2$	$4r+1$ $4r''-1$ $4r'-1$ $4r'-2$	$4r-2$ $4r''-2$ $4r'-1$ $4r'$	$4r$ $4r''-2$ $4r'+1$ $4r'$	$4r-2$ $4r''-1$ $4r'+1$ $4r'-1$	$4r-2$ $4r''$ $4r'+1$ $4r'$	$4r-1$ $4r''-2$ $4r'-1$ $4r'+1$

4 diamonds, equally distant

$4r-1$ $4r'''$ $4r'$ $4r''-1$	$4r-1$ $4r'''+1$ $4r'+1$ $4r''-1$	$4r$ $4r'''+1$ $4r'+1$ $4r''$	$4r+1$ $4r'''-2$ $4r'$ $4r''-1$	$4r+1$ $4r'''-2.$ $4r'-1$ $4r''$	$4r-1$ $4r'''$ $4r'+1$ $4r''-2$	$4r+1$ $4r'''-2$ $4r'$ $4r''-1$	$4r$ $4r'''$ $4r'$ $4r''$
$4r-1$ $4r'''-2$ $4r'-2$ $4r''-1$	$4r$ $4r'''-1$ $4r'-1$ $4r''$	$4r$ $4r'''-2$ $4r'-2$ $4r''$	$4r+1$ $4r'''-1$ $4r'-1$ $4r''+1$	$4r+1$ $4r'''$ $4r'$ $4r''+1$	$4r$ $4r'''-1$ $4r'+1$ $4r''-2$	$4r-1$ $4r'''$ $4r'-2$ $4r''+1$	
$4r-2$ $4r'''-1$ $4r'-1$ $4r''-2$	$4r-2$ $4r'''$ $4r'$ $4r''-2$	$4r-2$ $4r'''+1$ $4r'-1$ $4r''$	$4r-2$ $4r'''+1$ $4r'$ $4r''-1$	$4r+1$ $4r'''-2$ $4r'+1$ $4r''-2$	$4r+1$ $4r'''-2$ $4r'-2$ $4r''+1$	$4r-1$ $4r'''-1$ $4r'-1$ $4r''-1$	

4 diamonds, shifted up / down

$4r-1$ $4r'''$ $4r'+1$ $4r''+1$	$4r-2$ $4r'''$ $4r'$ $4r''+1$	$4r-2$ $4r'''$ $4r'+1$ $4r''$	$4r-2$ $4r'''-2$ $4r'-1$ $4r''$	$4r-1$ $4r'''-2$ $4r'-1$ $4r''+1$	$4r$ $4r'''-1$ $4r'+1$ $4r''+1$	$4r+1$ $4r'''$ $4r'-2$ $4r''$	$4r-2$ $4r'''-2$ $4r'$ $4r''-1$	$4r-2$ $4r'''-1$ $4r'+1$ $4r''-1$	$4r-2$ $4r'''-1$ $4r'-1$ $4r''+1$
$4r$ $4r'''-1$ $4r'-2$ $4r''-2$	$4r$ $4r'''+1$ $4r'-2$ $4r''$	$4r$ $4r'''+1$ $4r'$ $4r''-2$	$4r+1$ $4r'''+1$ $4r'$ $4r''-1$	$4r+1$ $4r'''-1$ $4r'-2$ $4r''-1$	$4r$ $4r'''-2$ $4r'$ $4r''+1$	$4r-1$ $4r'''+1$ $4r'-1$ $4r''-2$	$4r-1$ $4r'''+1$ $4r'-2$ $4r''-1$	$4r-1$ $4r'''$ $4r'-2$ $4r''-2$	

Table 4.2: All pairings between diamonds for knot $TK_{2|p|+2}$. The five local symmetries are underlined.

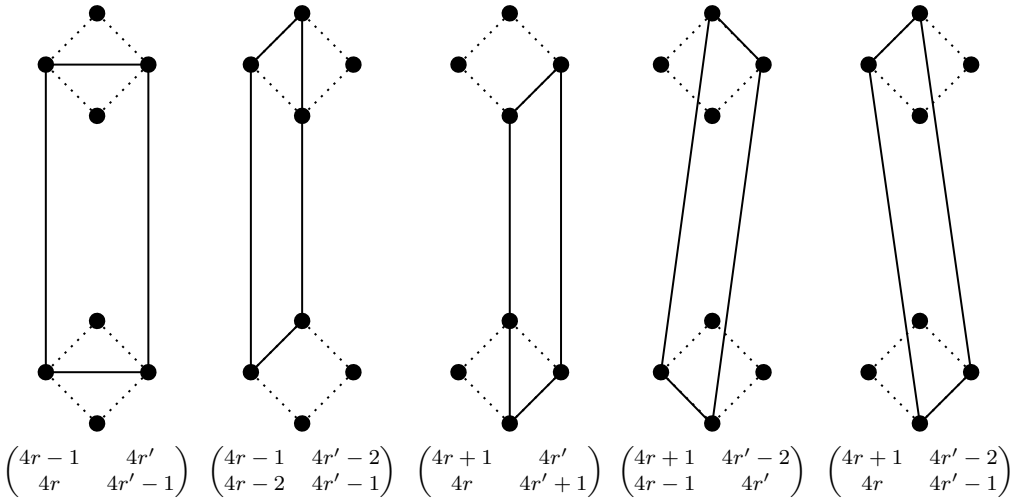

Figure 4.9: Pairings between two homology diamonds labelled by r and r'.

We now show that the five underlined pairings in table 4.2 are local symmetries. The detailed analysis of four of them is given in table 4.3. The top-right pairing in this table is a particular case of another pairing

$$\begin{pmatrix} 4r+1 & 4r''-2 \\ 4r'+1 & 4r'-2 \end{pmatrix} \tag{4.57}$$

From the sub-matrix

$$\begin{matrix} a = 4r+1 \\ b = 4r'-2 \\ c = 4r+5 \\ d = 4r'-6 \end{matrix} \quad \begin{pmatrix} 2r-4 & 2r-2 & 2r-4 & 2r-2-\delta_{r+1,r'} \\ 2r-2 & 2r' & 2r & 2r'-2 \\ 2r-4 & 2r & 2r-2 & 2r-\delta_{r+2,r'} \\ 2r-2-\delta_{r+1,r'} & 2r'-2 & 2r-\delta_{r+2,r'} & 2r'-2 \end{pmatrix} \tag{4.58}$$

we see that $r' = r+2$ is the only candidate for a symmetry (otherwise $|C_{ab} - C_{cd}| = 1$ is not

$a = 4r-1$
$b = 4r'$
$c = 4r$
$d = 4r'-1$

$$\begin{pmatrix} 2r-3 & 2r-2 & 2r-2 & 2r-3 \\ 2r-2 & 2r'-1 & 2r-1 & 2r'-2 \\ 2r-2 & 2r-1 & 2r-1 & \boxed{2r-1} \\ 2r-3 & 2r'-2 & \boxed{2r-1} & 2r'-3 \end{pmatrix}$$

$\underline{r < r'' < r' :}$

$4r''-2$	$2r-1+2r''-1 = 2r+2r''-2$
$4r''-1$	$2r-3+2r''-2 \neq 2r-1+2r''-3$
$4r''$	$2r-2+2r''-1 = 2r-1+2r''-2$
$4r''+1$	$2r-4+2r''-2 = 2r-3+2r''-3$

$\underline{r < r' < r'' :}$

$4r''-2$	$2r-1+2r' = 2r+2r'-1$
$4r''-1$	$2r-3+2r'-1 = 2r-1+2r'-3$
$4r''$	$2r-2+2r'-1 = 2r-1+2r'-2$
$4r''+1$	$2r-4+2r'-3 = 2r-3+2r'-4$

$\underline{r'' < r < r' :}$

$4r''-2$	$2r''-4+2r''-1 = 2r''-1+2r''-4$
$4r''-1$	$2r''-3+2r''-2 = 2r''-2+2r''-3$
$4r''$	$2r''-1+2r''-1 = 2r''-1+2r''-1$
$4r''+1$	$2r''-4+2r''-2 = 2r''-2+2r''-4$

$4r+1$
$4r'-2$
$4r+5$
$4r'-6$

$$\begin{pmatrix} 2r-4 & 2r-2 & 2r-4 & 2r-2 \\ 2r-2 & 2r' & 2r & 2r'-2 \\ 2r-4 & 2r & 2r-2 & \boxed{2r-1} \\ 2r-2 & 2r'-2 & \boxed{2r-1} & 2r'-2 \end{pmatrix}$$

$\underline{\text{The left vertical axis:}}$

$\ldots, 4r-9, 4r-5$	$2r-6+2r-3 = 2r-6+2r-3$
$4r-1$	$2r-4+2r-1 = 2r-4+2r-1$
$4r+3$	$2r-3+2r+1 = 2r-2+2r$
$4r+7, 4r+11, \ldots$	$2r-3+2r+2 = 2r-1+2r$

$\underline{\text{The right vertical axis:}}$

$\ldots, 4r-8, 4r-4$	$2r-5+2r-2 = 2r-5+2r-2$
$4r$	$2r-3+2r = 2r-3+2r$
$4r+4$	$2r-2+2r+2 = 2r-1+2r+1$
$4r+8, 4r+12, \ldots$	$2r-2+2r+3 = 2r+2r+1$

$\underline{\text{The middle vertical axis:}}$

$4r''-2, r'' \leq p$	$2r''-3+2r'' = 2r''-3+2r''$
$4r+9, 4r+13, \ldots$	$2r-4+2r+1 = 2r-2+2r-1$

$4r-1$
$4r'-2$
$4r-2$
$4r'-1$

$$\begin{pmatrix} 2r-3 & \boxed{2r-1} & 2r-2 & 2r-3 \\ \boxed{2r-1} & 2r' & 2r & 2r'-2 \\ 2r-2 & 2r & 2r & 2r-2 \\ 2r-3 & 2r'-2 & 2r-2 & 2r'-3 \end{pmatrix}$$

$\underline{r'' < r < r' :}$

$4r''-2$	$2r''-4+2r''-2 = 2r''-2+2r''-4$
$4r''-1$	$2r''-3+2r''-1 = 2r''-1+2r''-3$
$4r''$	$2r''-1+2r'' = 2r''+2r''-1$
$4r''+1$	$2r''-4+2r''-2 = 2r''-2+2r''-4$

$\underline{r < r'' < r' :}$

$4r''-2$	$2r-1+2r'' \neq 2r+2r''-2$
$4r''-1$	$2r-3+2r''-1 \neq 2r-2+2r''-3$
$4r''$	$2r-2+2r'' = 2r-1+2r''-1$
$4r''+1$	$2r-4+2r''-2 \neq 2r-1+2r''-3$

$\underline{r < r' < r'' :}$

$4r''-2$	$2r-1+2r' = 2r+2r'-1$
$4r''-1$	$2r-3+2r'-2 = 2r-2+2r'-3$
$4r''$	$2r-2+2r'-2 = 2r-2+2r'-2$
$4r''+1$	$2r-4+2r'-3 = 2r-3+2r'-4$

$4r+1$
$4r'$
$4r$
$4r'+1$

$$\begin{pmatrix} 2r-4 & \boxed{2r-2} & 2r-3 & 2r-4 \\ \boxed{2r-2} & 2r'-1 & 2r-1 & 2r'-3 \\ 2r-3 & 2r-1 & 2r-1 & 2r-3 \\ 2r-4 & 2r'-3 & 2r-3 & 2r'-4 \end{pmatrix}$$

$\underline{r'' < r < r' :}$

$4r''-2$	$2r''-3+2r''-1 = 2r''-1+2r''-3$
$4r''-1$	$2r''-4+2r''-2 = 2r''-2+2r''-4$
$4r''$	$2r''-3+2r''-1 = 2r''-1+2r''-3$
$4r''+1$	$2r''-4+2r''-2 = 2r''-2+2r''-4$

$\underline{r < r'' < r' :}$

$4r''-2$	$2r-2+2r''-3 \neq 2r+2r''-3$
$4r''-1$	$2r-3+2r''-2 = 2r-1+2r''-4$
$4r''$	$2r-2+2r''-1 \neq 2r-1+2r''-3$
$4r''+1$	$2r-4+2r''-2 \neq 2r-3+2r''-4$

$\underline{r < r' < r'' :}$

$4r''-2$	$2r-2+2r'' = 2r+2r''-2$
$4r''-1$	$2r-3+2r''-1 = 2r-1+2r''-3$
$4r''$	$2r-2+2r''-1 = 2r-1+2r''-2$
$4r''+1$	$2r-4+2r''-3 = 2r-3+2r''-4$

Table 4.3: The four pairings which are local symmetries only when $r' = r+1$.

satisfied). The fifth case corresponds to

$$\begin{matrix} a = 4r+1 \\ b = 4r'-2 \\ c = 4r \\ d = 4r'-1 \end{matrix} \quad \begin{pmatrix} 2r-4 & 2r-2 & 2r-3 & 2r-3 \\ 2r-2 & 2r' & 2r & 2r'-2 \\ 2r-3 & 2r & 2r-1 & \boxed{2r-1} \\ 2r-3 & 2r'-2 & \boxed{2r-1} & 2r'-3 \end{pmatrix} \tag{4.59}$$

$$
\begin{array}{ll}
s=4 & (-1)+(2) \neq (1)+(1) \\
s=5 & (-2)+(0) \neq (0)+(-1) \\
\underline{r<r''<r'}: & \\
s=4r-1 & (2r-4)+(2r-1)=(2r-2)+(2r-3) \\
s=4r-2 & (2r-3)+(2r)=(2r-1)+(2r-2) \\
s=4r' & (2r-2)+(2r'-1)=(2r-1)+(2r'-2) \\
s=4r'+1 & (2r-4)+(2r'-3)=(2r-3)+(2r'-4) \\
s=4r'' & (2r-2)+(2r'')=(2r-1)+(2r''-1) \\
\underline{r<r'<r''}: & \\
s=4r''-1 & (2r-3)+(2r'-2) \neq (2r-1)+(2r'-3) \\
s=4r''-2 & (2r-2)+(2r') \neq (2r)+(2r'-1)
\end{array}
$$

We see here that some conditions fail and deduce that (4.59) is a symmetry if and only if $r=1$ and $r'=p$. For example, $r=p=1$ corresponds to the unique symmetry for the figure eight knot.

Summing up, all five cases in the top of figure 4.7 are indeed non-trivial local symmetries. It turns out that all other pairings listed in table 4.2 fail to be a (non-trivial) symmetry. This happens because of the two reasons: when $C_{ab} \neq C_{cd}$, either the condition $|C_{ab}-C_{cd}|=1$ fails in general (which we have verified using the Mathematica program), or it is satisfied only when some diamonds collide and gives again the same five cases.

4.5.3 Twist knots TK_{2p+1}: $3_1, 5_2, 7_2, 9_2, \ldots$

For this family of knots, some local symmetries agree (up to a relabelling of quiver nodes) with those for $TK_{2|p|+2}$ knots (we denote them by $\mathcal{S}^T_{2|p|+2}$ in proposition 4.3.1). This is because the main building blocks (diamonds) for their HOMFLY-PT homologies have essentially the same structure. The difference comes from a zig-zag, which for $TK_{2|p|+2}$ knots is degenerated to a dot, while for TK_{2p+1} knot it takes form of a single wedge of length 3 (compare the two homology diagrams in figure 4.5). In what follows, we only need to study the interaction between this zig-zag and an arbitrary diamond. There are five potential cases:

$$
\begin{pmatrix} 2 & 4r+1 \\ 3 & 4r \end{pmatrix}, \begin{pmatrix} 1 & 4r+2 \\ 3 & 4r \end{pmatrix}, \begin{pmatrix} 2 & 4r+3 \\ 3 & 4r+2 \end{pmatrix}, \begin{pmatrix} 1 & 4r+3 \\ 3 & 4r+1 \end{pmatrix}, \begin{pmatrix} 1 & 4r+2 \\ 2 & 4r+1 \end{pmatrix}, \tag{4.60}
$$

where $r=1,\ldots p-1$. It turns out that one such case is actually trivial

$$
\begin{array}{l} a=1 \\ b=4r+2 \\ c=3 \\ d=4r \end{array} \qquad \begin{pmatrix} 2 & 1 & 2 & 1 \\ 1 & 2r-2 & 2 & 2r-3 \\ 2 & 2 & 3 & 1 \\ 1 & 2r-3 & 1 & 2r-3 \end{pmatrix} \tag{4.61}
$$

The other four pairings are analysed in table 4.4. In the top-left case the only possibility for a symmetry is $r=p-1$, which proves the bottom-right symmetry in figure 4.7. Likewise, the top-right case corresponds to the bottom-left symmetry in figure 4.7, and the rightmost pairing in (4.60) is a symmetry as well, see figure 4.7 (bottom-middle). However, $\lambda_1\lambda_{4r+3}=\lambda_3\lambda_{4r+1}$

does not lead to a symmetry because of the spectator constraint for $s = 2$.

Pairing $(2, 4r+1, 3, 4r)$:

$a = 2$, $b = 4r+1$, $c = 3$, $d = 4r$

$$\begin{pmatrix} 0 & \boxed{2} & 1 & 0 \\ \boxed{2} & 2r & 3 & 2r-2 \\ 1 & 3 & 3 & 1 \\ 0 & 2r-2 & 1 & 2r-3 \end{pmatrix}$$

$s = 1$	$1 + 2 = 2 + 1$
$s = 4r+2$	$0 + 2r + 1 = 2 + 2r - 1$
$s = 4r+3$	$1 + 2r + 2 = 3 + 2r$
$1 < r' < r$:	
$s = 4r'$	$0 + 2r' - 2 = 1 + 2r' - 3$
$s = 4r'+1$	$2 + 2r' = 3 + 2r' - 1$
$s = 4r'+2$	$0 + 2r' = 2 + 2r' - 2$
$s = 4r'+3$	$1 + 2r' + 1 = 3 + 2r' - 1$
$r < r'$:	
$s = 4r'$	$0 + 2r - 1 \neq 1 + 2r - 3$

Pairing $(2, 4r+3, 3, 4r+2)$:

$a = 2$, $b = 4r+3$, $c = 3$, $d = 4r+2$

$$\begin{pmatrix} 0 & 1 & 1 & 0 \\ 1 & 2r+3 & 3 & 2r+1 \\ 1 & 3 & 3 & \boxed{2} \\ 0 & 2r+1 & \boxed{2} & 2r \end{pmatrix}$$

$s = 1$	$1 + 2 = 2 + 1$
$s = 4r$	$0 + 2r = 1 + 2r - 1$
$s = 4r+1$	$2 + 2r + 2 = 3 + 2r + 1$
$1 < r' < r$:	
$s = 4r'$	$0 + 2r' = 1 + 2r' - 1$
$s = 4r'+1$	$2 + 2r' + 2 = 3 + 2r' + 1$
$s = 4r'+2$	$0 + 2r' + 1 \neq 2 + 2r'$
$s = 4r'+3$	$1 + 2r' + 3 \neq 3 + 2r' + 2$
$r < r'$:	
$s = 4r'$	$0 + 2r - 1 = 1 + 2r - 2$
$s = 4r'+1$	$2 + 2r + 1 = 3 + 2r$
$s = 4r'+2$	$0 + 2r = 2 + 2r - 2$
$s = 4r'+3$	$1 + 2r + 1 = 3 + 2r - 1$

Pairing $(2, 4r+1, 1, 4r+2)$:

$a = 2$, $b = 4r+1$, $c = 1$, $d = 4r+2$

$$\begin{pmatrix} 0 & \boxed{2} & 1 & 0 \\ \boxed{2} & 2r+2 & 2 & 2r+1 \\ 1 & 2 & 2 & 1 \\ 0 & 2r+1 & 1 & 2r \end{pmatrix}$$

$s = 3$	$1 + 3 = 2 + 2$
$s = 4r$	$0 + 2r = 1 + 2r - 1$
$s = 4r+3$	$1 + 2r + 2 = 2 + 2r + 1$
$1 < r' < r$:	
$s = 4r'$	$0 + 2r' - 2 = 1 + 2r' - 3$
$s = 4r'+1$	$2 + 2r' \neq 2 + 2r' - 2$
$s = 4r'+2$	$0 + 2r' \neq 1 + 2r' - 2$
$s = 4r'+3$	$1 + 3r' + 1 = 2 + 2r'$
$r < r'$:	
$s = 4r'$	$0 + 2r - 1 = 1 + 2r - 2$
$s = 4r'+1$	$2 + 2r = 2 + 2r$
$s = 4r'+2$	$0 + 2r - 1 = 1 + 2r - 2$
$s = 4r'+3$	$1 + 2r = 2 + 2r - 1$

Pairing $(1, 4r+3, 3, 4r+1)$:

$a = 1$, $b = 4r+3$, $c = 3$, $d = 4r+1$

$$\begin{pmatrix} 2 & 2 & 2 & 2 \\ 2 & 2r+3 & 3 & 2r+2 \\ 2 & 3 & 3 & \boxed{3} \\ 2 & 2r+2 & \boxed{3} & 2r+2 \end{pmatrix}$$

$s = 2$	$1 + 1 \neq 1 + 2$

Table 4.4: The non-trivial pairings between the wedge and a diamond.

4.5.4 $6_2, 6_3, 7_3$ knots

In the last part of this chapter we determine the local symmetries for knots $6_2, 6_3$ and 7_3 and their quiver matrices found in [21] and [23].

6_2 **knot** Let us start from the knot 6_2. The quiver from [21] reads

$$C = \begin{bmatrix} -2 & -2 & -1 & -1 & -1 & -1 & 0 & -1 & 1 & 1 & 1 \\ -2 & -1 & -1 & 0 & 0 & 0 & 1 & 0 & 1 & 2 & 2 \\ -1 & -1 & 0 & 1 & 0 & 0 & 1 & 0 & 1 & 2 & 2 \\ -1 & 0 & 1 & 0 & 0 & 0 & 1 & 0 & 2 & 1 & 1 \\ -1 & 0 & 0 & 0 & 1 & 1 & 1 & 1 & 2 & 2 & 2 \\ -1 & 0 & 0 & 0 & 1 & 1 & 1 & 1 & 2 & 2 & 2 \\ 0 & 1 & 1 & 1 & 1 & 1 & 2 & 1 & 2 & 2 & 2 \\ -1 & 0 & 0 & 0 & 1 & 1 & 1 & 2 & 2 & 3 & 3 \\ 1 & 1 & 1 & 2 & 2 & 2 & 2 & 2 & 3 & 3 & 3 \\ 1 & 2 & 2 & 1 & 2 & 2 & 2 & 3 & 3 & 3 & 3 \\ 1 & 2 & 2 & 1 & 2 & 2 & 2 & 3 & 3 & 3 & 4 \end{bmatrix}, \qquad \boldsymbol{\lambda} = \begin{bmatrix} q^{-2}(-t)^{-2} \\ a^2q^{-4}(-t)^{-1} \\ a^2q^{-2} \\ q^2 \\ a^2(-t) \\ a^2(-t) \\ a^2q^2(-t)^2 \\ a^4q^{-2}(-t)^2 \\ a^4(-t)^3 \\ a^2q^4(-t)^3 \\ a^4q^2(-t)^4 \end{bmatrix}. \tag{4.62}$$

There are eight local symmetries associated to (4.62) for the following pairings:

$$\begin{aligned} &\lambda_1\lambda_7 = \lambda_3\lambda_4, && \lambda_1\lambda_{11} = \lambda_4\lambda_8, && \lambda_5\lambda_{11} = \lambda_8\lambda_{10}, && \lambda_6\lambda_{11} = \lambda_8\lambda_{10}, \\ &\lambda_1\lambda_9 = \lambda_3\lambda_5, && \lambda_1\lambda_9 = \lambda_3\lambda_6, && \lambda_2\lambda_7 = \lambda_3\lambda_5, && \lambda_2\lambda_7 = \lambda_3\lambda_6. \end{aligned}$$

Their graphical representation, together with the homology diagram, is given in figure 4.10.

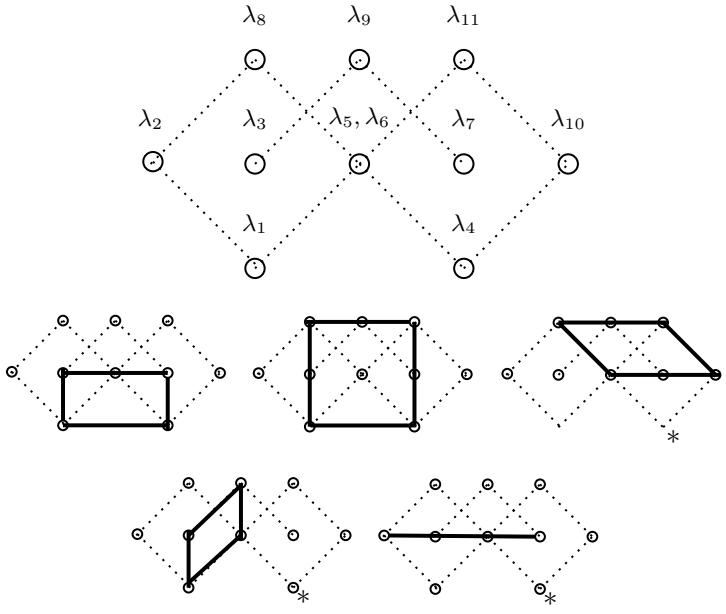

Figure 4.10: Homology diagram and local symmetries for 6_2 knot, each picture marked with * corresponds to two symmetries, due to double-valued nodes λ_5 and λ_6.

6_3 **knot** For 6_3 the quiver matrix from [21] is given by

$$C = \begin{bmatrix}
0 & 0 & 0 & -1 & -1 & 0 & 0 & -1 & -1 & 0 & 0 & -1 & -1 \\
0 & 1 & 0 & -1 & -2 & 1 & 0 & -1 & -2 & 1 & 1 & 0 & -1 \\
0 & 0 & 0 & -1 & -2 & 1 & 0 & 0 & -2 & 1 & 1 & 0 & 0 \\
-1 & -1 & -1 & -2 & -3 & 0 & -1 & -2 & -3 & -1 & 0 & -2 & -2 \\
-1 & -2 & -2 & -3 & -3 & -1 & -1 & -2 & -3 & -1 & -1 & -2 & -2 \\
0 & 1 & 1 & 0 & -1 & 2 & 1 & 0 & -1 & 2 & 1 & 1 & -1 \\
0 & 0 & 0 & -1 & -1 & 1 & 1 & 0 & -1 & 2 & 1 & 1 & 0 \\
-1 & -1 & 0 & -2 & -2 & 0 & 0 & -1 & -2 & 0 & 0 & -1 & -2 \\
-1 & -2 & -2 & -3 & -3 & -1 & -1 & -2 & -2 & 0 & -1 & -1 & -2 \\
0 & 1 & 1 & -1 & -1 & 2 & 2 & 0 & 0 & 3 & 2 & 1 & 0 \\
0 & 1 & 1 & 0 & -1 & 1 & 1 & 0 & -1 & 2 & 2 & 1 & 0 \\
-1 & 0 & 0 & -2 & -2 & 1 & 1 & -1 & -1 & 1 & 1 & 0 & -1 \\
-1 & -1 & 0 & -2 & -2 & -1 & 0 & -2 & -2 & 0 & 0 & -1 & -1
\end{bmatrix}, \quad \boldsymbol{\lambda} = \begin{bmatrix}
1 \\
a^2q^{-2}(-t) \\
1 \\
q^{-4}(-t)^{-2} \\
a^{-2}q^{-2}(-t)^{-3} \\
a^2(-t)^2 \\
q^2(-t) \\
q^{-2}(-t)^{-1} \\
a^{-2}(-t)^{-2} \\
a^2q^2(-t)^3 \\
q^4(-t)^2 \\
1 \\
a^{-2}q^2(-t)^{-1}
\end{bmatrix}. \tag{4.63}$$

For (4.63) there are six local symmetries for the following pairings:

$$\begin{aligned}
&\lambda_2\lambda_8 = \lambda_4\lambda_6, && \lambda_2\lambda_{12} = \lambda_4\lambda_{10}, && \lambda_3\lambda_8 = \lambda_4\lambda_7, \\
&\lambda_3\lambda_9 = \lambda_5\lambda_7, && \lambda_3\lambda_{13} = \lambda_5\lambda_{11}, && \lambda_6\lambda_{13} = \lambda_8\lambda_{11},
\end{aligned}$$

which graphical representation, together with the homology diagram, is given in figure 4.11.

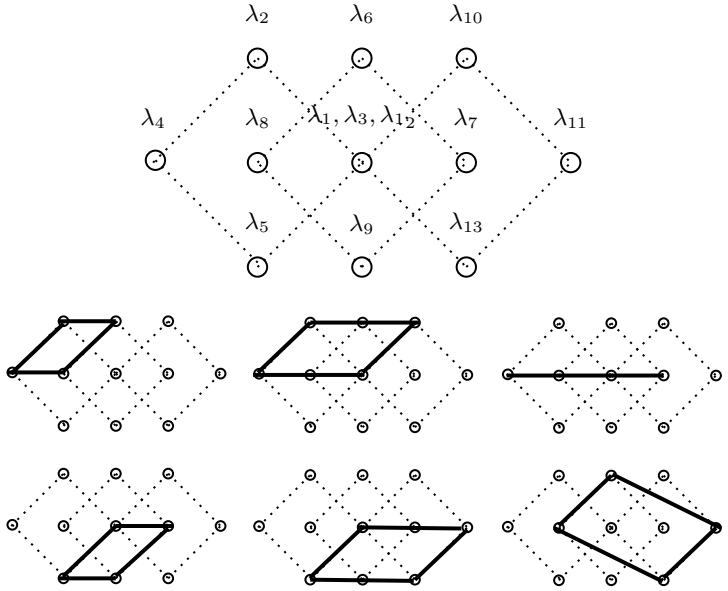

Figure 4.11: Homology diagram and local symmetries for 6_3 knot.

7_3 knot As the last isolated example we consider the 7_3 knot. The quiver from [23] reads

$$C = \begin{bmatrix} 2 & 0 & 3 & 2 & 1 & 5 & 4 & 3 & 3 & 2 & 5 & 4 & 3 \\ 0 & 0 & 1 & 1 & 0 & 3 & 3 & 2 & 1 & 1 & 3 & 3 & 2 \\ 3 & 1 & 4 & 2 & 2 & 5 & 4 & 4 & 4 & 2 & 5 & 4 & 4 \\ 2 & 1 & 2 & 2 & 1 & 3 & 3 & 3 & 3 & 2 & 3 & 3 & 3 \\ 1 & 0 & 2 & 1 & 1 & 3 & 2 & 2 & 2 & 1 & 3 & 2 & 2 \\ 5 & 3 & 5 & 3 & 3 & 6 & 4 & 4 & 6 & 4 & 6 & 4 & 4 \\ 4 & 3 & 4 & 3 & 2 & 4 & 4 & 3 & 5 & 4 & 5 & 4 & 3 \\ 3 & 2 & 4 & 3 & 2 & 4 & 3 & 3 & 4 & 3 & 5 & 4 & 3 \\ 3 & 1 & 4 & 3 & 2 & 6 & 5 & 4 & 5 & 3 & 6 & 5 & 4 \\ 2 & 1 & 2 & 2 & 1 & 4 & 4 & 3 & 3 & 3 & 4 & 4 & 3 \\ 5 & 3 & 5 & 3 & 3 & 6 & 5 & 5 & 6 & 4 & 7 & 5 & 5 \\ 4 & 3 & 4 & 3 & 2 & 4 & 4 & 4 & 5 & 4 & 5 & 5 & 4 \\ 3 & 2 & 4 & 3 & 2 & 4 & 3 & 3 & 4 & 3 & 5 & 4 & 4 \end{bmatrix}, \qquad \boldsymbol{\lambda} = \begin{bmatrix} a^6q^{-4}(-t)^2 \\ a^4q^{-4} \\ a^6(-t)^4 \\ a^4(-t)^2 \\ a^4q^{-2}(-t) \\ a^6q^4(-t)^6 \\ a^4q^4(-t)^4 \\ a^4q^2(-t)^3 \\ a^8q^{-2}(-t)^5 \\ a^6q^{-2}(-t)^3 \\ a^8q^2(-t)^7 \\ a^6q^2(-t)^5 \\ a^6(-t)^4 \end{bmatrix}. \tag{4.64}$$

For (4.64) there are seven local symmetries for the following pairings, also shown in figure 4.12.

$$\lambda_1\lambda_{10} = \lambda_2\lambda_9, \qquad \lambda_2\lambda_{11} = \lambda_3\lambda_{10}, \qquad \lambda_3\lambda_{10} = \lambda_4\lambda_9, \qquad \lambda_3\lambda_{12} = \lambda_4\lambda_{11},$$
$$\lambda_4\lambda_{13} = \lambda_5\lambda_{12}, \qquad \lambda_6\lambda_{12} = \lambda_7\lambda_{11}, \qquad \lambda_7\lambda_{13} = \lambda_8\lambda_{12}.$$

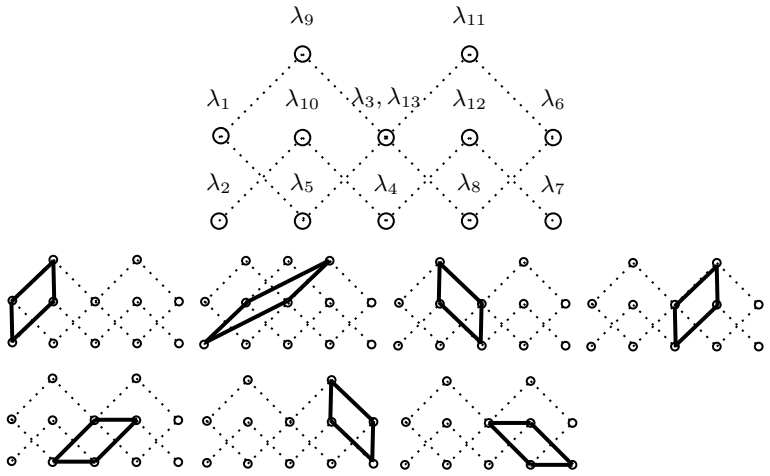

Figure 4.12: Homology diagram and local symmetries for 7_3 knot.

To sum up, we analysed some examples of knots and computed their local symmetries for quiver matrices from [21, 23]. Such symmetries are shown as parallelograms on the homology diagram of a knot, and give rise to equivalent quivers which differ by a single transposition of arrows. In this chapter we studied the local equivalence, and did not identify all possible equivalent quivers for a given knot (except for the cases of 3_1 and 4_1 knots). However, this step can be done by a successive application of theorem 4.3.1 to such pairs of equivalent quivers, as shown in [60]. One of the most promising directions is to find the relation to colored homology differentials which can be possibly obtained from the diagrams of symmetries.

Summary

The main theme of this thesis revolves around Nahm sums, appearing in many areas of contemporary theoretical physics: two-dimensional conformal field theory, Chern-Simons theory, certain class of supersymmetric gauge theories associated to three-manifolds, and others. Remarkably, all these theories turn out to be related by dualities, and the occurrence of Nahm sums in seemingly distant contexts suggests their common physical origin. We mainly focused on the Nahm sums which encode motivic Donaldson-Thomas invariants for a symmetric quiver, such that a suitable quiver also encodes quantum knot invariants, as stated by the knots-quivers correspondence. We studied the recursive structures from these q-series, including quantum A-polynomials, topological recursion, WKB expansions, and also local equivalence relation for quivers.

In the second chapter we have shown that quiver A-polynomial, defined as the semi-classical limit of the corresponding Nahm sum, is quantizable for a class of quivers. Moreover, we have found an interesting combinatorial formula which computes the Newton polytope for such quivers. As a consequence, we expect such quivers to have nice interpretation also in terms of topological string A-model (and the B-model defined from the quiver A-polynomial).

In the third chapter we have used the fact that quiver A-polynomial is quantizable, and applied the topological recursion in order to reconstruct the Nahm sum and quantum quiver A-polynomial from classical quiver A-polynomials. The conjectural correspondence between the topological recursion wave function and the Nahm sum was explicitly checked and confirmed for several examples, with a single exception in which we expect more complicated relation to take place. Besides, we also studied quantum Airy structures which generalize the topological recursion, and defined the case which governs spectral curves with non-simple ramification points of an arbitrary order. We studied the case of cubic operators in a greater detail and confirmed that it corresponds to the algebra of extended conformal symmetries in 2d CFTs.

In the fourth chapter we studied the uniqueness aspect in the knots-quivers correspondence and defined the local equivalence relation for symmetric quivers, allowing to find recursively all equivalent quivers for a given knot. We also studied this conditions for several families of knots, and determined quivers which differ by a single local transformation from those previously known.

Summing up, these results help to understand the role of Nahm sums in physics, to relate seemingly distant theories involving quantum knot invariants and knot homologies and shed some light on the relation between knots, quivers, topological strings and other structures, leaving the scope for further research.

Bibliography

[1] Gerard 't Hooft. "A Planar Diagram Theory for Strong Interactions". In: *Nucl. Phys. B* 72 (1974). Ed. by J. C. Taylor, p. 461. DOI: 10.1016/0550-3213(74)90154-0.

[2] P. Di Francesco, Paul H. Ginsparg, and Jean Zinn-Justin. "2-D Gravity and random matrices". In: *Phys. Rept.* 254 (1995), pp. 1–133. DOI: 10.1016/0370-1573(94)00084-G. arXiv: hep-th/9306153.

[3] B. Eynard. "Topological expansion for the 1-Hermitian matrix model correlation functions". In: *JHEP* 11 (2004), p. 031. DOI: 10.1088/1126-6708/2004/11/031. arXiv: hep-th/0407261 [hep-th].

[4] Marcos Mariño. *Chern-Simons Theory, Matrix Models, and Topological Strings*. Oxford University Press, 2005.

[5] Bertrand Eynard, Taro Kimura, and Sylvain Ribault. "Counting surfaces". In: *Progress in Mathematical Physics* 70 (2016).

[6] A. A. Belavin, Alexander M. Polyakov, and A. B. Zamolodchikov. "Infinite Conformal Symmetry in two-dimensional Quantum Field Theory". In: *Nucl. Phys.* B241 (1984), pp. 333–380. DOI: 10.1016/0550-3213(84)90052-X.

[7] Jacques Distler and Hikaru Kawai. "Conformal Field Theory and 2D Quantum Gravity". In: *Nucl. Phys. B* 321 (1989), pp. 509–527. DOI: 10.1016/0550-3213(89)90354-4.

[8] Ofer Aharony, Steven S. Gubser, Juan Martin Maldacena, Hirosi Ooguri, and Yaron Oz. "Large N field theories, string theory and gravity". In: *Phys. Rept.* 323 (2000), pp. 183–386. DOI: 10.1016/S0370-1573(99)00083-6. arXiv: hep-th/9905111.

[9] Werner Nahm, Andreas Recknagel, and Michael Terhoeven. "Dilogarith Identities in Conformal Field Theory". In: *Mod. Phys. Lett.* (1993). arXiv: hep-th/9211034.

[10] Werner Nahm. "Conformal field theory and torsion elements of the Bloch group". In: *Frontiers in number theory, physics, and geometry 2: On random matrices, zeta functions and dynamical systems. Proceedings, Meeting, Les Houches, France, March 9-21, 2003* (2007), pp. 67–132. DOI: 10.1007/978-3-540-30308-4_2. arXiv: hep-th/0404120 [hep-th].

[11] Gregory W. Moore and Nathan Seiberg. "Polynomial Equations for Rational Conformal Field Theories". In: *Phys. Lett. B* 212 (1988), pp. 451–460. DOI: 10.1016/0370-2693(88)91796-0.

[12] Gregory W. Moore and Nathan Seiberg. "Taming the Conformal Zoo". In: *Phys. Lett. B* 220 (1989), pp. 422–430. DOI: 10.1016/0370-2693(89)90897-6.

[13] Timothy J. Hollowood and Paul Mansfield. "Rational Conformal Field Theories At, and Away From, Criticality as Toda Field Theories". In: *Phys. Lett. B* 226 (1989), p. 73. DOI: 10.1016/0370-2693(89)90291-8.

[14] Erik Verlinde. "Conformal Field Theory and its Applications to Strings". In: *PhD thesis* (1988). eprint: https://inis.iaea.org/collection/NCLCollectionStore/_Public/20/024/20024924.pdf?r=1&r=1.

[15] Sergey Mozgovoy and Markus Reineke. "On the number of stable quiver representations over finite fields". In: *Journal of Pure and Applied Algebra* 213.4 (2009), pp. 430–439. ISSN: 0022-4049. DOI: https://doi.org/10.1016/j.jpaa.2008.07.019.

[16] Maxim Kontsevich and Yan Soibelman. "Stability structures, motivic Donaldson-Thomas invariants and cluster transformations". In: *arXiv preprint* (2008). arXiv: 0811.2435 [math.AG].

[17] Markus Reineke. "Degenerate Cohomological Hall algebra and quantized Donaldson-Thomas invariants for m-loop quivers". In: *Doc. Math.* 17 (2012), p. 1. arXiv: 1102.3978 [math.RT].

[18] E. Guadagnini, M. Martellini, and M. Mintchev. "Wilson Lines in Chern-Simons Theory and Link Invariants". In: *Nucl. Phys. B* 330 (1990), pp. 575–607. DOI: 10.1016/0550-3213(90)90124-V.

[19] Michael Francis Atiyah. *The geometry and physics of knots*. Cambridge University Press, 1990.

[20] Hirosi Ooguri and Cumrun Vafa. "Knot invariants and topological strings". In: *Nucl. Phys. B* 577 (2000), pp. 419–438. DOI: 10.1016/S0550-3213(00)00118-8. arXiv: hep-th/9912123.

[21] Piotr Kucharski, Markus Reineke, Marko Stosic, and Piotr Sulkowski. "Knots-quivers correspondence". In: *Adv. Theor. Math. Phys.* 23.7 (2019), p. 1685. arXiv: 1707.04017 [hep-th].

[22] Piotr Kucharski, Markus Reineke, Marko Stosic, and Piotr Sulkowski. "BPS states, knots and quivers". In: *Phys. Rev. D* 96 (2017), p. 121902. DOI: 10.1103/PhysRevD.96.121902. arXiv: 1707.02991 [hep-th].

[23] Marko Stosic and Paul Wedrich. "Rational Links and DT Invariants of Quivers". In: *International Mathematics Research Notices* (Jan. 2019). rny289. ISSN: 1073-7928. DOI: 10.1093/imrn/rny289. arXiv: 1711.03333 [math.QA]. URL: https://doi.org/10.1093/imrn/rny289.

[24] Tobias Ekholm, Piotr Kucharski, and Pietro Longhi. "Physics and geometry of knots-quivers correspondence". In: *Commun. Math. Phys.* 379.2 (2020), pp. 361–415. DOI: 10.1007/s00220-020-03840-y. arXiv: 1811.03110 [hep-th].

[25] Tobias Ekholm, Piotr Kucharski, and Pietro Longhi. "Multi-cover skeins, quivers, and 3d $\mathcal{N} = 2$ dualities". In: *JHEP* 02 (2020), p. 018. DOI: 10.1007/JHEP02(2020)018. arXiv: 1910.06193 [hep-th].

[26] Marko Stosic and Paul Wedrich. "Tangle addition and the knots-quivers correspondence". In: *arXiv preprint* (Apr. 2020). arXiv: 2004.10837 [math.QA].

[27] Tobias Ekholm, Piotr Kucharski, and Pietro Longhi. "Knot homologies and generalized quiver partition functions". In: *arXiv preprint* (Aug. 2021). arXiv: 2108.12645 [hep-th].

[28] Edward Witten. "Quantum field theory and the Jones polynomial". In: *Comm. Math. Phys.* 121.3 (1989), pp. 351–399. ISSN: 0010-3616. URL: http://projecteuclid.org/euclid.cmp/1104178138.

[29] E. Cremmer, S. Ferrara, L. Girardello, and Antoine Van Proeyen. "Yang-Mills Theories with Local Supersymmetry: Lagrangian, Transformation Laws and SuperHiggs Effect". In: *Nucl. Phys. B* 212 (1983). Ed. by A. Salam and E. Sezgin, p. 413. DOI: 10.1016/0550-3213(83)90679-X.

[30] N. Seiberg and Edward Witten. "Monopoles, duality and chiral symmetry breaking in N=2 supersymmetric QCD". In: *Nucl. Phys. B* 431 (1994), pp. 484–550. DOI: 10.1016/0550-3213(94)90214-3. arXiv: hep-th/9408099.

[31] Philip C. Argyres and Michael R. Douglas. "New phenomena in SU(3) supersymmetric gauge theory". In: *Nucl. Phys. B* 448 (1995), pp. 93–126. DOI: 10.1016/0550-3213(95)00281-V. arXiv: hep-th/9505062.

[32] Michael R. Douglas and Gregory W. Moore. "D-branes, quivers, and ALE instantons". In: *arXiv preprint* (Mar. 1996). arXiv: hep-th/9603167.

[33] Edward Witten. "Solutions of four-dimensional field theories via M theory". In: *Nucl. Phys. B* 500 (1997), pp. 3–42. DOI: 10.1016/S0550-3213(97)00416-1. arXiv: hep-th/9703166.

[34] Hee-Joong Chung, Tudor Dimofte, Sergei Gukov, and Piotr Sułkowski. "3d-3d Correspondence Revisited". In: *JHEP* 04 (2016), p. 140. DOI: 10.1007/JHEP04(2016)140. arXiv: 1405.3663 [hep-th].

[35] Sergei Gukov, Satoshi Nawata, Ingmar Saberi, Marko Stosic, and Piotr Sulkowski. "Sequencing BPS Spectra". In: *JHEP* 03 (2016), p. 004. DOI: 10.1007/JHEP03(2016)004. arXiv: 1512.07883 [hep-th].

[36] Sergei Gukov, Pavel Putrov, and Cumrun Vafa. "Fivebranes and 3-manifold homology". In: *JHEP* 07 (2017), p. 071. DOI: 10.1007/JHEP07(2017)071. arXiv: 1602.05302 [hep-th].

[37] Sungbong Chun, Sergei Gukov, Sunghyuk Park, and Nikita Sopenko. "3d-3d correspondence for mapping tori". In: *JHEP* 09 (2020), p. 152. DOI: 10.1007/JHEP09(2020)152. arXiv: 1911.08456 [hep-th].

[38] Rajesh Gopakumar and Cumrun Vafa. "On the gauge theory/geometry correspondence". In: *Adv. Theor. Math. Phys* (1999), p. 1415.

[39] Marcos Marino. "Les Houches lectures on matrix models and topological strings". In: 2004. arXiv: hep-th/0410165 [hep-th]. URL: http://weblib.cern.ch/abstract?CERN-PH-TH-2004-199.

[40] Hirosi Ooguri and Cumrun Vafa. "Knot invariants and topological strings". In: *Nucl.Phys.* B577 (2000), pp. 419–438. DOI: 10.1016/S0550-3213(00)00118-8. arXiv: hep-th/9912123 [hep-th].

[41] Stavros Garoufalidis and Thang T. Q. Le. "Nahm sums, stability and the colored Jones polynomial". In: (Dec. 2011). arXiv: 1112.3905 [math.GT].

[42] Tudor Dimofte and Stavros Garoufalidis. "The quantum content of the gluing equations". In: *Geometry & Topology* 17.3 (2013), pp. 1253–1315. DOI: 10.2140/gt.2013.17.1253. URL: https://doi.org/10.2140/gt.2013.17.1253.

[43] Bertrand Eynard. "All orders asymptotic expansion of large partitions". In: *J. Stat. Mech.* 0807 (2008), P07023. DOI: 10.1088/1742-5468/2008/07/P07023. arXiv: 0804.0381 [math-ph].

[44] Bertrand Eynard and Olivier Marchal. "Topological expansion of the Bethe ansatz, and non-commutative algebraic geometry". In: *JHEP* 03 (2009), p. 094. DOI: 10.1088/1126-6708/2009/03/094. arXiv: 0809.3367 [math-ph].

[45] L. Chekhov. "Genus one correlation to multicut matrix model solutions". In: *Theor. Math. Phys.* 141 (2004). [Teor. Mat. Fiz.141,358(2004)], pp. 1640–1653. DOI: 10.1023/B:TAMP.0000049759.01361.79. arXiv: hep-th/0401089 [hep-th].

[46] D. Cooper, M. Culler, H. Gillet, D. D. Long, and P. B. Shalen. "Plane curves associated to character varieties of 3-manifolds". In: *Invent. Math.* 118.1 (1994), pp. 47–84. ISSN: 0020-9910. DOI: 10.1007/BF01231526.

[47] Sergei Gukov. "Three-dimensional quantum gravity, Chern-Simons theory, and the A polynomial". In: *Commun. Math. Phys.* 255 (2005), pp. 577–627. DOI: 10.1007/s00220-005-1312-y. arXiv: hep-th/0306165.

[48] Sergei Gukov and Piotr Sulkowski. "A-polynomial, B-model, and Quantization". In: *JHEP* 1202 (2012), p. 070. DOI: 10.1007/JHEP02(2012)070. arXiv: 1108.0002 [hep-th].

[49] Gaëtan Borot and Bertrand Eynard. "All order asymptotics of hyperbolic knot invariants from non-perturbative topological recursion of A-polynomials". In: *Quantum Topology* 6.1 (2015), pp. 39–138.

[50] Hiroyuki Fuji, Sergei Gukov, and Piotr Sulkowski. "Super-A-polynomial for knots and BPS states". In: *Nucl. Phys. B* 867 (2013), pp. 506–546. DOI: 10.1016/j.nuclphysb.2012.10.005. arXiv: 1205.1515 [hep-th].

[51] Hiroyuki Fuji and Piotr Sulkowski. "Super-A-polynomial". In: *Proc. Symp. Pure Math.* 90 (2015). Ed. by Ron Donagi, Sheldon Katz, Albrecht Klemm, and David R. Morrison, pp. 277–304. DOI: 10.1090/pspum/090. arXiv: 1303.3709 [math.AG].

[52] Maxim Kontsevich and Yan Soibelman. "Airy structures and symplectic geometry of topological recursion". In: *arXiv e-prints*, arXiv:1701.09137 (Jan. 2017), arXiv:1701.09137. arXiv: 1701.09137 [math.AG].

[53] Jorgen Ellegaard Andersen, Gaëtan Borot, Leonid O. Chekhov, and Nicolas Orantin. "The ABCD of topological recursion". In: *arXiv e-prints*, arXiv:1703.03307 (Mar. 2017), arXiv:1703.03307. arXiv: 1703.03307 [math-ph].

[54] Vincent Bouchard, Paweł Ciosmak, Leszek Hadasz, Kento Osuga, Blazej Ruba, and Piotr Sułkowski. "Super Quantum Airy Structures". In: *Commun. Math. Phys.* 380.1 (2020), pp. 449–522. DOI: 10.1007/s00220-020-03876-0. arXiv: 1907.08913 [math-ph].

[55] S. Kharchev, A. Marshakov, A. Mironov, A. Morozov, and A. Zabrodin. "Unification of all string models with $c < 1$". In: *Physics Letters B* 275.3 (1992), pp. 311–314. ISSN: 0370-2693. DOI: https://doi.org/10.1016/0370-2693(92)91595-Z.

[56] E. Brezin and S. Hikami. "The intersection numbers of the p-spin curves from random matrix theory". In: *JHEP* 02 (2013), p. 035. DOI: 10.1007/JHEP02(2013)035. arXiv: 1212.6096 [math-ph].

[57] Gaëtan Borot, Vincent Bouchard, Nitin K. Chidambaram, Thomas Creutzig, and Dmitry Noshchenko. "Higher Airy structures, W algebras and topological recursion". In: (Dec. 2018). arXiv: 1812.08738 [math-ph].

[58] Helder Larraguivel, Dmitry Noshchenko, Miłosz Panfil, and Piotr Sułkowski. "Nahm sums, quiver A-polynomials and topological recursion". In: *JHEP* 07 (2020), p. 151. DOI: 10.1007/JHEP07(2020)151. arXiv: 2005.01776 [hep-th].

[59] Dmitry Noshchenko. "Combinatorics of Nahm sums, quiver resultants and the K-theoretic condition". In: *JHEP* 03 (2021), p. 236. DOI: 10.1007/JHEP03(2021)236. arXiv: 2007.15398 [hep-th].

[60] Jakub Jankowski, Piotr Kucharski, Hélder Larraguível, Dmitry Noshchenko, and Piotr Sułkowski. "Permutohedra for knots and quivers". In: (May 2021). arXiv: 2105.11806 [hep-th].

[61] S. Dotsenko. "Lectures on Conformal Field Theory". In: *Conformal Field Theory and Solvable Lattice Models*. Ed. by M. Jimbo, T. Miwa, and A. Tsuchiya. Academic Press, 1988, pp. 123–170. ISBN: 978-0-12-385340-0. DOI: https://doi.org/10.1016/B978-0-12-385340-0.50008-5.

[62] S. Dotsenko and A.M. Polyakov. "Fermion Representations for the 2D and 3D Ising Models". In: *Conformal Field Theory and Solvable Lattice Models*. Ed. by M. Jimbo, T. Miwa, and A. Tsuchiya. Academic Press, 1988, pp. 171–203. ISBN: 978-0-12-385340-0. DOI: https://doi.org/10.1016/B978-0-12-385340-0.50009-7.

[63] Francisco C. Alcaraz, Michael N. Barber, and Murray T. Batchelor. "Conformal Invariance, the Xxz Chain and the Operator Content of Two-dimensional Critical Systems". In: *Annals Phys.* 182 (1988), pp. 280–343. DOI: 10.1016/0003-4916(88)90015-2.

[64] A.A. Belavin, A.M. Polyakov, and A.B. Zamolodchikov. "Infinite conformal symmetry in two- dimensional quantum field theory". In: *Nuclear Physics B* 241.2 (1984), pp. 333–380. ISSN: 0550-3213. DOI: https://doi.org/10.1016/0550-3213(84)90052-X.

[65] Paul Ginsparg. "Applied Conformal Field Theory (lecture notes)". In: (1989). arXiv: hep-th/9108028.

[66] John Cardy. "Conformal Field Theory and Statistical Mechanics (lecture notes)". In: (2008). arXiv: 0807.3472.

[67] Ralph Blumenhagen and Erik Plauschinn. *Introduction to conformal field theory: with applications to string theory*. Vol. 779. Springer Science & Business Media, 2009.

[68] R. E. Borcherds. "Vertex Algebras for Beginners". In: *Bulletin of the London Mathematical Society* 30.2 (1998), pp. 196–223.

[69] A. B. Zamolodchikov. "Integrable field theory from conformal field theory". In: *Adv. Stud. Pure Math.* 19 (1989). Ed. by M. Jimbo, T. Miwa, and A. Tsuchiya, pp. 641–674.

[70] Vladimir V. Bazhanov, Sergei L. Lukyanov, and Alexander B. Zamolodchikov. "Integrable structure of conformal field theory. 2. Q operator and DDV equation". In: *Commun. Math. Phys.* 190 (1997), pp. 247–278. DOI: 10.1007/s002200050240. arXiv: hep-th/9604044.

[71] M. E. Fisher. "Yang-Lee Edge Singularity and phi**3 Field Theory". In: *Phys. Rev. Lett.* 40 (1978), pp. 1610–1613. DOI: 10.1103/PhysRevLett.40.1610.

[72] John L. Cardy. "Conformal Invariance and the Yang-lee Edge Singularity in Two-dimensions". In: *Phys. Rev. Lett.* 54 (1985), pp. 1354–1356. DOI: 10.1103/PhysRevLett.54.1354.

[73] David J. Gross and Alexander A. Migdal. "Nonperturbative Solution of the Ising Model on a Random Surface". In: *Phys. Rev. Lett.* 64 (1990), p. 717. DOI: 10.1103/PhysRevLett.64.717.

[74] Paul H. Ginsparg. "Applied Conformal Field Theory". In: *Les Houches Summer School in Theoretical Physics: Fields, Strings, Critical Phenomena*. Sept. 1988. arXiv: hep-th/9108028.

[75] John L. Cardy. "Operator Content of Two-Dimensional Conformally Invariant Theories". In: *Nucl. Phys. B* 270 (1986), pp. 186–204. DOI: 10.1016/0550-3213(86)90552-3.

[76] George E. Andrews, Jethro van Ekeren, and Reimundo Heluani. "The singular support of the Ising model". In: (2020). arXiv: 2005.10769.

[77] Markus Reineke. "Cohomology of quiver moduli, functional equations, and integrality of Donaldson–Thomas type invariants". In: *Compositio Mathematica* 147 (03 May 2011), pp. 943–964. ISSN: 1570-5846. DOI: 10.1112/S0010437X1000521X. URL: http://Journals.cambridge.org/article_S0010437X1000521X.

[78] Maxim Kontsevich and Yan Soibelman. "Cohomological Hall algebra, exponential Hodge structures and motivic Donaldson-Thomas invariants". In: *Commun. Num. Theor. Phys.* 5 (2011), pp. 231–352. DOI: 10.4310/CNTP.2011.v5.n2.a1. arXiv: 1006.2706 [math.AG].

[79] Alexander Soibelman. "Lecture Notes On Quiver Representations And Moduli Problems In Algebraic Geometry". In: *arXiv preprint* (2019). arXiv: 1909.03509.

[80] Alexander I. Efimov. "Cohomological Hall algebra of a symmetric quiver". In: *Compositio Mathematica* 148.4 (2012), pp. 1133–1146. DOI: 10.1112/S0010437X12000152. arXiv: 1103.2736.

[81] Davide Gaiotto, Gregory W Moore, and Andrew Neitzke. "Wall-crossing, Hitchin systems, and the WKB approximation". In: *Advances in Mathematics* 234 (2013), pp. 239–403. arXiv: 0907.3987.

[82] Davide Gaiotto, Gregory W. Moore, and Andrew Neitzke. "Four-dimensional wall-crossing via three-dimensional field theory". In: *Commun. Math. Phys.* 299 (2010), pp. 163–224. DOI: 10.1007/s00220-010-1071-2. arXiv: 0807.4723 [hep-th].

[83] Andrew Neitzke. "What is a BPS state?" In: *Lecture notes* (2016). URL: https://web.ma.utexas.edu/users/neitzke/expos/bps-expos.%20pdf.

[84] V. Jones. "Hecke algebra representations of braid groups and link polynomials". In: *Ann. of Math.* 126 (1987), p. 335.

[85] Mikhail Khovanov. "A categorification of the Jones polynomial". In: *Duke Math. J.* 101 (2000), pp. 359–426. arXiv: math/9908171 [math].

[86] Nathan M. Dunfield, Sergei Gukov, and Jacob Rasmussen. "The superpolynomial for knot homologies". In: *Experiment. Math.* 15.2 (2006), pp. 129–159. ISSN: 1058-6458. arXiv: math/0505662 [math.GT]. URL: http://projecteuclid.org/euclid.em/1175789736.

[87] Mikhail Khovanov and Lev Rozansky. "Matrix factorizations and link homology". In: *Fund. Math.* 199 (2008), pp. 1–91. arXiv: math/0401268 [math.QA].

[88] Mikhail Khovanov and Lev Rozansky. "Matrix factorizations and link homology II". In: *Geom. & Topol.* 12 (2008), pp. 1387–1425. arXiv: math/0505056 [math.QA].

[89] Sergei Gukov and Marko Stosic. "Homological Algebra of Knots and BPS States". In: *Proc. Symp. Pure Math.* 85 (2012), pp. 125–172. DOI: 10.1090/pspum/085/1377,10.2140/gtm.2012.18.309. arXiv: 1112.0030 [hep-th].

[90] Eugene Gorsky, Sergei Gukov, and Marko Stosic. "Quadruply-graded colored homology of knots". In: *Fundamenta Mathematicae* 243 (Apr. 2013). DOI: 10.4064/fm30-11-2017. arXiv: 1304.3481 [math.QA].

[91] Tudor Dimofte and Sergei Gukov. "Chern-Simons Theory and S-duality". In: *JHEP* 05 (2013), p. 109. DOI: 10.1007/JHEP05(2013)109. arXiv: 1106.4550 [hep-th].

[92] Victor V. Batyrev. "Dual polyhedra and mirror symmetry for Calabi-Yau hypersurfaces in toric varieties". In: *J. Alg. Geom.* 3 (1994), pp. 493–545. arXiv: alg-geom/9310003.

[93] Naichung Conan Leung and Cumrun Vafa. "Branes and toric geometry". In: *Adv. Theor. Math. Phys.* 2 (1998), pp. 91–118. DOI: 10.4310/ATMP.1998.v2.n1.a4. arXiv: hep-th/9711013.

[94] Mina Aganagic, Albrecht Klemm, Marcos Marino, and Cumrun Vafa. "Matrix model as a mirror of Chern-Simons theory". In: *JHEP* 0402 (2004), p. 010. DOI: 10.1088/1126-6708/2004/02/010. arXiv: hep-th/0211098 [hep-th].

[95] Edward Witten. "Chern-Simons gauge theory as a string theory". In: *The Floer Memorial Volume*. Ed. by Helmut Hofer, Clifford H. Taubes, Alan Weinstein, and Eduard Zehnder. Basel: Birkhäuser Basel, 1995, pp. 637–678. ISBN: 978-3-0348-9217-9. DOI: 10.1007/978-3-0348-9217-9_28. URL: https://doi.org/10.1007/978-3-0348-9217-9_28.

[96] Robbert Dijkgraaf and Cumrun Vafa. "Matrix models, topological strings, and supersymmetric gauge theories". In: *Nuclear Physics B* 644.1 (2002), pp. 3–20. ISSN: 0550-3213. DOI: https://doi.org/10.1016/S0550-3213(02)00766-6.

[97] André Miemiec and Igor Schnakenburg. "Basics of M-theory". In: *Fortschritte der Physik: Progress of Physics* 54.1 (2006), pp. 5–72.

[98] Stavros Garoufalidis, Aaron D. Lauda, and Thang T. Q. Le. "The colored HOMFLYPT function is q-holonomic". In: (2016). arXiv: 1604.08502 [math.GT].

[99] Milosz Panfil and Piotr Sulkowski. "Topological strings, strips and quivers". In: *JHEP* 01 (2019), p. 124. DOI: 10.1007/JHEP01(2019)124. arXiv: 1811.03556 [hep-th].

[100] N. Seiberg and Edward Witten. "Electric - magnetic duality, monopole condensation, and confinement in N=2 supersymmetric Yang-Mills theory". In: *Nucl. Phys. B* 426 (1994). [Erratum: Nucl.Phys.B 430, 485–486 (1994)], pp. 19–52. DOI: 10.1016/0550-3213(94)90124-4. arXiv: hep-th/9407087.

[101] Nikita A. Nekrasov. "Seiberg-Witten prepotential from instanton counting". In: *ICM proceedings*. June 2003. arXiv: hep-th/0306211.

[102] Bertrand Eynard and Nicolas Orantin. "Weil-Petersson volume of moduli spaces, Mirzakhani's recursion and matrix models". In: (2007). arXiv: 0705.3600.

[103] Mina Aganagic, Robbert Dijkgraaf, Albrecht Klemm, Marcos Marino, and Cumrun Vafa. "Topological strings and integrable hierarchies". In: *Commun. Math. Phys.* 261 (2006), pp. 451–516. DOI: 10.1007/s00220-005-1448-9. arXiv: hep-th/0312085.

[104] Robbert Dijkgraaf, Lotte Hollands, Piotr Sulkowski, and Cumrun Vafa. "Supersymmetric gauge theories, intersecting branes and free fermions". In: *JHEP* 02 (2008), p. 106. DOI: 10.1088/1126-6708/2008/02/106. arXiv: 0709.4446 [hep-th].

[105] Leonid Chekhov, Bertrand Eynard, and Nicolas Orantin. "Free energy topological expansion for the 2-matrix model". In: *JHEP* 12 (2006), p. 053. DOI: 10.1088/1126-6708/2006/12/053. arXiv: math-ph/0603003.

[106] Bertrand Eynard and Nicolas Orantin. "Invariants of algebraic curves and topological expansion". In: *Commun. Num. Theor. Phys.* 1 (2007), pp. 347–452. DOI: 10.4310/CNTP.2007.v1.n2.a4. arXiv: math-ph/0702045.

[107] Vincent Bouchard, Albrecht Klemm, Marcos Marino, and Sara Pasquetti. "Remodeling the B-Model". In: *Commun. Math. Phys.* 287 (2009), pp. 117–178. DOI: 10.1007/s00220-008-0620-4. eprint: 0709.1453.

[108] Bertrand Eynard and Nicolas Orantin. "Computation of Open Gromov–Witten Invariants for Toric Calabi–Yau 3-Folds by Topological Recursion, a Proof of the BKMP Conjecture". In: *Commun. Math. Phys.* 337.2 (2015), pp. 483–567. DOI: 10.1007/s00220-015-2361-5. arXiv: 1205.1103 [math-ph].

[109] Bohan Fang, Chiu-Chu Melissa Liu, and Zhengyu Zong. "On the Remodeling Conjecture for Toric Calabi-Yau 3-Orbifolds". In: *J. Am. Math. Soc.* 33.1 (2020), pp. 135–222. DOI: 10.1090/jams/934. arXiv: 1604.07123 [math.AG].

[110] Jonh Milnor. *Introduction to Algebraic K-theory*. Princeton University Press & University of Tokyo Press, 1971.

[111] F. Rodriguez Villegas. "Modular Mahler measures I". In: *Topics in Number Theory*. S.D. Ahlgren, G.E. Andrews and K. Ono, ed. Dordrecht: Kluwer, 1999, pp. 17–48.

[112] David W. Boyd, Fernando Rodriguez-Villegas, and Nathan M. Dunfield. "Mahler's measure and the dilogarithm (II)". In: *Canadian Journal of Mathematics* 54 (2002), pp. 468–492. arXiv: math/0308041v2.

[113] Israel Gelfand, Mikhail Kapranov, and Andrei Zelevinsky. *Discriminants, Resultants, and Multidimensional Determinants. The Science of Microfabrication*. Wiley, 1994.

[114] Bernd Sturmfels. "On the Newton Polytope of the Resultant". In: *Journal of Algebraic Combinatorics* 3.3 (1994), pp. 207–236.

[115] Carlos D'Andrea, Gabriela Jeronimo, and Martin Sombra. "The Canny-Emiris conjecture for the sparse resultant". In: *arXiv preprint* (2020). arXiv: 2004.14622.

[116] Israel M. Gelfand, Mikhail M. Kapranov, and Andrei V. Zelevinsky. "Newton Polytopes of the Classical Resultant and Discriminant". In: *Advances in Mathematics* 84 (1990), pp. 237–254.

[117] Hidetoshi Awata, Sergei Gukov, Piotr Sulkowski, and Hiroyuki Fuji. "Volume Conjecture: Refined and Categorified". In: *Adv. Theor. Math. Phys.* 16.6 (2012), pp. 1669–1777. DOI: 10.4310/ATMP.2012.v16.n6.a3. arXiv: 1203.2182 [hep-th].

[118] L. Chekhov and B. Eynard. "Hermitean matrix model free energy: Feynman graph technique for all genera". In: *JHEP* 03 (2006), p. 014. DOI: 10.1088/1126-6708/2006/03/014. arXiv: hep-th/0504116 [hep-th].

[119] Leonid Chekhov, Bertrand Eynard, and Nicolas Orantin. "Free energy topological expansion for the 2-matrix model". In: (2006). arXiv: math-ph/0603003.

[120] Bertrand Eynard and Nicolas Orantin. "Invariants of algebraic curves and topological expansion". In: *Commun. Num. Theor. Phys.* 1 (2007), pp. 347–452. DOI: 10.4310/CNTP.2007.v1.n2.a4. arXiv: math-ph/0702045 [math-ph].

[121] Bertrand Eynard. "A short overview of the "Topological recursion"". In: *preprint arXiv:1412.3286* (2014).

[122] Bertrand Eynard, Taro Kimura, and Sylvain Ribault. "Random matrices". In: (2015). arXiv: 1510.04430.

[123] Vincent Bouchard and Bertrand Eynard. "Think globally, compute locally". In: *JHEP* 02 (2013), p. 143. DOI: 10.1007/JHEP02(2013)143. arXiv: 1211.2302 [math-ph].

[124] Vincent Bouchard and Piotr Sulkowski. "Topological recursion and mirror curves". In: *Adv. Theor. Math. Phys.* 16.5 (2012), pp. 1443–1483. DOI: 10.4310/ATMP.2012.v16.n5.a3. arXiv: 1105.2052 [hep-th].

[125] Vincent Bouchard and Bertrand Eynard. "Reconstructing WKB from topological recursion". In: (2016). arXiv: 1606.04498 [math-ph].

[126] Paul Norbury. "Quantum curves and topological recursion". In: *String-Math 2014* 93 (2014), pp. 41–65.

[127] Stavros Garoufalidis, Piotr Kucharski, and Piotr Sulkowski. "Knots, BPS states, and algebraic curves". In: *Commun. Math. Phys.* 346.1 (2016), pp. 75–113. DOI: 10.1007/s00220-016-2682-z. arXiv: 1504.06327 [hep-th].

[128] Stavros Garoufalidis and Thang T. Q. Lê. "A survey of q-holonomic functions". In: *Enseign. Math.* 62 (2016), pp. 501–525. DOI: 10.4171/LEM/62-3/4-7. eprint: 1601.07487.

[129] Stavros Garoufalidis, Thang T Q Lê, and Zeilberger Meets Jones. "The colored Jones function is q-holonomic". In: *Geometry and Topology* (2005), pp. 1253–1293.

[130] Marc Culler. *A-Polynomials-gluing Equations*. Aug. 2021. URL: https://knotinfo.math.indiana.edu/descriptions/a_polys_table_glueing.html.

[131] Vincent Bouchard and Piotr Sulkowski. "Topological recursion and mirror curves". In: *Adv. Theor. Math. Phys.* 16 (2012), pp. 1443–1483. DOI: 10.4310/ATMP.2012.v16.n5.a3. arXiv: 1105.2052 [hep-th].

[132] Milosz Panfil, Marko Stosic, and Piotr Sulkowski. "Donaldson-Thomas invariants, torus knots, and lattice paths". In: *Phys. Rev.* D98.2 (2018), p. 026022. DOI: 10.1103/PhysRevD.98.026022. arXiv: 1802.04573 [hep-th].

[133] Robbert Dijkgraaf, Hiroyuki Fuji, and Masahide Manabe. "The volume conjecture, perturbative knot invariants, and recursion relations for topological strings". In: *Nuclear Phys. B* 849.1 (2011), pp. 166–211. ISSN: 0550-3213. DOI: 10.1016/j.nuclphysb.2011.03.014. URL: http://dx.doi.org/10.1016/j.nuclphysb.2011.03.014.

[134] B. łażej Ruba. "Analyticity of the free energy for quantum Airy structures". In: *J. Phys. A* 53.8 (2020), p. 085201. DOI: 10.1088/1751-8121/ab69a4. arXiv: 1906.00043 [math-ph].

[135] Gaëtan Borot, Reinier Kramer, and Yannik Schüler. "Higher Airy Structures and Topological Recursion for Singular Spectral Curves". In: *arXiv preprint* (Oct. 2020). arXiv: 2010.03512 [math-ph].

[136] Vincent Bouchard and Kieran Mastel. "A New Class of Higher Quantum Airy Structures as Modules of $\mathcal{W}(\mathfrak{gl}_r)$-Algebras". In: *arXiv preprint* (Sept. 2020). arXiv: 2009.13047 [math-ph].

[137] Robbert Dijkgraaf, Cumrun Vafa, Erik P. Verlinde, and Herman L. Verlinde. "The Operator Algebra of Orbifold Models". In: *Commun. Math. Phys.* 123 (1989), p. 485. DOI: 10.1007/BF01238812.

[138] M. Kontsevich. "Intersection theory on the moduli space of curves and the matrix Airy function". In: *Commun. Math. Phys.* 147 (1992), pp. 1–23. DOI: 10.1007/BF02099526.

[139] Peter Bouwknegt and Kareljan Schoutens. "W symmetry in conformal field theory". In: *Phys. Rept.* 223 (1993), pp. 183–276. DOI: 10.1016/0370-1573(93)90111-P. arXiv: hep-th/9210010.

[140] Mina Aganagic, Miranda C. N. Cheng, Robbert Dijkgraaf, Daniel Krefl, and Cumrun Vafa. "Quantum Geometry of Refined Topological Strings". In: *JHEP* 11 (2012), p. 019. arXiv: 1105.0630 [hep-th].

[141] Vincent Bouchard, Joel Hutchinson, Prachi Loliencar, Michael Meiers, and Matthew Rupert. "A generalized topological recursion for arbitrary ramification". In: *Annales Henri Poincare* 15 (2014), pp. 143–169. DOI: 10.1007/s00023-013-0233-0. arXiv: 1208.6035 [math-ph].

[142] I. Bakas. "The structure of the W $_\infty$ algebra". In: *Communications in Mathematical Physics* 134.3 (Dec. 1990), pp. 487–508. DOI: 10.1007/BF02098443.

[143] Satoshi Nawata, P. Ramadevi, and Vivek Kumar Singh. "Colored HOMFLY-PT polynomials that distinguish mutant knots". In: *J. Knot Theor. Ramifications* 26.14 (2017), p. 1750096. DOI: 10.1142/S0218216517500961. arXiv: 1504.00364 [math.GT].